

Pertanika Journal of

SCIENCE &

TECHNOLOGY

JST

VOL. 33 (S4) 2025

A Special Issue devoted to
**Synergizing Innovation and Practicality:
Bridging the Gap in Applied Engineering**

Guest Editors

Siti Anom Ahmad, Nashiren Farzilah Mailah and Roseliza Kadir Basha



PERTANIKA
JOURNALS

A scientific journal published by Universiti Putra Malaysia Press

PERTANIKA JOURNAL OF SCIENCE & TECHNOLOGY

About the Journal

Overview

Pertanika Journal of Science & Technology is an official journal of Universiti Putra Malaysia. It is an open-access online scientific journal. It publishes original scientific outputs. It neither accepts nor commissions third party content.

Recognised internationally as the leading peer-reviewed interdisciplinary journal devoted to the publication of original papers, it serves as a forum for practical approaches to improve quality on issues pertaining to science and engineering and its related fields.

Pertanika Journal of Science & Technology currently publishes 6 issues a year (*January, March, April, July, August, and October*). It is considered for publication of original articles as per its scope. The journal publishes in **English** and it is open for submission by authors from all over the world.

The journal is available world-wide.

Aims and scope

Pertanika Journal of Science & Technology aims to provide a forum for high quality research related to science and engineering research. Areas relevant to the scope of the journal include: bioinformatics, bioscience, biotechnology and bio-molecular sciences, chemistry, computer science, ecology, engineering, engineering design, environmental control and management, mathematics and statistics, medicine and health sciences, nanotechnology, physics, safety and emergency management, and related fields of study.

History

Pertanika Journal of Science & Technology was founded in 1993 and focuses on research in science and engineering and its related fields.

Vision

To publish a journal of international repute.

Mission

Our goal is to bring the highest quality research to the widest possible audience.

Quality

We aim for excellence, sustained by a responsible and professional approach to journal publishing. Submissions can expect to receive a decision within 90 days. The elapsed time from submission to publication for the articles averages 180 days. We are working towards decreasing the processing time with the help of our editors and the reviewers.

Abstracting and indexing of Pertanika

Pertanika Journal of Science & Technology is now over 33 years old; this accumulated knowledge and experience has resulted the journal being abstracted and indexed in SCOPUS (Elsevier), Journal Citation Reports (JCR-Clarivate), EBSCO, ASEAN CITATION INDEX, Microsoft Academic, Google Scholar, and MyCite.

Citing journal articles

The abbreviation for Pertanika Journal of Science & Technology is *Pertanika J. Sci. & Technol.*

Publication policy

Pertanika policy prohibits an author from submitting the same manuscript for concurrent consideration by two or more publications. It prohibits as well publication of any manuscript that has already been published either in whole or substantial part elsewhere. It also does not permit publication of manuscript that has been published in full in proceedings.

Code of Ethics

The *Pertanika* journals and Universiti Putra Malaysia take seriously the responsibility of all of its journal publications to reflect the highest in publication ethics. Thus, all journals and journal editors are expected to abide by the journal's codes of ethics. Refer to *Pertanika's Code of Ethics* for full details, or visit the journal's web link at http://www.pertanika.upm.edu.my/code_of_ethics.php

Originality

The author must ensure that when a manuscript is submitted to *Pertanika*, the manuscript must be an original work. The author should check the manuscript for any possible plagiarism using any program such as Turn-It-In or any other software before submitting the manuscripts to the *Pertanika* Editorial Office, Journal Division.

All submitted manuscripts must be in the journal's acceptable similarity index range:
≤ 20% – PASS; > 20% – REJECT.

International Standard Serial Number (ISSN)

An ISSN is an 8-digit code used to identify periodicals such as journals of all kinds and on all media—print and electronic.

Pertanika Journal of Science & Technology: e-ISSN 2231-8526 (Online).

Lag time

A decision on acceptance or rejection of a manuscript is reached in 90 days (average). The elapsed time from submission to publication for the articles averages 180 days.

Authorship

Authors are not permitted to add or remove any names from the authorship provided at the time of initial submission without the consent of the journal's Chief Executive Editor.

Manuscript preparation

For manuscript preparation, authors may refer to *Pertanika*'s **INSTRUCTION TO AUTHORS**, available on the official website of *Pertanika*.

Editorial process

Authors who complete any submission are notified with an acknowledgement containing a manuscript ID on receipt of a manuscript, and upon the editorial decision regarding publication.

Pertanika follows a **double-blind peer-review** process. Manuscripts deemed suitable for publication are sent to reviewers. Authors are encouraged to suggest names of at least 3 potential reviewers at the time of submission of their manuscripts to *Pertanika*, but the editors will make the final selection and are not, however, bound by these suggestions.

Notification of the editorial decision is usually provided within 90 days from the receipt of manuscript. Publication of solicited manuscripts is not guaranteed. In most cases, manuscripts are accepted conditionally, pending an author's revision of the material.

The journal's peer review

In the peer-review process, 2 to 3 referees independently evaluate the scientific quality of the submitted manuscripts. At least 2 referee reports are required to help make a decision.

Peer reviewers are experts chosen by journal editors to provide written assessment of the **strengths and weaknesses** of written research, with the aim of improving the reporting of research and identifying the most appropriate and highest quality material for the journal.

Operating and review process

What happens to a manuscript once it is submitted to *Pertanika*? Typically, there are 7 steps to the editorial review process:

1. The journal's Chief Executive Editor and the Editor-in-Chief examine the paper to determine whether it is relevance to journal needs in terms of novelty, impact, design, procedure, language as well as presentation and allow it to proceed to the reviewing process. If not appropriate, the manuscript is rejected outright and the author is informed.
2. The Chief Executive Editor sends the article-identifying information having been removed, to 2 to 3 reviewers. They are specialists in the subject matter of the article. The Chief Executive Editor requests that they complete the review within 3 weeks.

Comments to authors are about the appropriateness and adequacy of the theoretical or conceptual framework, literature review, method, results and discussion, and conclusions. Reviewers often include suggestions for strengthening of the manuscript. Comments to the editor are in the nature of the significance of the work and its potential contribution to the research field.

3. The Editor-in-Chief examines the review reports and decides whether to accept or reject the manuscript, invite the authors to revise and resubmit the manuscript, or seek additional review reports. In rare instances, the manuscript is accepted with almost no revision. Almost without exception, reviewers' comments (to the authors) are forwarded to the authors. If a revision is indicated, the editor provides guidelines for attending to the reviewers' suggestions and perhaps additional advice about revising the manuscript.
4. The authors decide whether and how to address the reviewers' comments and criticisms and the editor's concerns. The authors return a revised version of the paper to the Chief Executive Editor along with specific information describing how they have addressed the concerns of the reviewers and the editor, usually in a tabular form. The authors may also submit a rebuttal if there is a need especially when the authors disagree with certain comments provided by reviewers.
5. The Chief Executive Editor sends the revised manuscript out for re-review. Typically, at least 1 of the original reviewers will be asked to examine the article.
6. When the reviewers have completed their work, the Editor-in-Chief examines their comments and decides whether the manuscript is ready to be published, needs another round of revisions, or should be rejected. If the decision is to accept, the Chief Executive Editor is notified.
7. The Chief Executive Editor reserves the final right to accept or reject any material for publication, if the processing of a particular manuscript is deemed not to be in compliance with the S.O.P. of *Pertanika*. An acceptance letter is sent to all the authors.

The editorial office ensures that the manuscript adheres to the correct style (in-text citations, the reference list, and tables are typical areas of concern, clarity, and grammar). The authors are asked to respond to any minor queries by the editorial office. Following these corrections, page proofs are mailed to the corresponding authors for their final approval. At this point, **only essential changes are accepted**. Finally, the manuscript appears in the pages of the journal and is posted on-line.

Pertanika Journal of
**SCIENCE
& TECHNOLOGY**

A Special Issue devoted to
**Synergizing Innovation and Practicality:
Bridging the Gap in Applied Engineering**

Vol. 33 (S4) 2025

Guest Editors
Siti Anom Ahmad, Nashiren Farzilah Mailah and Roseliza Kadir Basha



A scientific journal published by Universiti Putra Malaysia Press

UNIVERSITY PUBLICATIONS COMMITTEE

CHAIRMAN

Zamberi Sekawi

EDITOR-IN-CHIEF

Luqman Chuah Abdullah
Chemical Engineering

EDITORIAL STAFF

Journal Officers:

Ellyyanur Puteri Zainal
Siti Zuhaila Abd Wahid
Tee Syin Ying

Editorial Assistants:

Siti Juridah Mat Arip
Zulinaardawati Kamarudin

English Editor:

Norhanizah Ismail

PRODUCTION STAFF

Pre-press Officers:

Ku Ida Mastura Ku Baharom
Nur Farrah Dila Ismail

WEBMASTER

IT Officer:

Kiran Raj Kaneswaran

EDITORIAL OFFICE

JOURNAL DIVISION

Putra Science Park
1st Floor, IDEA Tower II
UPM-MTDC Technology Centre
Universiti Putra Malaysia
43400 Serdang, Selangor Malaysia.

General Enquiry

Tel. No: +603 9769 1622

E-mail:

executive_editor.pertanika@upm.edu.my

URL: <http://www.pertanika.upm.edu.my>

PUBLISHER

UPM Press

Universiti Putra Malaysia
43400 UPM, Serdang, Selangor, Malaysia.
Tel: +603 9769 8855

E-mail: dir.penerbit@upm.edu.my

URL: <http://penerbit.upm.edu.my>



PENERBIT
UPM
UNIVERSITI PUTRA MALAYSIA
P R E S S



PERTANIKA
JOURNALS

ASSOCIATE EDITOR

2024-2026

Miss Laiha Mat Kiah

Security Services Sn: Digital Forensic, Steganography, Network Security, Information Security, Communication Protocols, Security Protocols
Universiti Malaysia, Malaysia

Saidur Rahman

Renewable Energy, Nanofluids, Energy Efficiency, Heat Transfer, Energy Policy
Sunway University, Malaysia

EDITORIAL BOARD

2024-2026

Abdul Latif Ahmad

Chemical Engineering
Universiti Sains Malaysia, Malaysia

Hsiu-Po Kuo

Chemical Engineering
National Taiwan University, Taiwan

Mohd. Ali Hassan

Bioprocess Engineering, Environmental Biotechnology
Universiti Putra Malaysia, Malaysia

Ahmad Zaharin Aris

Hydrochemistry, Environmental Chemistry, Environmental Forensics, Heavy Metals
Universiti Putra Malaysia, Malaysia

Ivan D. Rukhlenko

Nonlinear Optics, Silicon Photonics, Plasmonics and Nanotechnology
The University of Sydney, Australia

Nor Azah Yusof

Biosensors, Chemical Sensor, Functional Material
Universiti Putra Malaysia, Malaysia

Azlina Harun@

Kamaruddin
Enzyme Technology, Fermentation Technology
Universiti Sains Malaysia, Malaysia

Lee Keat Teong

Energy Environment, Reaction Engineering, Waste Utilization, Renewable Energy
Universiti Sains Malaysia, Malaysia

Norbahiah Misran

Communication Engineering
Universiti Kebangsaan Malaysia, Malaysia

Bassim H. Hameed

Chemical Engineering: Reaction Engineering, Environmental Catalysis & Adsorption
Qatar University, Qatar

Mohamed Othman

Communication Technology and Network, Scientific Computing
Universiti Putra Malaysia, Malaysia

Roslan Abd-Shukor

Physics & Materials Physics, Superconducting Materials
Universiti Kebangsaan Malaysia, Malaysia

Biswajeet Pradhan

Digital image processing, Geographical Information System (GIS), Remote Sensing
University of Technology Sydney, Australia

Mohd Shukry Abdul Majid

Polymer Composites, Composite Pipes, Natural Fibre Composites, Biodegradable Composites, Bio-Composites
Universiti Malaysia Perlis, Malaysia

Sodeifan Gholmosseini

Supercritical technology, Optimization, nanoparticles, Polymer nanocomposites
University of Kashan, Iran

Ho Yuh-Shan

Water research, Chemical Engineering and Environmental Studies
Asia University, Taiwan

Mohd Zulkifly Abdullah

Fluid Mechanics, Heat Transfer, Computational Fluid Dynamics (CFD)
Universiti Sains Malaysia, Malaysia

Wing Keong Ng

Aquaculture, Aquatic Animal Nutrition, Aqua Feed Technology
Universiti Sains Malaysia, Malaysia

INTERNATIONAL ADVISORY BOARD

2024-2027

Hiroshi Uyama

Polymer Chemistry, Organic Compounds, Coating, Chemical Engineering
Osaka University, Japan

Mohini Sain

Material Science, Biocomposites, Biomaterials
University of Toronto, Canada

Mohamed Pourkashanian

Mechanical Engineering, Energy, CFD and Combustion Processes
Sheffield University, United Kingdom

Yulong Ding

Particle Science & Thermal Engineering
University of Birmingham, United Kingdom

ABSTRACTING AND INDEXING OF PERTANIKA JOURNALS

Pertanika Journal of Science & Technology is indexed in Journal Citation Reports (JCR-Clarivate), SCOPUS (Elsevier), EBSCO, ASEAN Citation Index, Microsoft Academic, Google Scholar and MyCite.

The publisher of Pertanika will not be responsible for the statements made by the authors in any articles published in the journal. Under no circumstances will the publisher of this publication be liable for any loss or damage caused by your reliance on the advice, opinion or information obtained either explicitly or implied through the contents of this publication. All rights of reproduction are reserved in respect of all papers, articles, illustrations, etc., published in Pertanika. Pertanika provides free access to the full text of research articles for anyone, worldwide. It does not charge either its authors or author-institution for refereeing/publishing outgoing articles or user-institution for accessing incoming articles. No material published in Pertanika may be reproduced or stored on microfilm or in electronic, optical or magnetic form without the written authorization of the Publisher.

Copyright ©2021 Universiti Putra Malaysia Press. All Rights Reserved.

Pertanika Journal of Science & Technology
Vol. 33 (S4) 2025

Contents

Preface	i
<i>Siti Anom Ahmad, Nashiren Farzilah Mailah and Roseliza Kadir Basha</i>	
Bibliometric Review on Geopolymer Modified with Nanomaterials Using VOS Viewer	1
<i>Maryam Firas Al-Baldawi, Farah Nora Aznieta Abdul Aziz , Al Ghazali Noor Abbas, Noor Azline Mohd Nasir, Khalina Abdan and Norsuzailina Mohamed Sutan</i>	
Material Characterization and Electrical Performance of <i>Prosopis africana</i> Conductive Ink for Antenna Applications	27
<i>Suleiman Babani, Mohd Nizar Hamidon, Alyani Ismail, Haslina Jaafar, Intan Helina Hasan, Farah Nabilah Shafee, Ibrahim Garba Shitu, Jamila Lamido, Sani Halliru Lawan and Zainab Yunusa</i>	
Effect of Coil Diameter on the Performance of Interior and Embedded Permanent Magnet for Double-stator Generator	45
<i>Nur Amira Ibrahim, Norhisam Misron, Hairul Faizi Hairulnizam, Chockalingam Aravind Vaithilingam, Nashiren Farzilah Mailah and Ishak Aris</i>	
Psychology-informed Natural Language Understanding: Integrating Personality and Emotion-aware Features for Comprehensive Sentiment Analysis and Depression Detection	57
<i>Jing Jie Tan, Ban-Hoe Kwan, Danny Wee-Kiat Ng and Yan Chai Hum</i>	
Development of Digital Twin Data-driven Modelling for Gas Turbine Operation Behaviour	81
<i>Balbir Shah Mohd Irwan Shah, Asnor Juraiza Ishak, Mohd Khair Hassan and Nor Mohd Haziq Norsahperi</i>	
Evaluation of Multimodal Dataset for Continuous Air-writing Multidigit Number Recognition Using Wearable Sensor	99
<i>Yusuke Takei and Eiichi Inohira</i>	
Acoustic Partial Discharge Localization in Refined, Bleached and Deodorized Palm Oil (RBDPO) Based on the Savitzky-Golay and Moving Average Denoising Methods	115
<i>Nur Darina Ahmad, Norhafiz Azis, Jasronita Jasni, Khairil Anas Md Rezali, Mohd Aizam Talib, Nik Hakimi Nik Ali and Masahiro Kozako</i>	

Performance of Recycling Aggregate Self-Compacting Concrete Incorporating Supplementary Cementitious Materials: An Overview	129
<i>Said Mohammed Mostafa Aljamala, Nor Azizi Safiee, Noor Azline Mohd Nasir and Farah Nora Aznieta Abdul Aziz</i>	
Differences Between Research Log Datasets and Development Field Logs and the Creation of the Complexity Evaluation Index	161
<i>Hironori Uchida, Keitaro Tominaga, Hideki Itai, Yujie Li and Yoshihisa Nakatoh</i>	

Preface

This Special Issue of *Pertanika Journal of Science and Technology (JST)* features selected papers from the **Symposium on Applied Engineering and Sciences (SAES2023)**, held on 20th–21st November 2023 at Universiti Putra Malaysia. SAES, an annual conference co-organized by Universiti Putra Malaysia and Kyushu Institute of Technology, Japan, was established in 2013 to promote research exchange and collaboration between the two institutions. Over the years, SAES has become a vibrant platform for researchers from various institutions and disciplines to share innovations, insights, and solutions in applied engineering.

Applied engineering is the practical realization of scientific and engineering principles to solve real-world problems, improve systems, and create technologies that directly benefit society. It encompasses diverse fields such as mechanical, electrical, civil, and chemical engineering, as well as computer science, and emphasizes translating theory into impactful applications.

This special issue, “**Synergizing Innovation and Practicality: Bridging the Gap in Applied Engineering**,” reflects the essence of applied engineering—balancing technological advancement with real-world relevance. It underscores the importance of interdisciplinary collaboration and innovation in addressing complex societal and industrial challenges. Innovation in applied engineering fuels economic development and contributes to sustainability and improving the quality of life.

This issue features nine peer-reviewed papers covering a wide range of topics, including engineering, technology, and computer sciences. Each paper represents a novel contribution that bridges innovation and practicality, aligning with the theme and spirit of SAES.

We sincerely thank all authors, reviewers, and the editorial team for their contributions and commitment to academic excellence. We hope this special issue will inspire further research and collaboration in applied engineering and its many transformative possibilities.

Guest Editors

Siti Anom Ahmad (Prof. Ir. Dr.)

Nashiren Farzilah Mailah (Assoc. Prof. Dr.)

Roseliza Kadir Basha (Dr.)

Bibliometric Review on Geopolymer Modified with Nanomaterials Using VOS Viewer

Maryam Firas Al-Baldawi¹, Farah Nora Aznieta Abdul Aziz^{1*},
Al Ghazali Noor Abbas¹, Noor Azline Mohd Nasir¹, Khalina Abdan² and
Norsuzailina Mohamed Sutan³

¹Housing Research Centre (HRC), Department of Civil Engineering, Faculty of Engineering, Universiti Putra Malaysia UPM, 43400 Serdang, Selangor, Malaysia

²Institute of Tropical Forestry and Forest Products (INTROP), Universiti Putra Malaysia, University Putra Malaysia UPM, 43400 Serdang, Selangor, Malaysia

³Department of Civil Engineering, Faculty of Engineering, Universiti Malaysia Sarawak, 94300 Kota Samarahan, Sarawak, Malaysia

ABSTRACT

Geopolymer composites modified with nanomaterials have gained significant interest in recent years due to their improved properties. The nanoparticles can form extra C-S-H gel, reducing porosity and generating a denser microstructure. Manual reviews cannot effectively manage the immense bibliometric data. Therefore, this manuscript reviews nanomaterials in geopolymer by adopting a scientometric evaluation as a form of analysis via visualization of similarities software in the VOS viewer. A bibliometric network is created and depicted to analyze the annual distribution and growth pattern, prominent sources, frequent keywords, top articles, and leading countries of geopolymer modified with nanomaterials via the searched words in the Scopus database of “geopolymer” and “nanomaterial” that successfully achieved 529 documents from 2008 to

October 2023. The results of the scientometric study indicate that *Construction and Building Materials* appears as the top publication source, in terms of article amount and citation count, and the most frequently utilized keywords in these publications are nanomaterial, geopolymers, and inorganic polymers. Furthermore, the countries that have demonstrated the highest levels of activity and contribution in terms of publications are China, India, and the United States. The inclusion of participating nations and researchers is facilitated through quantitative and graphical representations. This review has

ARTICLE INFO

Article history:

Received: 01 April 2024

Accepted: 10 April 2025

Published: 10 June 2025

DOI: <https://doi.org/10.47836/pjst.33.S4.01>

E-mail address:

mariamfrsas436@gmail.com (Maryam Firas Al-Baldawi)

farah@upm.edu.my (Farah Nora Aznieta Abdul Aziz)

na706050@gmail.com (Al-Ghazali Noor Abbas)

nazline@upm.edu.my (Noor Azline Mohd Nasir)

khalina@upm.edu.my (Khalina Abdan)

msnorsuzailina@unimas.my (Norsuzailina Mohamed Sutan)

*Corresponding author

the potential to provide valuable insights to academics in the field of forming collaborations and discussing novel ideas and methods. This is mostly due to the inclusion of visual and statistical depictions that showcase the participating nations and authors of the study.

Keywords: Geopolymer concrete (GPC), nanomaterial, VOS viewer, scientometric analysis

INTRODUCTION

Cement-based concrete is anticipated to be the most widely utilized substance worldwide after water, which contributes significantly to greenhouse gas emissions (Adesina, 2020). However, cement production is responsible for around 5%–8% of global carbon dioxide (CO₂) emissions (Teh et al., 2017). The annual consumption of cement exceeds 4000 million tons and is anticipated to exceed almost 6000 million tons by 2060 (Shahmansouri et al., 2020). Researchers have endeavored to develop substitute binders for concrete manufacturing to mitigate the environmental impact of CO₂ emissions on the Earth. Geopolymer concrete has developed as a promising replacement for ordinary concrete, demonstrating the potential for substitution (Shehata et al., 2022).

Portland cement is manufactured by heating limestone (CaCO₃) and clay at high temperatures (~1450 °C) in a kiln, resulting in significant CO₂ emissions from fuel burning and limestone decomposition. Conversely, geopolymer concrete employs industrial by-products like fly ash, slag, or metakaolin as its principal binder, which are activated with alkaline solutions (sodium hydroxide and sodium silicate). The absence of cement clinker production leads to significant CO₂ reduction. Geopolymers possess the ability to significantly decrease the carbon dioxide emissions associated with ordinary Portland cement (OPC) production by up to 80% (Duxson et al., 2007).

The word geopolymer was introduced in 1978 by a French scientist, Joseph Davidovits (Davidovits, 1979). It refers to a group of solid substances produced through the chemical reaction between an alumina silicate powder and an alkaline activator (Elie et al., 2021). Geopolymer has garnered more attention within the realm of academic research due to reduced CO₂ emissions (McLellan et al., 2011), reuse of waste materials (Kheimi et al., 2022), support for circular economy practices in solid waste management, enhanced thermal resistance (Turner & Collins, 2013), improved mechanical performance, resistance to acid and sulfate attacks (Zhao et al., 2021), decreased drying shrinkage, and increased resistance to freeze-thaw cycles (Davidovits, 1991; Matsimbe et al., 2022). Despite its numerous advantages, the utilization of geopolymer in technical applications remains limited because of its comparatively high porosity, inadequate interfacial bonding strength, and delayed development of strength during its final stages (Alomayri, 2019).

Recently, geopolymer composites modified with nanomaterials have gained significant interest. Nanomaterials can make more C-S-H gel, which reduces porosity and increases the

density of the microstructure (Jindal & Sharma, 2020; Mostafa et al., 2020) as illustrated in Figure 1. Nanomaterials enhance the formation of C-S-H gel, which reduces porosity and improves the density of the composite (Jindal & Sharma, 2020; Mostafa et al., 2020). Various types of nanomaterials used in geopolymers, such as nano-silica (Çevik et al., 2018), nano-alumina (Assaedi & Olawale, 2022), nano-titanium oxide (Jagadesh & Nagarajan, 2022), carbon nanotubes (Jagadesh & Nagarajan, 2022), and nano-clay (Li et al., 2022), are used to enhance their properties (Raj et al., 2023). Figure 1 illustrates the benefits of nanomaterial-based geopolymers. Nano silica is a specific type of nanomaterial that is most impactful due to its high reactivity with geopolymer compared to other nanomaterials.

Conventional literature reviews are insufficient and subject to bias in establishing an integrated and systematic relationship between different domains of scholarly work. The bibliometric analysis method illustrates the current trajectory of geopolymer concrete modified with nano materials knowledge development in numerous fields of science, furnishes data on the most productive writers and nations, and offers insight into past trends and projected futures of research areas worldwide. This approach is especially valuable as it permits researchers to identify new trends, cross-disciplinary collaborations,

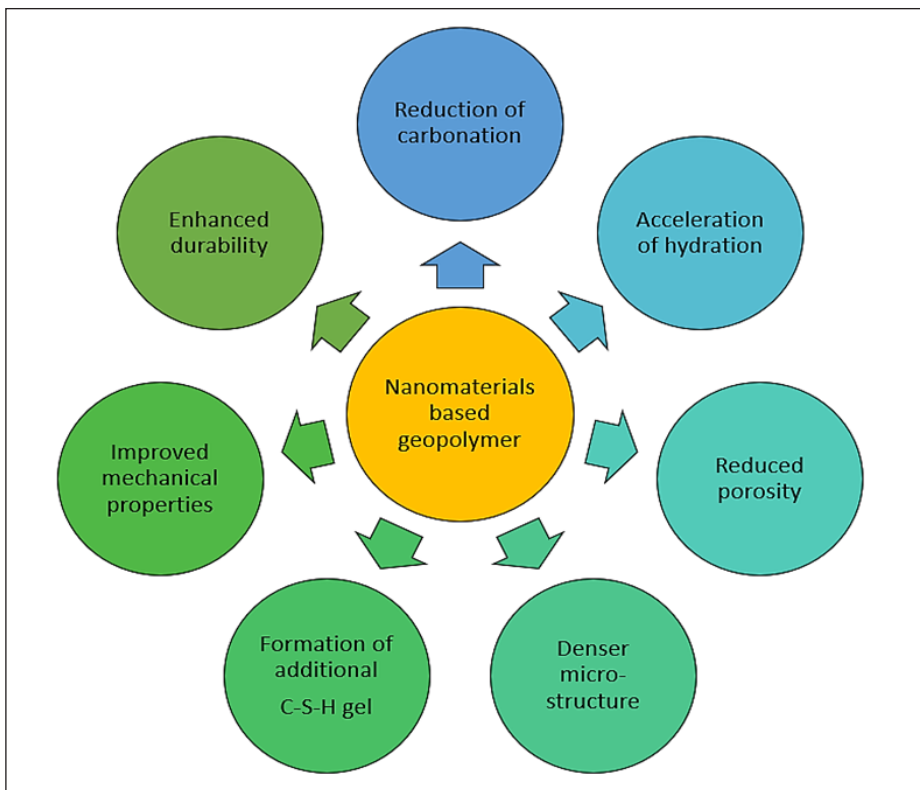


Figure 1. Benefits of nanomaterial-based geopolymers (created by the author)

and technological innovations essential to handling global sustainability obstacles in construction materials.

Several researchers use VOS viewer software to conduct bibliometric studies of geopolymers in various fields, developed in 2010 by Nees Jan van Eck and Ludo Waltman. The software was selected over other bibliometric tools, such as CiteSpace, R Bibliometrix and Google Scholar, because of its ability to visualize and exhibit maps that are easy to interpret. Besides, VOS viewer collects data from various scientific sources such as the Web of Science and Scopus. This enables users to share their maps as dynamic visualizations on the web. VOS viewer is also available on many devices and operating systems, and is free to access (Martins et al., 2024).

Matsimbe et al. (2023) carried out a bibliographic analysis study of geopolymer research in Sub-Saharan Africa using VOS viewer software. The researchers discovered that the terms exhibiting the most frequent occurrences are geopolymers, inorganic polymers, and compressive strength. Furthermore, the *Construction and Building Materials* journal is widely regarded as a prominent scholarly publication, with 41 published articles and an impressive citation record of around 1488. Cameroon, Nigeria, and South Africa are the nations that exhibit the largest volume of publications. Khan et al. (2022) conducted a review of research on the scientometric analysis of the research growth on geopolymers. The keywords used are geopolymer, fly ash, and compressive strength. The scientometric analysis shows that *Construction and Building Materials* publishes the most articles and citations. China, India, and Australia have published extensively. The quantitative and graphical depiction of the participating countries and scholars in this study may foster academic collaboration and creativity.

Tian et al. (2022) found that fly ash-based geopolymer development has three stages: replacing Portland cement, developing multifunctional materials, and reducing environmental impact through solid waste conversion. The author found that China, Australia, India, and the United States emerged as the leading nations in terms of articles, with 16.45%, 10.14%, 7.67%, and 6.68% of the 4352 total articles, respectively.

On the other hand, Yang et al. (2022) carried out a bibliometric analysis of geopolymer composites. The analysis revealed a significant growth in publications on geopolymer composites, particularly between 2011 and 2021, highlighting an increasing interest in eco-friendly construction materials. The top keywords, such as inorganic polymers, geopolymers, and geopolymer, emphasize sustainability and mechanical properties. *Construction and Building Materials* led with 666 publications, followed by Ceramics International. India, China and Australia emerged as top contributors. The bibliometric analysis identified Van Deventer J. S. J. as the most prolific author with 79 publications and 16,125 citations, followed by Chindaprasirt P. (77 publications) and Provis J. L. (70 publications, 13,382 citations).

Geopolymer technology solves environmental contamination by replacing Portland cement with a sustainable alternative. Elmesalami and Celik (2022) comprehensively reviewed Engineered Geopolymer Composites (EGCs). The report commences with a scientometric analysis employing science mapping techniques to summarize the current state of study advancements in EGCs. The review has uncovered the intriguing potential of EGCs as materials that possess both low-carbon and ultra-high-performance characteristics in the application field of construction. Nevertheless, the current phase of research on EGCs remains in its nascent stages, necessitating future inquiries to fully comprehend and use the complete capabilities of EGCs.

Ji and Pei (2019) conducted a review paper on the bibliographic and graphical analysis of the application of geopolymers in the immobilization of heavy metals. The data show that geopolymer research has grown fast in recent years and has been applied to various technical sectors. Geopolymers are manufactured from fly ash and metakaolin. The toxicity characteristic leaching procedure (TCLP) is the most commonly used leaching method because it is a standardized method recommended by the U.S. Environmental Protection Agency (EPA) to evaluate the leaching potential of heavy metals under simulated landfill conditions, heavy metals like Pb, Cr, Cu, Cd, and Zn are toxic elements commonly found in industrial by-products like fly ash. These metals pose environmental risks due to their potential to leach into soil and groundwater, contaminating ecosystems. Therefore, using this method makes it an ideal choice for this research.

Another study conducted by Firas et al. (2024) and Al-Baldawi (2024) on the "Performance of Hybrid Fiber Reinforced Geopolymer Composites (HFRGC): Scientometric and Conventional Review". The outcome indicated that India, China, and Australia were the most active countries in HFRGC research, revealing India as the leading contributor with 35 documents and 333 citations. *Construction and Building Materials* emerged as the most influential journal, publishing 15 articles with 441 citations, significantly outpacing others like *Lecture Notes in Civil Engineering* (10 articles, four citations) and *Materials* (five articles, 34 citations). Frequently used keywords include "geopolymers" and "inorganic polymers," each with 51 occurrences, and "compressive strength" with 31 occurrences. The analysis shows fluctuating publication growth, peaking in 2023 with 20 documents. These findings underscore key research hubs, journals, and trends, aiding collaboration and strategic direction for future HFRGC studies.

There has been a notable lack of studies of geopolymers modified with nanomaterials in bibliometric reviews and bibliometric studies. This deficiency extends to the search strings that have not been sufficiently broad to yield a comprehensive dataset. Consequently, there is a need for an impartial and less subjective illustration of the trends and advancements in this field. This study aims to elucidate the patterns and advancements observed in the most significant sources of publishing, keywords, publications, and nations in the field of geopolymer modified with nanomaterials from 2008 to 2023. The bibliometric analysis

conducted in this study offers significant statistical insights into the development and implementation of geopolymer modified with nanomaterials.

Consequently, it effectively highlights the prevailing and prospective research trends in this field. Furthermore, it clarifies the key issues and noteworthy contributions made by eminent publications and authors to the development of the discipline and enhances comprehension of the theoretical framework and core subjects of the subject area. Using network visualization in bibliometric co-occurrences and co-citations can help academics and research institutions share research skills and creative technologies, work together on unique research projects, and create new business partnerships. Therefore, this study aims to address this deficiency by performing a bibliographic evaluation of the geopolymer modified with nanomaterials research trends to establish empirical benchmarks for future studies.

RESEARCH STRATEGY AND DATA SOURCES

The current investigation employed a scientometric strategy-based review of geopolymers modified with nanomaterials to analyze scientific findings and generate bibliometric geographical maps. The chosen methodology is suitable for this type of assessment as it effectively examines and evaluates the progression of the study during a certain timeframe, utilizing an extensive collection of bibliographic data (Hosseini et al., 2018). Several articles have been released on the topic, and choosing a trustworthy search engine is crucial. Scopus and Web of Science are both highly accurate search platforms that are ideal. (Chadegani et al., 2013; Pranckutė, 2021). The bibliographic data for the geopolymer composite modified with nanomaterials study was acquired using Scopus, which academics highly recommend (Meho, 2019).

Scopus was selected as the principal data source because of its extensive coverage and thorough indexing of scientific literature compared to the Web of Science (Visser et al., 2021). Scopus indexes more than 20,000 journals, exceeding WoS's 13,600, thereby providing a more extensive overview of global research outputs (Mongeon & Paul-Hus, 2016). Nevertheless, the accuracy of citation data differs, as WoS faces issues with missing and incorrect references, while Scopus struggles with duplicate publications. These elements make Scopus preferred for larger disciplinary coverage, although both platforms have limitations impacting citation reliability (Liu et al., 2021).

VOS viewer, created by Eck and Waltman (2021), is a popular data visualization software. It is able to generate visualizations of researchers, journals, documents, and keywords using citations and co-occurrence data. Table 1 illustrates the selection standards applied when obtaining data in the Scopus database from 2008 until October 2023. The timeframe of 2008–2023 was selected because research on the application of nanomaterials in geopolymer technology began gaining significant interest around 2008. Furthermore, collecting literature up to the time of manuscript submission in October 2023

ensures the Review reflects the most recent advancements and trends.

This research focuses on the annual publication of documents, Science mapping of top publication sources, science mapping of co-occurrence keywords, authors, top-cited articles, and contributing nations. The words searched in the Scopus database of Geopolymer and nanomaterial successfully achieved 529 of 914 articles as of October

2023, after applying filtration to eliminate unnecessary papers. The journal article and journal review document types were chosen. The constraint of the language was specified as English. Non-English articles are excluded to prevent misleading data due to translation, interpretation, and accessibility issues because the VOS viewer gives metadata in English.

The subject areas of engineering and material science were chosen because Geopolymer and nanomaterials are categories in these two. By limiting the scope to these categories, the study ensures a focused and comprehensive bibliometric analysis that is feasible and relevant to the research objectives. The geopolymer data modified with nanomaterials obtained from the Scopus database have been retained in the comma-separated values (CSV) form to facilitate assessment via an appropriate program. The scientific map and visualization tool utilized in this study was VOS viewer (version 1.6.17). Figure 2 illustrates a diagram representing the scientometric strategy.

Table 1

Filter applied for extracting data from the Scopus website

Option	Filter used
Publication date	2008–2023
Language	English
Subject area	Material Science Engineering
Document type	Article Review

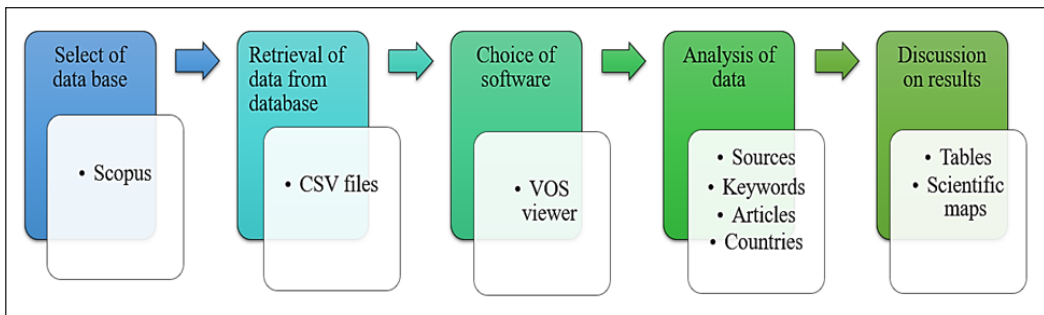


Figure 2. The Sequences of scientometric analysis followed in the geopolymer modified with nanomaterials research

RESULTS AND DISCUSSION

Annual Publication of Documents

The annual publication trend for the subject area is illustrated in Figure 3. The searched keywords, geopolymer and nanomaterial, resulted in 914 documents from 2008 to 2023.

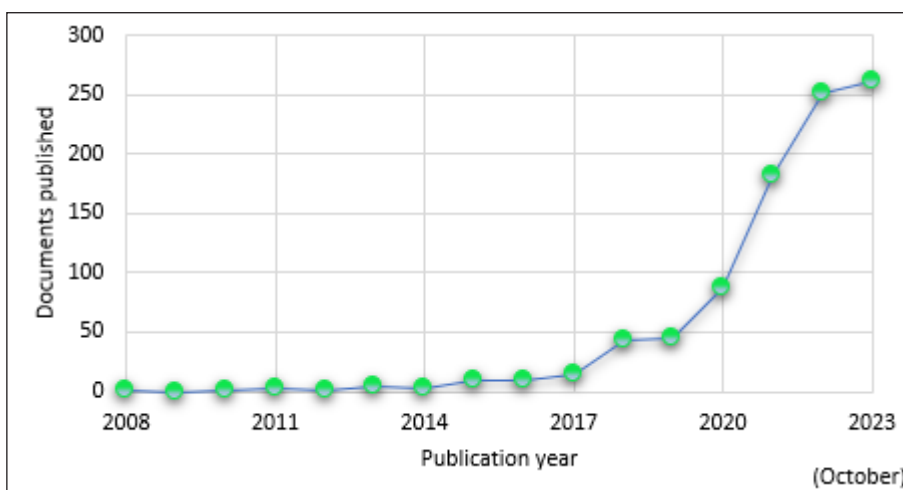


Figure 3. Annual publication trend on geopolymers modified with nanomaterials corpus from 2008 until 2023

According to the study conducted by Chen et al. (2022), the annual volume of publications can indicate the development path within a certain topic. According to the Scopus journal database, there have been a few research investigations on nanomaterial-based geopolymers between 2008 and 2017. Nevertheless, starting in 2018, there was a noticeable rise in published works, with a growth rate of over 50% compared to 2017. Since then, there has been an annual increase in the total and cumulative amount of documents on nanomaterial-based geopolymers, which peaked in 2023. The quantity of scholarly articles within the specific study domain is increasing yearly, with a total publication of 262 (October 2023).

Science Mapping Top Publication Sources

The use of source mapping techniques facilitates the analysis of innovation and development. These sources offer access to data that has some clearly stated limitations. The analysis was conducted using the VOS viewer software, which utilized bibliometric data from Scopus. The analysis type selected for this study was "bibliographic coupling" with the analysis unit "sources". The thresholds were fixed at a minimum number of five documents and a minimum citation source of 21. After the analysis, 203 publications met the conditions. Using 203 publications, the most related journals are identified by considering their total link strength, published related papers, and citation count. The result of the 10 most related journals is demonstrated in Table 2. *Construction and Building Materials*, *Materials*, and *Journal of Cleaner Production* are the three highest publication sources with 59, 25, and 20 research papers, respectively.

The aforementioned academic journals, *Construction and Building Materials*, *Journal of Cleaner Production*, and *Materials*, have received citation counts of 1918, 671, and 490,

Table 2

Top publication sources in the related research area

No.	Source	Number of publications	Citations	Link Strength
1	Construction and Building Materials	59	1918	496
2	Materials	25	490	138
3	Journal of Cleaner Production	20	671	105
4	Journal of Materials in Civil Engineering	14	93	64
5	Materials today: Proceedings	14	39	30
6	Case Studies in Construction Materials	12	142	301
7	Journal of Building Engineering	11	274	216
8	Polymers	11	97	12
9	Nanomaterials	10	198	140
10	Cement and Concrete Composites	10	294	102

respectively. This examination would establish a basis for future scientometric inquiries in geopolymer-modified nanomaterials research. Furthermore, previous conventional evaluations were incapable of producing visualizations of science maps. Figure 4(A) displays a network visualization of the journals that have been published.

The impact of the journal on the number of documents in the present research topic is reflected in the size of the node; a larger node indicates a greater impact. For instance, *Construction and Building Materials* have a bigger node size than the other categories, meaning they are a highly important source in the study. The artwork consists of five distinct clusters, each depicted using a unique color, namely red, green, blue, yellow, and purple. Groups are established according to the scope of the study sources or the frequency with which the sources are co-cited within similar works (Wuni et al., 2020). The number of connections among the research sources indicates the quantity of publications within the present study domain that feature co-citations.

Furthermore, the measure of connection strength provides insight into the frequency with which two journals are referenced in the same scholarly publication. For example, Construction and building materials had the most references compared to other studies (total link strength: 496). The relationships among the nodes in a cluster that are situated close together are more powerful compared to those that are farther apart. For instance, *Construction and Building Materials* are directly linked to case research studies on building materials compared to others. Different colors in Figure 4(B) represent different densities found in a journal. The largest concentration is red, followed by yellow, green, and blue.

The red hue of *Construction and Building Materials* represents the greater significance of the current study. Some journals related to the topic, such as the *International Journal of Geopolymer & Green Chemistry*, *Journal of Nano Research and Applications*, and *International Journal of Nanotechnology and Applications*, are worth mentioning. However, these journals are not in the Scopus database, so they are not captured in this research.

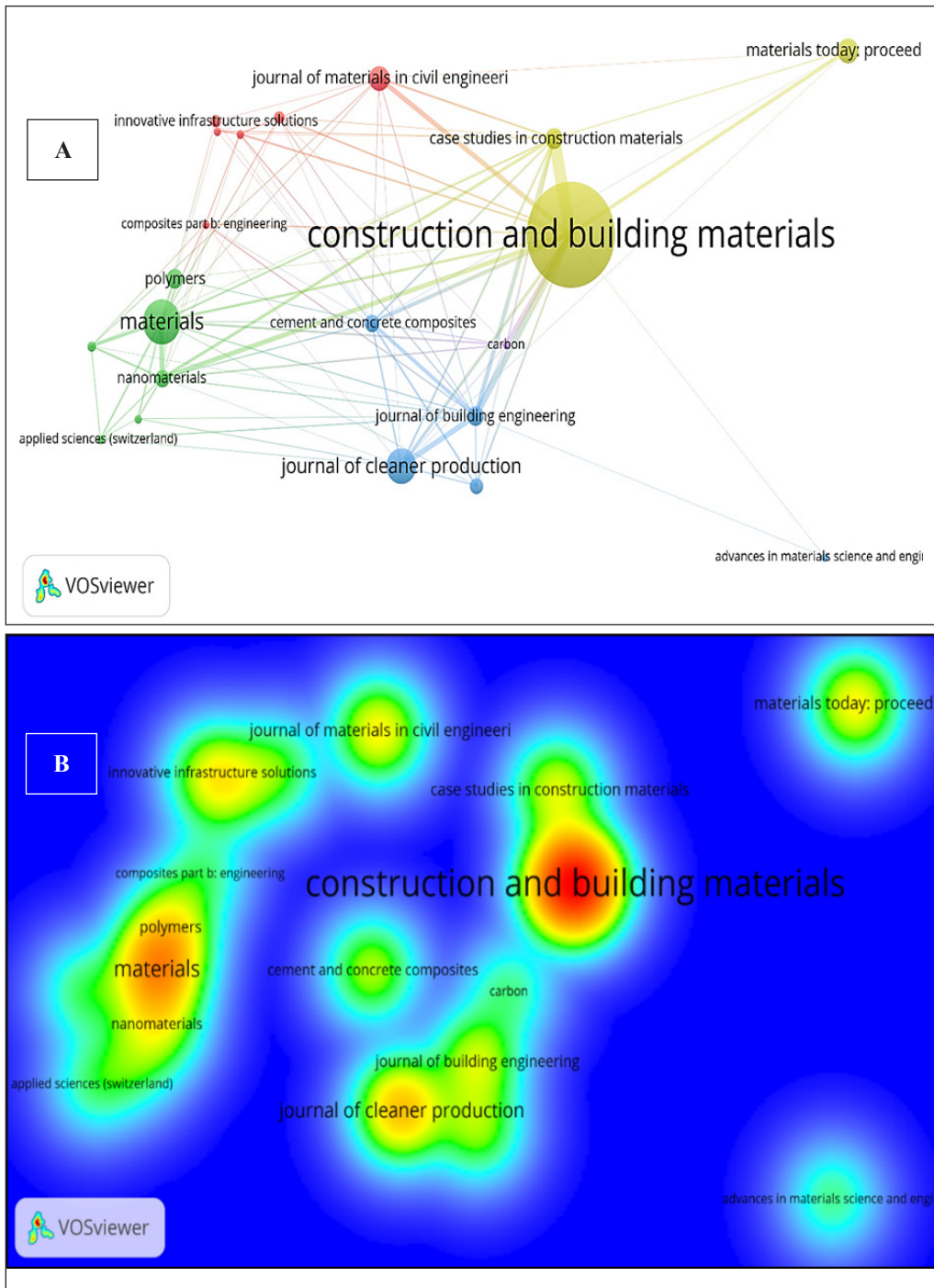


Figure 4. Science mapping of publication sources: (A) Network visualization; and (B) Density visualization

Science Mapping of Co-occurrence Keywords

Keywords have an essential function in academic study as they help to differentiate and demonstrate the fundamental topic of the studied area (Su & Lee, 2010). In the assessment, the data analysis type chosen was "co-occurrence," and the unit of analysis was specified as "all keywords." The minimum threshold for keyword repetition was maintained at 10, preserving 125 out of the total 5216 keywords. Table 3 displays the predominant keywords observed in geopolymer research modified with nanomaterials. Nanomaterials, geopolymers, and inorganic polymers are the top three most occurring keywords, with 59, 41, and 41 occurrences, respectively.

Table 3
The most frequent keywords in the research area

No.	Keywords	Occurrences	Total link strength
1	Nanomaterial	59	355
2	Geopolymers	41	365
3	Inorganic polymers	41	365
4	Nanoparticles	41	198
5	Geopolymer	36	299
6	Nanocomposites	35	186
7	Sustainable development	27	186
8	Nano silica	26	243
9	Nanomaterials	26	163
10	Titanium dioxide	25	156

Figure 5 (A) illustrates the visual representation of the main keywords within the research areas. The network visualization identifies four clusters: red, green, blue, and yellow. Moreover, the scientific visualization presented in the study reveals that the aforementioned keywords display larger nodes when compared to the other keywords. This observation indicates the importance of these keywords in the research area. In Figure 5(B), the varying colors indicate the dense concentration of keywords. The colors red, yellow, green, and blue are organized in ascending order based on their respective densities, with red having the highest density and blue having the lowest density.

The red zones, which include nanomaterial, geopolymer, "inorganic polymer, and nanoparticles, indicate areas of increased research activity, reflecting a substantial emphasis on nanomaterial and geopolymer collectively. Simultaneously, yellow zones that include terms like graphene oxides, composite materials, and sustainability represent emerging topics with moderate research activity that necessitate further exploration, particularly concerning their combined effects on mechanical and microstructural performance. The outer green and blue zones, which include composite material, nanotechnology, and polymer, represent underrepresented but important areas in

composite material and nanotechnology, highlighting opportunities to merge geopolymer research with polymer goals.

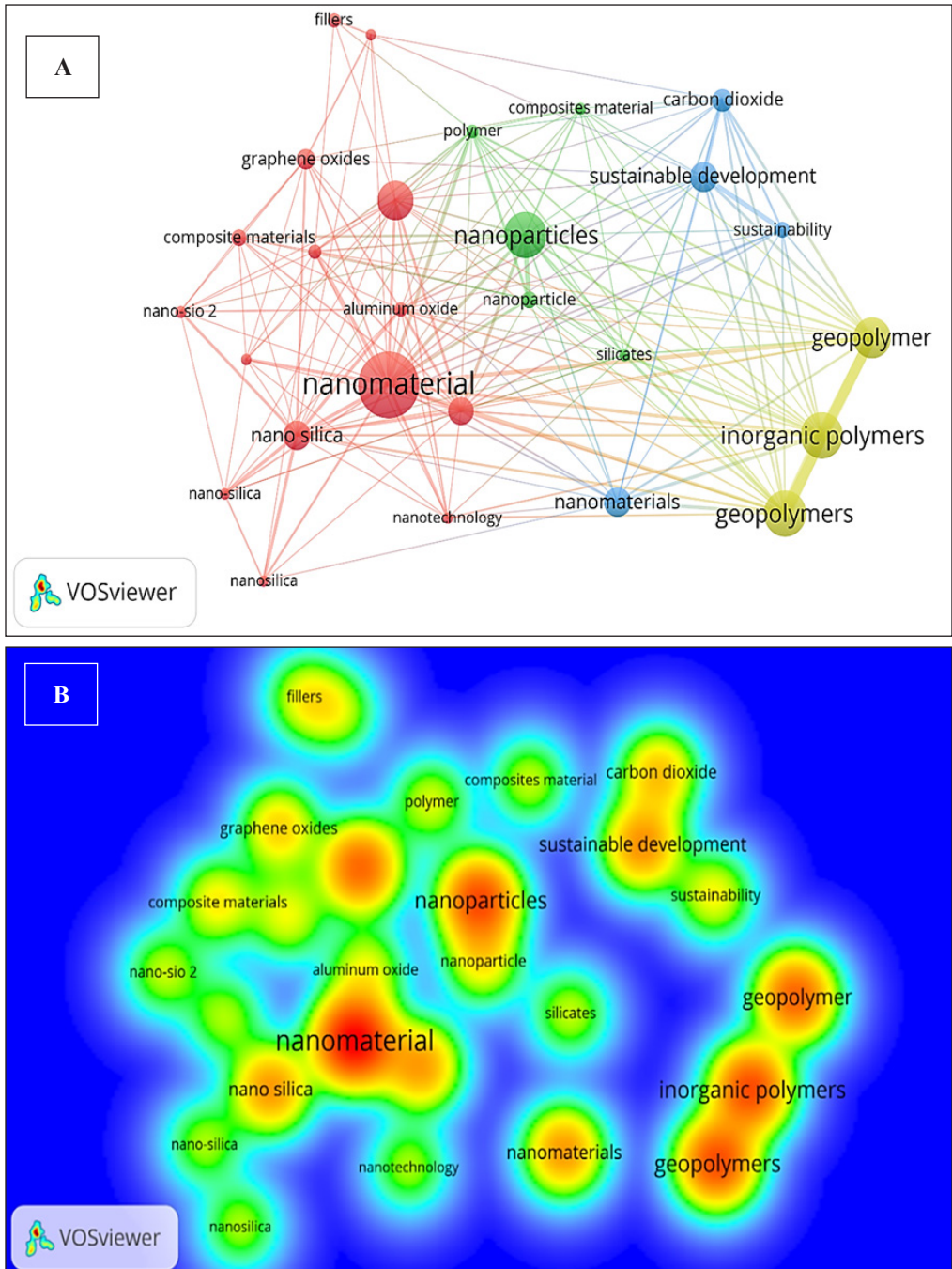


Figure 5. Science mapping of frequent keywords: (A) Network visualization; and (B) Density visualization

High-density topics such as nanomaterials, nanoparticles, and geopolymers suggest the need for deeper exploration into optimizing their properties and scalability for industrial applications. Medium-density areas, including sustainable development, carbon dioxide, and graphene oxides, point toward opportunities for interdisciplinary research on integrating nanomaterials with sustainable practices to address environmental challenges like carbon emissions. Low-density topics, such as fillers, silicates, and composite materials, represent emerging fields that could benefit from novel approaches to improve the performance and adaptability of geopolymers. Future research should focus on bridging these gaps, enhancing the synergy between sustainability and material science, and expanding the practical applications of nanomaterials in geopolymers for infrastructure, energy, and environmental solutions.

Science Mapping of Top-cited Articles

The total number of citations obtained by a document reflects its significance in the field of research. The evaluation of papers involved selecting "bibliographic coupling" as a method of analysis and "documents" as the investigation unit. Table 4 presents a compilation of the 10 most highly cited publications in the field of geopolymer modified with nanomaterials, encompassing the authors' names and relevant citation details. Liu et al. (2020) received 159 citations for their article "Review on the research progress of cement-based and geopolymer materials modified by graphene and graphene oxide" (Mohajerani et al., 2019), and Korayem et al. (2017) received 134 and 123 citations, respectively, selecting them among the top three most cited works.

Liu et al. (2020) addressed a substantial knowledge deficiency by integrating cementitious and geopolymer systems developments. The article's broad scope, relevance, and ability to connect emerging nanotechnology with sustainable materials research made it particularly impactful at a time of growing interest in advanced material science. This is measured by the high citation index of 159. Other papers are less impactful because the discussion is on the specified research output, lacks a comprehensive synthesis, and is not in an interdisciplinary area, with a smaller scope. Hence, the citation index is lower.

Liu et al. (2020) provide an innovative overview of graphene-based nanomaterials, including graphene and graphene oxide, for improving cement-based and geopolymer materials, emphasizing notable progress in mechanical strength, durability, thermal stability, and microstructure. Their research addressed a substantial knowledge deficiency by integrating developments in cementitious and geopolymer systems, emphasizing graphene-based materials' revolutionary capabilities for sustainable, high-performance construction applications. The article's broad scope, relevance, and ability to connect emerging nanotechnology with sustainable materials research made it particularly impactful at a time of growing interest in advanced material science.

Table 4
The most cited articles in the research area

No.	Article	Title	Citations
1	Liu et al., 2020	Review of the research progress of cement-based and geopolymer materials modified by graphene and graphene oxide	159
2	Mohajerani et al., 2019	Nanoparticles in construction materials and other applications, and implications of nanoparticle use	134
3	Korayem et al., 2017	A review of dispersion of nanoparticles in cementitious matrices: A Nanoparticle geometry perspective	123
4	Khater & Abd El Gawaad, 2016	Characterization of alkali-activated geopolymer mortar doped with MWCNT	122
5	Vishwakarma & Ramachandran, 2018	Green Concrete mix using solid waste and nanoparticles as alternatives. A review	112
6	Shah et al., 2015	Nano-modification of cementitious material: Toward a stronger and durable concrete	109
7	Faried et al., 2021	Mechanical and durability properties of ultra-high-performance concrete incorporated with various nano-waste materials under different curing conditions	108
8	Ebrahimi et al., 2018	A review of the impact of micro- and nanoparticles on freeze-thaw durability of hardened concrete: Mechanism perspective	98
9	Hajimohammadi et al., 2011	Time-resolved and spatially resolved infrared spectroscopic observation of seeded nucleation controlling geopolymer gel formation	94
10	Ahmed et al., 2022	The role of nanomaterials in geopolymer concrete composites: A state-of-the-art review	74

In contrast, other highly cited works like Mohajerani et al. (2019) and Korayem et al. (2017), although valuable, concentrated on more specialized subjects, such as the environmental implications of waste materials or particular impacts of nanomaterials on cementitious systems, lacking the comprehensive synthesis, interdisciplinary insights, or prospective analysis that Liu et al. provided. The context of the influence of this article is the transformative potential of nanomaterials in the construction and building industry, focusing on enhancing the performance of cement-based and geopolymer materials. The research by Liu et al. (2020) and Mohajerani et al. (2019) emphasizes the innovative application of materials like graphene and graphene oxide (GO) to address critical challenges in structural engineering, such as improving mechanical properties like (tensile and compressive strength), durability, and resistance to environmental stresses like freeze-thaw cycles and cracking. The important gap that the research found includes unresolved challenges such as variability in optimal content and gaps in the microstructural understanding of these materials.

Figure 6(A) demonstrates the map of related works according to citations and the relative importance of these articles in the current subject of study. The investigation showed that 359 papers were connected through citations. In addition, the density mapping depicted in Figure 6(B) illustrates a heightened concentration of articles among the top-ranked ones.

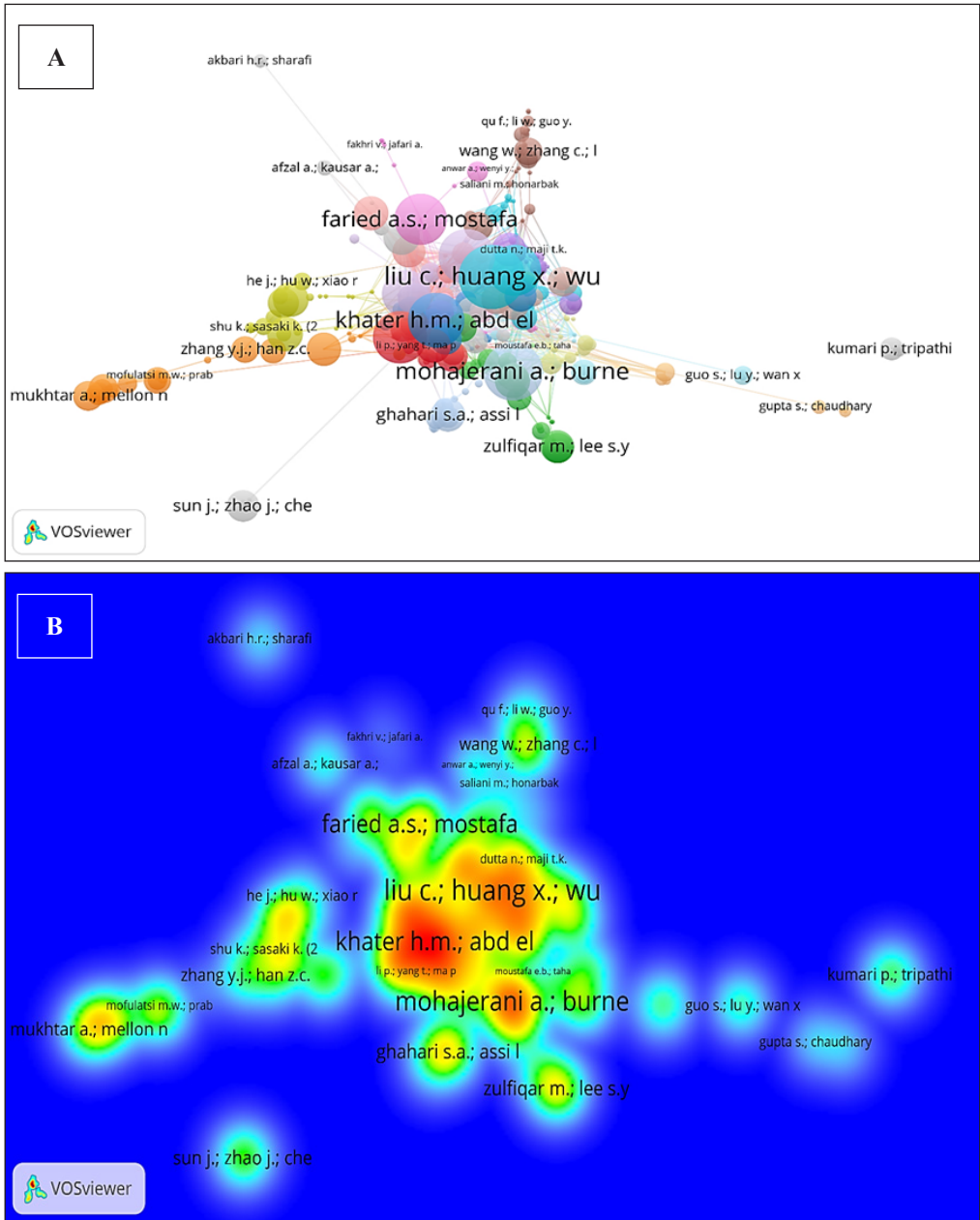


Figure 6. Science mapping of cited articles: (A) Network visualization; (B) Density visualization

Science Mapping of Country Contributions

Certain states have exhibited higher involvement and ongoing contributions in geopolymers modified with nanomaterials than others. The network was visualized to provide readers with a visual representation of the regions dedicated to the research domain. “Bibliographic coupling” was adopted as the “method of analysis”, and “countries” as the “unit of analysis”. The minimum number of documents restricted for a country was 5, and 32 of the 75 nations met the criteria.

The countries enumerated in Table 5 have produced at least ten publications on the present study subject. China, India, and the United States provided the most documents, with 164, 89, and 59, respectively. Moreover, the countries that received the most citations were China, the United States, and Australia, which received 4024, 2942, and 1319, respectively. The number of publications, references, and total link strength indicate the degree of influence each nation has had on the evolution of the subject area. Figure 7(A) depicts the science mapping visualization of nations joined through citations. The node size relates to the nation's contribution to the area of research. Four clusters of countries were found on the visualization network, each with its color. As shown in Figure 7(B), the countries with the highest level of participation possessed a larger density. The geographical trends highlight the significant influence of major hubs such as China, India, and the United States in promoting geopolymer research involving nanomaterials, facilitated by robust global and regional collaborations.

The four colors denote clusters of countries participating in regular collaboration within the study topic, with each hue indicating a unique group based on co-occurrence or similarity. The blue cluster, led by China, shows significant regional cooperation with nations including Saudi Arabia, Iraq, and Egypt. This indicates common interests in geopolymer concrete enhanced with nanomaterials in rapidly developing regions. China is a critical

Table 5
The top ten documents in the research area

No.	Country	Documents	Citations	Total link strength
1	China	164	4024	18336
2	India	89	683	5343
3	United States	59	2942	8511
4	Saudi Arabia	51	1097	17247
5	Malaysia	43	872	7242
6	Iran	38	1072	4860
7	Australia	35	1319	6967
8	Egypt	32	424	6645
9	Iraq	24	681	10365
10	Pakistan	23	280	5652

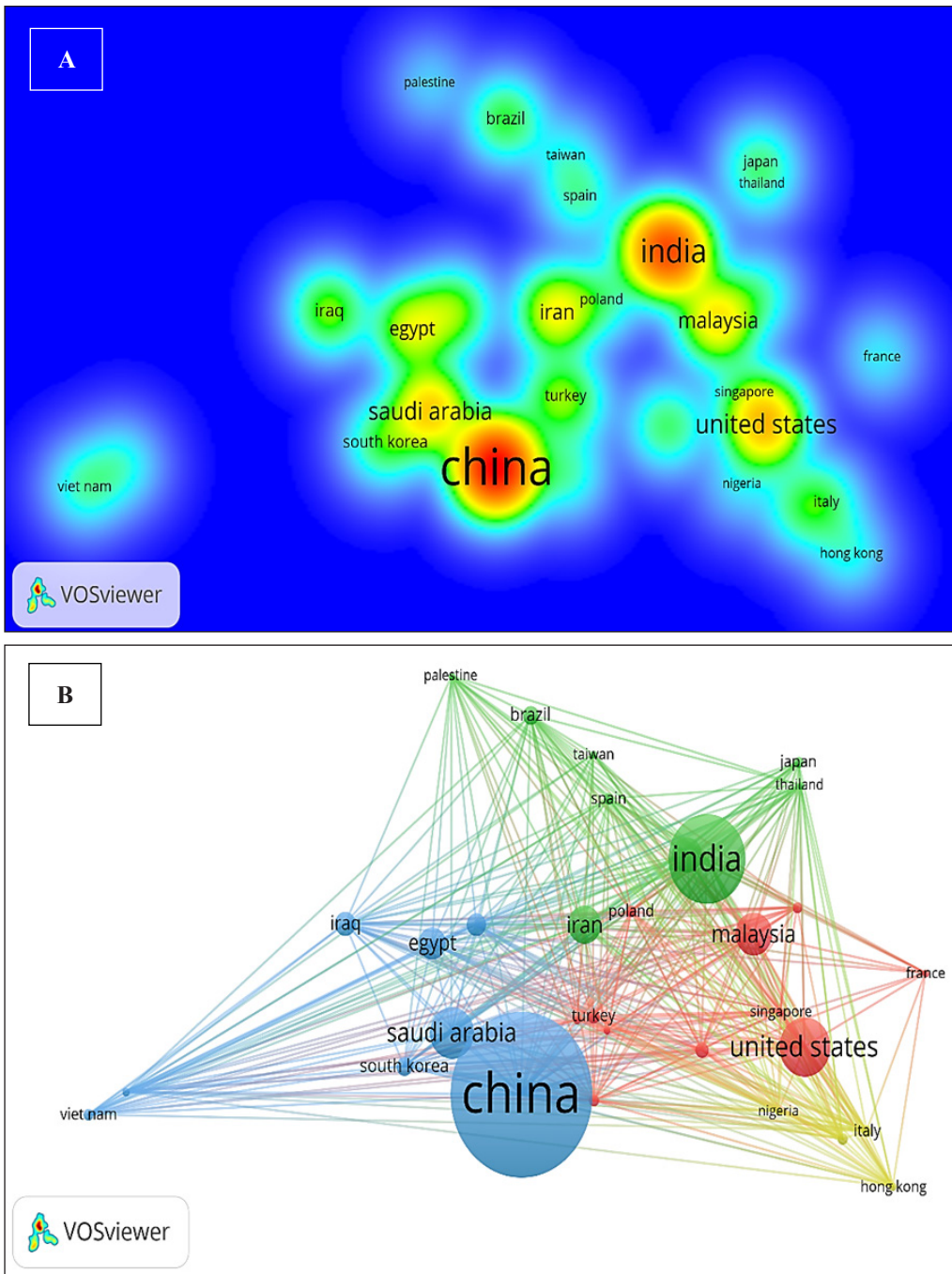


Figure 7. Science mapping of countries' contributions: (A) Network visualization; (B) Density visualization

hub, linking this group with multiple clusters via significant international collaborations. The green cluster, led by India, displays collaboration among developing countries such as Brazil and Iran, while also connecting with bigger hubs that incorporate international innovations. In contrast, based in the United States, the red cluster demonstrates advanced collaborations with countries such as Malaysia and Singapore, highlighting the importance of innovative nanomaterial uses and commercialization.

This cluster acts as a crucial link to the green and yellow clusters, facilitating information and technology transfer. The yellow cluster, which includes countries like Italy and Hong Kong, reflects smaller-scale contributions. While these countries play a less prominent role, they maintain connections with larger clusters, facilitating the exchange of innovative techniques and specialized knowledge. The connections between clusters, depicted by lines in the graphic, indicate the level of collaboration; larger lines imply stronger partnerships. The linkage among clusters illustrates a balanced global network, wherein regional centers such as China and India are crucial in linking developing academic fields with advanced technological centers like the United States, thus creating a collaborative environment for advancing geopolymer concrete incorporating nanomaterials.

The trends highlight the necessity of inclusive policies, investments in developing regions, and knowledge-sharing to enhance global advancements in geopolymer-nanomaterial innovations. The visual representation and data documentation of all the countries involved will facilitate young scientists in establishing scientific relationships, initiating collaborative initiatives, and sharing innovative methodologies and ideas. Academic researchers hailing from different countries with a vested interest in advancing the study of geopolymer modified with nanomaterials have the opportunity to engage in fruitful collaborations with established experts in this domain, thereby gaining valuable insights and benefiting from their extensive knowledge and experience.

DISCUSSIONS

The scientometric review conducted a comprehensive statistical evaluation and mapping of the available bibliographic data about research on geopolymers modified with nanomaterials. Prior literature reviews have demonstrated limitations in their ability to comprehensively and accurately establish connections between various research domains. Hence, the VOS viewer presents the connections within various domains.

The output of the present study has discovered the top sources of publications, such as the *Construction and Building Materials Journal*, which has produced 59 documents. The frequently utilized keywords are nanomaterial, geopolymers and inorganic polymers. Furthermore, this analysis also includes the top-cited article, Liu et al. (2020), which received 159 citations. The most important countries in this work are China, India, and the United States. The statistics and visualizations of the contributing countries will help

young researchers form scientific partnerships, start collaborative businesses, and share novel concepts and methods to achieve knowledge.

1. A comprehensive assessment of scholarly journals, encompassing studies on incorporating nanoparticles in geopolymers, has indicated that *Construction and Building Materials*, *Materials*, and *Journal of Cleaner Production* are the leading publication journals, including 59, 25, and 20 publications, respectively. *Construction and Building Materials*, *Journal of Cleaner Production*, and *Materials* have been identified as the top three in total citations, with citation counts of 1918, 671, and 490, respectively.
2. The analysis of keywords within the study field indicates that the most frequently used keywords are nanomaterials, geopolymers, and inorganic polymers, with 59, 41, and 41 occurrences, respectively. The keyword evaluation discovered that nanomaterials have mostly been studied for developing environmentally friendly building materials and enhancing the properties of geopolymer compounds.
3. The top-cited article is Liu et al. (2020), which received 159 citations. Mohajerani et al. (2019) and Korayem et al. (2017) received 134 and 123 citations, respectively, making them among the top three most cited works.
4. The investigation of the countries' contributions found that China, India, and the United States displayed the most papers, with 164, 89, and 59 papers, respectively. Moreover, the countries that received the most citations were China, the United States, and Australia, which received 4024, 2942, and 1319, respectively.

LIMITATION

This work provides a scientometric evaluation of nanomaterials in geopolymer, utilizing visualization of similarity software in the VOS viewer for analysis. A bibliometric network is constructed and illustrated to examine the annual distribution and growth trends, sources, keywords, leading articles, and prominent countries related to geopolymer modified with nanomaterials, based on the search terms "geopolymer" and "nanomaterial" in the Scopus database. The network yielded 529 documents from 2008 to October 2023.

The quality of VOS viewer outcomes is significantly influenced by the dataset employed. Incomplete or biased data, such as that derived from a singular database like Scopus, can result in misleading outcomes.

VOS viewer cannot evaluate the quality of research papers, as it depends only on bibliometric data like citation counts, which do not reflect the significance of a study. While self-citation may affect individual citation measurements, its overall effect on VOS viewer analyses is relatively minimal. Studies have shown that the median self-citation rate is usually below 15% across areas, resulting in just a tiny percentage of total citations (Frontiers in Research Metrics and Analytics, 2023; IJHS, 2023).

The VOS viewer does not analyze the research content, focusing only on bibliometric relationships such as citations, Authors, keywords and countries. This may limit detailed insights; hence, a traditional review should be made. Despite these limitations, the VOS viewer remains a powerful tool for visualizing bibliometric networks, relationships, and collaborations, provided its outputs are interpreted alongside other complementary analyses.

The findings based on reading showed that the utilization of nanomaterials in geopolymer composites shows considerable promise due to their ability to substantially enhance the mechanical properties of the materials with only a small quantity of nanoparticles. Further investigation is necessary to ascertain the exact number of nanocomposites in the geopolymer composite mixture. Additional research is required to investigate the impact of nanomaterials on both human health and the environment (Tortella et al., 2020).

Furthermore, conducting a comprehensive investigation into the mathematical modelling or artificial intelligence of nanomaterial-based geopolymer behavior is still possible. Because of the high cost of nanomaterials (Grieger et al., 2012) and the alkaline activator of geopolymers, there are further obstacles to their widespread use in the building industry (Mendes et al., 2021). Moreover, incorporating sufficient nanomaterials into geopolymers has enhanced their performance, decreased porosity, and enhanced mechanical qualities. Therefore, proper selection of the nanoparticle dosage is very important to attain optimal mechanical properties in the geopolymer composite (Dylla & Hassan, 2012). For example, when a greater quantity or proportion of nanoparticles is incorporated into the concrete mixture, a reduction in mechanical strength can be noticed due to the conglomeration of the nanoparticles with other components.

CONCLUSION AND FUTURE PERSPECTIVES

The current research paper conducts a scientometric review of the existing literature on geopolymers modified with nanomaterials to evaluate the annual distribution and growth pattern, prominent sources, frequent keywords, top articles, and leading countries on geopolymers modified with nanomaterials where the previous literature reviews have shown shortcomings in their ability to extensively and completely establish connections among different research domains. A search was conducted in the Scopus database using the VOS viewer, resulting in the finding of 529 publications that were relevant to the research topic.

The searched keywords, geopolymer and nanomaterial, resulted in 914 documents from 2008 to 2023, while the *Construction and Building Materials* journal was the highest publication source with 59 research papers and 1918 citations. Nanomaterials, geopolymers, and inorganic polymers are the top three most occurring keywords, with 59, 41, and 41 occurrences, respectively. Liu et al. (2020) received 159 citations for their article “Review on the research progress of cement-based and geopolymer materials modified by graphene

and graphene oxide China, India, and the United States provided the biggest number of documents, with 164, 89, and 59 documents, respectively.

Based on this VOS review, the reader could visualize the overall picture of the bibliographic data on geopolymers modified with nanomaterials. The scientometric analysis will aid researchers to identify important keywords, the highest-cited paper and key researchers in this area. Countries that contribute to the research are also identified. Based on these outputs, the future direction of research collaboration shall explore other continents, such as Africa, to enhance cooperative research, exchange ideas and expertise, and create joint ventures in research. The study reveals underrepresented areas, notably in Africa and smaller states, that require targeted research funding and collaboration to increase participation. Additionally, unexamined subfields encompass the environmental sustainability of nanomaterial-based geopolymers and their extensive industrial uses.

Future research based on the output of conventional research and application will find that the elevated expense of nanomaterials and alkaline activators presents a considerable obstacle to their extensive application in the construction sector. Practical obstacles, like the expansion of production and the assurance of cost-effectiveness, remain unaddressed. Connecting laboratory research with practical applications is crucial to address these problems and facilitate real-world implementation. By addressing these constraints, bridging data deficiencies, and surmounting practical obstacles, the next research can realize the complete potential of nanomaterial-modified geopolymers for sustainable and economical construction solutions.

ACKNOWLEDGEMENT

The authors express gratitude for the financial support for this research by the Ministry of Education, Malaysia, under the Fundamental Research Grant Scheme (FRGS/1/2020/TKO/UPM/02/32) with Vote no: 5540372 for research work entitled 'An investigation of characterization and parametric effect of kenaf bast fiber in the properties of geopolymer kenaf reinforced concrete.'

REFERENCES

- Adesina, A. (2020). Recent advances in the concrete industry to reduce its carbon dioxide emissions. *Environmental Challenges*, 1, Article 100004. <https://doi.org/10.1016/j.envc.2020.100004>
- Ahmed, H. U., Mohammed, A. A., & Mohammed, A. S. (2022). The role of nanomaterials in geopolymer concrete composites: A state-of-the-art review. *Journal of Building Engineering*, 49, Article 104062. <https://doi.org/10.1016/j.job.2022.104062>
- Al-Baldawi, M. F., Aziz, F. N. A. A., Abbas, A. G. N., Nasir, N. A. M., & Sutan, N. M. (2024). Performance of hybrid fiber reinforced geopolymer composites: Scientometric and conventional review. *Pertanika Journal of Science and Technology*, 32(S5), 41–73. <https://doi.org/10.47836/pjst.32.S5.03>

- Alomayri, T. (2019). Experimental study of the microstructural and mechanical properties of geopolymer paste with nano material (Al₂O₃). *Journal of Building Engineering*, 25, Article 100788. <https://doi.org/10.1016/j.jobe.2019.100788>
- Assaedi, H. S., & D. Olawale, M. (2022). Impact of nano-alumina on the mechanical characterization of PVA fibre-reinforced geopolymer composites. *Journal of Taibah University for Science*, 16(1), 828–835. <https://doi.org/10.1080/16583655.2022.2119735>
- Chadegani, A. A., Salehi, H., Yunus, M. M. M., Farhadi, H., Fooladi, M., Farhadi, M., & Ebrahim, N. A. (2013). A comparison between two main academic literature collections: Web of science and scopus databases. *Asian Social Science*, 9(5), 18–26. <https://doi.org/10.5539/ass.v9n5p18>
- Çevik, A., Alzebaree, R., Humur, G., Niş, A., & Gülşan, M. E. (2018). Effect of nano-silica on the chemical durability and mechanical performance of fly ash based geopolymer concrete. *Ceramics International*, 44(11), 12253–12264. <https://doi.org/10.1016/j.ceramint.2018.04.009>
- Chen, Y., Lin, M., & Zhuang, D. (2022). Wastewater treatment and emerging contaminants: Bibliometric analysis. *Chemosphere*, 297, Article 133932. <https://doi.org/10.1016/j.chemosphere.2022.133932>
- Davidovits, J. (1979). Geopolymers of the first generation. *Society*, 1, 49–67.
- Davidovits, J. (1991). Geopolymers - Inorganic polymeric new materials. *Journal of Thermal Analysis*, 37(8), 1633–1656. <https://doi.org/10.1007/BF01912193>
- Duxson, P., Provis, J. L., Lukey, G. C., & van Deventer, J. S. J. (2007). The role of inorganic polymer technology in the development of “green concrete.” *Cement and Concrete Research*, 37(12), 1590–1597. <https://doi.org/10.1016/j.cemconres.2007.08.018>
- Ebrahimi, K., Daiezadeh, M. J., Zakertabrizi, M., Zahmatkesh, F., & Korayem, A. H. (2018). A review of the impact of micro- and nanoparticles on freeze-thaw durability of hardened concrete: Mechanism perspective. *Construction and Building Materials*, 186, 1105–1113. <https://doi.org/10.1016/j.conbuildmat.2018.08.029>
- Elie, K., Valeria, A., Daniele, N., Davide, S., Isabella, L., Alberto, M., & Cristina, L. (2021). Dependence of the geopolymerization process and end-products to the nature of solid precursors: Challenge of the sustainability. *Journal of Cleaner Production*, 278, Article 123587. <https://doi.org/10.1016/j.jclepro.2020.123587>
- Elmesalami, N., & Celik, K. (2022). A critical review of engineered geopolymer composite: A low-carbon ultra-high-performance concrete. *Construction and Building Materials*, 346, Article 128491. <https://doi.org/10.1016/j.conbuildmat.2022.128491>
- Faried, A. S., Mostafa, S. A., Tayeh, B. A., & Tawfik, T. A. (2021). Mechanical and durability properties of ultra-high performance concrete incorporated with various nano waste materials under different curing conditions. *Journal of Building Engineering*, 43, Article 102569. <https://doi.org/10.1016/j.jobe.2021.102569>
- Firas, A. B. M., Aziz, F. N. A. A., Abbas, A. G. N., Nasir, N. A. M., & Safiee, N. A. (2024). Thermal performance of natural fiber-reinforced geopolymer concrete. In N. Sabtu (Ed.) *Lecture Notes in Civil Engineering* (Vol. 385, pp. 151–162). Springer Nature Singapore. https://doi.org/10.1007/978-981-99-6018-7_11

- Grieger, K. D., Laurent, A., Miseljic, M., Christensen, F., Baun, A., & Olsen, S. I. (2012). Analysis of current research addressing complementary use of life-cycle assessment and risk assessment for engineered nanomaterials: Have lessons been learned from previous experience with chemicals? *Journal of Nanoparticle Research*, 14(7), Article 958. <https://doi.org/10.1007/s11051-012-0958-6>
- Hajimohammadi, A., Provis, J. L., & van Deventer, J. S. J. (2011). Time-resolved and spatially-resolved infrared spectroscopic observation of seeded nucleation controlling geopolymer gel formation. *Journal of Colloid and Interface Science*, 357(2), 384–392. <https://doi.org/10.1016/j.jcis.2011.02.045>
- Hosseini, M. R., Martek, I., Zavadskas, E. K., Aibinu, A. A., Arashpour, M., & Chileshe, N. (2018). Critical evaluation of off-site construction research: A Scientometric analysis. *Automation in Construction*, 87, 235–247. <https://doi.org/10.1016/j.autcon.2017.12.002>
- Ji, Z., & Pei, Y. (2019). Bibliographic and visualized analysis of geopolymer research and its application in heavy metal immobilization: A review. *Journal of Environmental Management*, 231, 256–267. <https://doi.org/10.1016/j.jenvman.2018.10.041>
- Jagadesh, P., & Nagarajan, V. (2022). Effect of nano titanium di oxide on mechanical properties of fly ash and ground granulated blast furnace slag based geopolymer concrete. *Journal of Building Engineering*, 61, Article 105235. <https://doi.org/10.1016/j.jobe.2022.105235>
- Jindal, B. B., & Sharma, R. (2020). The effect of nanomaterials on properties of geopolymers derived from industrial by-products: A state-of-the-art review. *Construction and Building Materials*, 252, Article 119028. <https://doi.org/10.1016/j.conbuildmat.2020.119028>
- Khan, K., Ahmad, W., Amin, M. N., & Nazar, S. (2022). A scientometric-analysis-based review of the research development on geopolymers. *Polymers*, 14(17), Article 3676. <https://doi.org/10.3390/polym14173676>
- Khater, H. M., & El-Gawaad, H. A. A. (2016). Characterization of alkali activated geopolymer mortar doped with MWCNT. *Construction and Building Materials*, 102, 329–337. <https://doi.org/10.1016/j.conbuildmat.2015.10.121>
- Kheimi, M., Aziz, I. H., Abdullah, M. M. A. B., Almadani, M., & Razak, R. A. (2022). Waste material via geopolymerization for heavy-duty application: A review. *Materials*, 15(9), Article 3205. <https://doi.org/10.3390/ma15093205>
- Korayem, A. H., Tourani, N., Zakertabrizi, M., Sabziparvar, A. M., & Duan, W. H. (2017). A review of dispersion of nanoparticles in cementitious matrices: Nanoparticle geometry perspective. *Construction and Building Materials*, 153, 346–357. <https://doi.org/10.1016/j.conbuildmat.2017.06.164>
- Li, J., Si, J., Luo, F., Zuo, C., Zhang, P., Sun, Y., Li, W., & Miao, S. (2022). Self-compensating geopolymer utilizing nano-clay and chopped basalt fibers. *Construction and Building Materials*, 357, Article 129302. <https://doi.org/10.1016/j.conbuildmat.2022.129302>
- Liu, C., Huang, X., Wu, Y. Y., Deng, X., Liu, J., Zheng, Z., & Hui, D. (2020). Review on the research progress of cement-based and geopolymer materials modified by graphene and graphene oxide. *Nanotechnology Reviews*, 9(1), 155–169. <https://doi.org/10.1515/ntrev-2020-0014>
- Liu, W., Huang, M., & Wang, H. (2021). Same journal but different numbers of published records indexed in Scopus and Web of Science Core Collection: causes, consequences, and solutions. *Scientometrics*, 126(5), 4541–4550. <https://doi.org/10.1007/s11192-021-03934-x>

- Martins, J., Gonçalves, R., & Branco, F. (2024). A bibliometric analysis and visualization of e-learning adoption using VOSviewer. *Universal Access in the Information Society*, 23(3), 1177–1191. <https://doi.org/10.1007/s10209-022-00953-0>
- Matsimbe, J., Dinka, M., Olukanni, D., & Musonda, I. (2022). Geopolymer: A systematic review of methodologies. *Materials*, 15(19), Article 6852. <https://doi.org/10.3390/ma15196852>
- Matsimbe, J., Dinka, M., Olukanni, D., & Musonda, I. (2023). Bibliometric trends of geopolymer research in Sub-Saharan Africa. *Materials Today Communications*, 35, Article 106082. <https://doi.org/10.1016/j.mtcomm.2023.106082>
- McLellan, B. C., Williams, R. P., Lay, J., Van Riessen, A., & Corder, G. D. (2011). Costs and carbon emissions for geopolymer pastes in comparison to ordinary portland cement. *Journal of Cleaner Production*, 19(9–10), 1080–1090. <https://doi.org/10.1016/j.jclepro.2011.02.010>
- Meho, L. I. (2019). Using Scopus's CiteScore for assessing the quality of computer science conferences. *Journal of Informetrics*, 13(1), 419–433. <https://doi.org/10.1016/j.joi.2019.02.006>
- Mendes, B. C., Pedroti, L. G., Vieira, C. M. F., Marvila, M., Azevedo, A. R. G., Carvalho, J. M. F. D., & Ribeiro, J. C. L. (2021). Application of eco-friendly alternative activators in alkali-activated materials: A review. *Journal of Building Engineering*, 35, Article 102010. <https://doi.org/10.1016/j.jobe.2020.102010>
- Mohajerani, A., Burnett, L., Smith, J. V., Kurmus, H., Milas, J., Arulrajah, A., Horpibulsuk, S., & Kadir, A. A. (2019). Nanoparticles in construction materials and other applications, and implications of nanoparticle use. *Materials*, 12(19), Article 3052. <https://doi.org/10.3390/ma12193052>
- Mongeon, P., & Paul-Hus, A. (2016). The journal coverage of Web of Science and Scopus: A comparative analysis. *Scientometrics*, 106(1), 213–228. <https://doi.org/10.1007/s11192-015-1765-5>
- Mostafa, S. A., Faried, A. S., Farghali, A. A., El-Deeb, M. M., Tawfik, T. A., Majer, S., & Elrahman, M. A. (2020). Influence of nanoparticles from waste materials on mechanical properties, durability and microstructure of UHPC. *Materials*, 13(20), Article 4530. <https://doi.org/10.3390/ma13204530>
- Pranckutė, R. (2021). Web of Science (WoS) and Scopus: The titans of bibliographic information in today's academic world. *Publications*, 9(1), Article 12. <https://doi.org/10.3390/publications9010012>
- Raj, R. S., Arulraj, G. P., Anand, N., Kanagaraj, B., Lubloy, E., & Naser, M. Z. (2023). Nanomaterials in geopolymer composites: A review. *Developments in the Built Environment*, 13, Article 100114. <https://doi.org/10.1016/j.dibe.2022.100114>
- Shah, S. P., Hou, P., & Konsta-Gdoutos, M. S. (2015). Nano-modification of cementitious material: Toward a stronger and durable concrete. *Journal of Sustainable Cement-Based Materials*, 5(1), 1–22. <https://doi.org/10.1080/21650373.2015.1086286>
- Shahmansouri, A. A., Bengar, H. A., & Ghanbari, S. (2020). Compressive strength prediction of eco-efficient GGBS-based geopolymer concrete using GEP method. *Journal of Building Engineering*, 31, Article 101326. <https://doi.org/10.1016/j.jobe.2020.101326>
- Shehata, N., Mohamed, O. A., Sayed, E. T., Abdelkareem, M. A., & Olabi, A. G. (2022). Geopolymer concrete as green building materials: Recent applications, sustainable development and circular economy potentials. *Science of the Total Environment*, 836, Article 155577. <https://doi.org/10.1016/j.scitotenv.2022.155577>

- Su, H. N., & Lee, P. C. (2010). Mapping knowledge structure by keyword co-occurrence: A first look at journal papers in technology foresight. *Scientometrics*, 85(1), 65–79. <https://doi.org/10.1007/s11192-010-0259-8>
- Teh, S. H., Wiedmann, T., Castel, A., & Burgh, J. D. (2017). Hybrid life cycle assessment of greenhouse gas emissions from cement, concrete and geopolymer concrete in Australia. *Journal of Cleaner Production*, 152, 312–320. <https://doi.org/10.1016/j.jclepro.2017.03.122>
- Tian, Q., Pan, Y., Bai, Y., Yao, S., & Sun, S. (2022). A bibliometric analysis of research progress and trends on fly ash-based geopolymer. *Materials*, 15(14), Article 4777. <https://doi.org/10.3390/ma15144777>
- Tortella, G. R., Rubilar, O., Durán, N., Diez, M. C., Martínez, M., Parada, J., & Seabra, A. B. (2020). Silver nanoparticles: Toxicity in model organisms as an overview of its hazard for human health and the environment. *Journal of Hazardous Materials*, 390, Article 121974. <https://doi.org/10.1016/j.jhazmat.2019.121974>
- Turner, L. K., & Collins, F. G. (2013). Carbon dioxide equivalent (CO₂-e) emissions: A comparison between geopolymer and OPC cement concrete. *Construction and Building Materials*, 43, 125–130. <https://doi.org/10.1016/j.conbuildmat.2013.01.023>
- Eck, N. J. V., & Waltman, L. (2021). *Manual de VOSviewer*. Univeristeit Leiden. http://www.vosviewer.com/documentation/Manual_VOSviewer_1.6.1.pdf
- Vishwakarma, V., & Ramachandran, D. (2018). Green concrete mix using solid waste and nanoparticles as alternatives – A review. *Construction and Building Materials*, 162, 96–103. <https://doi.org/10.1016/j.conbuildmat.2017.11.174>
- Visser, M., Eck, N. J. V., & Waltman, L. (2021). Large-scale comparison of bibliographic data sources: Scopus, web of science, dimensions, crossref, and microsoft academic. *Quantitative Science Studies*, 2(1), 20–41. https://doi.org/10.1162/qss_a_00112
- Wuni, I. Y., Shen, G. Q., & Osei-Kyei, R. (2020). Sustainability of off-site construction: A bibliometric review and visualized analysis of trending topics and themes. *Journal of Green Building*, 15(4), 131–154. <https://doi.org/10.3992/jgb.15.4.131>
- Zhao, X., Wang, H., Zhou, B., Gao, H., & Lin, Y. (2021). Resistance of soda residue–Fly ash based geopolymer mortar to acid and sulfate environments. *Materials*, 14(4), Article 785. <https://doi.org/10.3390/ma14040785>

Material Characterization and Electrical Performance of *Prosopis Africana* Conductive Ink for Antenna Applications

Suleiman Babani^{1,3}, Mohd Nizar Hamidon^{1*}, Alyani Ismail², Haslina Jaafar²,
Intan Helina Hasan¹, Farah Nabilah Shafiee¹, Ibrahim Garba Shitu¹,
Jamila Lamido³, Sani Halliru Lawan³ and Zainab Yunusa⁴

¹Institute of Nanoscience & Nanotechnology (ION2), Universiti Putra Malaysia, 43400 UPM Serdang, Selangor, Malaysia

²Faculty of Engineering, Universiti Putra Malaysia, 43400 UPM Serdang, Selangor, Malaysia

³Department of Electrical Engineering, Faculty of Engineering, Bayero University Kano, PMB 3011 Kano, Nigeria

⁴Department of Electrical Engineering, University of Hafr Al Batin City, 39524, Saudi Arabia

ABSTRACT

This research explores the development and evaluation of a bio-based conductive ink derived from *Prosopis Africana* Char (PAC) for antenna applications, aiming to provide a sustainable, cost-effective alternative to conventional conductive materials in electronics. The study focuses on the structural, thermal, and electrical properties of the PAC-based ink to determine its suitability for printed antenna technology. The conductive ink was formulated by mixing PAC powder with an organic binder composed of m-xylene, linseed oil, and α -terpineol in a 45:55 wt% ratio, followed by mechanical stirring at 250 rpm for 3 hours at 40 °C to achieve a homogeneous paste. This mixture

was screen-printed onto an FR4 substrate and thermally treated at 300 °C. Characterization techniques such as field emission scanning electron microscopy (FESEM), Raman spectroscopy, thermogravimetric analysis (TGA), and four-point probe conductivity measurements were used to analyze the ink's morphology, composition, and electrical behavior. The PAC ink demonstrated a high conductivity of 4.678 S/m, strong adhesion, and excellent printability and environmental stability under variable temperature and humidity. Antenna performance assessments revealed promising results, including a return loss of $|S_{11}| = -16.50$ dB, a resonant frequency of 9.5

ARTICLE INFO

Article history:

Received: 01 April 2024

Accepted: 10 April 2025

Published: 10 June 2025

DOI: <https://doi.org/10.47836/pjst.33.S4.02>

E-mail address:

sbabani.ele@buk.edu.ng (Suleiman Babani)

mnh@upm.edu.my (Mohd Nizar Hamidon)

alyani@upm.edu.my (Alyani Ismail)

jhaslina@upm.edu.my (Haslina Jaafar)

i_helina@upm.edu.my (Intan Helina Hassan)

farahnabilahshafiee@gmail.com (Farah Nabilah Shafiee)

ibrahimgarbashitu@gmail.com (Ibrahim Garba Shitu)

sumailajamila@gmail.com (Jamila Lamido)

shlawan.ele@buk.edu.ng (Sani Halliru Lawan)

zainaby@uhb.edu.sa (Zainab Yunusa)

*Corresponding author

GHz, a bandwidth of 1.32 GHz, a peak gain of 6.62 dB, a VSWR of 1.25, and an efficiency of 80%. These outcomes indicate that the PAC thick film enhances bandwidth and radiation efficiency due to its favorable dielectric characteristics. Overall, the study confirms the potential of *Prosopis africana* as a viable, eco-friendly conductive material for flexible, lightweight antennas, offering a promising direction for sustainable innovation in wireless communication technologies.

Keywords: Bandwidth, electrical conductivity, material analysis, micrometersized PAC powder, *Prosopis africana* conductive ink, sustainable patch antenna fabrication, thick film

INTRODUCTION

The conventional microstrip patch antenna (MPA) design consists of three main components: a radiating patch, a substrate, and a ground plane. Unlike traditional microwave antennas, microstrip patch antennas offer several advantages, such as being lightweight, flat profile, cost-effective, and easy to fabricate. However, choosing an MPA over traditional antennas requires careful consideration of some limitations, including low efficiency and narrow bandwidth (Bansal, 2008). Therefore, selecting the right substrate material is crucial in achieving optimal performance tailored to the specific requirements or application of the device. Microstrip antennas were first developed in the 1950s, and since then, there have been significant advancements in printed circuit board (PCB) technology, particularly in the 1970s. These antennas come in different shapes and sizes, but rectangular and circular patches are the most common due to their ease of design and suitability for array configurations (Garg et al., 2001). Patch antennas have traditionally been made using copper as the primary radiating material (Babani et al., 2015). However, producing copper can cause environmental pollution, and the oxidation that occurs after fabrication can lead to a decrease in the performance of the antenna (Ram et al., 2021). Therefore, finding an alternative material to replace copper in printed electronics remains a significant challenge.

Previous research has extensively examined the use of carbon-based materials, such as carbon nanotubes, graphene, carbon black, and graphite, as conductive patch elements. Some of the work has become increasingly interested in carbon-based material printed antennas (Lu et al., 2021; Quaranta et al., 2019), sensors (Bakar et al., 2023; Guo et al., 2021), energy storage and conversion (Husain et al., 2022) and electromagnetic devices (Alshahrani & Prakash, 2023; Huo et al., 2023), due to their excellent properties, such as electrical, mechanical, and chemical stability, cost-effectiveness, and lightweight characteristics (Khair et al., 2019; Lu et al., 2022).

In the study conducted by Ram et al. (2021) on graphene circular structures, a circular microstrip patch array (MPA) based on graphene was employed, resulting in an enhancement of gain by approximately 5 dBi. Another investigation has been documented, incorporating graphene properties into CST and COMSOL simulations (Su et al., 2016).

Song et al. (2019) conducted a separate research endeavor wherein a 2×2 rectangular patch array was fabricated through the laser engraving of a graphene film, followed by its transfer onto a substrate. This process is acknowledged for its complexity and high cost. Devi et al. (2017) introduced a novel rectangular microstrip antenna employing carbon nanotubes (CNTs) to achieve a broad bandwidth, and the antenna demonstrated a notable improvement with a 20% increase in impedance bandwidth.

Additionally, employing graphene-based materials as conductive patches, as highlighted by Azman et al. (2022), results in a notable 60% increase in bandwidth. In the field of communication systems, there is a crucial need to improve bandwidth for practical use. The challenges in designing radio frequency (RF) antennas that use nanomaterials are related to identifying the resonance of materials at lower or higher frequencies and establishing reliable electrical connections with nanomaterials to assess performance.

One of the most promising approaches is using natural materials, which provide sustainability and improve performance. In this regard, *Prosopis Africana*, a sustainable natural resource, has gained considerable interest due to its unique electrical characteristics and the practicality of producing conductive ink from its biomass (Babani et al., 2023).

However, a new proposal has emerged to investigate the conversion of *Prosopis africana* biomass into a similar carbon-based material. This idea is based on recognizing *Prosopis africana* as a versatile tree with significant economic importance in rural and urban communities across sub-Saharan Africa (Agboola, 2004; Nnamani et al., 2020).

The primary objective of this study is to present a novel approach to antenna design by harnessing the properties of *Prosopis africana* as a replacement for copper due to its higher conductivity, to develop a conductive ink-based patch antenna. The central focus of this research is on enhancing the bandwidth of patch antennas, a crucial parameter for modern communication systems, including Wi-Fi, 5G, and satellite communication.

Prosopis africana biomass, derived from the tree species native to sub-Saharan Africa, is recognized as a valuable and multifaceted natural resource. This biomass is extensively utilized across various domains, encompassing traditional roles in food production, medicinal practices, and timber supply, as well as modern applications in sustainable energy, environmental protection, and the development of advanced materials (Bishop et al., 2021). Additionally, the tree's pods serve as a source of nutrient-rich fodder and possess medicinal properties, underscoring their importance for livestock and human sustenance, particularly in arid environments (Yusuf et al., 2008).

Prosopis africana biomass is increasingly utilized for bioenergy production, serving as a renewable and environmentally friendly source of fuel and electricity (Kiflie et al., 2023). Additionally, its capacity to thrive in diverse climatic conditions and its potential to rehabilitate degraded landscapes underscore its importance in mitigating desertification and promoting land restoration. Pyrolysis, as the preliminary step in the thermochemical

conversion of biomass, involves complex mechanisms influenced by various factors, including the material's composition, particle size, heating rate, and other related parameters (Rao & Sharma, 1998).

Biochar, a carbon-rich substance generated through biomass pyrolysis, has gained attention as a promising material for diverse electronic applications (Yan et al., 2022). Its distinct characteristics, including high carbon content and excellent electrical conductivity, render it an appealing option for various electronic components. The material's significant surface area and porosity facilitate efficient charge storage, thereby enhancing its energy storage capacity (Leng et al., 2021). Moreover, the abundant carbon structure of biochar can be tailored or functionalized to enhance its electrochemical performance, positioning it as a versatile and sustainable solution for developing cost-effective energy storage technologies.

The compatibility of biochar with flexible electronics warrants particular attention. Its unique mechanical flexibility and electrical conductivity combination positions biochar as a promising candidate for use in flexible and wearable electronic devices (Rizwan et al., 2017). Incorporating biochar into electronic applications signifies progress toward developing sustainable and eco-friendly technological innovations (Tovar-Lopez, 2023).

Thick film processing is a popular method for electronic applications due to its simplicity, speed, and cost-effectiveness. This technique allows for incremental layer deposition, which can be tailored to the specific requirements of the application. It also contributes to the miniaturization of electronic devices (Shafee et al., 2020).

This study introduces a new approach to developing a thick film paste for PAC, which combines micro-sized powder and an organic binder. This unique paste formulation is an important contribution not previously documented. By using thick film technology, we are now able to create an MPA with improved performance utilizing the commonly used FR4 substrate.

METHOD AND MATERIAL

The study used raw material from *Prosopis africana*, a widespread plant species in northern Nigeria. The materials were collected from Duhun Karo farms in the Hadejia Local Government Area of Jigawa State, Nigeria. The *Prosopis africana* wood was subjected to controlled pyrolysis to obtain activated char. The carbonization process was carried out at optimized temperatures and durations, resulting in PAC with desired properties at 500 °C for 3 hours. Figure 1 shows a step-by-step process for synthesizing PAC through pyrolysis (Kiflie et al., 2023). The carbonized material was then crushed into powder using a mortar and pestle. After that, the PAC powder was sieved to a micrometer size of <20 microns, which served as the active material in fabricating thick film antennas (Figure 2).

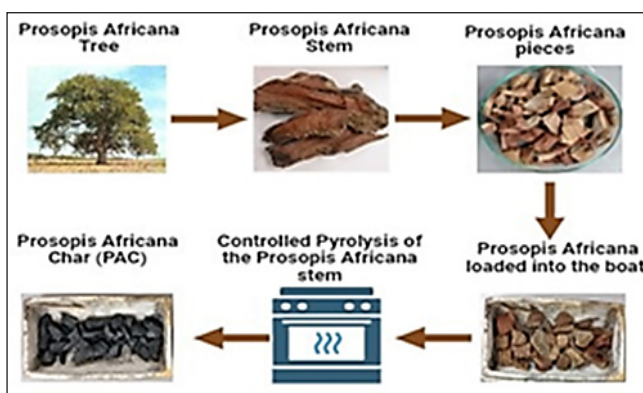


Figure 1. Preparation of activated char from *Prosopis africana* biomass (Babani et al., 2024a)



Figure 2. (a) The process of crushing PAC material using a mortar and pestle after carbonization, and (b) the process of sieving the PAC Powder using a < 20 micron sieve

The paste formulation commenced by blending PAC micrometer powder of 45 wt% with an organic binder of 55 wt%, comprising (M-X), (LO), and (α -T). The chemical composition remained unchanged post-purchase. The selection of the active powder ratio was informed by prior research (Hasan et al., 2018). The amalgamation was stirred at 250 rpm for 3 hours, maintaining a temperature of 40 °C using a magnetic stirrer to achieve a homogeneous consistency. Figure 3 illustrates the process formulation of organic volatiles (OV) and PAC powder employed for the thick film paste.

After mixing, the paste was applied onto an FR4 substrate using a silk screen with a rectangular design. The PAC thick film was given 10–15 minutes to level off, dried, and then fired in a box furnace at 300 °C for 60 minutes. This process aimed to eliminate the organic binder and securely bind the nano-powders to the substrate (Shafiee et al., 2020). Various techniques were used to characterize the thick, dried PAC film. Raman

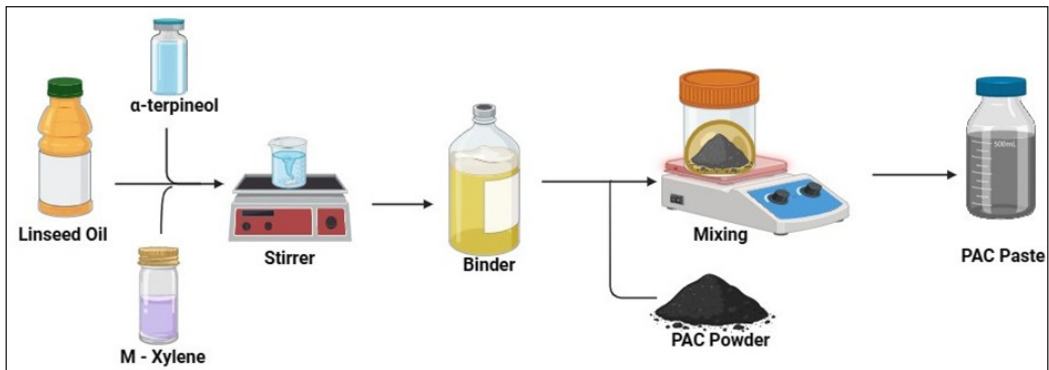


Figure 3. Formulation of organic binder and PAC paste thick film for screen printing

spectroscopy was used to assess the graphitic defects in the PAC powder, field emission scanning electron microscopy (FESEM) was used to analyze the structural morphology, and energy dispersive x-ray spectroscopy (EDX) was conducted for elemental analysis of the PAC thick film. A thermogravimetric analysis (TGA) was employed to determine the thermal stability of the PAC paste.

After characterization, a PAC thick film was printed onto a one-sided FR4 substrate, which served as both the antenna feedline and radiating patch. The antenna design was carefully simulated and optimized after inserting all the dimension values and associated PAC values as a new material into the CST software to determine the ideal and geometrical parameters, ensuring the desired bandwidth enhancement. After the design stage, the patch was printed and fired at 150 °C for 30 minutes. Then, an SMA connector was attached to the fabricated antenna to enable the measurement of resonant frequency, return loss, and bandwidth via the vector network analyzer (VNA). The structure of the antenna design and the physically fabricated MPA can be seen in Figure 4. This design was simulated to work at the resonant frequency of 9.50 GHz for airborne radar applications.

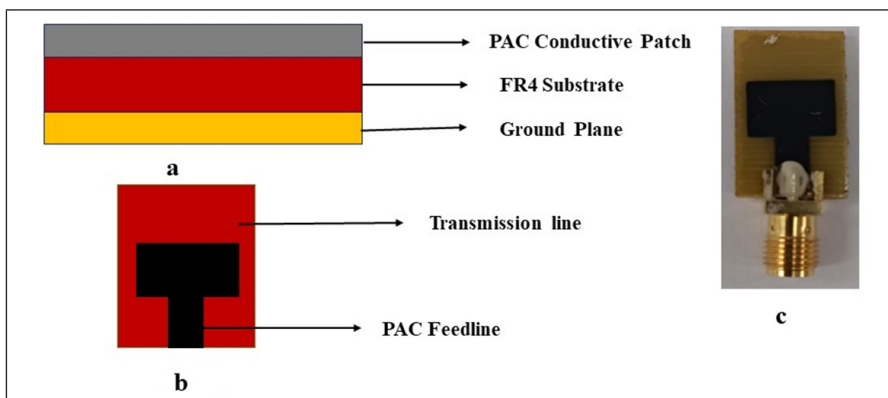


Figure 4. MPA structure: (a) view from the site, (b) view from the top, (c) fabrication prototype

RESULTS AND DISCUSSION

Graphitic materials are characterized by their black color and similar densities, which makes it crucial to distinguish between them accurately. Performing standard characterization procedures on sp² graphitic materials is customary before conducting any tests. Raman spectroscopy is the most effective method for such characterization (Kusaimi et al., 2018; Shitu et al., 2024). The results of Raman spectroscopy for the milled PAC powders are presented in Figure 5. In order to gain a better understanding of the graphitization process in activated charcoal, a Raman analysis was conducted. The graph shows two distinct peaks at 1358 cm⁻¹ and 1580 cm⁻¹, representing the defect mode (D band) and graphitic mode (G band). The calculated value of the ratio of defect intensity (I_D) to graphitic intensity (I_G), (I_D/I_G), is 0.98. This indicates a significant level of disorder associated with defects in the graphitic structure. These peaks are associated with graphene and graphite (Chen et al., 2016; Shitu et al., 2023).

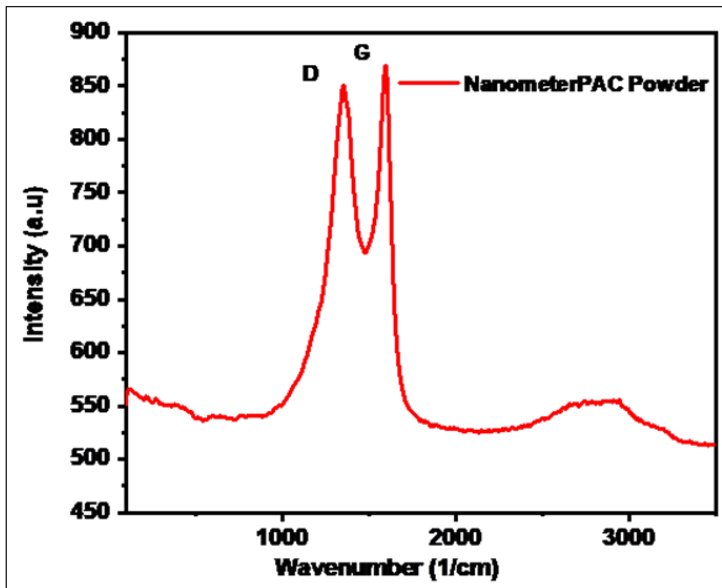


Figure 5. Raman of PAC powders

Figure 6 displays FESEM images illustrating the PAC thick film at room temperature and fired at 300 °C. Before being subjected to the specified temperature, the thick film was covered with a liquid organic binder (OB). Upon firing in the furnace, the binder underwent drying and evaporation, which encased the nanoparticles and bound them to the substrate. The OB, which contained linseed oil (LO), a drying oil, demonstrated polymerization upon exposure to the designated temperature. This property makes the oil suitable for a binder and a thick film paste. The FESEM image of the thick film fired at 300 °C shows a well-

dispersed arrangement of PAC powder, displaying nanoparticles within the range of 10 to 20 nm (Hasan & Hamidon, 2017; Yunusa & Musa, 2023).

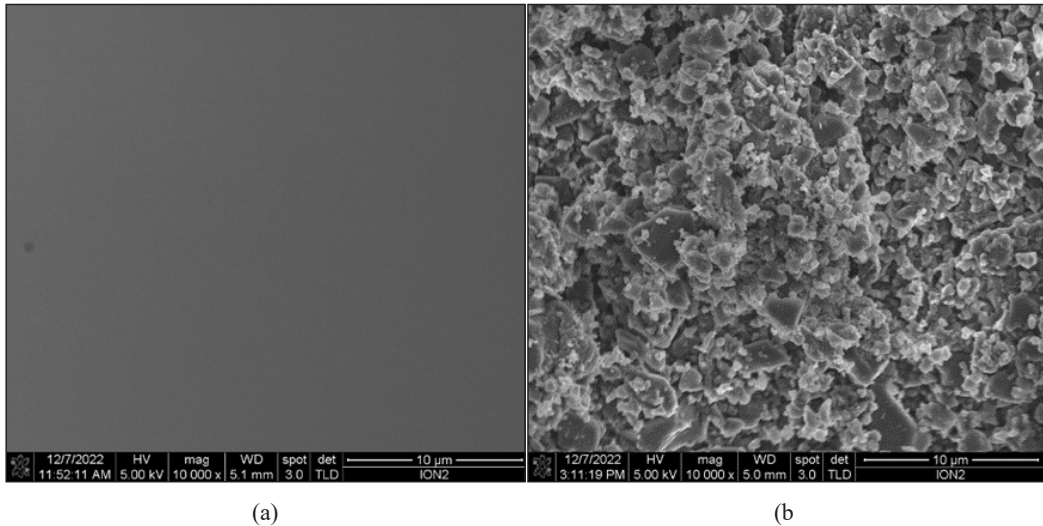


Figure 6. Morphology of PAC film (a) at room temperature and (b) firing at 300 °C

Figure 7 depicts the results of the EDX analysis conducted on both samples, which confirms the impact of firing temperature. The analysis revealed that the carbon component in the OV decreased while other elements associated with the PAC material increased as the firing temperature increased. These findings suggest that the elevated temperature facilitated the volatilization or desiccation of the OV, mainly composed of LO, exposing the nanoparticles underneath the oil layer (Babani et al., 2024b). To summarize, the analysis of samples processed at 300 °C showed conspicuous visibility of nanoparticles on the thick film's surface, which could affect the material's properties and overall performance (Abadi, 2010). After firing, the EDX analysis of the thick film surface indicates a higher carbon content in C: O elements, attributed to the presence of LO and other solvents at this stage.

Figure 8 shows the weight loss and decomposition rate of PAC paste in the temperature range of 25 to 1000 °C under an air atmosphere. The paste's volatile components evaporate between 50 °C and 255 °C, which corresponds to the flash point and boiling point of M-X (25 °C, 138 °C) and (α .T) (90 °C, 217 °C), respectively (Hasan et al., 2018). After that, non-volatile constituents, mainly LO, are removed. According to material specification documents, LO has a flash point of 300 °C and a boiling point of over 400 °C. The boiling of LO becomes prominent, with its boiling point reaching a maximum of 376 °C and beyond. In the final stages of this thermal process, a secondary decomposition event occurs within the temperature range of 400 °C to 500 °C, which is directly associated with the breakdown of linseed oil. Almost all the OV have evaporated and disintegrated by this point, leaving

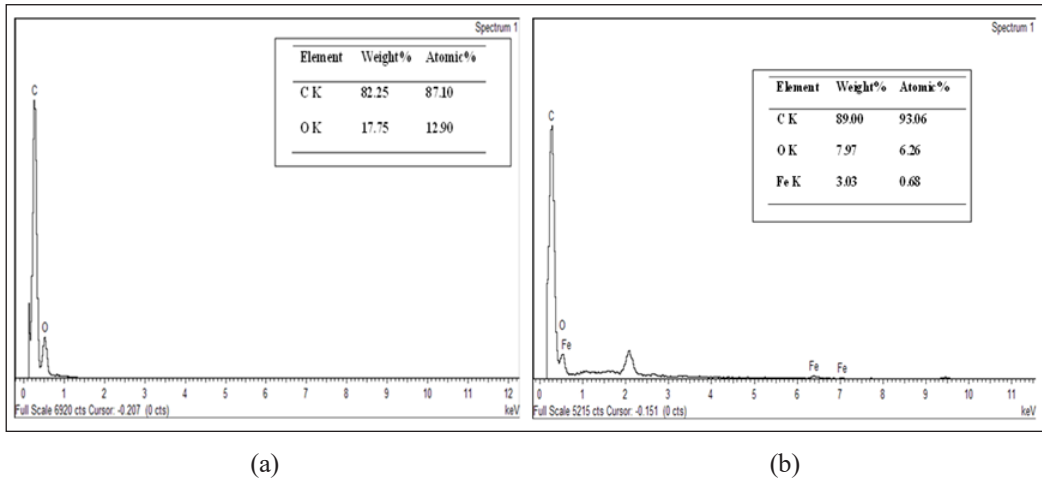


Figure 7. EDX of PAC film at (a) room temperature and (b) at firing temperature at 300 °C

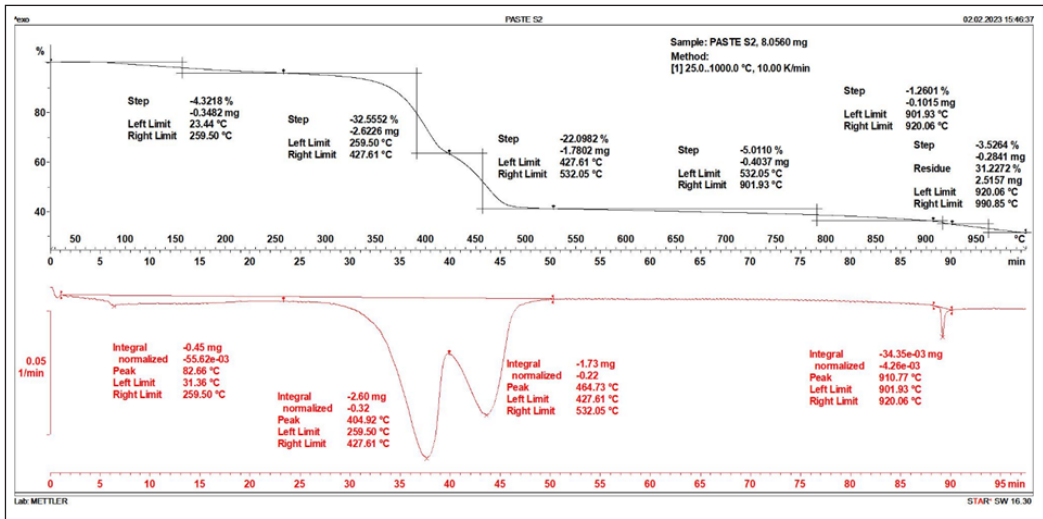


Figure 8. TGA measurement of PAC paste thick film

the PAC ashes firmly adhered to the alumina substrate. Therefore, it can be concluded that the optimal temperature range for PAC thick films, using LO as its OV, is between 400 °C and 500 °C. LO is a suitable organic vehicle within this range for formulating viscous films that can withstand lower firing temperatures (Sumaila et al., 2023a).

The electrical characterization was conducted using a four-point probe setup to determine the electrical resistance of the thick films. The relevant electrical parameters, such as sheet resistance, resistivity, and conductivity, were calculated using the appropriate formulas:

$$\text{From Ohm's law } R = \frac{V}{I} \quad [1]$$

$$R_S = R * R_{CF} \quad [2]$$

$$\rho = R_S * t \quad [3]$$

$$\delta = \frac{1}{\rho} \quad [4]$$

where R is the resistance in Ω , R_{CF} is the correctional factor that depends on the thickness of the film, ρ is the resistivity in Ω/m , t is the thickness of the PAC thick film in μm , and δ is the conductivity in S/m. From four points, the values of $R = 2.10E3$, $R_{CF} = 8.186$, $R_S = 1.7191E4$, and $t = 12.43 \mu m$ are the average thickness from the cross-sectional FESEM. Therefore, we calculated the resistivity and conductivity from the above formula as $\rho = 0.2137 \Omega/m$ and $\delta = 4.679$ S/m, respectively. From Table 1, it shows that the summary of the 45 wt% of PAC has good electrical conductivity, which is due to the amount of binder removed during the annealing process and the particle shape, size, and particle interconnection, similar to studies (Babani et al., 2025; Sumaila et al., 2023b).

Table 1
The electrical conductivity of the PAC thick film

Material	Resistance (Ω)	Sheet Resistance (Ω/sqr)	Resistivity (Ω/m)	Conductivity (S/m)
PAC	2.10E3	1.7191E4	0.2137	4.679

A preliminary simulation was conducted to prepare for the fabrication of the MPA component. The goal was to determine the design parameters and dimensions for both the substrate and the radiating patch. Even small changes to these dimensions can significantly affect the MPA's performance, making the simulation phase a crucial step in the fabrication process. In this study, the operational frequency for the MPA was set at 9.50 GHz, complying with ITU regulations for the X-band specifications. FR4 was selected as the substrate material, and PAC paste was used for the feedline and patch during the simulation to define the dimensions of both the substrate and the patch. The thickness and substrate height of the radiating patch, represented by 't' and 'h', respectively, are usually kept below the wavelength. The FR4 substrate is characterized by a relative permittivity of 4.3 and has a thickness of 1.6mm, a 0.035 mm copper thickness, and a conductive PAC thickness of 0.01923 mm.

Figure 9 also presents the analysis of MPA performance with PAC thick film on an FR4 substrate within a frequency range of 8 to 11 GHz. Both simulation and experimental measurements were conducted to assess the impact of the PAC thick film as a conductive radiating patch on the simulated resonant frequency of 9.5 GHz.

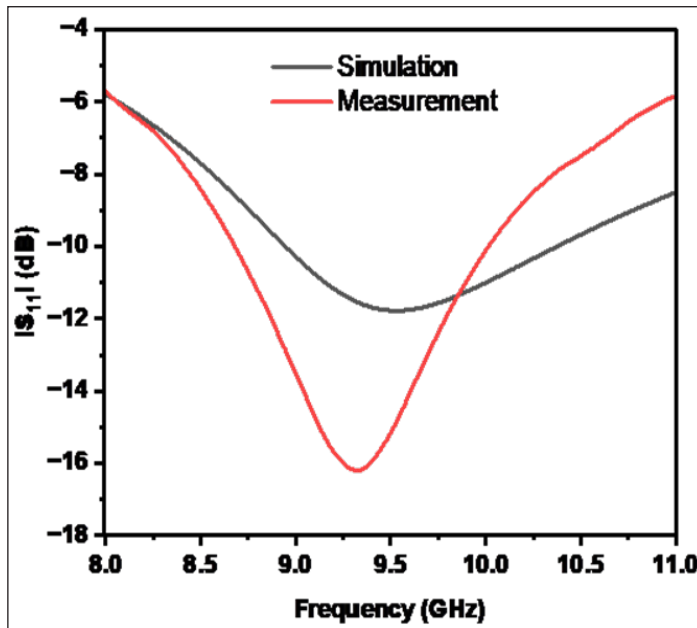


Figure 9. Return loss of the simulated and measured results of the PAC thick film MPA

A detailed comparison between simulation and measurement results is provided, and a summary of all data is tabulated in Table 2. These findings reveal that the MPA fabricated with the PAC thick film significantly enhances return loss, bandwidth, and gain.

Table 2
Summary of simulated and measurement values

Parameters	Simulation Value	Measurement Value
Operating Frequency (GHz)	9.5	9.38
Return loss S ₁₁ (dB)	-11.50	-16.50
Bandwidth @ -10dB (GHz)	1.41	1.32

The graph showcases the 9.5 GHz frequency for $\Phi = 90^\circ$ and $\Phi = 0^\circ$, drawing attention to the variations and contrasts in radiation levels across the substrate. By providing a clear depiction of the frequency's behavior in a two-dimensional plane, it becomes easier to pinpoint areas of differing radiation intensities, as demonstrated in Figure 10. This type of analysis is vital for applications that depend on accurate frequency control and enhanced signal optimization (Musa et al., 2023).

A simulation was performed to analyze the peak realization gain on the substrate. The analysis at 9.5 GHz offers critical insights into the system's robustness and reliability. This frequency-specific information is essential for optimizing the system's performance

and ensuring its functionality under optimal conditions. Such detailed evaluation plays a pivotal role in developing and refining frequency-sensitive technologies, improving their effectiveness. Figure 11 presents the simulated peak realization gain, measured at 6.68 dB.

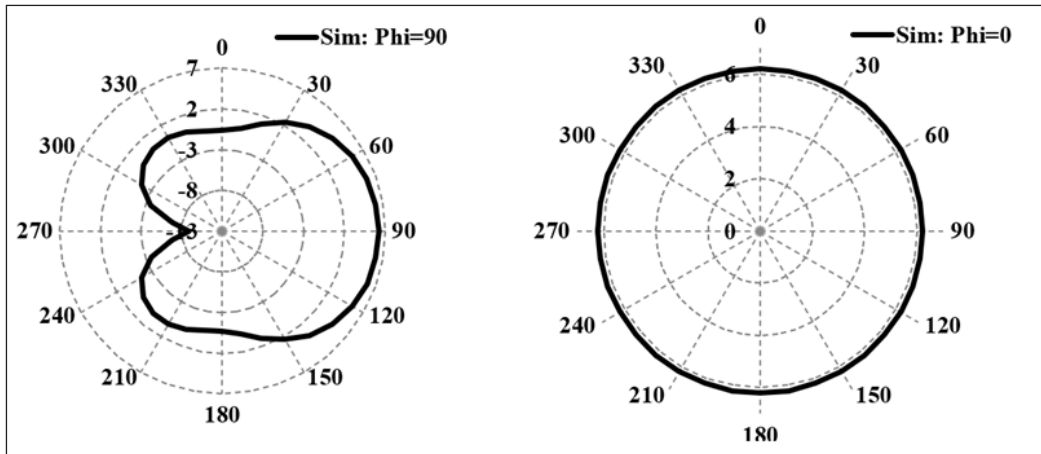


Figure 10. The simulated 2D radiation pattern of the proposed antenna

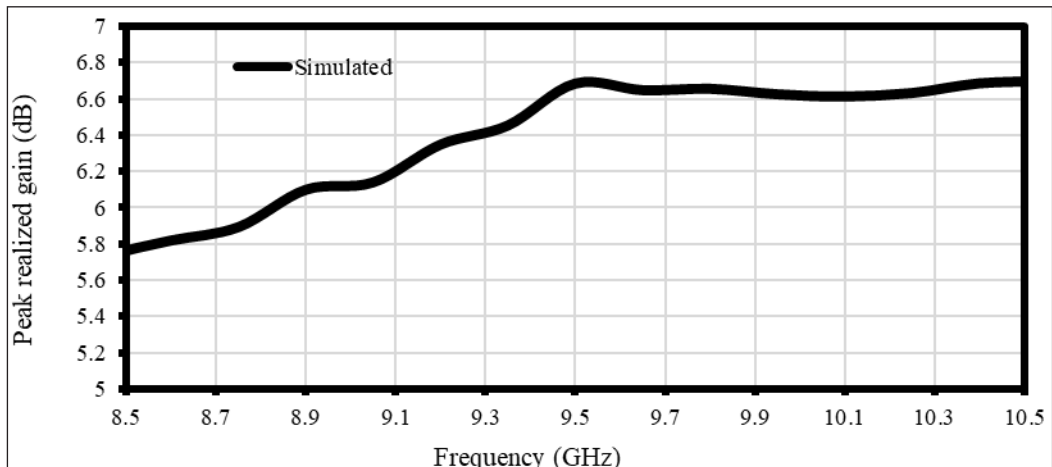


Figure 11. The simulated peak realized gain vs frequency on the substrate

As shown in Table 3, this research marks an important progression in enhancing the bandwidth of MPAs to meet the increasing requirements of modern communication and sensing systems. The effective implementation of PAC ink suggests novel opportunities for incorporating sustainable materials into radar technologies, fostering advancements in antenna design and materials science. The outcomes of this study motivate further investigation into achieving more sustainable and efficient wireless communication and radar systems (Babani et al., 2024a; Muhammad et al., 2021; Musa et al., 2023).

Table 3
 Comparison study of patch antennas over different carbon materials on X Band

Antenna	f_0 (GHz)	Conductive Patch Material	$ S_{11} $ (dB)	BW (GHz)	Gain (dB)	Application	Ref.
<i>R</i>	10.00	MWCNT	-15.50	N.A	1.20	X- Band	(Dakshayani & Suryanarayana, 2022)
<i>R</i>	10	MWCNT	-11.64	2.5	0.81	BW enhancement	(Devi et al., 2017)
<i>R</i>	11.04	Graphene	-12.05	1.45	N.A	5G	(Sa'don et al., 2019)
<i>R</i>	11.0	Graphene	-16.20	0.814	6.54	Military satellites	(Yunusa & Shehu, 2022)
This Work	9.5	PAC	-16.50	1.32	6.68	Airborne Radar	

R = Rectangular Patch Antenna

CONCLUSION

Material characterization and performance analysis serve as essential tools for evaluating the suitability of materials in various applications. This study emphasized the relationship between intrinsic properties, processing methods, and performance outcomes, offering an in-depth understanding of the material behavior under specific conditions. The research outcomes underscore the importance of leveraging advanced characterization techniques to refine material properties and enhance functionality. This work bridges the gap between theoretical material science and practical engineering applications by correlating experimental data with application-specific requirements. Ultimately, this study contributes to the ongoing efforts to innovate in material selection and design, addressing current challenges and future opportunities. Continued exploration into emerging materials and cutting-edge analysis techniques will be critical in shaping the next generation of high-performance materials.

In conclusion, this article contributes to the growing body of knowledge on material characterization and performance by presenting a detailed and practical framework for evaluating materials for any electronics applications that require electrical conductivity, like antenna and sensor applications, because of the higher electrical conductivity of 4.46 S/m. The research underscores the necessity of linking characterization data to real-world performance to drive innovation in material design and development. Future work could explore [specific suggestions] to further refine the material's applicability across broader contexts and enhance its role in advancing technological solutions.

ACKNOWLEDGEMENTS

This work was supported by the Petroleum Technology Development Fund (PTDF) of Nigeria. The Faculty of Engineering's Putra-IPS Grant/2022/9735300 and the Institute of Nanotechnology and Nanoscience (ION2) at Universiti Putra Malaysia (UPM) also provided financial assistance.

REFERENCES

- Abadi, M. H. N. S. (2010). *Development of nanocrystalline thick film gas sensors* [Unpubliss doctoral thesis]. Universiti Putra Malaysia.
- Agboola, D. A. (2004). *Prosopis africana* (Mimosaceae): Stem, roots, and seeds in the economy of the savanna areas of Nigeria. *Economic Botany*, 58(1), S34-S42. [https://doi.org/10.1663/0013-0001\(2004\)58\[s34:pamsra\]2.0.co;2](https://doi.org/10.1663/0013-0001(2004)58[s34:pamsra]2.0.co;2)
- Alshahrani, H., & Prakash, V. R. A. (2023). Development of highly flexible electromagnetic interference shielding composites for electronic applications using Cobalt/ Hevea brasiliensis seed husk carbon dots/ Bamboo microfibre-polyvinyl alcohol. *Industrial Crops and Products*, 191(PA), Article 115967. <https://doi.org/10.1016/j.indcrop.2022.115967>
- Azman, N. I. Z., Othman, M. K., Zaini, N. A. A., & Jusoh, M. A. (2022). Graphene-based materials for microstrip patch antenna. *Progress In Electromagnetics Research C*, 126, 207–216. <https://doi.org/10.2528/PIERC22090505>
- Babani, S., Hamidon, M. N., Ismail, A., & Jaafar, H. (2024a). Advancing microstrip patch antennas through *Prosopis africana* conductive ink-based thick films for enhanced bandwidth in radar applications. *Progress In Electromagnetics Research B*, 105, 17–29. <https://doi.org/10.2528/PIERB23122102>
- Babani, S., Nizar, M., Alyani, H., Haslina, I., Intan, J., & Hassan, H. (2024b). Development and characterization of screen - Printed *Prosopis Africana* Char thick film for electronic applications. *Journal of the Australian Ceramic Society*, 60(2), 643-652. <https://doi.org/10.1007/s41779-024-00999-8>
- Babani, S., Hamidon, M. N., Ismail, A., Jaafar, H., Bakar, A. A., & Lawal, I. (2023, September 12-13). *Impact of micrometer and nanometer-sized particles on the electrical properties of Prosopis africana biochar thick films*. [Paper presentation]. In 7th International Symposium on Advanced Materials and Nanotechnology (iSAMN2023), Serdang, Selangor.
- Babani, S., Hamidon, M. N., Ismail, A., Jaafar, H., Hassan, I. H., Shafee, F. N., Shitu, I. G., Yunusa, Z., Lamido, J., & Muhammad, S. (2025). Deployment of *Prosopis Africana* biomass material as a conductive thick film paste for electronic applications. In *Proceedings of the International Conference on Sustainability: Developments and Innovations* (pp. 125-132). Springer Nature Singapore. https://doi.org/10.1007/978-981-97-8712-8_16
- Babani, S., Khamis, N. H. H., Bala, B. D., & Ahmed Mohammed, T. A. (2015). A compact microstrip patch antenna for ADS-B operation. In *2014 IEEE Asia-Pacific Conference on Applied Electromagnetics (APACE)* (pp. 250-252). IEEE.. <https://doi.org/10.1109/APACE.2014.7043793>
- Bakar, A. A., Hamidon, M. N., Yaacob, M. H., Paiman, S., Jaafar, H., Jusoh, W. N. W., Shffee, F. N., & Hasan, I. H. (2023). An ohmic contact behavior of flexible thick film carbon-based electrode with TiO₂ layer

at different operating temperature. *International Journal of Chemical and Biochemical Sciences*, 24(7), 246-252

- Bansal, R. (2008). Antenna theory; analysis and design. *Proceedings of the IEEE* 72(7), 989-990. <https://doi.org/10.1109/proc.1984.12959>
- Bishop, B., Abang, F. B. P., & Attah, S. (2021). Effect of Fermentation with rumen content on the feeding value of boiled iron tree (*Prosopis Africana*) seedcoat on haematology and serum biochemistry of broiler chickens. *Annual Research & Review in Biology*, 36, 70–77. <https://doi.org/10.9734/arrb/2021/v36i1230464>
- Chen, J., Li, J., Xiong, D., He, Y., Ji, Y., & Qin, Y. (2016). Preparation and tribological behavior of Ni-graphene composite coating under room temperature. *Applied Surface Science*, 361, 49–56. <https://doi.org/10.1016/j.apsusc.2015.11.094>
- Dakshayani, P., & Suryanarayana, V. (2022). Investigation of conformal CPW fed copper and multiwalled carbon nanotube microstrip antennas in X- band applications. *International Journal of Innovative Research and Practices*, 10(8), 6–11.
- Devi, K. S. C., Angadi, B., & Mahesh, H. M. (2017). Multiwalled carbon nanotube-based patch antenna for bandwidth enhancement. *Materials Science & Engineering B*, 224, 56–60. <https://doi.org/10.1016/j.mseb.2017.07.005>
- Garg, R., Bhartia, P., Bahl, I. J., & Ittipiboon, A. (2001). *Microstrip antenna design handbook*. Artech House.
- Guo, Y., Wei, X., Gao, S., Yue, W., Li, Y., & Shen, G. (2021). Recent advances in carbon material-based multifunctional sensors and their applications in electronic skin systems. *Advanced Functional Materials*, 31(40), Article 2104288. <https://doi.org/10.1002/adfm.202104288>
- Hasan, I. H., & Hamidon, M. N. (2017). Yttrium iron garnet thick film inclusion for enhanced microstrip patch antenna performance. In *2017 IEEE Regional Symposium on Micro and Nanoelectronics (RSM)* (pp. 131-134). IEEE. <https://doi.org/10.1109/RSM.2017.8069168>
- Hasan, I. H., Hamidon, M. N., Ismail, A., Ismail, I., Mekki, A. S., Mohd Kusaimi, M. A., Azhari, S., & Osman, R. (2018). YIG thick film as substrate overlay for bandwidth enhancement of microstrip patch antenna. *IEEE Access*, 6, 32601–32611. <https://doi.org/10.1109/ACCESS.2018.2842749>
- Huo, K. L., Yang, S. H., Zong, J. Y., Chu, J. J., Wang, Y. D., & Cao, M. S. (2023). Carbon-based EM functional materials and multi-band microwave devices: Current progress and perspectives. *Carbon*, 213, Article 118193. <https://doi.org/10.1016/j.carbon.2023.118193>
- Husain, Z., Shakeelur Rahman, A. R., Ansari, K. B., Pandit, A. B., Khan, M. S., Qyyum, M. A., & Lam, S. S. (2022). Nano-sized mesoporous biochar derived from biomass pyrolysis as electrochemical energy storage supercapacitor. *Materials Science for Energy Technologies*, 5, 99–109. <https://doi.org/10.1016/j.mset.2021.12.003>
- Khair, N., Islam, R., & Shahariar, H. (2019). Carbon-based electronic textiles: Materials, fabrication processes and applications. *Journal of Materials Science*, 54(14), 10079–10101. <https://doi.org/10.1007/s10853-019-03464-1>

- Kiffie, Z., Solomon, M., & Kassahun, S. K. (2023). Statistically optimized charcoal production from *Prosopis juliflora* for use as alternative fuel in cement factories. *Biomass Conversion and Biorefinery*, 13(3), 1539–1552. <https://doi.org/10.1007/s13399-020-01172-4>
- Kusaimi, M. A., Hamidon, M. N., & Azhari, S. (2018). Importance of annealing temperature on the electrical conductivity of screen printed graphite organic paste. *eProceedings Chemistry*, 3, 22-24.
- Leng, L., Xiong, Q., Yang, L., Li, H., Zhou, Y., Zhang, W., Jiang, S., Li, H., & Huang, H. (2021). An overview on engineering the surface area and porosity of biochar. *Science of the Total Environment*, 763, Article 144204. <https://doi.org/10.1016/j.scitotenv.2020.144204>
- Lu, G., Wang, J., Xie, Z., & Yeow, J. (2022). Carbon-based THz microstrip antenna design: A review. *IEEE Open Journal of Nanotechnology*, 3, 15–23. <https://doi.org/10.1109/OJNANO.2021.3135478>
- Lu, G., Wang, J., Xie, Z., & Yeow, J. T. W. (2021). Carbon-based THz microstrip antenna design: A review. *IEEE Open Journal of Nanotechnology*, 3, 15–23. <https://doi.org/10.1109/OJNANO.2021.3135478>
- Muhammad, S., Tiang, J. J., Wong, S. K., Iqbal, A., Smida, A., & Azizi, M. K. (2021). A compact dual-port multi-band rectifier circuit for RF energy harvesting. *Computer Materials & Continua*, 68(1), 167-184. <https://doi.org/10.32604/cmc.2021.016133>
- Musa, U., Babani, S., Babale, S. A., Ali, A. S., Yunusa, Z., & Lawan, S. H. (2023). Bandwidth enhancement of millimeter-wave microstrip patch antenna array for 5G mobile communication networks. *Bulletin of Electrical Engineering and Informatics*, 12(4), 2203–2211. <https://doi.org/10.11591/eei.v12i4.4680>
- Nnamani, P. O., Shinde, J. A., Jadhav, R. N., Sanandam, M. R., & Lokhande, C. D. (2020). Fundamental properties of *Prosopis Africana* peel powders (PAPPs) as drug delivery excipient. *African Journal of Pharmaceutical Research & Development*, 12(1), 119–133.
- Quaranta, S., Giorcelli, M., & Savi, P. (2019). Graphene and MWCNT printed films: Preparation and RF electrical properties study. *Journal of Nanomaterials*, 2019(1), Article 4658215. <https://doi.org/10.1155/2019/4658215>
- Ram, P., Yadav, A., Suman, M. K., & Kumar, A. (2021). Graphene based circular shaped micro strip patch antenna array for 2.45 GHz ISM band application. *Wireless Personal Communications*, 116(3), 1613–1620. <https://doi.org/10.1007/s11277-020-07751-y>
- Rao, T. R., & Sharma, A. (1998). Pyrolysis rates of biomass materials. *Energy*, 23(11), 973-978.
- Rizwan, M., Member, S., Waqas, M., Khan, A., Member, S., Syd, L., Virkki, J., & Ukkonen, L. (2017). Flexible and stretchable brush-painted wearable antenna on a three-dimensional (3-D) printed substrate. *IEEE Antennas and Wireless Propagation Letters*, 16, 3108-3112. <https://doi.org/10.1109/LAWP.2017.2763743>
- Sa'don, S. N. H., Jamaluddin, M. H., Kamarudin, M. R., Ahmad, F., & Dahlan, S. H. (2019). A 5G graphene antenna produced by screen printing method. *Indonesian Journal of Electrical Engineering and Computer Science*, 15(2), 950–1055. <https://doi.org/10.11591/ijeecs.v15.i2.pp950-955>
- Shafee, F. N., Hamidon, M. N., Wahid, M. H., Shaari, A. H., Ertugrul, M., Abdullah, N. H., Kusaimi, M. A. M., Mustafa, M. S., & Ibrahim, I. R. (2020). Effect of nanometric and micronic particles size on physical and electrical properties of graphite thick film. *International Journal of Nanotechnology*, 17(11–12), 825–839. <https://doi.org/10.1504/IJNT.2020.112385>

- Shitu, I. G., Katibi, K. K., Muhammad, A., Chiromawa, I. M., Tafida, R. A., Amusa, A. A., & Babani, S. (2023). Effects of irradiation time on the structural, elastic, and optical properties of hexagonal (wurtzite) zinc oxide nanoparticle synthesised via microwave-assisted hydrothermal route. *Optical and Quantum Electronics*, 56(2), 266. <https://doi.org/10.1007/s11082-023-05867-6>
- Shitu, I. G., Katibi, K. K., Tafida, R. A., Iya, S. G. D., Alotaibi, K. M., Babani, S., Amusa, A. A., Elbidi, M., Katibi, M. T., & Mallik, S. (2024). Synthesis and characterization of magnetic biochar nanocomposite from oil palm fronds for efficient copper (II) ion removal from leachate. *Clean Technologies and Environmental Policy*. <https://doi.org/10.1007/s10098-024-03041-4>
- Song, R., Huang, G., Liu, C., Zhang, N., Zhang, J., Liu, C., Wu, Z. P., & He, D. (2019). High-conductive graphene film based antenna array for 5G mobile communications. *International Journal of RF and Microwave Computer-Aided Engineering*, 29(6), Article e21692.
- Su, Y., Guo, Z., Huang, W., Liu, Z., Gong, T., He, Y., & Yu, B. (2016). Ultra-sensitive graphene photodetector with plasmonic structure. *Applied Physics Letters*, 109(17), Article 173107. <https://doi.org/10.1063/1.4966597>
- Sumaila, J. L., Sani, D., Aibu, S., Hamidon, M. N., Yunusa, Z., Magaji, N., Abubakar, A., Shafiee, F. N., & Babani, S. (2023a). Morphology and electrical properties of pristine and composite rice husk ash nano / micro particles thick films for gas sensing applications. In *2023 IEEE Regional Symposium on Micro and Nanoelectronics (RSM)* (pp. 90-93). IEEE. <https://doi.org/10.1109/RSM59033.2023.10327321>
- Sumaila, J. L., Sani, D., Magaji, N., & Yunusa, Z. (2023b). Rice husk ash (RHA) nano particles as new materials for hydrogen gas sensor. In *Proceeding of 7th International Symposium on Advanced Materials and Nanotechnology* (pp. 136–139). Institut of Nanoscience and Nanotechnology Universiti Putra Malaysia.
- Tovar-Lopez, F. J. (2023). Recent progress in micro- and nanotechnology-enabled sensors for biomedical and environmental challenges. *Sensors*, 23(12), Article 5406. <https://doi.org/10.3390/s23125406>
- Yan, B., Zheng, J., Feng, L., Du, C., Jian, S., Yang, W., Wu, Y. A., Jiang, S., He, S., & Chen, W. (2022). Wood-derived biochar as thick electrodes for high-rate performance supercapacitors. *Biochar*, 4(1), Article 50. <https://doi.org/10.1007/s42773-022-00176-9>
- Yunusa, Z., & Musa, U. (2023). Rheological properties of *Prosopis Africana* Char paste thick film for antenna applications. In *2023 IEEE International Conference on Sensors and Nanotechnology (SENNANO)* (pp. 37-40). IEEE. <https://doi.org/10.1109/SENNANO57767.2023.10352532>
- Yunusa, Z., & Shehu, A. A. (2022). Comparative study of single-slot and multi-slot graphene-based microstrip patch antenna for X-band application. *NanoEra*, 2(1), 1-4.
- Yusuf, N. D., Ogah, D. M., Hassan, D. I., Musa, M. M., & Doma, U. D. (2008). Effect of decorticated fermented prosopis seed meal (*Prosopis Africana*) on growth performance of broiler chicken. *International Journal of Poultry Science*, 7(11), 1054–1057. <https://doi.org/10.3923/ijps.2008.1054.1057>

Effect of Coil Diameter on the Performance of Interior and Embedded Permanent Magnet for Double-stator Generator

Nur Amira Ibrahim¹, Norhisam Mison^{1,2,3*}, Hairul Faizi Hairulnizam¹, Chockalingam Aravind Vaithilingam⁴, Nashiren Farzilah Mailah¹ and Ishak Aris¹

¹Faculty of Engineering, Universiti Putra Malaysia, Serdang, Selangor 43400, Malaysia

²Institute of Nanoscience and Nanotechnology, Universiti Putra Malaysia, Serdang, Selangor 43400, Malaysia

³Institute of Plantation Studies, Universiti Putra Malaysia, Serdang, Selangor 43400, Malaysia

⁴Clean Technology Impact Lab, Taylor's University, Subang Jaya, Selangor 47500, Malaysia

ABSTRACT

The permanent magnet synchronous motor (PMSM) intended for low-speed, high-torque applications generally possesses a substantial physical size, and the internal space of the permanent magnet rotor is frequently underutilized. The rising electrical demands in electric machines have necessitated enhancements in power density, especially in double-stator systems featuring interior and embedded permanent magnets. Nevertheless, research on motors employing copper coils of differing sizes is restricted. This paper analyses the performance of an interior and embedded permanent magnet double-stator generator using JMAG software by varying the coil diameter, establishing an inverse proportionality between coil diameter and the number of turns per slot. Performance analysis under different loads and speeds showed that a 1.0 mm coil diameter achieved the highest average power (293W) at 2 ohms for speeds of 200 rpm and 1662 W at 1 ohms for 800 rpm. Larger diameters did not guarantee higher output; 0.75 mm and 1.0 mm were the best performers. A 1.0 mm coil also exhibited the best power efficiency (56%–75%) across all speeds, outperforming 0.5 mm (below 55% efficiency) and 1.5 mm (efficiency above 73% but with a steep slope in load resistance variation).

ARTICLE INFO

Article history:

Received: 01 April 2024

Accepted: 10 April 2025

Published: 10 June 2025

DOI: <https://doi.org/10.47836/pjst.33.S4.03>

E-mail address:

nuraamiraibrahim@gmail.com (Nur Amira Ibrahim)

norhisam@upm.edu.my (Norhisam Mison)

GS67769@student.upm.edu.my (Hairul Faizi Hairulnizam)

aravindv@ieec.org (Chockalingam Aravind Vaithilingam)

nashiren@upm.edu.my (Nashiren Farzilah Mailah)

ishak_ar@upm.edu.my (Ishak Aris)

*Corresponding author

Keywords: Electrical power, PMSM, power efficiency, speed

INTRODUCTION

Permanent Magnet Synchronous Machines (PMSMs) have attracted significant attention due to their efficiency, power density, and

precise control capabilities (Krause et al., 2013; Lin et al., 2013; Mehrjou et al., 2017). They excel in regulating various parameters such as speed, torque, and position with high accuracy and responsiveness. PMSMs achieve this by directly converting mechanical energy into electrical energy through the shaft, eliminating the need for a gearbox and thereby improving efficiency (Rahman et al., 2010; Wang, 2008; Wu et al., 2009; Yasa & Mese, 2014). Gearboxes are prone to noise production, increased energy losses, and frequent maintenance requirements, leading to significant periods of inactivity.

The performance of PMSMs can be evaluated based on their structure and parameter design. They can be classified into three types based on stator and rotor numbers: single-stator single-rotor (Gieras et al., 2008), double-stator single-rotor (Chau et al., 2006; Liu et al., 2008; Feng et al., 2004; Gul et al., 2020; Norhisam et al., 2009; Wang et al., 2015; Zhang et al., 2020), and single-stator double-rotor (Zheng et al., 2013). The single-stator PMSMs require a significant number of poles and slots to generate more power. However, this approach can lead to unutilized space in the middle of the rotor. To address this issue, maintaining the size of the single-stator and adding another stator in the middle of the rotor can result in higher generated power. This is due to reduced magnetic flux leakages that flow in the direction of the shaft. This concept is supported by Feng et al. (2004), who conducted a performance analysis of a double-stator starter generator. Their study demonstrated that double-stator machines outperform single-stator ones. This is primarily attributed to the larger output torque of the armature winding in series, which acts as a motor at low speeds, and the ability to alter the two stator windings' relative positions when operating as a generator.

Zhang et al. (2020) demonstrated that double-stator PMSMs offer higher torque density, starting torque, and electric machine utilization compared to traditional single-stator machines. In contrast, the maximum output of a single-stator inner rotor permanent magnet motor is only 65.9% of that of a double-stator double-stator PMSM, indicating that the former is underutilized, acting primarily as rotor support. Li (2022) investigated a wind turbine power generation system using a double-rotor machine configuration, which showed benefits such as reduced harmonic generation, lower costs, and improved reliability compared to traditional PMSGs. However, the mechanical complexity of double-rotor machines, requiring two separate shafts (a constant speed shaft for the inner rotor and a variable speed shaft for the outer rotor), led to their exclusion from this study.

Regarding the permanent magnet rotor structure, the researchers (Chau et al., 2006; Liu et al., 2008; Feng et al., 2004; Gieras et al., 2008; Gul et al., 2020; Li, 2022; Norhisam et al., 2009; Wang et al., 2015; Zhang et al., 2020) mostly utilized surface-mounted PMSMs, except for reference (Zheng et al., 2013), which employed an interior-mounted PMSM. Wu et al. (2022) explored various rotor structures for double-stator PMSMs, highlighting that surface-mounted permanent magnets only produce electromagnetic torque due to a

closer-to-sine-wave air gap flux density waveform, with the d-axis and q-axis being the same. In contrast, interior permanent magnets can produce electromagnetic and reluctance torque because of a flat-top air gap flux density waveform, resulting in different d-axis and q-axis properties. Asgari and Mirsalim (2019) noted that surface-mounted permanent magnets can pose mechanical challenges, as they are more susceptible to dislodging at high perimeter speeds. Consequently, interior and embedded permanent magnet double-stator PMSMs were favored due to their high power density, efficiency, and reduced risk of permanent magnet dislodgement.

Several design parameters can enhance the performance of PMSMs, including the diameter of the copper coil. Qiu et al. (2024) observed that decreasing the number of turns or increasing the copper coil size in a PMSM results in non-linear growth in magnetic density, with local regions exceeding 2T. They also noted that eddy current density and loss vary synchronously in a V-shaped curve with changes in the number of turns. The eddy current loss is minimized at 26 turns and increases by 2 times with a 23% reduction in turns. Therefore, determining the suitable coil size is crucial to maximizing PMSM performance. However, a comparison of various copper sizes for an interior and embedded permanent magnet double-stator PMSM has not yet been presented.

This research investigates the impact of coil diameter on the performance of an interior and embedded permanent magnet double-stator PMSM. An S-shaped permanent magnet is utilized, as it has shown superior performance compared to U-shaped and V-shaped permanent magnets. The coil diameter varies from 0.5 mm to 1.5 mm, and the number of turns is calculated based on it. The performance of the interior and embedded permanent magnet double-stator PMSM is analyzed in terms of generated power using a two-dimensional finite element method.

STRUCTURAL CONFIGURATION AND DESIGN SPECIFICATION

Traditional PMSMs consist of a single stationary and rotating part, leading to lower generated power due to the unutilized space in the middle of the rotor. In contrast, double-stator generators feature two stationary parts and a rotating part, enabling full space utilization and increased power generation as shown in Figure 1. Neodymium iron boron (NdFeB) permanent magnets are chosen for their straightforward construction, low operating costs, and high-power efficiency. Two sizes are employed: 16 mm × 6 mm for embedded permanent magnets and 6 mm × 3 mm for interior permanent magnets. The 16 mm × 6 mm magnets are classified as embedded permanent magnets because one surface faces the air gap, while the 6 mm × 3 mm magnets are categorized as interior permanent magnets because none of their surfaces face the air gap, and the permanent magnet arrangement resembles the shape of a capital “S”. The three-phase PMSM is designed with 45 slots and 30 poles. The specification of the designed PMSM is shown in Table 1.

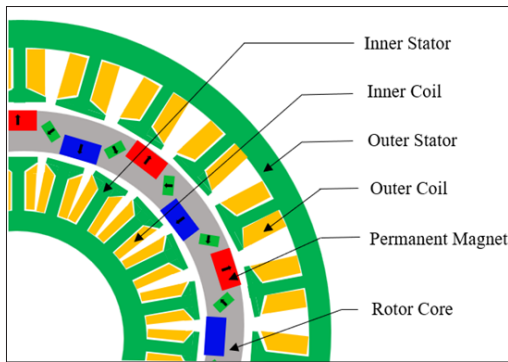


Table 1

Design specification of the designed PMSM

Design Parameter	Value
Inner Diameter [mm]	175
Outer Diameter [mm]	300
Airgap [mm]	3
Slots Number	45
Poles Number	30
Magnet Material	NdFeB
Rotor Core and Stator Material	50H800

Figure 1. Structure of the designed PMSM

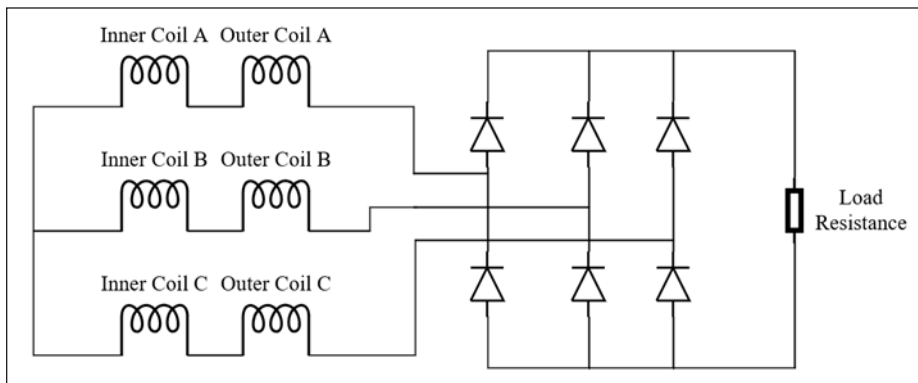


Figure 2. Coil connection of the proposed PMSM

The proposed PMSM consists of an inner coil for the inner stator and an outer coil for the outer stator. Each stator phase has 15 slots, making a total of 45 slots for the complete stator. Each coil is connected in series with the others, and the inner coil and outer coil are also connected in series for each phase, as illustrated in Figure 2. The output of each phase is then connected to a three-phase rectifier to convert the alternating current (AC) to direct current (DC). After the AC to DC conversion, a load resistor is connected and varied from 0.1 ohms to 30 ohms to observe the average power produced by the proposed PMSM.

EVALUATION METHOD

JMAG is a finite element analysis software tailored for the simulation and analysis of electrical machines. It enables the modeling of various operating conditions and facilitates the optimization of designs to enhance performance, efficiency, and reliability. The two-dimensional finite element method is enough to observe the performance of the PMSM, as its accuracy is less than 10% compared to the three-dimensional finite element method,

and simulation can be done in minimal time. The diameter of the copper coil is inversely proportional to the number of turns in each slot and also depends on the coil space of the inner and outer stator. The relationship of the coil diameter with the number of turns and coil space is represented in Equation 1:

$$N = \frac{A_{winding}}{A_{coil}} \times C_{coefficient} \quad [1]$$

where N represents the number of turns, $A_{winding}$ represents the area of winding space in the stator, A_{coil} represents the area of the copper coil, and $C_{coefficient}$ represents the coil coefficient.

To validate the simulation and experimental results, the proposed PMSM was fabricated and assembled according to Figure 3, and the validation results are presented in Figure 4. The model numbers of the equipment used in the experiments are as follows: The motor controller is HPC300 72300, the DC motor is HPM05KW-12-PZ, and the torque sensor is TRB-10K. The fabricated PMSM uses a 1 mm coil diameter for validation, with the coil resistance for each phase measured at 1.04 ohms using an LCR meter (model LCR-8110G). The graph in Figure 4 shows the percentage differences in generated power between the simulation and experimental data, with a difference of 12%. This indicates that the disparities between the simulation and experimental results are relatively minor, suggesting that the simulation results are trustworthy and applicable.

Therefore, the fundamental design parameters are maintained constant, including the number of slots and poles, the size of the proposed PMSM, the air gap, and the permanent

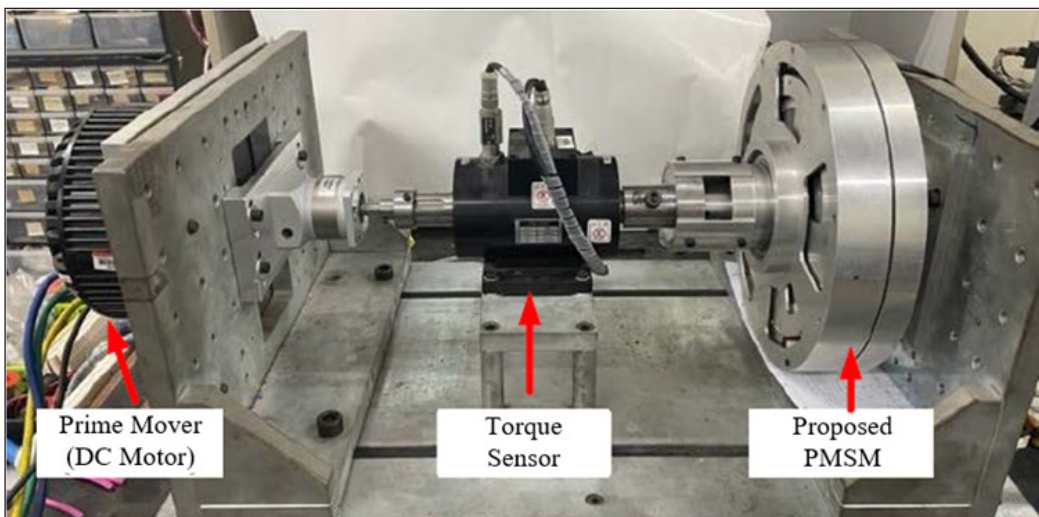


Figure 3. Experimental setup of the proposed PMSM

magnet. The number of turns for the inner and outer stators varies depending on the coil diameter, which ranges from 0.5 mm to 2.0 mm. The specific number of turns for each stator is presented in Table 2. The table indicates that the inner stator has fewer turns than the outer stator due to the limited winding space. Additionally, the number of turns decreases for each stator as the coil diameter increases.

The data includes electrical power measurements and total losses, which were obtained using JMAG-designer software. The average power and power losses represent the electrical power and losses that the proposed generator produces for each load resistance. The maximum average power is the peak power obtained from the graph, as in Figure 5. The efficiency of the power is calculated based on Equation 2:

$$E_{power} (\%) = \frac{P_{max}}{P_{losses} + P_{max}} \times 100 \quad [2]$$

where E_{power} represents the power efficiency, P_{max} represents the maximum average power, and P_{losses} represents the power losses for the proposed generator.

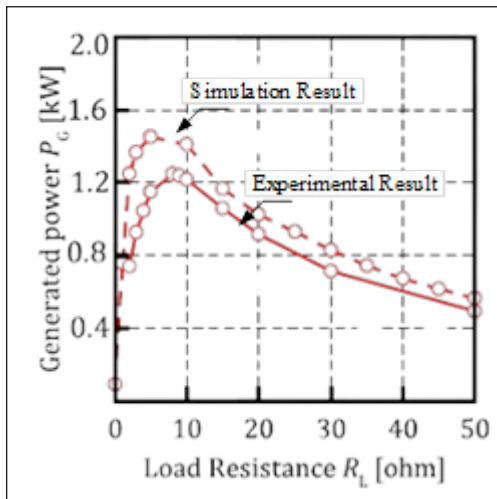


Figure 4. Validation result of proposed PMSM

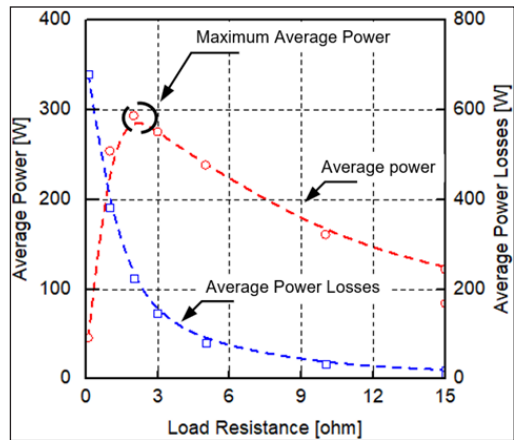


Figure 5. Data evaluation

POWER CHARACTERISTICS FOR DIFFERENT COIL DIAMETERS

Load Variation

The performance of the proposed PMSM is evaluated based on the generated power produced by the PMSM for different loads

Table 2

Number of turns for each coil diameter

Coil Diameter [mm]	Number of Turns	
	Inner Stator	Outer Stator
0.5	52	79
0.75	23	35
1.00	13	20
1.50	6	9
2.0	3	5

and speeds. The load resistance was varied from 0.1 ohms to 30 ohms to observe the effect of coil diameter on the performance of the proposed PMSM. The maximum average power and the load resistance at which the maximum power occurs are recorded and analyzed. Figure 6 illustrates the load variation analysis, with the load resistance on the X-axis and the average power on the Y-axis for speeds of 200 and 800 rpm.

Based on the analysis for speeds of 200 rpm and 800 rpm, the highest average power is achieved with a coil diameter of 1.0 mm for 200 rpm, which is 293 W at a load resistance of 2 ohms and 1662 W with a coil diameter of 1.5 mm at a load resistance of 1 ohm for 800 rpm. Even though the coil diameter of 1.5 mm shows the highest average power at 800 rpm, the slope gradient drastically drops, yielding 800 W at a load resistance of 6 ohms. In contrast, the average power for a coil diameter of 1.0 mm does not drop drastically, to 1500 W at a load resistance of 6 ohms. The results indicate that a larger coil diameter does not necessarily result in higher power output, nor guarantees a lower gradient of the average power slope. Based on the load resistance analysis, the best coil diameters were determined to be 1.0 mm, as they produce more power while maintaining a low gradient of the slope.

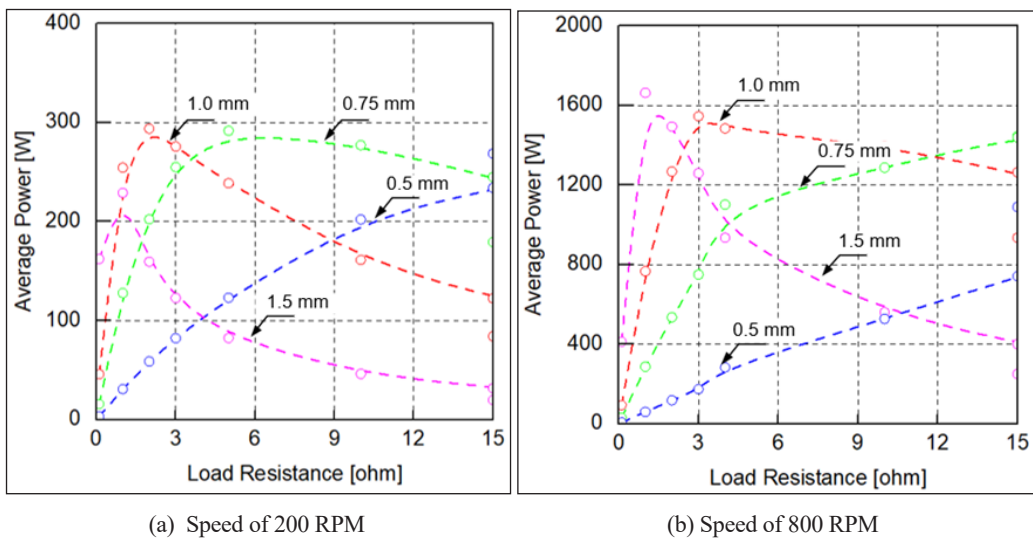


Figure 6. Load variation

Power Efficiency

Power efficiency is crucial for minimizing energy wastage in each coil diameter. Figure 7 illustrates the total power versus speed graph, where the total power comprises the average power and power losses. Analyzing the graph for a coil diameter of 0.5 mm reveals that the power losses generated by the proposed PMSM are nearly equal to the average power at every speed. For instance, at 300 rpm, the power losses amount to 421 W, while the

average power is 464 W. This indicates that a coil diameter of 0.5 mm is unsuitable for the proposed PMSM, as it results in losses comparable to the average power output. In contrast, for coil diameters of 1.0 mm and 1.5 mm, the average power at 800 rpm is 1545 W and 1662 W, respectively, with corresponding power losses of 896 W and 600 W. This suggests that these diameters are more favorable, as they yield higher average power outputs compared to the power losses incurred.

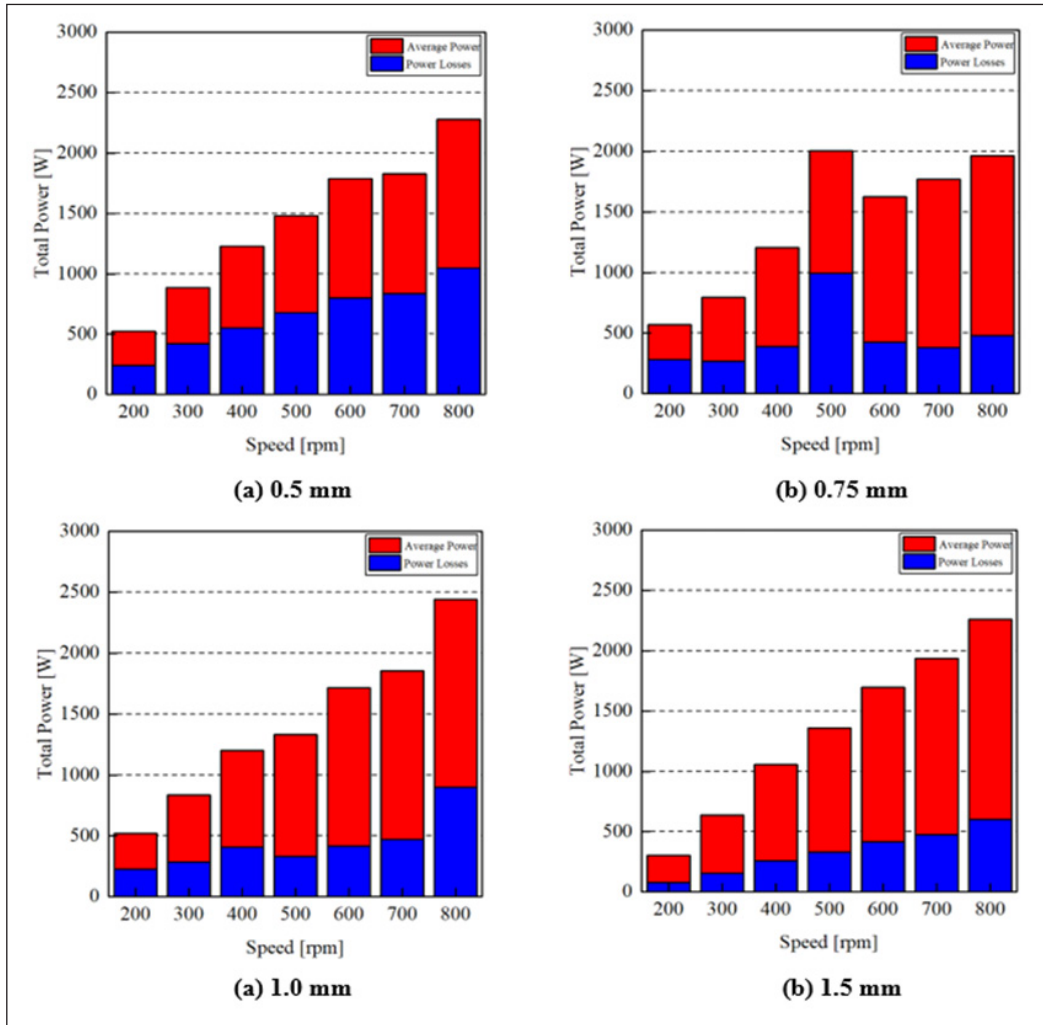


Figure 7. Average power and power losses for each coil diameter

Table 3 shows the power efficiency, which is one of the analyses to observe the performance of the proposed PMSM when varying the coil diameter. The lowest efficient coil diameter is 0.5 mm because it is achieved below 55% for every speed of the proposed

PMSM. Even though 1.5 mm reached 73% and above, it has a drawback: the slope of the graph was very steep when varying the load resistance. The coil diameter of 1.0 mm can be considered the best-performing size because the power efficiency is more than 55% for every speed, ranging from 56% to 75%.

Table 3
Power efficiency for each coil diameter

Speed (rpm)	Power Efficiency (%)			
	0.5 mm	0.75 mm	1.0 mm	1.5 mm
200	53.8	51.0	56.6	75.0
300	52.4	66.7	65.9	75.6
400	55.2	67.7	66.4	75.7
500	54.4	50.5	75.4	75.8
600	55.2	73.7	75.7	75.6
700	54.3	78.5	74.8	75.5
800	54.0	75.5	63.3	73.5

CONCLUSION

The study was conducted using JMAG software and focused on analyzing the performance of a permanent magnet synchronous motor (PMSM) by varying the coil diameter. The relationship between the coil diameter, number of turns, and coil space in the stator was established, indicating an inverse proportionality between the coil diameter and the number of turns per slot. The study maintained constant fundamental design parameters, such as the number of slots and poles, PMSM size, air gap, and permanent magnet properties. The number of inner and outer stator turns varied based on the coil diameter, ranging from 0.5 mm to 1.5 mm. Performance evaluation was conducted by analyzing the generated power under different loads and speeds. The analysis showed that a coil diameter of 1.0 mm achieved the highest average power (293W) at a load resistance of 2 ohms for speeds of 200 rpm and 1662 W at a load resistance of 1 ohms for 800 rpm. Larger coil diameters did not necessarily result in higher power output, and the best-performing coil diameters were found to be 0.75 mm and 1.0 mm, producing more power while maintaining a low gradient of the average power slope. Power efficiency analysis showed that a coil diameter of 1.0 mm performed the best, with power efficiency ranging from 56% to 75% for all speeds, compared to 0.5 mm, which consistently achieved below 55% efficiency, and 1.5 mm, which had efficiency above 73% but exhibited a steep slope in the graph when varying the load resistance.

ACKNOWLEDGEMENT

This work is supported by Universiti Putra Malaysia (UPM) and Ministry of Higher Education (PRGS-5543000).

REFERENCE

- Asgari, S., & Mirsalim, M. (2019). A Novel Dual-stator radial-flux machine with diametrically magnetized cylindrical permanent magnets. *IEEE Transactions on Industrial Electronics*, 66(5), 3605–3614. <https://doi.org/10.1109/TIE.2018.2856211>
- Chau, K. T., Li, Y. B., Jiang, J. Z., & Chunhua, L. (2006). Design and analysis of a stator-doubly-fed doubly-salient permanent-magnet machine for automotive engines. *IEEE Transactions on Magnetics*, 42(10), 3470-3472. <https://doi.org/10.1109/TMAG.2006.879440>
- Liu, C., Chau, K. T., Jiang, J. Z., & Jian, L. (2008). Design of a new outer-rotor permanent magnet hybrid machine for wind power generation. *IEEE Transactions on Magnetics*, 44(6), 1494–1497. <https://doi.org/10.1109/TMAG.2007.916503>
- Feng, C., Cui, S., & Kang, C. (2004). Performance analysis of double-stator starter generator for the hybrid electric vehicle. In *2004 12th Symposium on Electromagnetic Launch Technology* (pp. 499-502). IEEE. <https://doi.org/10.1109/ELT.2004.1398131>
- Gieras, J., Wang, R. J., & Kamper, M. (2008). *Axial Flux Permanent Magnet brushless machines*. Springer Science & Business Media.
- Gul, W., Gao, Q., & Lenwari, W. (2020). Optimal design of a 5-MW double-stator single-rotor PMSG for offshore direct drive wind turbines. *IEEE Transactions on Industry Applications*, 56(1), 216–225. <https://doi.org/10.1109/TIA.2019.2949545>
- Krause, P., Wasynczuk, O., & Sudhoff, S. (2013). *Analysis of electric machinery and drive systems*. John Wiley & Sons, Ltd.
- Li, Y. (2022). Study of the double rotor double machine wind turbine generation system. *Energy Reports*, 8, 85–95. <https://doi.org/10.1016/J.EGYR.2022.05.063>
- Lin, H., Hwang, K. Y., & Kwon, B. Il. (2013). An improved flux observer for sensorless permanent magnet synchronous motor drives with parameter identification. *Journal of Electrical Engineering and Technology*, 8(3), 516–523. <https://doi.org/10.5370/JEET.2013.8.3.516>
- Mehrjou, M. R., Mariun, N., Mison, N., Radzi, M. A. M., & Musa, S. (2017). Broken rotor bar detection in LS-PMSM based on startup current analysis using wavelet entropy features. *Applied Sciences*, 7(8), Article 845. <https://doi.org/10.3390/app7080845>
- Norhisam, M., Norafiza, M., & Sia, C. Y. (2009). Double stator type permanent magnet generator. In *2009 IEEE Student Conference on Research and Development (SCOREd)* (pp. 316-319). IEEE. <https://doi.org/10.1109/SCORED.2009.5443010>
- Qiu, H., Zhang, Y., Yang, C., & Yi, R. (2024). Influence of the number of turns on the performance of permanent magnet synchronous motor. *Bulletin of the Polish Academy of Sciences Technical Sciences*, 68, 429–436. <https://doi.org/10.24425/bpasts.2020.133375>

- Rahman, M. L., Oka, S., & Shirai, Y. (2010). Hybrid power generation system using offshore-wind turbine and tidal turbine for power fluctuation compensation (HOT-PC). *IEEE Transactions on Sustainable Energy*, 1(2), 92–98. <https://doi.org/10.1109/TSTE.2010.2050347>
- Wang, Y., Niu, S., & Fu, W. (2015). Electromagnetic performance analysis of novel flux-regulatable permanent magnet machines for wide constant-power speed range operation. *Energies*, 8(12), 13971–13984. <https://doi.org/10.3390/en81212407>
- Wang, Z. (2008). *Simulation analysis of control system of direct-drive square wave permanent synchronous wind generator*. [Unpublished doctoral thesis]. Tianjin University.
- Wu, F., Zhang, X. P., & Ju, P. (2009). Small signal stability analysis and control of the wind turbine with the direct-drive permanent magnet generator integrated to the grid. *Electric Power Systems Research*, 79(12), 1661–1667. <https://doi.org/10.1016/J.EPSR.2009.07.003>
- Wu, J., Hu, Y., Zhang, B., Feng, G., & Liu, Z. (2022). Comparison and analysis of different rotor structures of double-stator permanent magnet synchronous motor. *IET Electric Power Applications*, 16(6), 685–700. <https://doi.org/10.1049/elp2.12186>
- Yasa, Y., & Mese, E. (2014). Design and analysis of generator and converters for outer rotor direct drive gearless small-scale wind turbines. In *2014 International Conference on Renewable Energy Research and Application (ICRERA)* (pp. 689–694). IEEE. <https://doi.org/10.1109/ICRERA.2014.7016474>
- Zhang, J., Zhang, B., Feng, G., & Gan, B. (2020). Design and analysis of a low-speed and high-torque dual-stator permanent magnet motor with inner enhanced torque. *IEEE Access*, 8, 182984–182995. <https://doi.org/10.1109/ACCESS.2020.3028425>
- Zheng, P., Wu, Q., Bai, J., Tong, C., & Song, Z. (2013). Analysis and experiment of a novel brushless double rotor machine for power-split hybrid electrical vehicle applications. *Energies*, 6(7), 3209–3223. <https://doi.org/10.3390/en6073209>

Psychology-informed Natural Language Understanding: Integrating Personality and Emotion-aware Features for Comprehensive Sentiment Analysis and Depression Detection

Jing Jie Tan, Ban-Hoe Kwan*, Danny Wee-Kiat Ng and Yan Chai Hum

Department of Mechatronics and Biomedical Engineering, Lee Kong Chian Faculty of Engineering and Science, Universiti Tunku Abdul Rahman, 43000, Kajang, Malaysia

ABSTRACT

This paper presents a novel approach to natural language understanding, integrating personality and emotion-aware features for sentiment analysis and depression detection. This research aims to enhance the performance of natural language understanding tasks, specifically sentiment analysis and depression detection, while also promoting explainability by including interpretable insights into psychological factors, such as emotion and personality, that influence these tasks. We refer to this additional feature as the psychology-informed module, alongside attention and transformer models. We achieved a significant improvement in accuracy using only the emotion feature: 3.4% for sentiment analysis on the IMDb dataset and 3.1% for depression detection on the SDCNL dataset. Similarly, using the personality feature led to a 2.5% improvement in sentiment analysis on the Polarity dataset and a 2.9% improvement in depression detection on the SDCNL dataset. On the other hand, the culmination of combining both psychological features achieves an accuracy of 0.8775 and 0.9053 for sentiment analysis on the Polarity and IMDb datasets, respectively. Additionally, notable results were obtained for depression detection, with accuracies of 0.8533 and 0.7177 on the Twitter (now known as X platform) and SDCNL datasets, respectively. These advancements enhance model accuracy and improve explainability, fostering versatile real-world applications. We thoroughly examined the factors, advantages, and limitations associated with this approach (psychology-informed module), providing a

ARTICLE INFO

Article history:

Received: 01 April 2024

Accepted: 10 April 2025

Published: 10 June 2025

DOI: <https://doi.org/10.47836/pjst.33.S4.04>

E-mail address:

tanjingjie@utar.my (Jing Jie Tan)

kwanbh@utar.edu.my (Ban-Hoe Kwan)

ngwk@utar.edu.my (Danny Wee-Kiat Ng)

humyc@utar.edu.my (Yan Chai Hum)

*Corresponding author

comprehensive discussion within the scope of our study. The findings pave the way for future research to explore innovative techniques, further expanding the interdisciplinary impact of psychology-informed natural language understanding.

Keywords: Depression detection, emotion-aware recognition, machine learning, natural language processing, natural language understanding, personality-aware recognition, psychology-informed models, sentiment analysis

INTRODUCTION

In the contemporary digital era, Natural Language Understanding (NLU) is rapidly advancing and finding versatile applications in diverse domains such as recommendation systems, depression detection, sentiment analysis, and more. As we witness the growing influence of NLU in shaping technology-driven solutions, a compelling question arises: Can integrating psychological insights into text analysis enhance its performance?

Prior work has focused on enhancing sentiment classification performance in textual messages through integrating personality recognition (Tan et al., 2023). Building upon this foundation, the current study delves deeper into the potential synergy between Natural Language Understanding (NLU) and psychology. This research aims to improve model performance by incorporating psychological information (referred to as the psychology-informed module) into text analysis, contributing to more nuanced and enhanced outcomes. Subsequently, this research study examines the significance of improvements in this approach compared to the baseline using statistical testing.

By delving into the intricacies of human emotion, personality, and cognitive processes, we seek to elevate the capabilities of NLU, paving the way for more nuanced and contextually aware applications. This exploration is motivated by the belief that a deeper understanding of the psychological dimensions within language can unlock new possibilities for refining the accuracy and effectiveness of NLU systems in various real-world scenarios.

Incorporating a psychology-informed module enhances the performance of natural language understanding tasks. It promotes explainability by providing interpretable insights into the underlying psychological factors influencing sentiment analysis and depression detection. This emphasis on transparency contributes to a more trustworthy and comprehensible framework for decision-making in NLU applications. This approach holds unlimited potential; for instance, in real-time, harnessing emotions not only improves depression detection but also facilitates context-aware emotion labelling or user personality labelling, empowering the algorithm to deliver personalized recommendations to other users, thus achieving a dual benefit with a singular, versatile approach.

LITERATURE REVIEW

Psychology Informed Model

This research defines the psychology-informed model as a classical model enhanced with a psychology-informed module, incorporating features derived from personality recognition and emotion recognition.

Personality Recognition

Various personality theories propose distinct dimensions (Cervone & Pervin, 2022), including the Eysenck Personality Questionnaire (EPQ) with the Big-3 model (Eysenck & Eysenck, 1975), the Myers-Briggs type indicator (MBTI) represents the Big-4 model, and the widely accepted Big-5 model encompasses "openness, conscientiousness, extraversion, agreeableness, and neuroticism" (OCEAN) (Goldberg, 1993). Additionally, the Big-6 model, incorporating "honesty-humility, emotionality, extraversion, agreeableness, conscientiousness, and openness" (HEXACO) (Ashton et al., 2004) provides another perspective on personality dimensions. According to Moreno et al. (2021), personality traits of an individual are shown in his or her written text.

Mairesse et al. (2007) made a significant contribution by conducting a state-of-the-art research focused on psycholinguistic features. Their study on the Essays corpus employed correlational analysis to identify key features influencing personality classification. In addition, Sun et al. (2019) justified topic word extraction through lexicons and word2vec for measuring personal traits in specific aspects using user-generated text. These techniques demonstrate significant diversity among individuals in affect and social interaction, revealing correlations with personality traits. In addition, transformer embedding includes Bidirectional Encoder Representations from Transformers (BERT) with SenticNet (a psychological lexicon), which shows improvement in personality recognition (Ren et al., 2021). These show the potential of personality recognition to improve the natural language understanding model.

Emotion Recognition

Emotions serve as immediate indicators of our psychological state. Circumplex Model of Affect is a widely acknowledged framework that categorizes emotions within a two-dimensional space defined by valence (pleasant-unpleasant) and arousal (low-high), offering a structured representation of diverse emotional experiences and their relationships (Posner et al., 2005). The seven common emotions are joy, anger, fear, surprise, sadness, disgust, and contempt. However, we can further fine-grain emotions such as admiration, love, and others. Hence, several datasets such as the ISEAR dataset (Scherer & Wallbott, 1994), the DENS dataset (C. Liu et al., 2019), and the GoEmotions dataset (Demszky et

al., 2020) featured varying numbers of classes, commonly utilized in emotion machine learning research.

Notably, for concise text, long short-term memory (LSTM) demonstrates superior performance with an accuracy of 97.50%, surpassing Linear Support Vector Classifier, which achieves only 89% (Alfarizi et al., 2022). Subsequent advancements involve transformer embeddings, revealing enhanced results with accuracy scores of 0.7431, 0.7299, 0.7009, and 0.6693 for its variations, namely RoBERTa, XLNet, BERT, and DistilBERT, respectively (Adoma et al., 2020). Therefore, this study delves into evaluating the efficacy of extracting emotional information features from transformer models as opposed to traditional statistical models.

Natural Language Understanding

To validate our hypothesis, which incorporates insights from psychological information, specifically personality and emotion, we focus on two natural language understanding tasks: sentiment analysis and depression detection.

Sentiment Analysis

In today's digital age, understanding and effectively classifying sentiments expressed in textual messages has become crucial for a wide range of applications. Sentiment analysis plays a pivotal role in enhancing various aspects of communication, business, and social interactions. (Yang et al., 2020; Yarkoni, 2010; Lin et al., 2017). It involves binary classification tasks, commonly applied to datasets that include movie reviews from movie and shopping platforms such as IMDb (Maas et al., 2011a) and Amazon Review (Keung et al., 2020).

Researchers explored the combination of lexicon-based methods and neural networks for sentiment analysis, achieving comparable accuracy of 90% when employing a recurrent neural network (RNN) and their variant, long short-term memory (LSTM), on the IMDb dataset (Qaisar, 2020; Shaukat et al., 2020). Meanwhile, on the Amazon Review dataset, a TF-IDF approach with logistic regression yielded an accuracy of 0.9; similarly, a BERT model achieved a comparable level of accuracy (Durairaj & Chinnalagu, 2021; Rajat et al., 2021). The observed identical accuracies prompt a consideration for potentially adopting a more efficient or lightweight approach to achieve similar results in sentiment analysis tasks.

Depression Detection

Depression detection models are significant as a screening tool to facilitate early treatment (Souza Filho et al., 2021). According to Havige et al. (2019), there is a strong positive correlation between a written message and the risk or the degree of depression in an individual. Hence, research has shown the possibility of detecting a person's depression

based on a text message that he or she posted or commented on. A study on postpartum depression also supported that the linguistic style in a message's content is a major indicator that is able to predict whether a person has depression or not (De Choudhury et al., 2014). There are widely used datasets, such as the Reddit and SDCNL datasets, which were collected through web scraping from users' self-reports on social media platforms (Haque et al., 2021; Yates et al., 2017).

Choudhury et al. (2016) proved the positive correlation between emotion and linguistic style labelled by LIWC and depression. Using a support vector machine classifier, the overall depression detection accuracy is 0.68. According to Kamal et al. (2018), the highest accuracy achieved in depression classification is 0.73 using the decision tree algorithm.

Tadesse et al. (2019) explored various combinations of lexicon features and models, finding that the combination of linguistic inquiry and word count (LIWC) + Latent Dirichlet Allocation (LDA) + bigram with a multi-layer perceptron (MLP) classifier achieved a noteworthy 91% accuracy. This underscores the significance of incorporating psychological insights, as lexicons carry nuanced meanings. Additionally, Figuerêdo et al. (2022) conducted further experiments, revealing that the semantic mapping of emoticons resulted in a 0.05 improvement in F1 score, highlighting the potential impact of emotion in text on depression detection.

METHODS

We aim to enhance natural language understanding (NLU), specifically in sentiment and depression classification, by integrating a classical NLU model with a psychology-informed module, incorporating personality recognition and/or emotion recognition results. This integration provides additional insights into the psychological status of the classifier. Our experiments encompass various combinations, including utilizing psychology-informed models and datasets, to enhance the overall performance of the classification tasks.

As illustrated in Figure 1, we commence the process by training a psychology-aware model to achieve this. This model will then generate psychological features for subsequent NLU model training. Finally, we employ this model for evaluation.

The related resources (algorithm repository and split datasets for reproducibility) are all in one place: <https://research.jingjietan.com/?q=PSYCHONLU>.

Datasets

Table 1 provides an overview of the datasets utilized in this research. Two widely recognized and relevant datasets were selected for each model's task domain. This choice allows for a comparative analysis that may offer additional evidence to support the research hypothesis. Selection criteria focused on datasets with an average size of approximately 1,000 to 100,000 records—ideal for training and analysis without being excessively large.

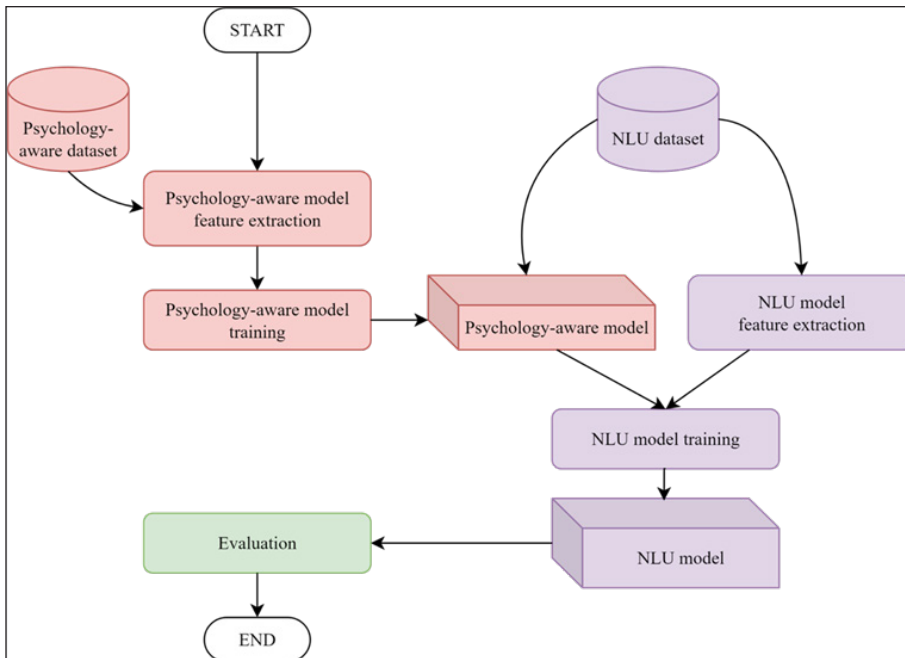


Figure 1. The block diagram of the proposed model architecture

Table 1
The datasets used in the experiments

Type	Model Task	Dataset	Description & Splitting
Psycho	Personality Recognition	Kaggle-MBTI-PersonalityCafe (Mitchell, 2017)	The dataset was gathered from Reddit and comprises documents labelled with MBTI (Myers-Briggs Type Indicator) types, which include 16 specific types or four binary labels. https://huggingface.co/datasets/jingjietan/kaggle-mbti (Tan, 2024b)
		Reddit-MBTI (Deimann et al., 2023)	The dataset, available upon request, was gathered from Reddit and consists of documents labelled with MBTI types, encompassing 16 distinct personality types or four binary category labels.
	Emotion Recognition	GoEmotions (Demszky et al., 2020)	Gathered from Reddit, this dataset includes text and categorizes it into 27 distinct emotions and a neutral category. https://huggingface.co/datasets/willcb/go-emotion (Demszky et al., 2020)
		CombinedDataset (Hartmann, 2022)	Merged from six open datasets, this combined dataset was refined by removing certain classes, resulting in a final set of seven classes. https://huggingface.co/j-hartmann/emotion-english-distilroberta-base (Hartmann, 2022)

Table 1 (continue)

Type	Model Task	Dataset	Description & Splitting
NLU	Sentiment Analysis	Polarity (v2.0) (Pang & Lee, 2004)	Comprising 1,000 movie review comments, this dataset is labelled with positive or negative sentiments. https://huggingface.co/datasets/jingjietan/polarity-sentiment (Tan, 2024c)
		IMDb (Maas et al., 2011a)	Composed of 50,000 comments on movie reviews, expressed in positive or negative terms. https://huggingface.co/datasets/jingjietan/imdb-sentiment (Tan, 2024a)
	Depression Detection	Twitter (now known as X) (Shinde, 2022)	Derived from Twitter posts, this dataset consists of 20,000 entries labelled as either indicating depression or not. https://huggingface.co/datasets/jingjietan/twitter-depression (Tan, 2024e)
		SDCNL (Haque et al., 2021)	Gathered from 1,895 Reddit posts, this dataset is labelled based on the presence of suicide intent. https://huggingface.co/datasets/jingjietan/sdcnl-suicide (Tan, 2024d)

Psychology-informed Modelling

We utilize the model parameters from the paper or train the model using the prepared dataset.

Personality Recognition

We employ the Kaggle-MBTI-PersonalityCafe dataset to train a **TF-IDF** model. TF-IDF (term frequency-inverse document frequency) is a numerical representation of the importance of a word in a document within a collection of documents, emphasizing terms that are frequent in a specific document but rare across the entire collection (Aizawa, 2003). The four binary features: I/E, S/N, T/F, or P/J represent distinct dimensions of the Myers-Briggs type indicator (MBTI), capturing preferences in terms of introversion/extraversion (I/E), sensing/intuition (S/I), thinking/feeling (T/F), and judging/perceiving (J/P), respectively (Sonmezoz et al., 2020). The formula for TF-IDF is represented by Equation 1, where tf_s represent the frequency of the term t in document s , while N is the number of documents in d , and df_t is the number of documents containing the term t .

$$TF - IDF(t, s) = TF(t, s) \times IDF(t) = tf_s \times \ln \frac{N}{df_t} \quad [1]$$

Here, we have prepared four binary classifiers, each producing a label for an MBTI dimension. The data pre-processing involves text cleaning to remove irrelevant links and symbols, followed by tokenization, as in Algorithm I.

Algorithm I: Data Pre-processing

Input: Dataset D
 Regex for link $R_LINK \leftarrow https?://[^s<>"]+|www\.[^s<>"]+$
 Regex for symbol $R_SYMBOL \leftarrow "[^0-9a-z]"$

Output Dataset D

- 1 # Assume N dimension is available in this dataset
GET texts **FROM** D_d
- 2 # Loop all the text
FOR $text \in$ texts **DO**:
- 3 $text \leftarrow$ Lower($text$)
- 4 $text \leftarrow$ regex.sub(R_LINK , , $text$).sub(R_SYMBOL , , $text$)
- 5 $text \leftarrow$ text.split()
- 6 **ENDDO**
- 7 **RETURN** D

We process both the training set and test set using the same tokenizer. Subsequently, we compute the TF-IDF for each word in the dataset, resulting in floating-point values. To maintain consistent input lengths for the neural network model, we set the maximum length to 5000. The Algorithm II outlines the training process for the multilayer perceptron model.

Algorithm II: Multilayer Perceptron Model Training

Input: Dataset D
 Model, M
 Hyperparameter ($epochs, \theta \dots$)

Output Model, M

- 1 **FOR** ($text, label$) \in (D_{text}, D_{label}) **DO**:
- 2 **SET** $text, label$ **TO** trainloader
- 3 **FOR** e **IN** $epochs$
- 4 **FOR** $inputs, targets$ **IN** trainloader
- 5 $outs \leftarrow$ FeedForward($M, inputs$)
- 6 $loss \leftarrow$ Loss($outs, targets$)
- 7 **UPDATE** $M, M \leftarrow M - \theta \frac{\partial L(\hat{y}, y)}{\partial M}$ # Back propagate with learning rate θ :
- 8 **ENDDO**
- 9 **ENDDO**
- 10 **ENDDO**
- 11 **RETURN** M

We prepared a model utilizing the parameters that were pre-trained from ALBERT (Robert Deimann et al., 2023) using the Reddit-MBTI Dataset. ALBERT (A Lite BERT) addresses challenges in scaling up model size during pretraining, offering parameter-reduction techniques to enhance memory efficiency and training speed (Lan et al., 2019). This model is a multiclass model that outputs the probability for each MBTI class.

The overall process begins with data cleaning and removing HTML tags and irrelevant information, as outlined in Algorithm I. Subsequently, we utilize the tokenizer from the respective transformer to tokenize the text. Finally, we feed the tokenized values into the transformer model, including the output layer, to obtain the informed features.

There are two ways to incorporate psychology-informed features. First, with ALBERT-first, we use the highest probability as the recognition output, such as INFP, resulting in four binary features with values of 0 or 1. Second, we included all classes as features with the **ALBERT-list**, resulting in 16 features, each corresponding to an MBTI type, such as INFP.

Emotion Recognition

Likewise, we employ Algorithm I and Algorithm II in personality recognition to train a **TF-IDF** model on the GoEmotions dataset. We also included three additional models, producing psychology-informed results using parameters from transformer models, as detailed in Algorithm III.

Algorithm III: Model Inference from Pretrained or Referenced Model

Input: Dataset D_{in}

Output Dataset D_{out}

- ¹ **MAKE** *tokenizer* **FROM** *vocabulary*
- ² **CONSTRUCT** *model* **USING** *pretrained or referenced parameters*
- ³ $D_{tokenise} \leftarrow tokenizer(D_{in})$
- ⁴ $D_{out} \leftarrow tokenizer(D_{tokenise})$
- ⁵ **RETURN** D_{out}

Firstly, we employ the **BERT** model parameters fine-tuned by Raw (2021) on the CombinedDataset, yielding six emotion feature labels. BERT is a transformer model developed by Devlin et al. (2018) that represents a cornerstone in natural language processing due to its versatility and effectiveness in capturing contextual information in text.

Next, we leverage RoBERTa, an optimized transformer model utilizing dynamic masking during pretraining. This alteration enhances the model's capture of contextual information, improving performance across various natural language processing tasks (Y.

Liu et al., 2019). This model has two variations: the distilled (light) version, **DistilRoBERTa** and the standard **RoBERTa**. For the former, reconstructing with parameters from Hartmann (2022) results in a 7-class multiclass output. Subsequently, utilizing Lowe's (2023) model parameters, we obtain a 28-multilabel model.

Natural Language Understanding

Despite the availability of various feature extraction methods and models for NLU tasks, we opted for TF-IDF and a multilayer perceptron to ensure a fair comparison. We utilize the psychology-informed models mentioned above to generate features for NLU, specifically for **sentiment analysis** and **depression detection**. These features serve as additional support alongside the traditional data cleaning and TF-IDF feature extraction processes outlined in Algorithm I. The resulting 5000 features are concatenated with the psychology features and fed into a neural network, as illustrated in Figure 2.

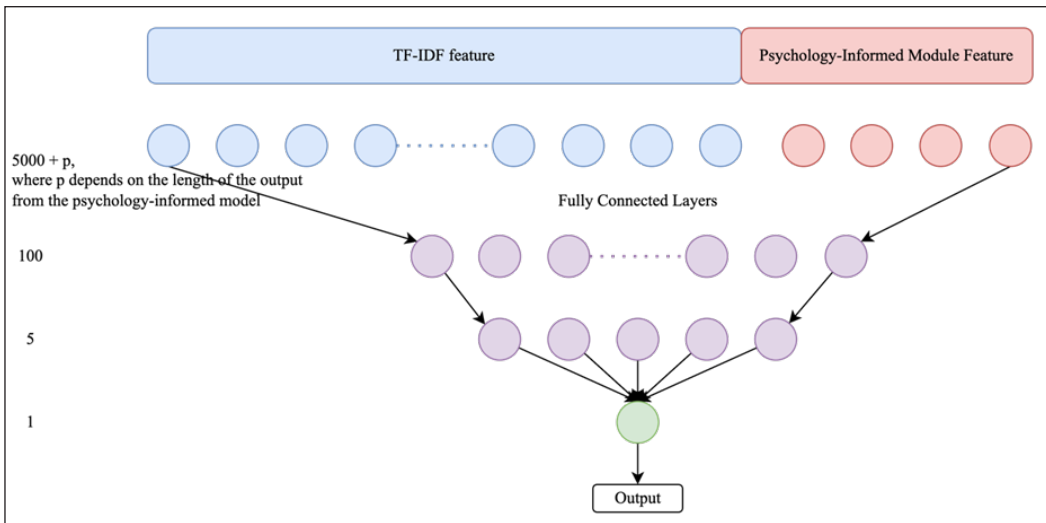


Figure 2. Illustration of combining psychology-informed model features with TF-IDF for multilayer perceptron (MLP) training by concatenation: e.g., the four personality outputs (represented by red circles) are included alongside TF-IDF features (represented by blue circles) for sentiment analysis

However, the concatenation process does impact the total number of parameters. Nevertheless, we have found that its impact is negligible, as the additional features contribute minimally. The mathematical proof is provided below:

The number of parameters between layers is $= n^{[l]} \times n^{[l+1]} + n^{[l+1]}$, where $n^{[0]}$ indicates the number of neurons in layer l .

Hence, the equation is to ensure an equal number of parameters for the normal model and the psychology-informed model, as shown in Equation 2:

$$\begin{aligned} & \left(n_{norm}^{[0]} \times n_{norm}^{[1]} + n_{norm}^{[1]} \right) + \left(n_{norm}^{[1]} \times n_{norm}^{[2]} + n_{norm}^{[2]} \right) \\ & = \left(n_{psyc\ ho}^{[0]} \times n_{psyc\ ho}^{[1]} + n_{psyc\ ho}^{[1]} \right) + \left(n_{psyc\ ho}^{[1]} \times n_{psyc\ ho}^{[2]} + n_{psyc\ ho}^{[2]} \right) \end{aligned} \quad [2]$$

Then, by arranging,

$$\begin{aligned} n_{psyc\ ho}^{[1]} = & \\ & \frac{\left(n_{norm}^{[0]} \times n_{norm}^{[1]} + n_{norm}^{[1]} \right) + \left(n_{norm}^{[1]} \times n_{norm}^{[2]} + n_{norm}^{[2]} \right) - n_{psyc\ ho}^{[2]}}{1 + n_{psyc\ ho}^{[2]} + n_{psyc\ ho}^{[0]}} \end{aligned} \quad [3]$$

As shown in Figure 2, substituting for the normal case values, where the input features, $n_{norm}^{[0]}$ is set to 5000, and the first hidden layer, $n_{norm}^{[1]}$, is set to 100. For input features of the psychology-informed model, it is the summation of TF-IDF features and psychology-informed features, denoted as $n_{psyc\ ho}^{[0]}$, equal to 5000 + 28, (28 being the highest number of features throughout the experiments. Lastly, the second hidden layer is the same for both models, $n_{norm}^{[2]} = n_{psyc\ ho}^{[2]} = 5$.

$$n_{psyc\ ho}^{[1]} = \frac{(5000 \times 100 + 100) + (100 \times 5 + 5) - 5}{1 + 5 + 5028} = 99.44 \approx 99 \quad [4]$$

From Equation 3, the suggested number of neurons is rounded to 99 (the normal setting is 100, which is not significantly different). We conducted experiments to further examine this setting and observed no noteworthy impact.

Evaluation

Lastly, the experiment was designed with a data split of 80% for training and 20% for testing, where the training set was further divided into an 80:20 ratio for the training set and the validation set. The test set remains invisible during training. The evaluation metric used is accuracy, formulated as Equation 5, where TP represents True Positive, TN is True Negative, FP is a False Positive, and FN is False Negative.

$$Accuracy = \frac{\text{number of correct prediction}}{\text{number of sample}} = \frac{TP + TN}{TP + TN + FP + FN} \quad [5]$$

Moving on, to demonstrate the significance of the proposed psychology-informed module, we employ the McNemar test—a statistical method for analyzing paired categorical

data (Smith & Ruxton, 2020). This test helps assess whether the intervention (the proposed psychology-informed module) leads to a statistically significant change in the model's classification outcomes (e.g., correct vs. incorrect predictions) compared to the performance with and without the module.

The null hypothesis (H_0) and alternative hypothesis (H_1) for the McNemar test are formulated as follows:

- **Null Hypothesis (H_0):** There is no significant difference in the outcomes of the model with and without the psychology-informed module.
- **Alternative Hypothesis (H_1):** There is a significant difference in the outcomes of the model with and without the psychology-informed module, indicating that the module leads to a significant change in the outcomes.

The McNemar test specifically examines the count of discordant pairs in the data, cases where outcomes differ between the two conditions. The test statistic, χ^2 , is calculated as shown in Equation 6:

$$\chi^2 = \frac{(b - c)^2}{b + c} \quad [6]$$

where:

- b is the number of cases where the model's prediction was correct before the addition of the psychology-informed module but incorrect after,
- c is the number of cases in which the prediction was incorrect before the addition of the psychology-informed module, but was correct after.

To evaluate statistical significance, we calculate the p-value using the cumulative distribution function (CDF) of the chi-squared distribution with degrees of freedom (df) set to 1, using Equation 7:

$$p = 1 - CDF(\chi, df = 1) \quad [7]$$

We then compare the p-value to a common significance level, $\alpha = 0.05$. If the p-value is less than 0.05, we reject the null hypothesis, indicating that the psychology-informed module has a statistically significant effect on the model's outcomes. Conversely, suppose the p-value is greater than or equal to 0.05. In that case, we fail to reject the null hypothesis, suggesting insufficient evidence to conclude that the module significantly affects model performance.

RESULTS AND DISCUSSION

The results are presented in a table, highlighting the improvements achieved by the proposed psychology-informed module compared to the regular method. Improvements with a highly significant p-value ($p \leq 0.01$) are indicated with an asterisk in **bold***. Additionally, improvements with a p-value between 0.01 and 0.05 ($0.01 < p < 0.05$) are also shown in **bold**. Any outcomes that do not show a significant improvement (where the null hypothesis is not rejected) are displayed in regular font, indicating no statistically significant difference between the model with and without the psychology-informed module.

Sentiment Analysis

As evident in Tables 2 and 3, there is a notable improvement in sentiment classification achieved through applying psychology-informed modules. Nevertheless, the Polarity dataset is smaller ($\sim 25\times$ smaller) compared to the IMDb dataset, which may lead to certain models failing to meet the statistical significance threshold for the hypothesis.

Table 2

Sentiment analysis results with personality-aware techniques

Dataset	Personality-aware Model	Accuracy	Improvement
Polarity	Regular (None)	0.8375	-
	TF-IDF	0.8625	0.0250
	ALBERT (list)	0.8525	0.0150
	ALBERT (first)	0.8600	0.0225
IMDb	Regular (None)	0.8710	-
	TF-IDF	0.8854	0.0144*
	ALBERT (list)	0.8740	0.0030
	ALBERT (first)	0.8845	0.0135*

Table 3

Sentiment analysis results with emotion-aware techniques

Dataset	Emotion-aware Model	Accuracy	Improvement
Polarity	Regular (None)	0.8375	-
	TF-IDF	0.8600	0.0225
	BERT	0.8600	0.0225
	RoBERTa	0.8600	0.0225
	DistilRoBERTa	0.8650	0.0275
IMDb	Regular (None)	0.8710	-
	TF-IDF	0.8923	0.0213*
	BERT	0.8748	0.0038*
	RoBERTa	0.9051	0.0341*
	DistilRoBERTa	0.8929	0.0219*

However, some psychology-informed modules still yield p-values less than 0.05, indicating a statistically significant impact, albeit at a lower confidence level. This is sufficient to demonstrate the effectiveness of the module within the smaller dataset. In contrast, the IMDb dataset shows stronger significance, with most models achieving p-values well below 0.05, further validating the module's effectiveness in a larger dataset.

Moving on, particularly noteworthy is the observation that emotion-aware models exhibit more substantial enhancements compared to their personality-aware counterparts. Specifically, the RoBERTa model, when applied to the IMDb dataset, demonstrates a notable improvement of 3.4%. This significant boost can be attributed to its capacity to tabulate 28 classes of emotion in probability, providing the model with valuable information for determining the overall sentiment.

In contrast, the performance of the BERT model in the IMDb dataset, which outputs six classes of features, shows the lowest accuracy. A similar limitation is observed with DistilRoBERTa, which outputs seven classes, merely 1% away from the more comprehensive RoBERTa model. This constraint in class representation underscores the significance of having a more extensive set of classes, influencing the model's capacity to discern nuanced sentiments in complex textual data.

Next, the RoBERTa and DistilRoBERTa emotion-aware models do not exhibit a significant difference in accuracy on the Polarity dataset. Upon further examination of both datasets, it is evident that the text in the Polarity dataset is relatively shorter (~4x) than that in the IMDb dataset. This difference leads to the conclusion that the information from the psychology-informed model does not have a substantial impact, as it is likely insufficient for the model to conduct a deep analysis of emotion. This explanation clarifies why the DistilRoBERTa model, which outputs seven features, performs similarly to the RoBERTa model, which outputs 28 features in the Polarity dataset.

Additionally, it is essential to note that transformer-based psychology-informed models do not manifest a significant improvement over the TF-IDF method. This observation underscores the notion that a sophisticated psychology-informed model is unnecessary to achieve enhanced accuracy. Nevertheless, using RoBERTa and DistilRoBERTa typically yields better results than the BERT model in psychology-informed applications, as they benefit from enhanced training strategies, including larger datasets and extended training periods without the Next Sentence Prediction task (Y. Liu et al., 2019).

Depression Detection

As evident in Tables 4 and 5, there is a notable improvement in depression detection achieved through the application of psychology-informed modules. Nevertheless, the Twitter dataset is approximately 10 times larger compared to the SDCNL dataset. This larger sample size enhances the statistical power of the analysis, making it more likely to

detect significant differences. As a result, the models on the Twitter dataset exhibit stronger statistical significance, with p-values well below the threshold of 0.05, indicating a clear and meaningful impact of the psychology-informed module. In contrast, the smaller SDCNL dataset may not provide enough data to achieve similar levels of statistical significance, which might result in less pronounced findings.

Table 4
Depression detection results with personality-aware techniques

Dataset	Personality-aware Model	Accuracy	Improvement
Twitter	Regular (None)	0.8485	-
	TF-IDF	0.8523	0.0037
	ALBERT (list)	0.8515	0.0030
	ALBERT (first)	0.8525	0.0040*
SDCNL	Regular (None)	0.6834	-
	TF-IDF	0.7071	0.0237
	ALBERT (list)	0.6939	0.0106
	ALBERT (first)	0.7124	0.0290

Table 5
Depression detection results with emotion-aware techniques

Dataset	Emotion-aware Model	Accuracy	Improvement
Twitter	Regular (None)	0.8485	-
	TF-IDF	0.8555	0.0070*
	BERT	0.8505	0.0020
	RoBERTa	0.8540	0.0055*
	DistilRoBERTa	0.8560	0.0075*
SDCNL	Regular (None)	0.6834	-
	TF-IDF	0.7098	0.0264
	BERT	0.6939	0.0106
	RoBERTa	0.7018	0.0185
	DistilRoBERTa	0.7150	0.0317

In both datasets, it is generally observed that ALBERT (list) consistently performs worse than ALBERT (first). This discrepancy can be attributed to the distinction between the personality-aware and emotion-aware models. The former necessitates using only the highest possible value, as individuals typically belong to one personality type. In contrast, an emotion-aware model acknowledges the potential coexistence of multiple emotions simultaneously. For instance, in scenarios like a birthday party context, emotions such as surprise and joy can co-occur.

Additionally, the BERT model shows little improvement compared to the DistilRoBERTa model, which outputs 28 emotion probabilities. This observation underscores, once again,

the importance of having a sufficient number of generated features from psychology-informed modules.

Personality Recognition

In addition, personality recognition is considered part of Natural Language Understanding (NLU), with emotion as the psychology-informed module. This approach is based on the premise that emotions expressed in a given context can potentially reflect aspects of an individual's personality. Table 6 illustrates the potential of leveraging emotion for MBTI classification, with results typically showing significant improvements in certain personality dimensions, particularly in the **P/J** (perceiving/judging) and **T/F** (thinking/feeling) dimensions. These dimensions are more likely to be influenced by the emotion-based insights, highlighting the value of incorporating emotional context into personality recognition models.

Table 6
Personality recognition results with emotion-aware techniques

Personality Dimension	Emotion-aware Model	Accuracy	Improvement
S/N	Regular (None)	0.8818	-
	RoBERTa	0.8835	0.0017
	DistilRoBERTa	0.8888	0.0068
P/J	Regular (None)	0.7608	-
	RoBERTa	0.7740	0.0133*
	DistilRoBERTa	0.7671	0.0063
I/E	Regular (None)	0.8249	-
	RoBERTa	0.8251	0.0002
	DistilRoBERTa	0.8329	0.0081
T/F	Regular (None)	0.8104	-
	RoBERTa	0.8202	0.0098*
	DistilRoBERTa	0.8294	0.0190*

However, it is crucial to note that further experiments are needed to better understand why certain personality traits contribute more strongly to emotional expression, especially when considering factors such as dataset imbalance and the data collection method. For example, individuals with certain personality types may be less inclined to post on social media, resulting in a lower representation of these personality types in the dataset. This imbalance can influence the model's ability to generalize and may lead to skewed results, underscoring the need for additional research to account for these factors.

Benchmark

To obtain the final evaluation of the model, we combine two psychology-informed features: personality (ALBERT (first)) and emotion (RoBERTa). The improvement is tabulated based on the highest accuracy achieved by a single model, as shown in Equation 8.

$$\begin{aligned} \textit{improvement} = & \textit{accuracy}_{\textit{combine}} \\ & - \max(\textit{accuracy}_{\textit{regular}}, \textit{accuracy}_{\textit{personality}}, \textit{accuracy}_{\textit{emotion}}) \end{aligned} \quad [8]$$

Table 7 shows that the improvement is relatively limited when combining personality and emotion modules, lacking significant significance compared to the individual (only personality or emotion module) models. Nonetheless, the Polarity dataset shows a noteworthy improvement of 1.7% (p-value = 0.10), which, while marginally above the typical significance threshold, is considered meaningful given the dataset's limited size. This finding suggests potential in the psychology-informed models for short text lengths. It highlights the need for further investigation in future work to better understand the model's performance on brief text data. Nevertheless, all observed improvements for psychology-informed NLU models are statistically significant compared to the regular approach models.

Table 7

Proposed approach: Psychology-informed NLU (Personality-aware (ALBERT) + Emotion-aware (RoBERTa))

Dataset	Reference Accuracy			Accuracy (Personality- aware (ALBERT) + Emotion-aware (RoBERTa))	Improvement	
	Regular (None)	Personality (ALBERT (first))	Emotion (RoBERTa)		Compared to Regular (None)	Compared to Single Feature (Personality or Emotion) (Best)
Polarity	0.8375	0.8600	0.8600	0.8775	0.0400	0.0175
IMDb	0.8710	0.8845	0.9051	0.9053	0.0343*	0.0002
Twitter	0.8485	0.8525	0.8540	0.8553	0.0068*	0.0013
SDCNL	0.6834	0.7124	0.7018	0.7177	0.0343	0.0053

Last but not least, we tabulate results from other researchers in Table 8 for comparative analysis. This comparison reaffirms that psychology-informed models demonstrate the capability to enhance accuracy, even when compared to heavy transformer models.

Even with a simple TF-IDF-based psychology-informed model, such as emotion-aware recognition for sentiment analysis on the IMDB dataset, our approach achieves an accuracy of 0.8923 (refer to Table 3), surpassing the 0.8905 achieved by the benchmark ALBERT

model (refer to Table 8). Notably, our approach maintains superiority with significantly lower computational costs due to its lightweight design. This underscores the potential effectiveness of integrating psychological insights into the NLU framework for improved performance.

Table 8

Benchmark comparison of proposed approach: Psychology-informed NLU (Personality-aware (ALBERT) + Emotion-aware (RoBERTa))

Dataset	Approach	Accuracy
Polarity	Proposed Psychology-Informed Approach	0.8775
	Support Vector Machine (SVM) + Information Gain (Maulana et al., 2020)	0.8565
	Bernoulli Naive Bayes (Rahman & Hossen, 2019)	0.8750
	Radial Basis Function (Maulana et al., 2020)	0.8305
IMDb	Proposed Psychology-Informed Approach	0.9053
	ALBERT (Ding et al., 2021)	0.8905
	LSTM (Qaisar, 2020)	0.8990
	Gate Recurrent Unit (Ding et al., 2021)	0.8631
	Logistic Regression (Qaisar, 2020)	0.8914
	Max Entropy Random Forest (Das & Chakraborty, 2018)	0.8991
Twitter	Proposed Psychology-Informed Approach	0.8553
	Gaussian Naive Bayes (Celebi, 2023)	0.7722
	Multinomial Naïve Bayes (Deshpande & Rao, 2017)	0.8300
SDCNL	Proposed Psychology-Informed Approach	0.7177
	Support Vector Machine (Gupta et al., 2023)	0.7000
	Logistic Regression (Gupta et al., 2023)	0.7100
	BERT-Dense (Haque et al., 2021)	0.7050
	BERT-Bidirectional LSTM (Haque et al., 2021)	0.7150
	Mental FLAN (Large Language Model) (Xu et al., 2023)	0.6770

Our findings suggest we can achieve effective results without training additional complex models. We can reduce costs and training time by leveraging simple methods or existing classification models already integrated within the system. This approach enhances explainability, providing clearer insights into classifications without adding more hidden layers for complexity.

CONCLUSION

In conclusion, the integration of personality and emotion-aware features into natural language understanding models, particularly for sentiment analysis and depression detection, has been validated through various experiments and statistical hypothesis testing, demonstrating their effectiveness in enhancing model performance. This approach improves model accuracy by up to 3.4% in sentiment analysis (IMDb dataset) and depression detection (SDCNL dataset). However, it also enhances model explainability, making it more transparent and interpretable compared to a complex model.

While the model demonstrated improved accuracy without relying strongly on complexity, it includes some features that may not contribute significantly. Therefore, we suggest exploring techniques such as principal component analysis (PCA) or other feature selection methods in future work to eliminate unimportant features and further optimize model performance.

This research has established a foundation for improving explainability and could be expanded to examine additional psychological factors or explore different natural language understanding (NLU) tasks. The future work in this area holds exciting possibilities. For example, future studies could use this approach to assess public intentions regarding vaccination or gauge people's perceptions of policy-making. All these applications aim to enhance public welfare while avoiding the complexity of advanced models. Subsequently, the next phase of work could involve incorporating psychology-informed model features into embeddings without relying solely on recognition results. This approach aims to explore alternative methods of leveraging the model's insights.

ACKNOWLEDGEMENT

The authors would like to express their sincere appreciation for the support provided by the Universiti Tunku Abdul Rahman Research Fund (IPSR/RMC/UTARRF/2021-C1/K03) and Greotech Integration (M) Sdn. Bhd. under project number 8084/0006.

REFERENCES

Adoma, A. F., Henry, N. M., & Chen, W. (2020). Comparative analyses of bert, roberta, distilbert, and xlnet for text-based emotion recognition. In *2020 17th International Computer Conference on Wavelet Active Media*

- Technology and Information Processing (ICCWAMTIP)* (pp. 117-121). IEEE. <https://doi.org/10.1109/ICCWAMTIP51612.2020.9317379>
- Aizawa, A. (2003). An information-theoretic perspective of TF-IDF measures. *Information Processing & Management*, 39(1), 45–65. [https://doi.org/10.1016/S0306-4573\(02\)00021-3](https://doi.org/10.1016/S0306-4573(02)00021-3)
- Alfarizi, M. I., Syafaah, L., & Lestandy, M. (2022). Emotional text classification using TF-IDF (term frequency-inverse document frequency) and LSTM (long short-term memory). *JUITA: Jurnal Informatika*, 10(2), 225-232. <https://doi.org/10.30595/juita.v10i2.13262>
- Ashton, M. C., Lee, K., Perugini, M., Szarota, P., De Vries, R. E., Di Blas, L., Boies, K., & De Raad, B. (2004). A six-factor structure of personality-descriptive adjectives: Solutions from psycholexical studies in seven languages. *Journal of Personality and Social Psychology*, 86(2), 356-366. <https://doi.org/10.1037/0022-3514.86.2.356>
- Celebi, M. E. (2023). *Nlp for depression prediction*. Kaggle. <https://www.kaggle.com/code/merencelebi/nlp-for-depression-prediction>
- Cervone, D. & Pervin, L. A. (2022). *Personality: Theory and research*. John Wiley & Sons. <https://doi.org/10.48550/arXiv.1806.06407>
- Das, B., & Chakraborty, S. (2018). *An improved text sentiment classification model using TF-IDF and next word negation*. arXiv:1806.06407. <https://doi.org/10.48550/arXiv.1806.06407>
- Deimann, R., Preidt, T., Roy, S. & Stanicki, J. (2023). *Is personality prediction possible based on Reddit comments?* arXiv:2408.16089. <https://arxiv.org/abs/2408.16089>
- Demszky, D., Movshovitz-Attias, D., Ko, J., Cowen, A., Nemade, G. & Ravi, S. (2020). GoEmotions: A dataset of fine-grained emotions. In *Proceedings of the 58th Annual Meeting of the Association for Computational Linguistics* (pp. 4040–4054). Association for Computational Linguistics.
- Demszky, D., Movshovitz-Attias, D., Ko, J., Cowen, A., Nemade, G., & Ravi, S. (2020). *GoEmotions: A dataset of fine-grained emotions*. arXiv:2005.00547. <https://doi.org/10.48550/arXiv.2005.00547>
- Deshpande, M., & Rao, V. (2017). Depression detection using emotion artificial intelligence. In *2017 International Conference on Intelligent Sustainable Systems (ICISS)* (pp. 858–862). IEEE. <https://doi.org/10.1109/ISS1.2017.8389299>
- Devlin, J., Chang, M. W., Lee, K., & Toutanova, K. (2018). BERT: Pre-training of deep bidirectional transformers for language understanding. In *Proceedings of the 2019 Conference of the North American Chapter of the Association for Computational Linguistics: Human Language Technologies* (pp. 4171–4186). Association for Computational Linguistics.
- Ding, Z., Qi, Y., & Lin, D. (2021). Albert-based sentiment analysis of movie review. In *2021 4th International Conference on Advanced Electronic Materials, Computers and Software Engineering (AEMCSE)* (pp. 1243-1246). IEEE. <https://doi.org/10.1109/AEMCSE51986.2021.00254>
- Durairaj, A. K., & Chinnalagu, A. (2021). Transformer based contextual model for sentiment analysis of customer reviews: A fine-tuned BERT. *International Journal of Advanced Computer Science and Applications*, 12(11), 474-480. <https://doi.org/10.14569/IJACSA.2021.0121153>

- Eysenck, H. J., & Eysenck, S. B. G. (1975). *Manual of the Eysenck Personality Questionnaire (Junior & Adult)*. Hodder and Stoughton Educational. <https://doi.org/10.1111/j.2044-8341.1977.tb02414.x>
- Figuerêdo, J. S. L., Maia, A. L. L. M., & Calumby, R. T. (2022). Early depression detection in social media based on deep learning and underlying emotions. *Online Social Networks and Media*, 31, Article 100225. <https://doi.org/10.1016/j.osnem.2022.100225>
- Goldberg, L. R. (1993). The structure of phenotypic personality traits. *American Psychologist*, 48(1), 26-34. <https://doi.org/10.1037/0003-066X.48.1.26>
- Gupta, S., Sinha, A. M., Proadhan, D., Ghosh, N., & Modak, S. (2023). Detecting depression and suicidal ideation from texts using machine learning & deep learning techniques. *International Journal of Computer Sciences and Engineering*, 11(1), 29–35.
- Haque, A., Reddi, V., & Giallanza, T. (2021). Deep learning for suicide and depression identification with unsupervised label correction. In I. Farkaš, P. Masulli, S. Otte & S. Wermter (Eds.) *Artificial Neural Networks and Machine Learning – ICANN 2021* (pp. 436–447). Springer. https://doi.org/10.1007/978-3-030-86383-8_35
- Hartmann, J. (2022). *Emotion-english-distilroberta-base*. Huggingface. <https://huggingface.co/j-hartmann/emotion-english-distilroberta-base>
- Lan, Z., Chen, M., Goodman, S., Gimpel, K., Sharma, P., & Soricut, R. (2019). *ALBERT: A lite BERT for self-supervised learning of language representations*. arXiv:1909.11942. <https://doi.org/10.48550/arXiv.1909.11942>
- Lin, J., Mao, W., & Zeng, D. D. (2017). Personality-based refinement for sentiment classification in microblog. *Knowledge-Based Systems*, 132, 204–214. <https://doi.org/10.1016/J.KNOSYS.2017.06.031>
- Liu, C., Osama, M. & de Andrade, A. (2019). *DENS: A dataset for multi-class emotion analysis*. arXiv:1910.11769. <https://doi.org/10.48550/arXiv.1910.11769>
- Liu, Y., Ott, M., Goyal, N., Du, J., Joshi, M., Chen, D., Levy, O., Lewis, M., Zettlemoyer, L., & Stoyanov, V. (2019). *RoBERTa: A robustly optimized BERT pretraining approach*. arXiv:1907.11692. <https://doi.org/10.48550/arXiv.1907.11692>
- Lowe, S. (2023). *Roberta base go emotion*. Dataloop https://dataloop.ai/library/model/samlowe_roberta-base-go_emotions/
- Maas, A., Daly, R. E., Pham, P. T., Huang, D., Ng, A. Y., & Potts, C. (2011). Learning word vectors for sentiment analysis. In *Proceedings of the 49th Annual Meeting of the Association for Computational Linguistics: Human Language Technologies* (pp. 142-150). Association for Computational Linguistics
- Mairesse, F., Walker, M. A., Mehl, M. R., & Moore, R. K. (2007). Using linguistic cues for the automatic recognition of personality in conversation and text. *Journal of Artificial Intelligence Research*, 30, 457–500. <https://doi.org/10.1613/jair.2349>
- Maulana, R., Rahayuningsih, P. A., Irmayani, W., Saputra, D., & Jayanti, W. E. (2020). Improved accuracy of sentiment analysis movie review using support vector machine based information gain. *Journal of Physics: Conference Series*, 1641(1), Article 012060. <https://doi.org/10.1088/1742-6596/1641/1/012060>

- Mitchell, J. (2017). *Myers-briggs personality type dataset*. Kaggle. <https://www.kaggle.com/datasets/datasnaek/mbti-type>
- Moreno, J. D., Martínez-Huertas, J., Olmos, R., Jorge-Botana, G., & Botella, J. (2021). Can personality traits be measured analyzing written language? A meta-analytic study on computational methods. *Personality and Individual Differences*, 177, Article 110818. <https://doi.org/10.1016/J.PAID.2021.110818>
- Pang, B., & Lee, L. (2004). *A sentimental education: Sentiment analysis using subjectivity summarization based on minimum cuts*. arXiv:cs/0409058. <https://doi.org/10.48550/arXiv.cs/040905>
- Posner, J., Russell, J. A., & Peterson, B. S. (2005). The circumplex model of affect: An integrative approach to affective neuroscience, cognitive development, and psychopathology. *Development and Psychopathology*, 17(3), 715–734. <https://doi.org/10.1017/S0954579405050340>
- Qaisar, S. M. (2020). Sentiment analysis of IMDb movie reviews using long short-term memory. In *2020 2nd International Conference on Computer and Information Sciences (ICCCIS)* (pp. 1-4). IEEE. <https://doi.org/10.1109/ICCCIS49240.2020.9257657>
- Rahman, A. & Hossen, Md. S. (2019). Sentiment analysis on movie review data using machine learning approach. *2019 International Conference on Bangla Speech and Language Processing (ICBSLP)*, 1–4. <https://doi.org/10.1109/ICBSLP47725.2019.201470>
- Rajat, R., Jaroli, P., Kumar, N., & Kaushal, R. K. (2021). A sentiment analysis of amazon review data using machine learning model. In *2021 6th International Conference on Innovative Technology in Intelligent System and Industrial Applications (CITISIA)* (pp. 1-6). IEEE. <https://doi.org/10.1109/CITISIA53721.2021.9719909>
- Raw, N. (2021). *Bert base uncased emotion*. Huggingface. <https://huggingface.co/nateraw/bert-base-uncased-emotion>
- Ren, Z., Shen, Q., Diao, X., & Xu, H. (2021). A sentiment-aware deep learning approach for personality detection from text. *Information Processing & Management*, 58(3), Article 102532. <https://doi.org/10.1016/j.ipm.2021.102532>
- Scherer, K. R., & Wallbott, H. G. (1994). Evidence for universality and cultural variation of differential emotion response patterning. *Journal of Personality and Social Psychology*, 66(2), 310-328.
- Shaukat, Z., Zulfqar, A. A., Xiao, C., Azeem, M., & Mahmood, T. (2020). Sentiment analysis on IMDB using lexicon and neural networks. *SN Applied Sciences*, 2(2), Article 148. <https://doi.org/10.1007/s42452-019-1926-x>
- Shinde, V. (2022). *Twitter dataset*. Kaggle. <https://www.kaggle.com/datasets/infamouscoder/mental-health-social-media>
- Smith, M. Q. R. P., & Ruxton, G. D. (2020). Effective use of the McNemar test. *Behavioral Ecology and Sociobiology*, 74(11), Article 133. <https://doi.org/10.1007/s00265-020-02916-y>
- Sönmezöz, K., Uğur, Ö., & Diri, B. (2020). MBTI personality prediction with machine learning. In *2020 28th Signal Processing and Communications Applications Conference (SIU)* (pp. 1-4). IEEE. <https://doi.org/10.1109/SIU49456.2020.9302239>

- Sun, G., Guo, A., Ma, J., & Wei, J. (2019). Personal trait analysis using word2vec based on user-generated text. In *2019 IEEE SmartWorld, Ubiquitous Intelligence & Computing, Advanced & Trusted Computing, Scalable Computing & Communications, Cloud & Big Data Computing, Internet of People and Smart City Innovation (SmartWorld/SCALCOM/UIC/ATC/CBDCOM/IOP/SCI)* (pp. 1131-1137). IEEE. <https://doi.org/10.1109/SmartWorld-UIC-ATC-SCALCOM-IOP-SCI.2019.00213>
- Tadesse, M. M., Lin, H., Xu, B., & Yang, L. (2019). Detection of depression-related posts in reddit social media forum. *IEEE Access*, 7, 44883–44893. <https://doi.org/10.1109/ACCESS.2019.2909180>
- Tan, J. J. (2024a). *IMDb sentiment dataset splitting*. Huggingface. <https://huggingface.co/datasets/jingjietan/imdb-sentiment>
- Tan, J. J. (2024b). *MBTI-personalitycafe-MBTI personality dataset splitting*. Huggingface. <https://huggingface.co/datasets/jingjietan/kaggle-mbti>
- Tan, J. J. (2024c). *Polarity sentiment dataset splitting*. Huggingface. <https://huggingface.co/datasets/jingjietan/polarity-sentiment>
- Tan, J. J. (2024d). *SDCNL suicide dataset splitting*. Huggingface. <https://huggingface.co/datasets/jingjietan/sdcnl-suicide>
- Tan, J. J. (2024e). *Twitter depression dataset splitting*. Huggingface. <https://huggingface.co/datasets/jingjietan/twitter-depression>
- Tan, J. J., Kwan, B. H., Ng, D. W. K., & Hum, Y. C. (2023, December 14-15). *Enhancing performance in sentiment classification of textual messages through personality recognition integration*. [Paper presentation]. 11th International Symposium on Applied Engineering and Sciences, Selangor, Malaysia.
- Xu, X., Yao, B., Dong, Y., Gabriel, S., Yu, H., Hendler, J., Ghassemi, M., Dey, A. K., & Wang, D. (2023). Mental-llm: Leveraging large language models for mental health prediction via online text data. *Proceedings of the ACM on Interactive, Mobile, Wearable and Ubiquitous Technologies*, 8(1), 1-32. <https://doi.org/10.1145/3643540>
- Yang, W., Yuan, T., & Wang, L. (2020). Micro-blog sentiment classification method based on the personality and bagging algorithm. *Future Internet*, 12(4), 75. <https://doi.org/10.3390/fi12040075>
- Yarkoni, T. (2010). Personality in 100,000 words: A large-scale analysis of personality and word use among bloggers. *Journal of Research in Personality*, 44(3), 363–373. <https://doi.org/10.1016/j.jrp.2010.04.001>
- Yates, A., Cohan, A., & Goharian, N. (2017). Depression and self-harm risk assessment in online forums. In *Proceedings of the 2017 Conference on Empirical Methods in Natural Language Processing* (pp. 2968–2978). Association for Computational Linguistics

Development of Digital Twin Data-driven Modelling for Gas Turbine Operation Behaviour

Balbir Shah Mohd Irwan Shah, Asnor Juraiza Ishak*, Mohd Khair Hassan and Nor Mohd Haziq Norsahperi

Department of Electrical and Electronic Engineering, Faculty of Engineering, Universiti Putra Malaysia, 43400 UPM, Serdang, Selangor, Malaysia

ABSTRACT

Digital twins have recently gained attention as digital solutions in "Energy 4.0" that will reshape the future of the power generation industry toward the digital era. It is supported by the rapid advancement of data connectivity and computational power to intensify the potential of digital twin technology in addressing the energy trilemma. The energy trilemma has been identified as a global challenge to transform the power generation industry landscape to be more efficient and competitive. Digital twins have been identified as a key enabler to address the impacts of this global challenge on power plants due to several factors such as ageing, performance degradation, and high operating costs. This study will evaluate the concept of the digital twin approach by developing the gas turbine digital twin to provide future insights into operational performance and optimisation. The gas turbine digital twin model is developed through a cutting-edge data-driven approach, utilising an artificial neural network (ANN) to deliver superior performance in advanced monitoring applications. The digital twin model is constructed structurally in four steps: process identification, data collection, pre-processing, and developing the digital twin plant model. The gas turbine operating parameters are analysed for critical parameter verification to emulate the gas turbine operation behaviour environment. The best deep learning structure for data-driven methods is identified based on a lower Mean Squared Error (MSE) and an average error of less than 0.5% of the predicted value. The findings indicate that the digital twin data-driven modelling can be applied to future advanced monitoring of gas turbines in the power generation industry.

ARTICLE INFO

Article history:

Received: 01 April 2024

Accepted: 10 April 2025

Published: 10 June 2025

DOI: <https://doi.org/10.47836/pjst.33.S4.05>

E-mail address:

balbirshahpd@gmail.com (Balbir Shah Mohd Irwan Shah)

asnorji@upm.edu.my (Asnor Juraiza Ishak)

khair@upm.edu.my (Mohd Khair Hassan)

nmhaziq@upm.edu.my (Nor Mohd Haziq Norsahperi)

*Corresponding author

Keywords: Artificial Neural Network (ANN), data-driven, digital twin, gas turbine, power plant, predictive modelling

INTRODUCTION

Digital twins play a significant role in addressing the Energy Trilemma, which has been identified as the global challenge of balancing energy security, environmental sustainability, and affordability. In the context of Industry 4.0, digital twins bring benefits to future power plants by optimizing operational and maintenance costs. A digital twin represents a real thing, system, process, environment, or entity that exists digitally. Physical data from various sources, including sensors, IoT devices, and other data streams, is gathered and integrated to produce a digital twin model. This replica can be utilized for analysis, modeling, monitoring, and control purposes to better understand and manage the physical counterpart. In addition, the digital twin can be developed to perform advanced applications such as operating behaviour emulation, anomaly detection (Wu et al., 2023), and performance optimization (Rahman et al., 2011).

In conjunction with Malaysia's electricity supply industry (MESI 2.0) initiatives, the government is committed to addressing the energy trilemma by introducing new enhanced dispatch arrangement (NEDA) rules to transform the industry into a more efficient and productive one. Under NEDA, generators are allowed to compete based on lower variable operating rates (VOR) and heat rates rather than a fixed rate. In the worst-case scenario, a power plant cannot dispatch due to process disruptions and equipment failures. This will likely result in a prolonged shutdown to investigate the root cause and perform corrective action. This condition will have a significant impact on national grid security and sustainability due to several factors, such as aging, performance degradation (Meher-Homji et al., 2001), restricted loading operations (Castillo et al., 2021), and high operating costs (Zhong et al., 2023). Therefore, the digital twin has been identified as a key enabler in the future to address the impacts of electricity liberalization on thermal power plant operation and performance. This will enhance competition in generation dispatch and result in more competitive energy prices.

The digital twin model is developed through four steps: process identification, data collection, data pre-processing, and digital twin plant modeling. Initially, the study examines critical gas turbine parameters for verification to develop a digital twin data-driven model for advanced monitoring. The digital twin is then modeled using a deep learning approach to predict gas turbine operating behaviour for anomaly detection and performance analysis applications. Finally, the best deep learning structure for data-driven methods is identified. The outcome will revolutionize the power plant industry for various Industry 4.0 applications.

Literature Review

This study found that adopting digital twins has led to the discovery of five categories of power generation in the distribution of digital twin applications. The publication trend

indicates that the adoption of the digital twin is dominated by coal-fired and gas turbine plant studies at 22.2%, followed by nuclear power and renewable energy at 18.5%, respectively. Meanwhile, the least studied renewable energy and cogeneration plants are 14.8% and 3.7%, respectively. Besides that, another finding indicates that a coal-fired power plant publication is focused on the study of components and processes at the same 50% rate. However, current studies on gas turbine plants predominantly focus on individual components rather than overall processes (Shah et al., 2024). As a result, this study will focus on developing a gas turbine digital twin, with a particular emphasis on process areas. The details of the digital twin study under the gas turbine application are shown in Table 1. The combined cycle power plant is a viable future alternative due to its high efficiency and capacity to address the energy trilemma while also realising the COP26 initiatives by 2030. The coexistence of this plant with renewable energy in the smart grid will help to rebalance the energy system between security and sustainability at an optimum cost. Hence, the gas turbine prospect can be explored to merge with renewable energy plants for smart grid implementation in the future. In addition, the emissions can be reduced further by introducing the new combustion technology that can generate energy from natural gas co-fired with clean fuel sources such as hydrogen, ammonia, and biomass.

Table 1

The summary of the digital twin study under the gas turbine application

Authors	Objective	Focus	Method	Category
Tsoutsanis et al., 2020	Health monitoring for transient operation	Parts	Machine Learning	Component
Marwaha & Kohn, 2019	Predictive maintenance	Compressor	Physic Model	Component
Ren et al., 2017	Life prediction	Rolling bearing	Deep Learning	Component
Polyakov et al., 2020	Failure identification and prediction	Component	ANN	Component
Nikolaev et al., 2019	Condition monitoring for maintenance	Flame tubes	ANN, Physics Model	Component
Malozemov et al., 2019	Performance monitoring and improvement	Diesel engine	Physic Model	Component
Dawes et al., 2019	Life Cycle Modelling for MRO	Turbine blade	Geometry Model	Component

METHODOLOGY

This study aims to develop a digital twin model for gas turbine power plant applications to simulate the dynamic operational behavior of the system. The scope will encompass critical aspects of gas turbine components and overall processes. Figure 1 provides an overview of the methodology applied in this study. An artificial neural network (ANN) has been selected as the data-driven approach for developing the gas turbine digital twin. Moreover, this study will incorporate an optimizer algorithm to enhance prediction accuracy and improve the model's performance. This approach is expected to outperform previous ANN models, which often required extended iteration times due to the complexity of hidden layers and neurons.

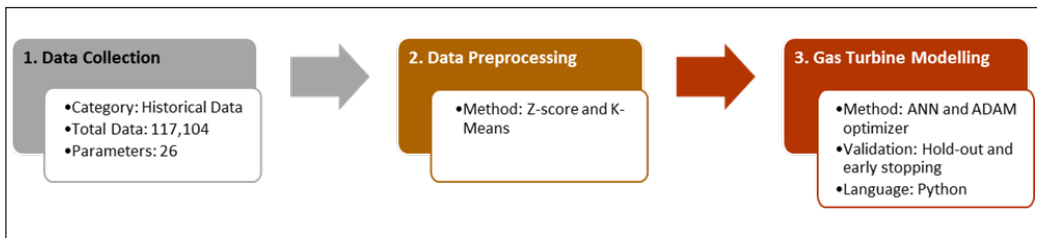


Figure 1. The summary of the methodology

Data Collection

The gas turbine's historical operating data is archived in a distributed control system (DCS) used to operate and control the power plant. The information is accumulated from a real power plant and recorded in CSV file format. The information was collected and categorised into four groups of periods that have been logged every minute for historical data collection. The Jupyter Notebook performs data analytics to provide an overview of data conditions and gas turbine operating profiles. The dataset contains a total of 117,104 data points and 26 parameters, comprising 24 inputs and 2 outputs.

The dataset is used to analyze variations, such as mean, median, mode, standard deviation, and maximum and minimum values of each parameter. Statistical analysis is essential for classifying values into different ranges and identifying the aberrant parameters and factors that impact performance and optimisation. Histogram plots are used to reveal outlier values during the operation of the gas turbine. In addition, the relationship between the parameters is presented using a correlation matrix. This matrix provides a quantitative indicator of the linear relationships between variables, helping to spot patterns and links within the data (Wagavkar, 2023).

Data Pre-processing

The dataset must be cleaned during the data pre-processing phase. Cleaning can standardise and structure data to maintain uniformity throughout a dataset and adding in fixing errors and inconsistencies to improve the accuracy of the data. This is crucial for data integrity and avoiding misleading and wrong analysis results. The dataset collected from the physical model is limited by the fact that anomalies and outliers can exist in the raw dataset for a variety of reasons, including data input mistakes, sensor failures, and unusual conditions. The actual and predicted input and output values may differ because of the presence of abnormal data points. Therefore, the dataset for the load in the generated output will be filtered as values higher than or equal to 125 MW will be used in this study.

The outlier removal methods, Z-score and K-means, will be applied in this study. In terms of standard deviations, the Z-score measures how much a data point deviates from the mean of a distribution. Outliers are often removed using Z-scores by defining a threshold over which data values are deemed outliers. Conversely, K-means is an iterative technique for grouping data that divides a dataset into a preset number of groups. To remove outliers, it seeks to minimise the within-cluster sum of squares, which indicates the compactness and similarity of data points within each cluster. The Z-scores and K-means techniques are utilised to eliminate the outliers from the dataset. Furthermore, a boxplot is constructed to visualise the data distribution before and after the data-cleaning process. Any value outside of the acceptable range has the probability of being an anomalous data point. Data points not within the acceptable range are considered an outliers. However, other statistical analyses and domain knowledge are still required to make informed decisions about the presence and handling of outliers.

Gas Turbine Modelling

The selected approach for a data-driven task is an artificial neural network (ANN) that utilizes backpropagation, a robust algorithm for supervised learning. Backpropagation is noteworthy for its ability to determine discrepancies between the network's predictions and actual outcomes. It works by switching the direction errors move through the network's layers. This lets neuron-associated weights be precisely adjusted to improve predictions. For the practical implementation of this ANN model, Jupyter Notebook has been chosen due to its compatibility with Python, which is renowned for rapid execution. Additionally, Jupyter Notebook supports a vast array of machine learning and deep learning libraries, making it an excellent tool for this study. Artificial neural networks are powerful tool within the domains of artificial intelligence and machine learning, adept at handling tasks like pattern recognition, classification, regression, and decision-making. The versatility of ANNs allows them to classify and train on data, enabling the generalisation of strategies for data interpretation during evaluations.

In this study, the ANN model is developed using the Keras library and structured with input, hidden, and output layers suitable for gas turbine applications. The model ensures data consistency by normalising input data to have a zero mean and unit variance. The composition of ANNs includes neurons, input layers, hidden layers, and output layers, arranged in a layered architecture. The hidden layer settings consists of three because a large amount of data requires attentive analysis to reduce errors and losses, which enhances the accuracy of the prediction results and achieves the desired outcomes. The connections between neurons are associated with weights. These weights determine the strength of the connection and are adjusted during training. The initial weights of connections are frequently chosen at random using initialisation methods. Each neuron in a layer calculates the weighted sum of its inputs, adds a bias term, and then uses an activation function. The bias factor increases the weighted sum before the activation function is used. The network output is compared to the desired target following a forward pass. The gradients of this comparison for the network weights are computed via backpropagation. The learning rate determines the step size of these weight updates. This procedure continues until the network converges or achieves a suitable performance level. The ANN will generate predictions on the original data after training.

Load and Pre-process Data

The StandardScaler from the Python scikit-learn Library is applied to load and pre-process datasets. The StandardScaler standardizes data on the output and input features by eliminating the mean and scaling to unit variance. Each input and output column is scaled using this approach by subtracting the mean and dividing by the standard deviation. The scaled features are then returned and provided with input and output values. The data is converted to a similar scale by standardizing the input attributes and output target. In addition, MinMaxScaler transform the data to a fixed range, usually between 0 and 1. Normalizing the variables can help alleviate these difficulties and boost the optimisation algorithm's convergence.

Model Training and Evaluation

The pre-processed data is split into training and testing sets. The model trains over multiple epochs, updating its parameters after processing batches of 32 samples. With a 70% training and 30% validation split, performance is monitored using holdout validation and early stopping. This approach is particularly effective, given the dataset of 117,104 data points and the hardware limitations that restrict extended training times for complex models. Early stopping enhances the holdout method by stopping training once the model reaches its best performance on the validation set, preventing overfitting. It halts training once optimal performance is achieved on the validation set, reducing overfitting. Meanwhile,

the scheduler technique is used to automatically adjust the learning rate based on validation loss, reducing it when improvement stagnates to help the model overcome local minima. This improves convergence without manual intervention, thereby optimizing the training process. After compiling the model with a loss function, optimizer, and metrics, a sequential model with three dense layers is created. The model is tested on a new dataset to minimize bias, and performance metrics are used to fine-tune hyperparameters.

Structure of the ANN Model

Figure 2 illustrates the structure of the Artificial Neural Network (ANN), consisting of three hidden layers. The first hidden layer utilizes the rectified linear unit (ReLU) activation function and contains 256 neurons. This layer's input data is characterized by 24 features. The second hidden layer also employs the ReLU activation function and consists of 128 neurons. The third and final layer uses a linear activation function with two output units. The activation functions are essential for introducing non-linearity to the model, allowing the network to capture complex patterns. The output layer uses a linear activation function because the problem is a regression task, where the model predicts continuous output values. The neuron counts in the hidden layers are powers of two, which optimize memory allocation and enhance performance.

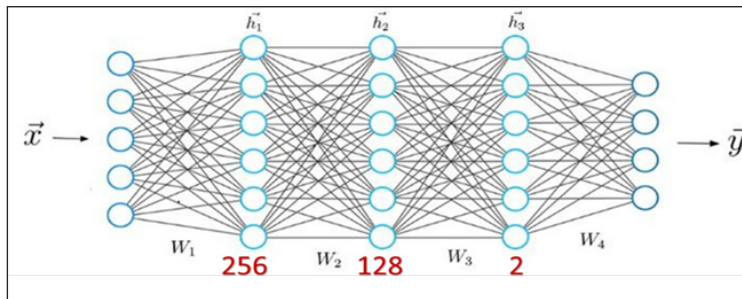


Figure 2. ANN development structure

RESULT AND DISCUSSION

The gas turbine digital twin was modeled using artificial neural networks (ANN) and achieved optimal performance by integrating the ADAM (adaptive moment estimation) optimizer. A thorough performance evaluation focused on critical metrics such as mean absolute error (MAE), root mean square error (RMSE), learning curves, gas turbine loss, test loss, regression values, prediction accuracy, and overall digital twin performance. This analysis clearly highlighted the transformative impact of data cleaning by comparing model performance before and after the process. The digital twin model's performance was rigorously tested, starting with a modest architecture of 256 neurons in the first layer

and 128 in the second. The model was progressively scaled to larger configurations, with the most effective setup found to be 2048 neurons in the first layer and 1024 in the second, optimized by the ADAM algorithm. This architecture was identified as the ideal structure for enhancing gas turbine performance. After completing the training and validation phases, the model's performance on the test dataset was carefully evaluated. As outlined in Table 2, both MAE and RMSE show significant reductions following data cleaning, indicating a substantial improvement in the model's predictive accuracy. The decrease in these metrics confirms that removing outliers effectively minimizes discrepancies between predicted and actual values. This demonstrates the model's robustness and reliability, setting a new benchmark for data-driven gas turbine performance analysis modelling.

Table 2
Overall data-driven model performance results

Model performance		
No.	Performance Indicator	Results
1	MAE	4.3758e-04
2	MSE	2.3419e-04
3	RMSE	0.1004
4	Test Accuracy	0.0101
5	R ²	1.00

Furthermore, the test accuracy improves after data cleaning compared to before. The increase in the number of neurons and the addition of hidden layer, as well as the use of the ADAM optimizer for prediction, result in lower test loss and higher test accuracy. The regression value (R²) indicates the relationship between the output and input variables. The negative coefficient indicates that the input and output are negatively correlated, meaning they tend to move in opposite directions; however, the regression value after data cleaning is positively correlated, implying that it tends to move in the same direction. An R² score of 1.0 indicates a perfect fit.

The loss function curves are plotted to display the training and validation accuracy and loss over time. Figure 3 shows the MSE loss function curve, illustrating the neural network model's training loss across epochs. Lower loss values during both training and validation indicate improved model performance. After data pre-processing, the validation loss is less than the training loss, signaling that overfitting has not occurred. Data pre-processing led to better overall performance, as it removed disturbances present in the previously trained and tested datasets. Before data cleaning, the validation line indicated overfitting, where the model performed well on training data but poorly on test data. This overfitting would have negatively impacted the gas turbine's output performance. Addressing this issue improved the model's robustness and generalizability.

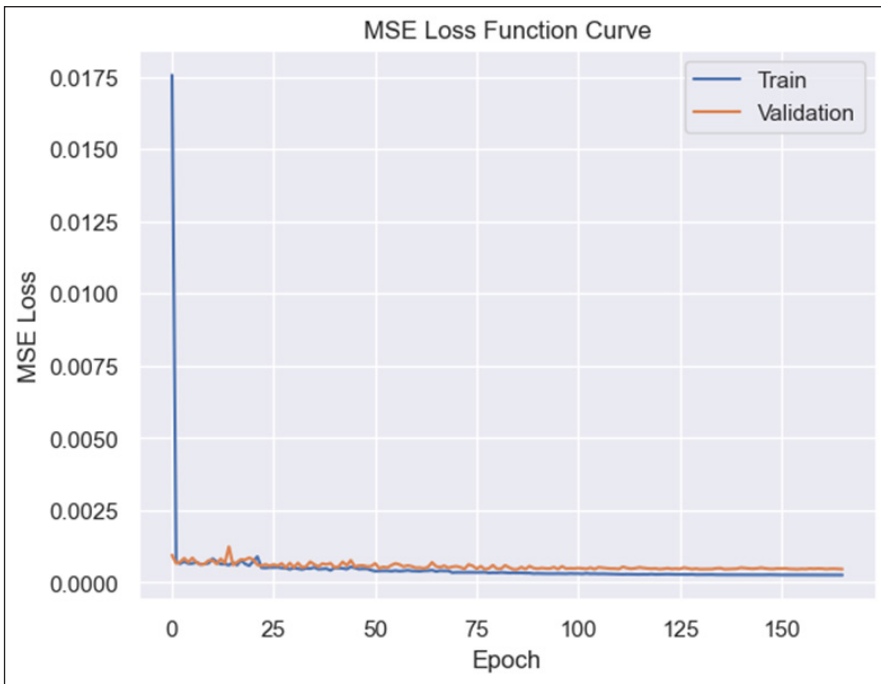


Figure 3. MSE loss function curve

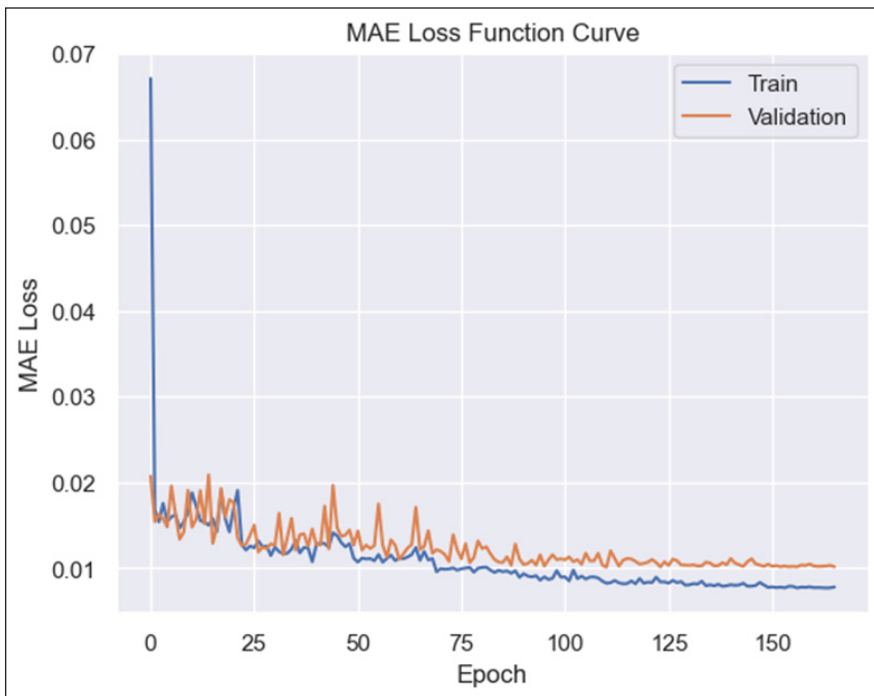


Figure 4. MAE loss function curve

The MAE is a key metric to evaluate the model's ability to generalize and predict new datasets. As shown in Figure 4, the MAE decreases with increasing epoch values, signifying that the model is progressively learning and improving. MAE validation is continuously monitored throughout the training process to ensure strong performance on unseen data, helping to avoid problems like overfitting or underfitting. An early stopping mechanism is applied during training, halting the process when validation MAE ceases to improve, thus preventing overfitting. The steady decline in errors and the minimal gap between training and validation MAE reflect stable validation, indicating that the model generalizes effectively without significant increases in validation error over time.

Separate graphs are created for each input and output variable to compare predicted values to actual values before data cleaning. According to Figure 5, the input predicted value overlaps with the actual value, implying that the predicted value is identical to the actual value. If the predicted value and actual value do not overlap and are far apart, it indicates that the actual value is not at the predicted value and is influenced by external disturbances in the gas turbine. After data cleaning, the predicted and actual values for all parameters are nearly identical. In contrast, the dataset before data cleaning contains a few data points that are not identical. This is because outliers and disturbances affect dataset learning and prediction accuracy. After data cleaning, the location of the data points changes because the outliers that affected the gas turbine's performance were eliminated.

Figure 6 illustrates the comparison between predicted and actual output values, showing a strong correlation as represented by a diagonal line. After data cleaning, the predicted values for gas turbine load and efficiency align closely with the actual values, highlighting the improved performance of the model. Prior to data cleaning, some predicted values exhibited deviations from the actual outputs, though the spread remained relatively narrow. A narrower spread signifies higher prediction accuracy, while a wider spread indicates greater variability in model performance. The dense clustering of predicted values after cleaning demonstrates high forecasting accuracy, whereas more dispersed plots before cleaning suggest increased variability. Overall, the improved alignment in the cleaned data underscores the enhanced accuracy and effectiveness of the data-driven model in predicting gas turbine load and efficiency.

The normal operational behaviour is illustrated by comparing real and predicted values of input and output parameters at specific loads, including 125 MW, 150 MW, 180 MW, 200 MW, and 220 MW. Table 3 presents samples of these values, along with the error percentages and cumulative error percentages. The results show that predictions after data cleaning are more accurate, with lower error percentages compared to those before data cleaning. The accuracy of predictions before data cleaning is compromised by outliers, which affect the model's ability to predict desired values accurately.

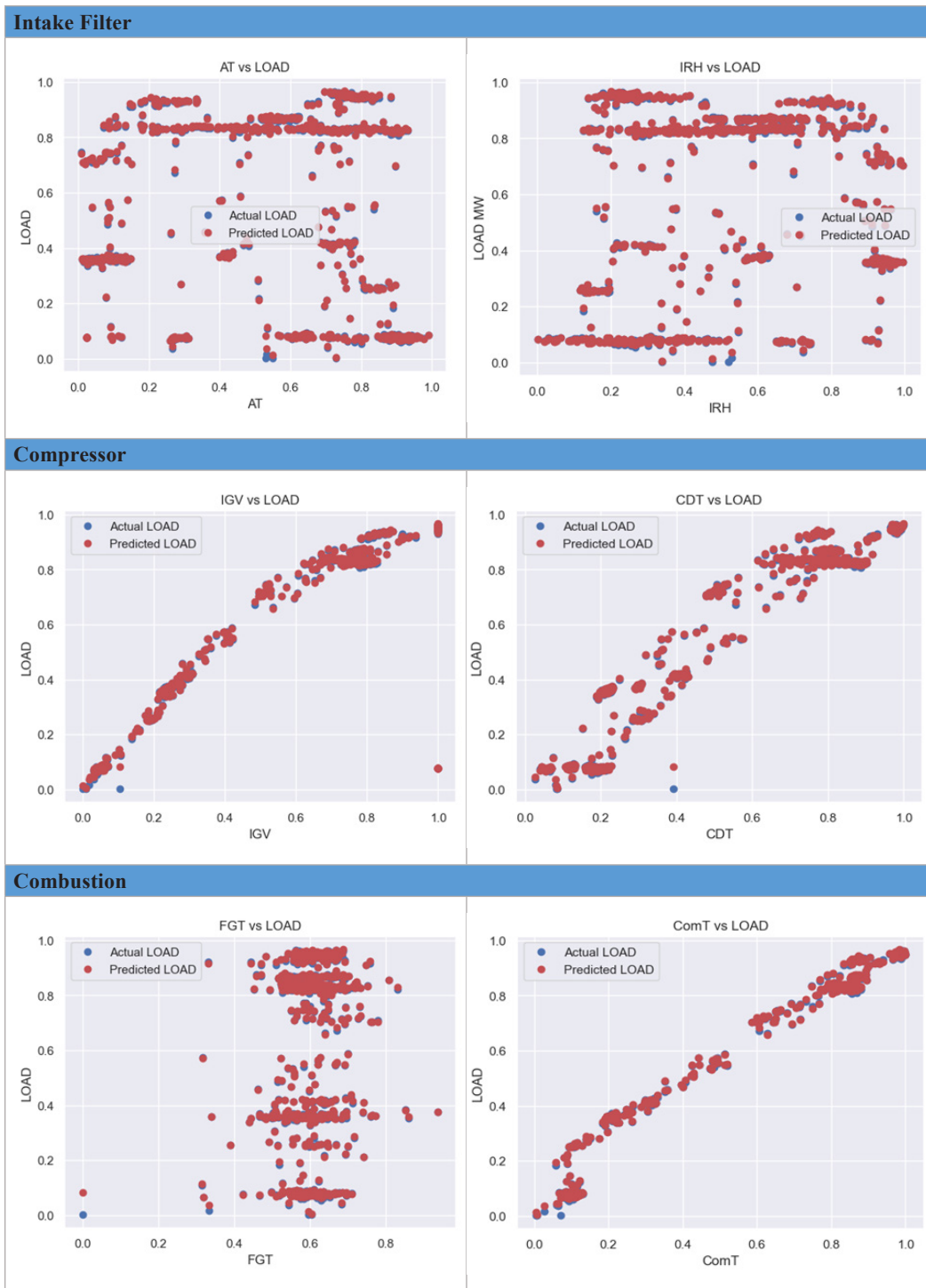


Figure 5. The comparison between the actual and predicted values of the input parameters

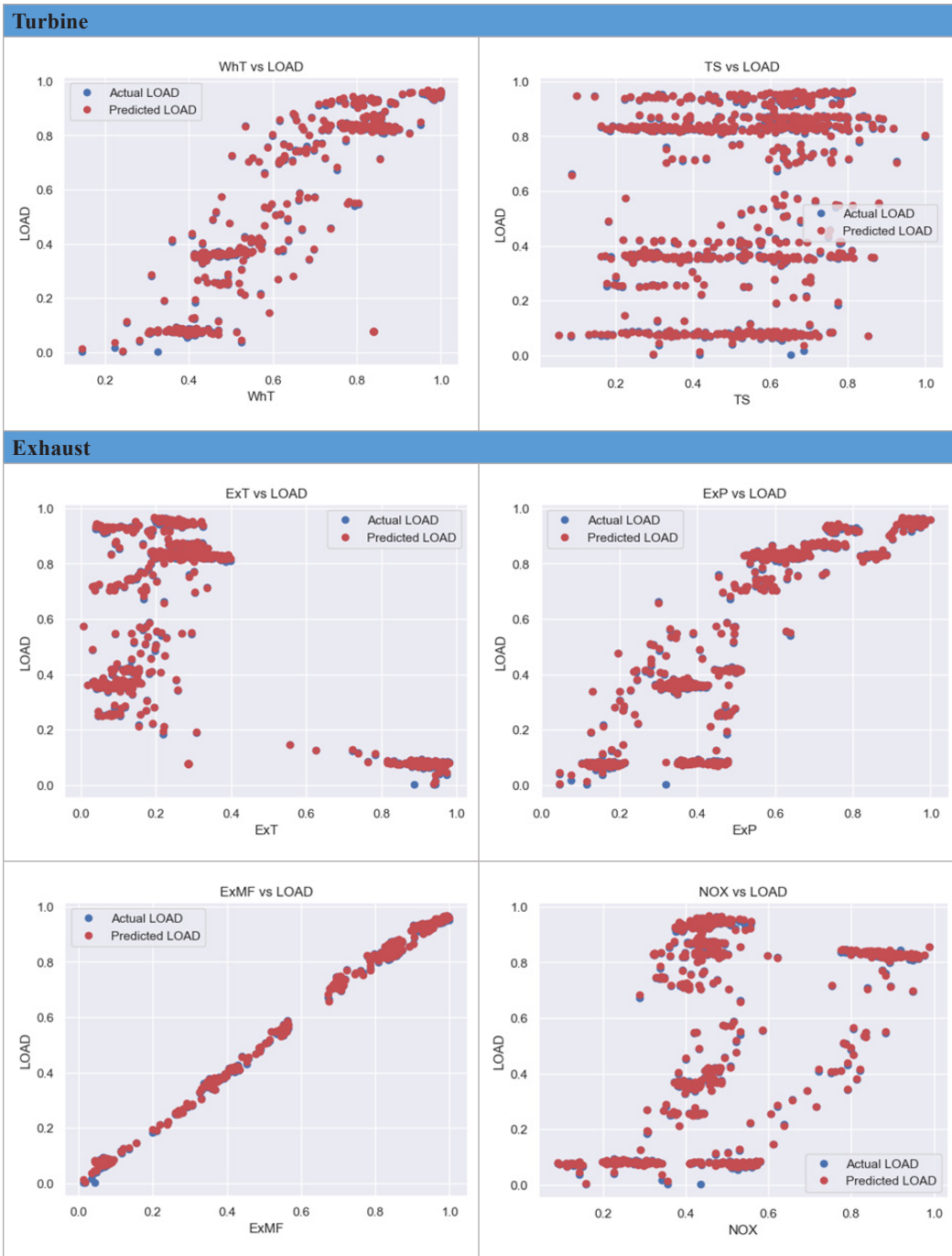


Figure 5 (continue)

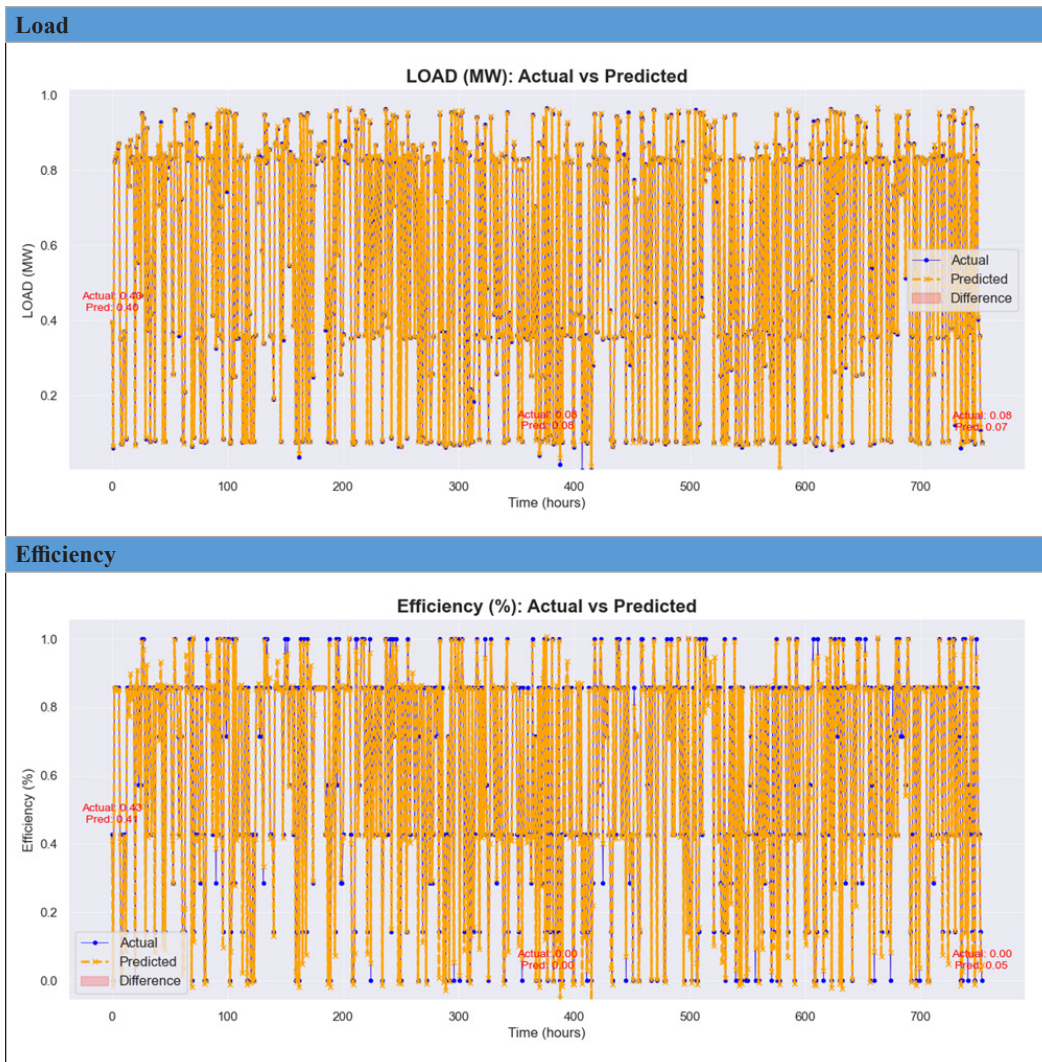


Figure 6. The comparison between the actual and predicted values of the output parameters

Table 3
 Predicted gas turbine operating parameters at 150 MW

Actual vs Predicted						
No	Operating Parameter		Real Value	Prediction Value	Error	% Error
1	Intake Filter	Ambient Temperature (degC)	25.84	25.9260	-0.0860	0.3328
		Pressure (Bar)	1.01	1.0055	0.0045	0.4455
		Relative Humidity	79.4	79.0366	0.3634	0.4577
		Mass Flow (m3/hr)	1615.92	1612.5670	3.3530	0.2075

Table 3 (continue)

Actual vs Predicted						
No	Operating Parameter		Real Value	Prediction Value	Error	% Error
2	Compressor	Inlet Guide Vanes (DEG)	55.18	54.6566	0.5234	0.9485
		Discharge Temperature (degC)	360.55	360.9410	-0.3910	0.1084
		Discharge Pressure (Bar)	10.31	10.3290	-0.0190	0.1843
3	Combustion	Fuel Gas Flow (t/hr)	35.71	35.7924	-0.0824	0.2307
		Fuel Gas Interstage Pressure (Bar)	26.84	26.8396	0.0004	0.0015
		Fuel Gas Temperature (degC)	185.24	185.3047	-0.0647	0.0349
		Speed Ratio Valve (%)	48.97	48.9502	0.0198	0.0404
		Fuel Stroke Reference (%)	50.77	50.7708	-0.0008	0.0016
		Gas Fuel LHV (Btu/scf)	935.93	934.3998	1.5302	0.1635
		Firing Temperature (degC)	1234.39	1235.3215	-0.9315	0.0755
4	Turbine	Wheelspace Temperature (degC)	442.88	442.4450	0.4350	0.0982
		Turbine Speed (RPM)	2999.37	2999.5833	-0.2133	0.0071
5	Exhaust	Temperature (degC)	633.73	633.6862	0.0438	0.0069
		Pressure (bar)	27.8	27.9665	-0.1665	0.5989
		Exhaust Mass Flow (t/hr)	1655.1	1657.1015	-2.0015	0.1209
		Nitrogen Oxides (Nox) (ppm)	20.04	20.0313	0.0087	0.0434
		Sulfur Dioxide (SO ₂) (ppm)	0.11	0.1117	-0.0017	1.5455
		Carbon Monoxide (CO) (ppm)	1.97	1.9772	-0.0072	0.3655
		Carbon Dioxide (CO ₂) (vol%)	4.08	4.0968	-0.0168	0.4118
6	Generated Output	Oxygen (O ₂) (vol%)	13.62	13.6015	0.0185	0.1358
		Load (MW)	150.16	149.8041	0.3559	0.2370
		Efficiency (%)	30	30.0840	-0.0840	0.2800
Total percentage of error (%)						7.0840

Table 4 comprehensively analyses predictive error percentages for gas turbine loadings ranging from 125 MW to 220 MW in a cumulative measure. This measure is derived from the sum of the error percentages for 26 different parameters. Notably, the determined

average for these predictive errors is 0.23%. This result demonstrates the effectiveness of the predictive models in action.

Table 4
Overall performance at various loads

Load	Error %	Ave Error %
125MW	7.8198	0.3008
150MW	7.0840	0.2725
180MW	5.1220	0.1970
200MW	6.4324	0.2474
220MW	4.3914	0.1689
Average error %		0.2373

CONCLUSION

The findings of this study mark a significant advancement in the realm of gas turbine performance analytics. This study rigorously built a digital twin model of a gas turbine using artificial neural networks (ANN) and achieved a commendable average error percentage of approximately 0.23% across various operating conditions. This exceptional precision indicates a highly successful model development process, demonstrating the effectiveness of the ANN methodology in capturing the complex performance dynamics of gas turbines. The ANN hyperparameters were optimized throughout the study, resulting in significant improvements in the model's predictive accuracy, as evidenced by substantial decreases in key performance metrics such as mean absolute error (MAE) and root mean squared error (RMSE). Such enhancements reinforce the model's robustness and highlight the diligent efforts to improve the analytical instrument. However, the study's insights are particularly valuable for gas turbine operations at load levels exceeding 50% capacity. The complexity of turbine behavior at lower loads presents additional challenges, making the current model less effective in these volatile conditions. Future research will address these challenges by enhancing the digital twin model's ability to perform under low-load conditions and incorporating predictions from a thermodynamic cycle perspective.

ACKNOWLEDGEMENT

The authors express their heartfelt gratitude to the management team of Tuanku Ja'afar Power Station and TNB Power Generation Sdn. Bhd. (Genco) for their invaluable support in this study. Their generosity in granting permission and assistance in gathering critical real-time data unequivocally contributed to the scholarly success of this research work. This collaboration shows the positive outcomes that can be achieved through industry-academic collaboration.

REFERENCES

- Castillo, I. G., Loboda, I., & Pérez Ruiz, J. L. (2021). Data-driven models for gas turbine online diagnosis. *Machines*, 9(12), 372. <https://doi.org/10.3390/machines9120372>
- Dawes, W. N., Meah, N., Kudryavtsev, A., Evans, R., Hunt, M., & Tiller, P. (2019, January 7-11). Digital geometry to support a gas turbine digital twin. [Paper presentation] *AIAA Scitech 2019 Forum*, San Diego, California. <https://doi.org/10.2514/6.2019-1715>
- Malozemov, A. A., Solomonenko, M. V., & Malozemov, G. A. (2019). Numerical simulation of power plants with reciprocating engines using Modelica language. In *2019 International Russian Automation Conference (RusAutoCon)* (pp. 1-5). IEEE. <https://doi.org/10.1109/RUSAUTOCON.2019.8867801>
- Marwaha, G., & Kohn, J. (2019). Predictive maintenance of gas turbine air inlet systems for enhanced profitability as a function of environmental conditions. In *Abu Dhabi International Petroleum Exhibition and Conference* (pp. SPE-197814). SPE. <https://doi.org/10.2118/197814-ms>
- Meher-Homji, C. B., Chaker, M. A., & Motiwala, H. M. (2001). Gas turbine performance deterioration. In *Proceedings of the 30th turbomachinery symposium*. Texas A&M University. Turbomachinery Laboratories.
- Nikolaev, S., Belov, S., Gusev, M., & Uzhinsky, I. (2019). Hybrid data-driven and physics-based modelling for prescriptive maintenance of gas-turbine power plant. In C. Fortin, L. Rivest, A. Bernard & A. Bouras (Eds.) *Product Lifecycle Management in the Digital Twin Era* (pp. 379–388). Springer. https://doi.org/10.1007/978-3-030-42250-9_36
- Polyakov, R., Paholkin, E., Kudryavcev, I., & Krupenin, N. (2020). Improving the safety of power plants by developing a digital twin and an expert system for adaptive-predictive analysis of the operability of gas turbine units. *Turbo Expo: Power for Land, Sea, and Air*, 84157, Article V006T09A001. <https://doi.org/10.1115/GT2020-14217>
- Rahman, M. M., Ibrahim, T. K., & Abdalla, A. N. (2011). Thermodynamic performance analysis of gas-turbine power-plant. *International Journal of the Physical Sciences*, 6(14), 3539-3550. <https://doi.org/10.5897/IJPS11.272>
- Ren, L., Cui, J., Sun, Y., & Cheng, X. (2017). Multi-bearing remaining useful life collaborative prediction: A deep learning approach. *Journal of Manufacturing Systems*, 43, 248–256. <https://doi.org/10.1016/j.jmsy.2017.02.013>
- Shah, B. S. M. I., Ishak, A. J., Hassan, M. K., & Norsahperi, N. M. H. (2024). Energy 4.0: Challenges and enablers of digital twin application in power plant. *ELEKTRIKA-Journal of Electrical Engineering*, 23(1), 103-124. <https://doi.org/http://dx.doi.org/10.11113/elektrika.v23n1.487>
- Tsoutsanis, E., Hamadache, M., & Dixon, R. (2020). Real-time diagnostic method of gas turbines operating under transient conditions in hybrid power plants. *Journal of Engineering for Gas Turbines and Power*, 142(10), Article 101002. <https://doi.org/10.1115/1.4048340>
- Wagavkar, S. (2023). *Introduction to the correlation matrix*. Builtin. <https://builtin.com/data-science/correlation-matrix>

- Wu, Z. Y., Chew, A., Meng, X., Cai, J., Pok, J., Kalfarisi, R., Lai, K. C., Hew, S. F., & Wong, J. J. (2023). High fidelity digital twin-based anomaly detection and localization for smart water grid operation management. *Sustainable Cities and Society*, *91*, Article 104446. <https://doi.org/10.1016/j.scs.2023.104446>
- Zhong, D., Xia, Z., Zhu, Y., & Duan, J. (2023). Overview of predictive maintenance based on digital twin technology. *Heliyon*, *9*(4), Article e14534. <https://doi.org/10.1016/j.heliyon.2023.e14534>

Evaluation of Multimodal Dataset for Continuous Air-writing Multidigit Number Recognition Using Wearable Sensor

Yusuke Takei¹ and Eiichi Inohira^{2*}

¹Graduate School of Engineering, Kyushu Institute of Technology, 1-1 Sensui-cho, Tobata-ku, Kitakyushu-shi, Fukuoka 804-8550, Japan

²Faculty of Engineering, Kyushu Institute of Technology, 1-1 Sensui-cho, Tobata-ku, Kitakyushu-shi, Fukuoka 804-8550, Japan

ABSTRACT

In recent years, there has been a significant increase in the research and development of technologies and products, such as wearable devices. Gesture input has emerged as a promising new input method well-suited to these technologies. However, developing a reliable method for recognizing continuous gestures that lack contextual relationships poses a significant challenge. This study introduces a novel approach for recognizing continuous multidigit numbers to address this issue. This method utilizes a deep learning model equipped with sample-level dense labeling and leverages a multimodal dataset comprising inertial measurement unit data from wearable sensors and camera data. The outcomes of our recognition experiment reveal that using a multimodal dataset to produce accurate training data enhances recognition accuracy by 13% compared to approaches that do not use a multimodal dataset. Additionally, using our two proposed methods, the recognition of continuous digit gestures comprising 5, 8, and 10 digits achieved a correct recognition rate exceeding 90%. These results underscore the efficacy of our proposed method in recognizing continuous air-writing character gestures.

Keywords: Air writing, gesture recognition, multimodal dataset, wearable sensor

ARTICLE INFO

Article history:

Received: 01 April 2024

Accepted: 10 April 2025

Published: 10 June 2025

DOI: <https://doi.org/10.47836/pjst.33.S4.06>

E-mail address:

takei.yusuke468@outlook.jp (Yusuke Takei)

inohira.eiichi402@mail.kyutech.jp (Eiichi Inohira)

*Corresponding author

INTRODUCTION

The advent of wearable technology has revolutionized how we interact with digital devices, paving the way for innovative methods of communication. Zhang et al. (2018) have applied a gesture input technique to off-the-shelf smartwatches. Schäfer et al. (2022) have proposed a gesture-based UI for controlling continuous

locomotion in Virtual Reality applications. Kim et al. (2023) have presented a gesture-based control system for an industrial manipulator with a robotic hand. Among these advancements, the development of air-writing gesture recognition stands out as a significant leap, offering a seamless and intuitive input mode for a wide range of applications. We have focused on wearable devices because they have no problem with occlusions with cameras and poor illumination. Numerous studies have explored the recognition of air-writing gestures using a variety of wearable devices. Tripathi et al. (2022) introduced a high-precision technique for recognizing English air-writing gestures, employing wristband-type inertial measurement unit (IMU) sensors. This method transforms sensor data into an image form for enhanced recognition accuracy. Zhang et al. (2022) have developed a wearable system attached to a finger and a CNN (convolutional neural network)-based classification model for digits and letters. Kim et al. (2014) tackled the challenge of limited hardware resources in air-writing gesture scenarios. They developed a computationally efficient and cost-effective approach using a stepwise lower-bound dynamic time warping algorithm. Wu et al. (2009) have used a Wiimote, which is the controller of the Nintendo Wii equipped with a 3-axis accelerometer and implements a gesture recognition system, including the air-writing gesture of Lu et al. (2014), and proposed a gesture recognition system using a mobile phone for digits. Dash et al. (2017) have proposed a gesture recognition system using a Myo armband and a model with CNN and GRU (gated recurrent unit). This system can recognize a single-digit number. Yin et al. (2019) focused on improving recognition accuracy in user-independent scenarios by converting sensor data into gesture contours. However, these studies have predominantly focused on recognizing gestures as isolated events. A significant issue in continuous gesture recognition is the need for pauses between gestures, significantly reducing input speed and degrading user experience. Studies have also investigated the recognition of gestures performed in a continuous sequence without pauses.

Lin et al. (2018) devised a technique for recognizing air writing gestures for text input on small-screen smartwatches, where conventional touch input is impractical. In their study, gestures were not performed continuously; short pauses were introduced between gestures to aid word recognition. Additionally, they improved tolerance for ambiguity in air-writing gestures by offering suggestions for four words based on input prefixes, utilizing a language database, and implementing automatic word completion. Amma et al. (2014) proposed applying methods used in gesture recognition to speech recognition. In this approach, the entire dataset of consecutively performed gestures is processed as a single input, rather than recognizing each gesture individually for character recognition. This method employs a hidden Markov model (HMM) decoding and language modeling to enable the recognition of words and sentences by interpreting a continuous stream of gesture data as input. Zhang et al. (2021) introduced an innovative end-to-end word-level recognition methodology.

This approach eschews the segmentation of each character and instead employs a deep learning framework, utilizing a connectionist temporal classification (CTC) decoder for streaming character output. They integrated an additional decoder with an attention layer within a CNN architecture to further refine character accuracy. This configuration ensures that a more precise word recognition result is achieved upon completion of character processing. Additionally, they incorporated a language model to enhance overall accuracy. Chen et al. (2021) developed ViFin, a novel approach for small-motion finger handwriting gesture recognition. This technique captures vibrations generated during air-drawn letters using a smartwatch with a finger and uses CTC and spell checking for continuous letter recognition. These studies prioritize words and sentences as their recognition targets and utilize the contextual dependency of letters and words. They employ advanced language models such as transformers and propose recognition methods that utilize dictionary-based interpolation. However, these methods may exhibit limited efficacy for newly coined words or for numbers and symbols that lack contextual dependencies.

In human activity recognition, segmentation of time-series data is important to identify the exact boundaries of an activity. Yao et al. (2018) have proposed dense labelling, which is a method for predicting the classification label of each sample (i.e., timestep). They pointed out that the conventional Sliding Window technique had problems with the best window length, sampling stride (window overlapping), and windows' labeling strategy. The windows lapping causes a multi-class window problem. Dense labelling avoids this problem because it has no windows and generates the label sequence of the same length as the input data. Zhang et al. (2019) have proposed a U-Net-based human activity recognition method.

We introduce a deep learning model with sample-level dense labeling, focusing on individual character recognition and accurately identifying numbers independent of preceding or subsequent characters. In this approach, the meticulous creation of precise sample-level labels is paramount for effectively training deep learning models with sample-level dense labeling. However, generating accurate labels from solely IMU data during gesture performance presents a challenge, owing to the inherent difficulty in discerning the exact duration of the gesture using only the IMU data without any cue data. In the previous work, the arm was intentionally immobilized after each gesture, exclusively during training data collection. This strategy facilitated the precise determination of gesture duration solely from IMU data. However, this study diverges from previous methodologies, such as the Sliding Window technique, since it directly inputs the entire dataset into the deep learning model for recognition. Consequently, sensor data obtained during the transitional phase between gestures could potentially influence the training of the deep learning model. To counteract this and improve the accuracy of the deep learning models, we advocate for creating precise labels using a multimodal dataset, consisting of IMU data from wearable sensors and camera data. After training the deep learning model, only the IMU data is

used for continuous air-writing multi-digit recognition. Then, our proposed approach is free from occlusions with cameras and poor illumination.

METHODS

Continuous Air-writing Multi-digit Recognition System

Our approach employed a deep learning model for continuously recognizing air-written multidigit numbers using wearable sensors, as depicted in Figure 1. The model used, U-Net (Ronneberger et al., 2015), is renowned for semantic segmentation and has demonstrated high accuracy in time-series data recognition. The configuration of the deep-learning mode allowed it to output two elements for each sample: a recognition label and a sine wave, as illustrated in Figure 2. The sine wave served to ascertain the number and duration of performed gestures.

The rationale for producing both sine wave and recognition labels is elucidated through specific examples. Consider the scenario where a user airwrites the two-digit number 55 without any temporal gap between the fives in the tens and units places. If the sensor's sampling frequency is not exceptionally high, the data representing the transitional period

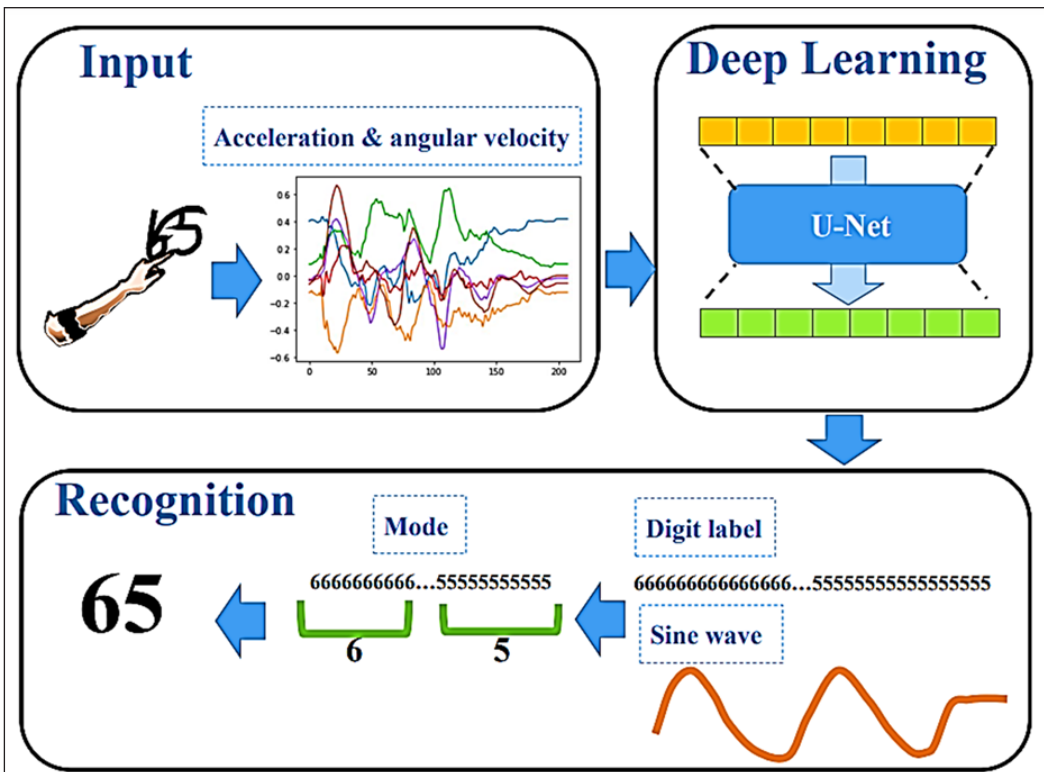


Figure 1. Overview of the continuous air-writing multidigit recognition system utilized in this study

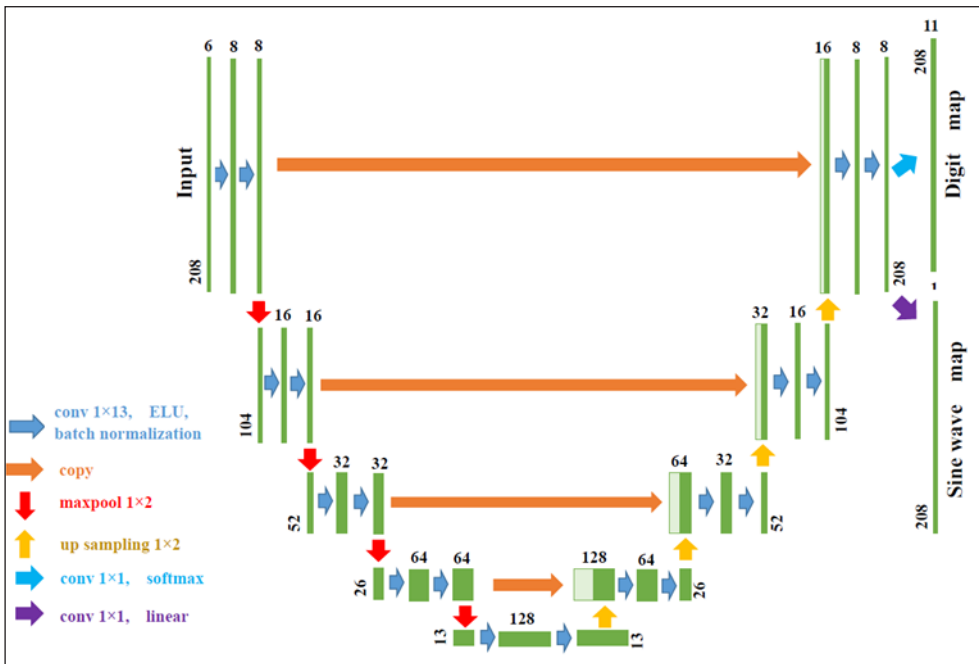


Figure 2. U-Net architecture was employed in this study

might be minimal, potentially as scarce as a single sample. In such instances, the output recognition labels from the deep learning model might only indicate a series of fives, represented as [5,5,5,5,5,...]. This output alone makes it challenging to determine whether the air-written number is a single five or a larger digit like 55 or 555.

To enhance the performance of the deep learning model, it was trained to produce one sine wave for each character. This configuration enables the recognition of any number of digits in a continuous sequence without restricting the count of consecutive digit inputs. The model generates two outputs: recognition labels and sine waves, both of which are per-sample outputs matching the temporal length of the input data. The recognition label is an 11-dimensional output, encompassing digits 0 to 9 and an additional value, 10, to signify non-gesture periods. The sine wave is trained to output values ranging from -1 to 1 for each sample. Therefore, obtaining precise data for each sample is crucial.

Experimental Setup

A multimodal dataset with accurate labels was constructed by integrating IMU and camera data. The process commenced with collecting video data using a webcam on a personal computer during the gesture performance, in conjunction with gathering IMU data from a wearable sensor on the arm. This process is depicted in Figure 3. We used a webcam on a laptop PC MSI GF63-11UC. The obtained video data has a resolution of 720 × 480

and a frame rate of 30 Hz. A participant wore a Myo armband on the forearm near the elbow and performed air-writing gestures in front of the webcam. We collected the IMU data using the Myo armband. The IMU data have three-dimensional acceleration sensor data, gyroscope sensor data, and a sampling rate of 50 Hz. A participant performed the designated air-writing gesture after a sound cue.

We recorded the IMU and camera data simultaneously for the predefined duration tailored to the number of digits, as shown in Table 1. The duration was so short that a pause during air-writing gestures was not allowed. The data for each gesture was recorded in separate files. As illustrated in Figure 4, Step 1 involved the utilization of Mediapipe, an open-source machine learning library. Mediapipe facilitates the implementation of Google's image recognition technology to detect faces, poses, and fingers in video recordings of air-written text gestures. In this study, the air-writing gestures were executed using only the index finger, allowing for determining the index fingertip's position coordinates from the identified landmarks. We obtained the index fingertip's position coordinates from each raw video data image via Mediapipe. The time series of these coordinates was obtained to trace the index finger's trajectory. In Step 2, the duration of each gesture in the video was ascertained from this trajectory, leading to

Table 1
Measurement time of multidigit numbers

Digits	2	5	8	10
Measurement time [s]	4	8	13	15

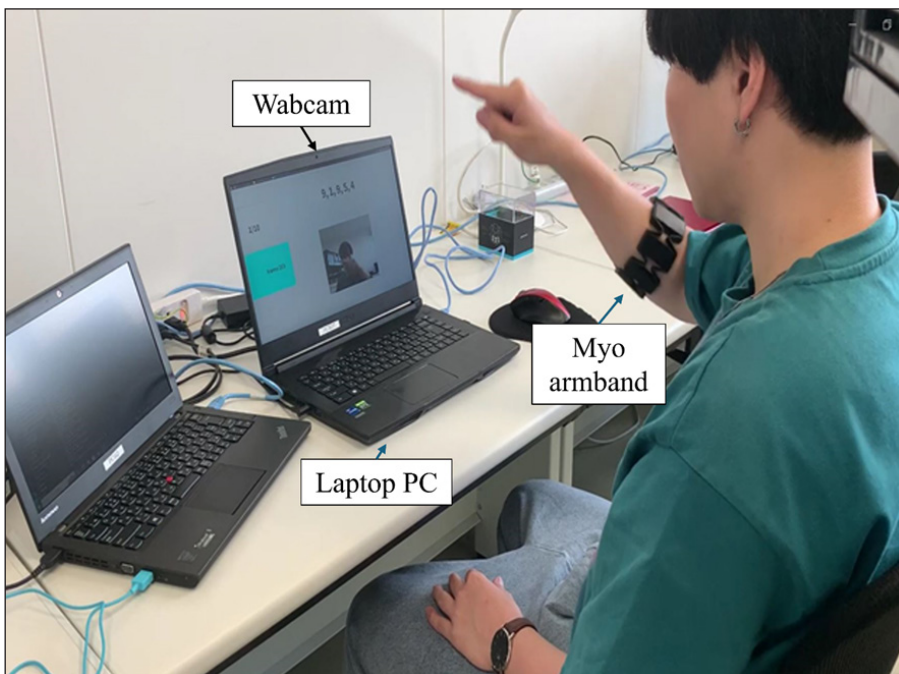


Figure 3. Experimental setup for data collection

the identification of the start and end times for each gesture. In Step 3, the corresponding start and end times in the sensor data for each gesture captured in the video were identified, enabling the creation of precise sample-level dense labels.

Datasets

To assess the multimodal dataset's effectiveness, an "Only-IMU dataset" was constructed, where only IMU data was collected using the wearable sensor. Labeling this dataset involved manual identification of corresponding waveform segments in the IMU data for each gesture. As shown in Step 3 of Figure 4, it is difficult to identify the start and end time of each continuous gesture because the motions before writing the first digit and between the first and second digits were recorded together, and the boundaries between the motions were unclear on the IMU data without camera data. Therefore, the Only-IMU dataset has an inaccuracy in the start and end times of the sample-level dense labels. In the Only-IMU dataset, the air-writing gestures of single-digit and continuous two-digit numbers were recorded. We collected data on the air-writing gesture of the 100 two-digit numbers ranging from 00 to 99 in a randomized order. This resulted in creating an Only-IMU dataset from 8 participants (8 male, 8 right-handed, 22 to 23 years old) and a multimodal dataset from 2 participants (2 male, 2 right-handed, 22 to 24 years old). These datasets were then utilized to train a user-dependent deep neural network model. The model's accuracy was evaluated using a 4-fold cross-validation approach. Each participant executed 100 trials comprising two types of air-writing gestures, forming 150 training and 50 test datasets per participant.

Moreover, two methodologies were employed to validate the effectiveness of recognizing continuous digit sequences in air-writing text gestures: one using a deep learning model with sample-level dense labeling, and another improving model accuracy by generating precise labels with a multimodal dataset combining IMU data and camera data. Recognition experiments involved collecting 5-digit, 8-digit, and 10-digit number gestures from two participants. The experiment included 50 trials for 5-digit numbers, 45 for 8-digit numbers, and 40 for 10-digit numbers, with 20 trials from each set designated as test data. As shown in Table 2, the multi-digit numbers were chosen as the appearance frequencies of each digit were equal. Consequently, 75 and 60 trials were allocated for training and testing, respectively.

Additionally, we used another multimodal dataset from 4 participants (2 males/1 female, 4 right-handed, 22 to 24 years old, 3 days) to evaluate the robustness of the recognition for another participant. Two participants of this dataset were in common with the previous multimodal dataset. Their data collection was conducted after several weeks.

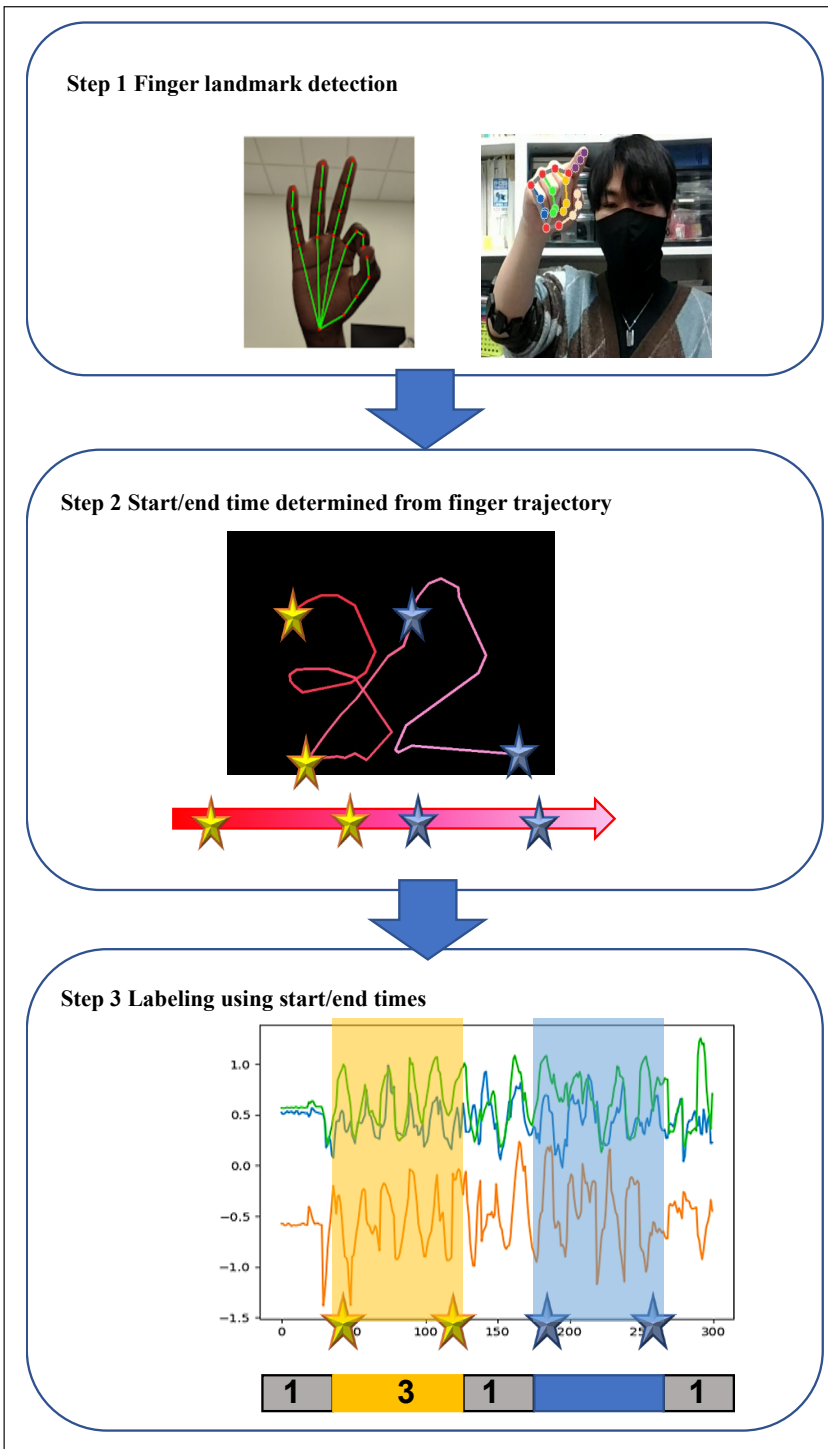


Figure 4. Process of time series data labeling using camera data

Table 2
The multidigit numbers for training and testing

Digits	Training	Test
2	None	23, 41, 80, 96, 98, 25, 12, 19, 10, 20, 30, 45, 54, 77, 66, 33, 69, 88, 75, 47
	56053, 03783, 52234, 82673, 42638, 02683, 90472, 96916, 23584, 86313, 83775, 81943, 06085, 12721, 90291, 90072, 05710, 81922, 65407, 44156, 86898, 51056, 69472, 94177, 97407,	08391, 63777, 61493, 63836, 95357, 09376, 55061, 82477, 80858, 98761, 54872, 82105, 09631, 90382, 15535, 70161, 04240, 42122, 42699, 44924,
8	54050611, 79161824, 78205757, 09033936, 98378568, 38254293, 07109104, 93891258, 85801886, 60666899, 66532268, 52842347, 56707414, 86926224, 06341128, 83491202, 78851040, 44715470, 69990556, 00766734, 09229570, 65429370, 25254451, 31413553, 41391777, 91337311,	84714903, 63716832, 52518516, 96660113, 88159682, 57819026, 37346495, 06574521, 08142977, 00993294, 93328847, 78332134, 22403008, 82974858, 22234867, 64796720, 33716979, 54605015, 15579940,
	2546030623, 8999541525, 2491348039, 0172482836, 2922403988, 9396843658, 0207013197, 8645101973, 9222887954, 0810865143, 5073511680, 5382770921, 7682468955, 6850667241, 7319567533, 0942800351, 9460773561, 4967727780, 2455417469, 1713464316,	2052286307, 5219346410, 6013820328, 7372505753, 2345757747, 8536225349, 5099736910, 3710321047, 4241288622, 2671683185, 9014071205, 1746011720, 0901145029, 0131256438, 8665665118, 4064895399, 5564398438, 7768833445, 8897798799, 4699696894,
10		

RESULTS AND DISCUSSION

Utilizing 10 datasets—eight from the Only-IMU group and two from the multimodal group—the training and evaluation process of the user-dependent deep neural network model was repeated 15 times, employing 4-fold cross-validation. This repetition was crucial to ascertain the true recognition accuracy, considering the initial parameter values of the deep neural network model and the potential variations in final parameters due to the training process. Consequently, accuracy was determined by averaging the correct answer percentages from the test dataset across 15 iterations.

The accuracy evaluation in this study is not based on the percentage of correctly identified individual digits within each number. Instead, it is determined by the accuracy of the entire number; a two-digit number is considered correctly recognized only if both digits precisely match the correct answer. Conversely, any discrepancy in even one digit results in the entire number being classified as incorrect.

Recognition of Two-digit Numbers

As depicted in Figure 5, the average percentages of correct responses using the Only-IMU dataset from the eight participants were as follows: 80.6%, 86.1%, 84.1%, 75.9%, 84.1%, 76.6%, 80.9%, and 75.7%. In contrast, when utilizing the multimodal dataset from two participants, the average percentages of correct responses were significantly higher at 94.3% and 92.9%. This represents an approximate 13% improvement in the average percentage of correct answers for the multimodal datasets compared to the Only-IMU datasets.

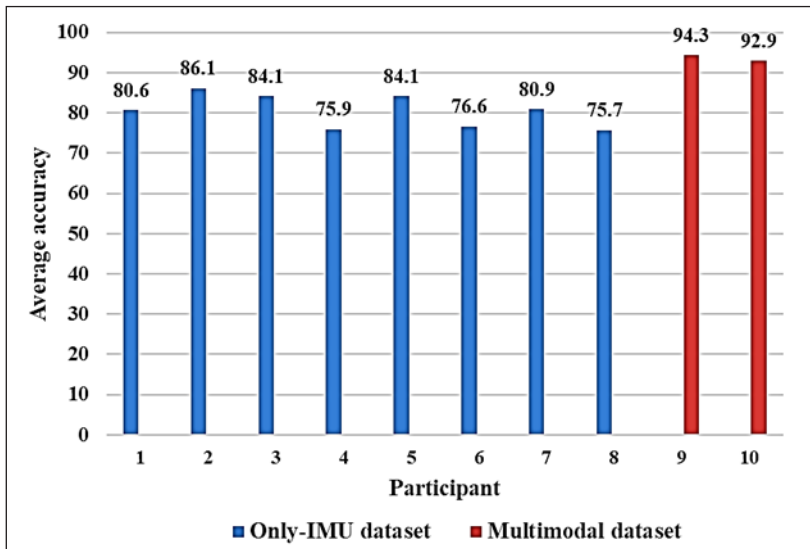


Figure 5. Comparative analysis of average accuracy: Only-IMU dataset vs. multimodal dataset

Additionally, the study examined confusion matrices of character recognition. The matrices, presented in Figures 6 and 7, indicated a notable reduction in misidentifications among numbers with similar gestures, such as 0, 6, 2, and 3. Figure 6 illustrates the results obtained using the Only-IMU dataset. The air-writing gesture for 0 was misrecognized as 6, a total of 63 times in the Only-IMU dataset. In contrast, as shown in Figure 7, the same misrecognition occurred only once when using the multimodal dataset. The misrecognition of 0, 2, and 3 also decreased similarly due to the multimodal dataset. This improvement is attributed to the more precise label data creation in the multimodal dataset. In the Only-IMU dataset, correct data was derived by manually identifying similar waveform segments in the IMU data for each gesture. However, this method proved less accurate, particularly for gestures with shared characteristics. In cases like 0, 6, 2, and 3, the IMU data waveforms were predominantly similar, with only minor differences at the beginning or end of the waveforms. These subtle differences, often represented by only a few samples, were occasionally overlooked in the labeling process, leading to the same waveform being

assigned different numerical labels. Consequently, the deep learning model was trained to map identical waveforms to diverse labels, potentially confusing the training phase. These findings underscore the effectiveness of the method that enhances the accuracy of deep-learning models by generating precise labels through a multimodal dataset, which integrates IMU data from wearable sensors and camera data.

0	420	10	3	1	4	2	64	1	0	3
1	12	396	6	5	8	4	18	31	1	7
2	0	2	428	53	7	0	0	5	0	4
3	0	1	17	436	0	0	0	0	2	0
4	2	6	2	7	428	1	4	8	8	2
5	0	1	9	2	0	427	3	2	8	1
6	61	13	2	0	4	1	432	1	1	2
7	2	15	5	2	6	0	0	432	1	5
8	0	0	5	5	0	0	2	0	431	0
9	3	1	0	0	2	0	2	6	0	415
	0	1	2	3	4	5	6	7	8	9

Figure 6. Confusion matrix from an experiment using the Only-IMU dataset

0	419	0	0	0	0	1	1	0	1	2
1	10	346	7	1	6	2	1	1	0	2
2	2	1	400	8	1	0	0	1	2	1
3	1	0	19	403	0	0	0	0	1	0
4	0	1	0	0	431	0	0	0	0	0
5	0	0	0	0	0	434	0	0	1	0
6	0	0	0	0	0	3	437	0	0	0
7	0	3	4	2	0	0	0	431	0	1
8	0	0	0	2	0	0	0	0	432	0
9	1	0	0	0	2	0	0	0	0	443
	0	1	2	3	4	5	6	7	8	9

Figure 7. Confusion matrix from an experiment using a multimodal dataset

Recognition of Multidigit Numbers

In a study focused on continuous air-writing of multidigit number gestures, 5-digit, 8-digit, and 10-digit sequences were collected from two participants. This experiment replicated the methodology of the previous study, including 15 training trials of the deep neural network model. The criterion for correct recognition remained consistent; a response was deemed accurate only if all digits of a number precisely matched the correct answer. Table 3 presents the average accuracy rates: 99% and 96.3% for 5-digit numbers, 99.6% and 97.6% for 8-digit numbers, and 99.3% and 93.3% for 10-digit numbers. These results suggest that the methods employed in this study were effective for recognizing air-writing gestures in continuous digit sequences.

Table 3
Average accuracy in multidigit recognition experiments (user-dependent)

Participant number	Accuracy rate for 5-digit numbers (%)	Accuracy rate for 8-digit numbers (%)	Accuracy rate for 10-digit numbers (%)
9	99.0	99.6	99.3
10	96.3	97.6	93.3

Compared to the accuracy rates for one- and two-digit numbers in the multimodal dataset verification experiment, it is noteworthy that the increased number of digits and the consequent rise in recognition complexity did not hinder accuracy. In the multimodal dataset experiment, the training data comprised 150 samples, divided equally between one-digit and two-digit numbers, amounting to 225 data points when considered individually. In contrast, the 5-digit, 8-digit, and 10-digit cases involved 30, 25, and 20 training data samples, culminating in 550 data points. This indicates that the training incorporated double the amount of data, which likely contributed to the improved accuracy rates despite the heightened complexity.

However, a persistent challenge was the tendency to overlook the recognition of the digit one in 5-digit, 8-digit, and 10-digit sequences. This issue is attributed to the variation in the time required to complete the gesture for each digit. Notably, the gesture time for digit one is significantly shorter compared to other digits, which potentially led to its under-recognition in these scenarios.

The deep learning model employed in this research was U-Net, with the kernel size of the convolutional layer maintained constant throughout the model. This fixed configuration might have contributed to the inadequate feature extraction of Gesture 1 during the deep learning process. As a result, enhancements in data preprocessing and the deep learning models are needed to ensure robust recognition of variations in the duration of each gesture.

Additionally, this study utilized user-dependent recognition. However, for the practical implementation of gesture input systems, it is preferable to distinguish between the users providing training data and those performing the actual gesture recognition. Relying on users to collect training data prior to actual use and subsequently training a deep learning model with this data is a time-consuming and labor-intensive process. This approach significantly detracts from the user experience as an input method, making it less feasible for practical applications.

Consequently, there is a pressing requirement for developing user-independent recognition systems. Such systems need to account for the diverse nature of user data, which can vary significantly in aspects like writing style, writing speed, arm position, and arm movement patterns. Therefore, designing a recognition system resilient to these user-specific variations is essential for successfully implementing gesture input technology.

Robustness

To investigate the robustness of multidigit number recognition, we conducted three-fold cross-validation, where the three participants were separated into two groups for training and one for testing. Table 4 shows the results of the cross-validation. In our method and dataset, the robustness is very low. The reason is that our dataset is too small. Air-writing gestures were highly dependent on participants. For instance, in the case of 2-digit numbers,

the accuracy varied significantly from 0.355 to 0.777. Another factor is the writing speed because we ask them to write multidigit numbers very fast. For instance, a participant should perform an air writing gesture of 10-digit numbers in 15 seconds. It is difficult to write digits fast and neatly.

Table 4
Accuracy in user-independent conditions

Test participant	2-digit	5-digit	8-digit	10-digit
P1	0.642	0.315	0.162	0.200
P2	0.777	0.357	0.260	0.277
P3	0.355	0.052	0.013	0.013
Average	0.591	0.241	0.163	0.092

Comparison with Other Studies

We compared our results with other studies using IMU-based approaches for recognizing digits. Singh and Koundal (2024) have achieved a recognition accuracy of 99.50% for the RealSense-Based 3D Trajectory Digit and Character (RTD-RTC) datasets (Image-based), which Alam et al. (2019; 2020) have collected, and a recognition accuracy of 96.30% for the 6DMG dataset (IMU-based), which Chen et al. (2012) have collected. Zhang et al. (2022) have achieved a recognition accuracy of 97.95% for the dataset using an IMU sensor attached to an index finger. Dash et al. (2017) have achieved a recognition accuracy of 96.7% for the user-dependent recognition and 91.7% for the user-independent recognition. Lamaakal et al. (2024) have achieved a testing recognition accuracy of 98.7%. These studies employed the sliding window technique. In the case of recognizing 10-digit numbers, the multi-class windows problem causes a decrease in the recognition accuracy. Here, a denotes a recognition accuracy of a single digit. A recognition accuracy of a 10-digit number is estimated to be a^{10} , which means 10 consecutive successes of recognition. Therefore, our recognition accuracy of 10-digit numbers in the user-dependent evaluation was higher because $0.987^{10} \approx 0.877$.

CONCLUSION

This study proposed a novel method for consecutive digit recognition, employing a deep learning model with sample-level dense labeling, diverging from the traditional Sliding Window technique of mapping a single label to one window. Additionally, the study advocated for enhancing deep-learning model accuracy by generating precise labels through a multimodal dataset that integrates IMU data from wearable sensors with camera data. The results of the recognition experiments conducted to validate the model's effectiveness demonstrated an average accuracy improvement of approximately 13% when using the

deep learning model trained on the multimodal dataset, compared to the model trained solely on the IMU dataset. The confusion matrix analysis revealed a significant reduction in misrecognition among numbers sharing similar gestures, such as 0, 6, 2, and 3, confirming the positive impact of accurate data creation using a multimodal dataset on the training of deep learning models. The participants in the study achieved an average correct response rate of over 90% in the recognition experiments for 5-digit, 8-digit, and 10-digit number gestures.

Notably, even with up to 10 consecutive digits, the correct answer rate was as high as 99.3% for the subject with the highest correct answer rate and 93.3% for the subject with the lowest correct answer rate, exceeding 90%. This indicated the proposed method's effectiveness for recognizing air-writing gestures in continuous digit sequences, employing a deep learning model with sample-level dense labeling and a multimodal dataset. However, future work is necessary to further verify and enhance the robustness of the recognition method in relation to variations in gesture duration and individual user differences. This will involve focusing on data preprocessing and advancing deep learning models to address these challenges.

ACKNOWLEDGEMENT

The authors acknowledge Mr. Kazuma Kodama for the data collection of air-writing gestures from eight participants.

REFERENCES

- Alam, M. S., Kwon, K. C., & Kim, N. (2019). Trajectory-based air-writing character recognition using convolutional neural network. In *2019 4th International Conference on Control, Robotics and Cybernetics (CRC)* (pp. 86-90). IEEE. <https://doi.org/10.1109/CRC.2019.00026>
- Alam, M. S., Kwon, K. C., Alam, M. A., Abbass, M. Y., Imtiaz, S. M., & Kim, N. (2020). Trajectory-based air-writing recognition using deep neural network and depth sensor. *Sensors*, *20*(2), Article 376. <https://doi.org/10.3390/s20020376>
- Amma, C., Georgi, M., & Schultz, T. (2014). Airwriting: A wearable handwriting recognition system. *Personal and Ubiquitous Computing*, *18*, 191-203. <https://doi.org/10.1007/s00779-013-0637-3>
- Dash, A., Sahu, A., Shringi, R., Gamboa, J., Afzal, M. Z., Malik, M. I., Dengel, A., & Ahmed, S. (2017). Airstript-creating documents in air. In *2017 14th IAPR International Conference on Document Analysis and Recognition (ICDAR)* (pp. 908-913). IEEE. <https://doi.org/10.1109/ICDAR.2017.153>
- Kim, D. W., Lee, J., Lim, H., Seo, J., & Kang, B. Y. (2014). Efficient dynamic time warping for 3D handwriting recognition using gyroscope equipped smartphones. *Expert Systems with Applications*, *41*(11), 5180-5189. <https://doi.org/10.1016/j.eswa.2014.03.011>
- Kim, E., Shin, J., Kwon, Y., & Park, B. (2023). EMG-based dynamic hand gesture recognition using edge AI for human-robot interaction. *Electronics*, *12*(7), Article 1541. <https://doi.org/10.3390/electronics12071541>

- Lamaakal, I., Ouahbi, I., El Makkaoui, K., Maleh, Y., Pławiak, P., & Alblehai, F. (2024). A TinyDL model for gesture-based air handwriting arabic numbers and simple arabic letters recognition. *IEEE Access*, *12*, 76589-7660. <https://doi.org/10.1109/ACCESS.2024.3406631>
- Lin, X., Chen, Y., Chang, X. W., Liu, X., & Wang, X. (2018). Show: Smart handwriting on watches. *Proceedings of the ACM on Interactive, Mobile, Wearable and Ubiquitous Technologies*, *1*(4), Article 151. <https://doi.org/10.1145/3161412>
- Lu, Z., Chen, X., Li, Q., Zhang, X., & Zhou, P. (2014). A hand gesture recognition framework and wearable gesture-based interaction prototype for mobile devices. *IEEE Transactions on Human-Machine Systems*, *44*(2), 293-299. <https://doi.org/10.1109/THMS.2014.2302794>
- Ronneberger, O., Fischer, P., Brox, T. (2015). U-Net: Convolutional networks for biomedical image segmentation. In N. Navab, J. Hornegger, W. M. Wells & A. F. Frangi (Eds.) *Medical Image Computing and Computer-Assisted Intervention – MICCAI* (pp. 234-241). Springer. https://doi.org/10.1007/978-3-319-24574-4_28
- Schäfer, A., Reis, G., Stricker, D. (2022). Controlling continuous locomotion in virtual reality with bare hands using hand gestures. In G. Zachmann, M. A. Raya, P. Bourdot, M. Marchal, J. Stefanucci & X. Yang (Eds.) *International Conference on Virtual Reality and Mixed Reality* (pp. 191-205). Springer International Publishing. https://doi.org/10.1007/978-3-031-16234-3_11
- Singh, A. K., & Koundal, D. (2024). A temporal convolutional network for modeling raw 3D sequences and air-writing recognition. *Decision Analytics Journal*, *10*, Article 100373. <https://doi.org/10.1016/j.dajour.2023.100373>
- Tripathi, A., Mondal, A. K., Kumar, L., & Prathosh, A. P. (2022). ImAiR: Airwriting recognition framework using image representation of IMU signals. *IEEE Sensors Letters*, *6*(10), Article 7003704. <https://doi.org/10.1109/LSENS.2022.3206307>
- Wu, J., Pan, G., Zhang, D., Qi, G., & Li, S. (2009). Gesture recognition with a 3-d accelerometer. In D. Zhang, M. Portmann, A. H. Tan & J. Indulska (Eds.) *Ubiquitous Intelligence and Computing: 6th International Conference, UIC* (pp. 25-38). Springer Berlin Heidelberg.
- Yao, R., Lin, G., Shi, Q., & Ranasinghe, D. C. (2018). Efficient dense labelling of human activity sequences from wearables using fully convolutional networks. *Pattern Recognition*, *78*, 252-266. <https://doi.org/10.1016/j.patcog.2017.12.024>
- Yin, Y., Xie, L., Gu, T., Lu, Y., & Lu, S. (2019). AirContour: Building contour-based model for in-air writing gesture recognition. *ACM Transactions on Sensor Networks (TOSN)*, *15*(4), 1-25. <https://doi.org/10.1145/3343855>
- Zhang, H., Chen, L., Zhang, Y., Hu, R., He, C., Tan, Y., & Zhang, J. (2022). A wearable real-time character recognition system based on edge computing-enabled deep learning for air-writing. *Journal of Sensors*, *2022*(1), Article 8507706. <https://doi.org/10.1155/2022/8507706>
- Zhang, Q., Wang, D., Zhao, R., Yu, Y., & Jing, J. (2021). Write, attend and spell: Streaming end-to-end free-style handwriting recognition using smartwatches. *Proceedings of the ACM on Interactive, Mobile, Wearable and Ubiquitous Technologies*, *5*(3), Article 138. <https://doi.org/10.1145/3478100>

- Zhang, Y., Gu, T., Luo, C., Kostakos, V., & Seneviratne, A. (2018). FinDroidHR: Smartwatch gesture input with optical heart rate monitor. *Proceedings of the ACM on Interactive, Mobile, Wearable and Ubiquitous Technologies*, 2(1), Article 56. <https://doi.org/10.1145/3191788>
- Zhang, Y., Zhang, Y., Zhang, Z., Bao, J., & Song, Y. (2018). Human activity recognition based on time series analysis using U-Net. *arXiv preprint arXiv:1809.08113*. <https://doi.org/10.48550/arXiv.1809.08113>

Acoustic Partial Discharge Localization in Refined, Bleached and Deodorized Palm Oil (RBDPO) Based on the Savitzky-Golay and Moving Average Denoising Methods

Nur Darina Ahmad^{1,2}, Norhafiz Azis^{1*}, Jasronita Jasni¹, Khairil Anas Md Rezali³, Mohd Aizam Talib⁴, Nik Hakimi Nik Ali⁵ and Masahiro Kozako⁶

¹*Advanced Lightning, Power and Energy Research Centre (ALPER), Department of Electrical and Electronics Engineering, Universiti Putra Malaysia, 43400 UPM Serdang, Selangor, Malaysia*

²*Electrical Engineering Studies, College of Engineering, Universiti Teknologi MARA, Pulau Pinang Branch, 13500 Permatang Pauh, Pulau Pinang, Malaysia*

³*Department of Mechanical and Manufacturing Engineering, Faculty of Engineering, Universiti Putra Malaysia, 43400 UPM Serdang, Selangor, Malaysia*

⁴*Advanced Diagnostic Services, TNB Labs Sdn Bhd, 43000 Kajang, Selangor, Malaysia*

⁵*School of Electrical Engineering, College of Engineering, Universiti Teknologi MARA (UiTM), 40450 Shah Alam, Selangor, Malaysia*

⁶*Department of Electrical and Electronic Engineering, Kyushu Institute of Technology, Kitakyushu-shi, Fukuoka, Japan*

ABSTRACT

This research describes an investigation on the localization of partial discharge (PD) in Refined, Bleached and Deodorized Palm Oil (RBDPO) with the applications of 2 denoising methods, namely Savitzky-Golay (SG) and Moving Average (MA). A needle-plane electrode setup was used to initiate the PD. The electrical PD signal measurement was carried out through the impedance matching circuit (IMC), and the acoustic PD signal was obtained by acoustic emission (AE) sensors. The AE sensors were attached to the tank's surface, and pre-amplifiers were used to boost the acquired

acoustic PD signal. A high-voltage AC supply initiated the PD within the test tank filled with RBDPO. Both electrical and acoustic PD signals were denoised by SG and MA methods. The 2 denoising methods were evaluated based on the signal-to-noise ratio (SNR), root mean squared error (RMSE) and correlation coefficient (CC) metrics. The denoised acoustic PD signals were then utilized in the time difference of arrival (TDOA) technique to perform PD localization. The SG was found to be more effective than the MA in denoising both the electrical and acoustic

ARTICLE INFO

Article history:

Received: 01 April 2024

Accepted: 10 April 2025

Published: 10 June 2025

DOI: <https://doi.org/10.47836/pjst.33.S4.07>

E-mail address:

nurdarina9183@uitm.edu.my (Nur Darina Ahmad)

norhafiz@upm.edu.my (Norhafiz Azis)

jas@upm.edu.my (Jasronita Jasni)

khairilanas@upm.edu.my (Khairil Anas Md Rezali)

aizam.talib@tnb.com.my (Mohd Aizam Talib)

hakimial@uitm.edu.my (Nik Hakimi Nik Ali)

kozako@ele.kyutech.ac.jp (Masahiro Kozako)

*Corresponding author

PD signals based on its low RMSE and high CC. The estimated PD source locations based on the SG-denoised acoustic PD signals are closer to the actual PD source than those derived from the MA-denoised signals.

Keywords: Acoustic partial discharge, moving average (MA), partial discharge localization, RBDPO (refined, bleach and deodorized palm oil), Savitzky-Golay (SG), time difference of arrival (TDOA)

INTRODUCTION

Partial discharge (PD) is a phenomenon that can affect the insulation in transformers. PD diagnostic is commonly employed due to its high sensitivity (Firuzi et al., 2019). Localization of PD can further be used to pinpoint the location of potential problems in the insulation system (Karami et al., 2020). Furthermore, it can help with the targeted maintenance scheme of transformers (Chan et al., 2023; Zhang et al., 2018).

The introduction of Refined, Bleached and Deodorized Palm Oil (RBDPO) as a possible substitute for mineral oil in transformers promotes sustainable initiatives in industries (Rafiq et al., 2015). Several studies have examined the suitability of RBDPO for this purpose (Azis et al., 2014; Mustam et al., 2023). Currently, the study related to acoustic PD source localization in RBDPO is still limited.

It is known that PD could be identified through electrical, chemical, acoustic and electromagnetic approaches. Acoustic PD signal often consists of both PD signal and noise components, necessitating denoising techniques to enhance detection accuracy (Hussain et al., 2021). The Savitzky-Golay (SG) is known as one of the denoising methods used in different types of applications, such as acoustic PD source localization in mineral oil, medical electromyography signal, on-load tap changer vibro-acoustic signal and sulfur hexafluoride corona discharge data (Dombi & Dineva, 2020; Feizifar et al., 2019; Li et al., 2021; Lonkwic et al., 2017; Seo, 2018a, 2018b; Yang et al., 2022). Moving Average (MA) is applied for electrical and acoustic PD source localization in mineral oil, communication echo signal/temperature data and photochemical and electrochemical reactor data (Ghosh et al., 2017; Guiñón et al., 2007; Hashim et al., 2023; Purnamasari et al., 2021). SG and MA methods are widely used in various applications due to their simplicity, efficiency and ability to preserve important signal features while reducing noise.

This study investigates the localization of the estimated PD source in RBDPO based on the electrical and acoustic PD signals denoised by SG and MA methods. These PD signals are acquired through an impedance matching circuit (IMC) and acoustic emission (AE) sensors. The acoustic PD source localization is based on the time difference of arrival (TDOA) outputs determined from the denoised acoustic PD signals. The performances of denoising methods are analyzed through signal-to-noise ratio (SNR), root mean squared

error (RMSE) and correlation coefficient (CC) metrics. The accuracy of the acoustic PD source localization is examined through location error analysis.

MATERIALS AND METHODS

Oil Preparation

Refined, Bleached and Deodorized Palm Oil (RBDPO) was used in this study, whereby the properties can be seen in Azis et al. (2014). The RBDPO was first subjected to filtration with a $0.22\ \mu\text{m}$ membrane filter. After filtration, the RBDPO was dried in an air-circulating oven at $85\ ^\circ\text{C}$ for 72 hours.

Experiment Setup

A steel test tank with dimensions of 40 cm in length, 25 cm in width, 25 cm in height and a maximum capacity of 20 liters was employed for the experiment. PD was produced through a needle-plane electrode setup with a gap distance between the needle tip and the surface of the plane electrode fixed at 50 mm throughout the experiment. The needle has a tip radius of $3\ \mu\text{m}$, and the diameter of the plane ground electrode is 50 mm. Figure 1 depicts the test circuit for electrical and acoustic PD measurement, whereby the measurement is carried out in accordance with IEC 61294 and IEC 60270 (Fuhr, 2005; Pattanadech & Muhr, 2017). Figure 2 illustrates an example of the AE sensors and needle-plane electrode placements. A 3D coordinate system was established for the steel tank, whereby one of the bottom corners of the tank was set as the origin (0, 0, 0) m, as shown in Figure 3. Based on this coordinate system, the actual PD source was set at (0.07, 0.08, 0.18) m.

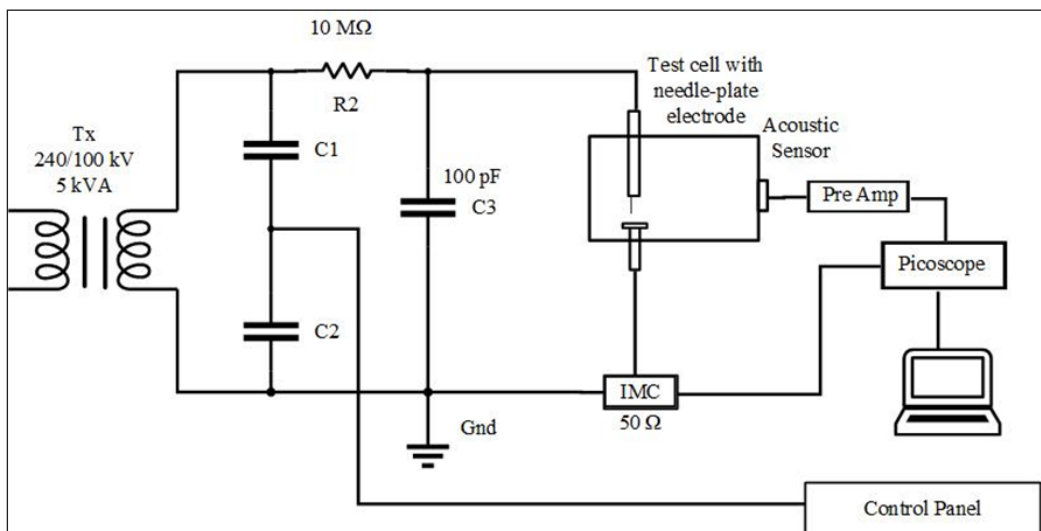


Figure 1. Experimental configuration for electrical and acoustic partial discharge measurements

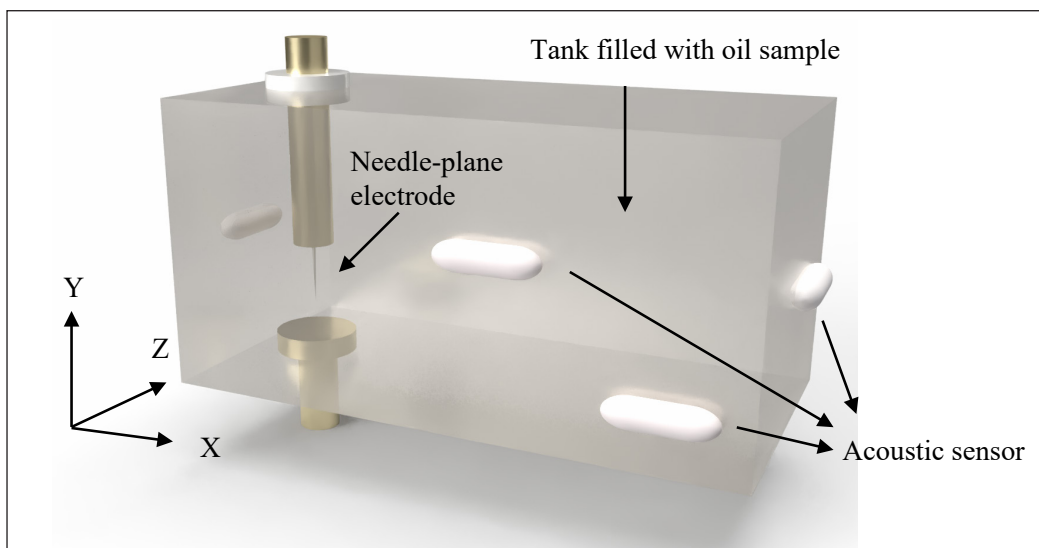


Figure 2. Example of needle-plane electrodes and acoustic emission sensor placements

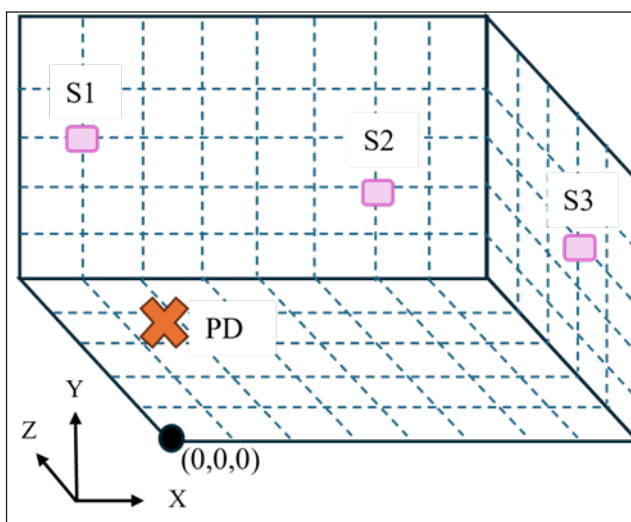


Figure 3. Coordinate marking for partial discharge localization

A high-voltage AC supply with a rating up to 100 kV was utilized to supply the voltage at the needle electrode, as shown in Figure 1. The supply voltage was increased at a constant step of 5 kV from 15 kV to 40 kV. In this study, 4 AE sensors were applied to capture the acoustic PD signals, as depicted in Figure 3. The operating frequency range of these AE sensors is between 20 and 180 kHz. Each AE sensor was connected to a pre-amplifier with 60 dB gain. The sensitivity of the AE sensor was checked based on IEEE C.57.127 (Ghosh et al., 2017). The electrical PD signal was acquired via an IMC with input and

output impedances of 50Ω respectively. The acoustic PD signals were collected once the electrical PD signals exceeded the partial discharge inception voltage (PDIV), which ranges from 120 pC to 140 pC, depending on the surrounding noise and weather. PicoScope 4824 with a sampling frequency up to 80 MS/s was used to acquire the electrical and acoustic PD signals simultaneously.

Acoustic Emission Sensors Positioning

Sixty-four different combinations of AE sensors' positions were used to collect the acoustic PD signals during the experiment. Each combination consisted of the positions for the 4 AE sensors, which were attached to the surface of the tank wall via magnetic holders. The various combinations were designed to ensure full coverage of the test tank's surface area. The AE sensors' position combinations are provided in Table 1.

Table 1
Examples of AE sensors' position combinations

Combination	AE Sensor	Sensor Position (cm)		
		x	y	z
1	Sensor 1	0	15	5
	Sensor 2	40	15	20
	Sensor 3	5	15	25
	Sensor 4	10	10	25
2	Sensor 1	0	10	5
	Sensor 2	40	10	20
	Sensor 3	5	10	25
	Sensor 4	40	5	10
3	Sensor 1	0	15	10
	Sensor 2	10	15	25
	Sensor 3	40	15	15
	Sensor 4	0	10	20

Denoising Technique

Once the measured data from the experimental work were acquired, the denoising technique was applied to electrical and acoustic PD signals.

Savitzky-Golay

The Savitzky-Golay (SG) is a time-domain method that performs least-squares polynomial fitting in a specific moving time window. As the time window moves across the input PD signals, a high level of smoothing without significant attenuation and minimal distortion can be generated based on Equation 1.

$$y(i) = \sum_{k=-nL}^{nR} (c_k)(s_{i+k}) \tag{1}$$

In Equation 1, $y(i)$ represents the denoised output for the electrical or acoustic PD signal, while s_{i+k} is the $(i+k)$ -th data point of the corresponding input electrical or acoustic PD signal. The nR and nL indicate the number of data points to the right and left of the current data point, i , respectively. c_k is the SG coefficient obtained from the least squares fitting process (Dombi & Dineva, 2020).

Moving Average

The Moving Average (MA) is a simple denoising method used to denoise a signal by calculating the average magnitude of the data points within a specific window. The MA of a PD signal can be computed based on Equation 2.

$$y(i) = \frac{1}{z} \sum_{k=-\frac{z-1}{2}}^{\frac{z-1}{2}} x(i+k) \tag{2}$$

In Equation 2, $y(i)$ represents the moving average at the i -th data point of the input electrical or acoustic PD signal, and $x(i+k)$ refers to the data points within a window of size z centered around the current data point $x(i)$.

Denoising Evaluation

SNR was utilized based on the equation in Yang et al. (2022) to assess the performance of the denoising methods. To assess the distortion of the waveforms for the denoised signal in comparison to the original signal, RMSE was employed based on the equation in Chaudhuri et al. (2023). The similarity of the denoised and original signals was evaluated using the correlation coefficient (CC) through the equation in Javandel et al. (2022).

PD Source Localization

In this study, the electrical PD signal served as the reference for acoustic PD signal detection for time of arrival calculation. This reference signal was crucial for synchronizing the acoustic PD signal to calculate the time delay. The PD source localization was subsequently performed using both time of arrival and TDOA, as outlined in Equation 3 (Ghosh et al., 2017; Sinaga et al., 2012). In this setup, sensor 2 was set as the reference sensor.

$$\begin{bmatrix} x \\ y \\ z \end{bmatrix} = - \begin{bmatrix} x_{12} & y_{12} & z_{12} \\ x_{32} & y_{32} & z_{32} \\ x_{42} & y_{42} & z_{42} \end{bmatrix}^{-1} \times \left\{ \begin{bmatrix} r_{12} \\ r_{32} \\ r_{42} \end{bmatrix} r_2 + \frac{1}{2} \begin{bmatrix} r_{12}^2 - K_1 + K_2 \\ r_{32}^2 - K_3 + K_2 \\ r_{42}^2 - K_4 + K_2 \end{bmatrix} \right\} \quad [3]$$

$$r_2 = \sqrt{[(x - x_2)^2 + (y - y_2)^2 + (z - z_2)^2]} \quad [4]$$

In Equation 3, x , y , and z represent the coordinates of the estimated PD source. The terms x_{j2} , y_{j2} , and z_{j2} jointly refer to the distance between sensor j and the reference sensor, while r_{j2} is the TDOA between sensor j and the reference sensor times the speed of the acoustic PD signal in RBDPO. The variable r_2 denotes the distance between the reference sensor and the estimated PD source, and K_j values are calculated as $K_j = x_j^2 + y_j^2 + z_j^2$. In the experiment, the velocity of the acoustic PD signal in RBDPO was set to 1528.22 ms^{-1} (Ahmad et al., 2023). For Equation 3, all the terms were known values except for r_2 . The x , y , and z coordinates were first expressed as functions of r_2 and then substituted into Equation 4. The positive solution for r_2 obtained from Equation 4 was substituted back into Equation 3 to solve the equation. The x , y , and z coordinates computed from Equation 3 represented the estimated PD source location based on the given positions of the AE sensors and the TDOA obtained from the denoised signals.

The TDOA between any pair of the AE sensors was computed as the difference between the time of arrival of the acoustic PD signal at each sensor. In order to determine the time of arrival of the acoustic PD signal for each of the AE sensors, the first peak method was selected according to Sarathi et al. (2014). The signal was first denoised and then converted to unipolar. Next, the signal was normalized by dividing the magnitude of each data point by the maximum magnitude of the signal. The first peak of the denoised acoustic PD signal that exceeded a pre-defined magnitude threshold was identified as the time of arrival for the particular sensor. Location error analysis was performed to evaluate the accuracy of the estimated PD source locations based on the equation in Kozako et al. (2012).

RESULT AND DISCUSSION

Partial Discharge Characteristic

Electrical Partial Discharge

Figure 4 shows an example of the electrical PD signal acquired at an applied voltage of 35 kV. The pattern of the electrical PD signal is in accordance with the standard IEC 60270 (CIGRE TB 676, 2017).

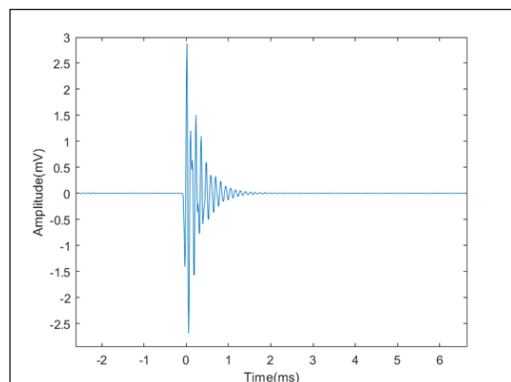


Figure 4. Typical electrical PD signal obtained from the PD experiment

Acoustic Emission Partial Discharge

The examples of acoustic PD signals with strong oil path and strong steel path characteristics can be seen in Figures 5(a) and 5(b), respectively. The contours of the acoustic PD signals are similar to those depicted in (CIGRE TB 676, 2017). The acoustic PD signal in Figure 5(a) propagates through oil over a total distance and time of 30.03 cm and 196.55 μ s. In Figure 5(b), the total distance and time for the acoustic PD signal to propagate along the steel wall are 16.34 cm and 106.94 μ s.

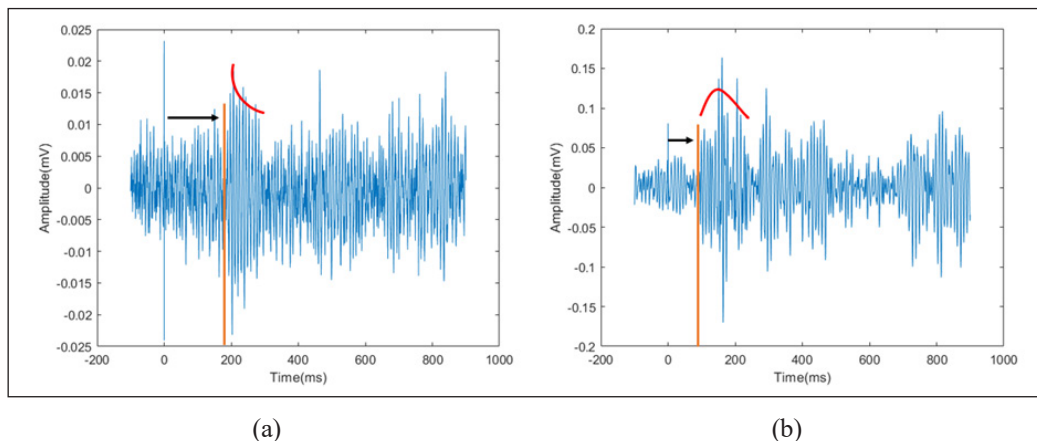


Figure 5. Acoustic PD signal with strong (a) oil and (b) steel path characteristics

Denoising Analysis

The original electrical and acoustic PD signals can be subjected to various kinds of noises such as mechanical noise, white noise and discrete spectral interference (Hashim et al., 2023). Thus, the denoising methods are applied to remove the noise from the original signals. Examples of original and denoised electrical and acoustic PD signals based on SG and MA can be found in Figures 6 and 7. It is shown that SG and MA can remove the reflection of the acoustic PD signal at the origin (Figure 7). As seen in Figure 8(a), while MA effectively smooths the ripples of the electrical PD signal, it also slightly reduces the magnitude of the electrical PD signal. The arrival time for the electrical PD signal using both methods shows almost the same result as the original signal. Although the starting time of SG- and MA-denoised acoustic PD signals is the same as the original signal, the first peak of the acoustic PD signal that is denoised by the MA is delayed by 0.7 μ s from the original signal, whereby it can affect the accuracy of time of arrival measurement, as illustrated in Figure 8(b). The SG can remove the noise and retain the essential characteristics of the original acoustic signal, such as peak and width, including a minor peak, as shown in Figure 8(b), whereby the arrival time is delayed by only 0.1 μ s.

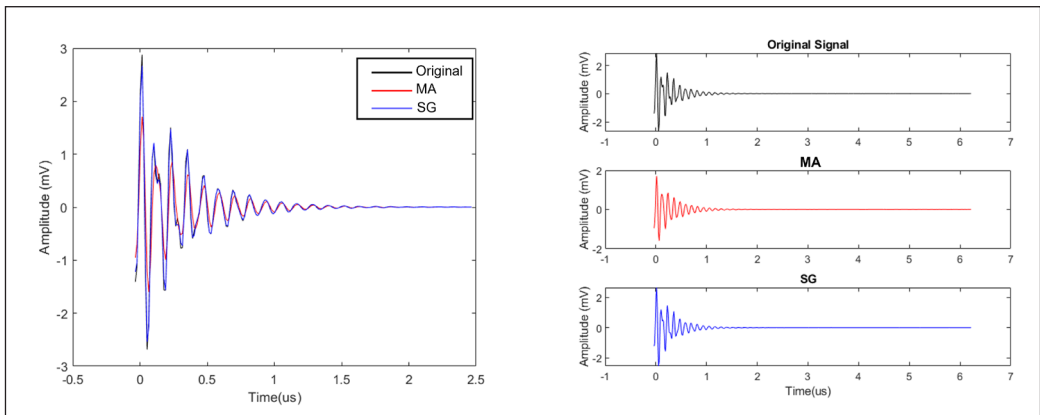


Figure 6. Original and denoised electrical PD signals based on SG and MA

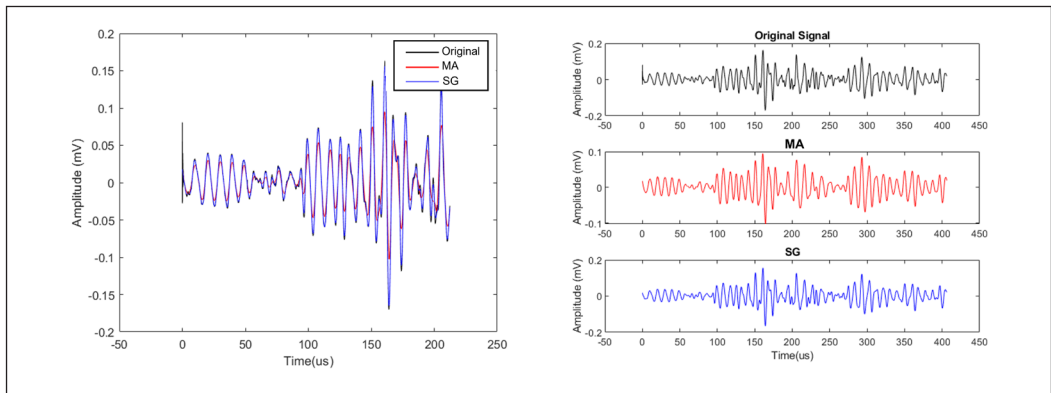


Figure 7. Original and denoised acoustic PD signals based on SG and MA

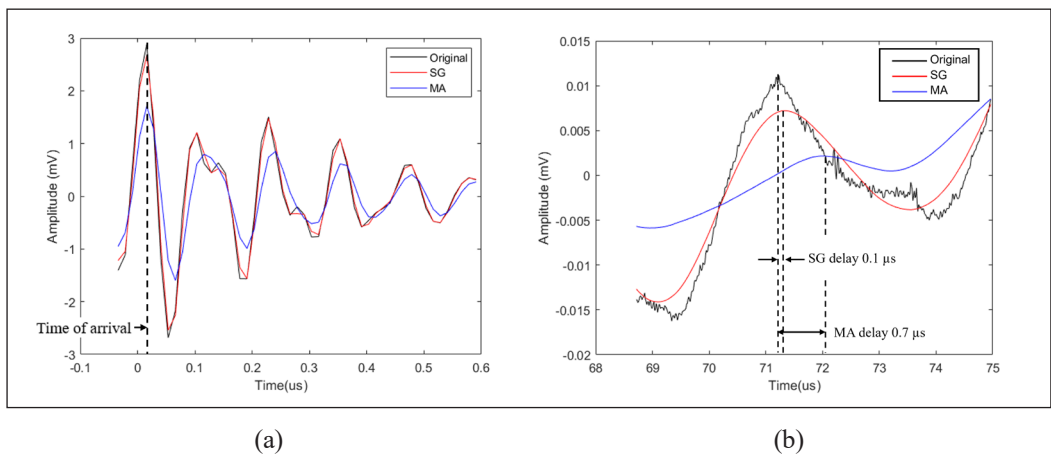


Figure 8. Time of arrival of (a) electrical and (b) acoustic PD signals based on SG and MA denoising methods

The denoising performances for SG and MA for the electrical and acoustic PD signals based on the SNR, RMSE and CC analyses can be seen in Table 2. The SG performs better than MA in denoising the electrical PD signals based on the lower RMSE of 0.1144 and higher CC of 0.9938. Although the MA achieves a higher SNR of 3.8816 than the SG, this may be due to the greater reduction in the magnitude of the MA-denoised signal. The SG also performs better for acoustic PD signals than the MA, as indicated by the low RMSE of 0.0018 and high CC of 0.9746. The high SNR by the MA is possibly due to the significant distortion in the denoised acoustic PD signal, as shown in Figure 8(b).

Table 2

Denoising performance of SG and MA based on the SNR, RMSE and CC analyses

Denoising Method	Signal	SNR	RMSE	CC
Savitzky-Golay	Electrical PD	0.3222	0.1144	0.9938
	Acoustic	1.1016	0.0018	0.9746
Moving Average	Electrical PD	3.8816	0.5160	0.8917
	Acoustic	6.4177	0.0061	0.6201

Partial Discharge Localization

Figure 9 shows examples of normalized and unipolar acoustic PD signals. The acoustic PD signal denoised by SG yields a higher amplitude than that of MA. The acoustic PD signal that is denoised by MA is smoother than that of SG. Compared to SG, the acoustic PD signal denoised by MA can be easily identified.

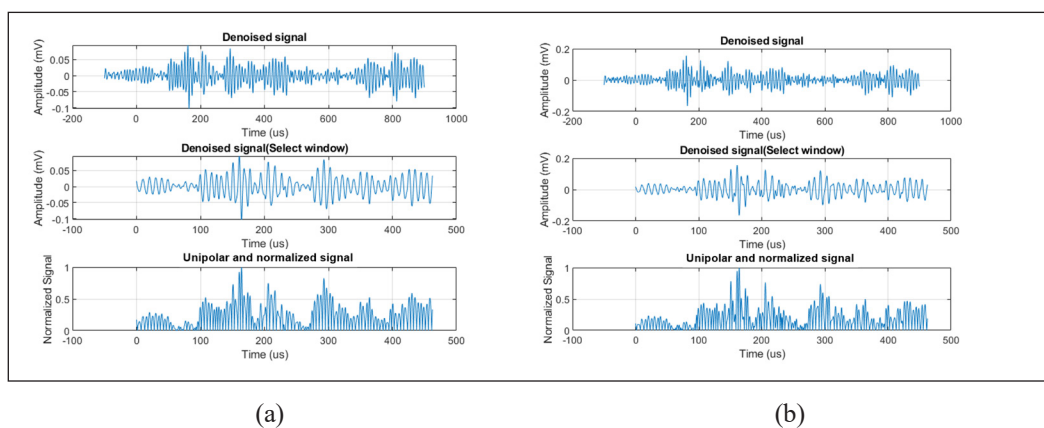


Figure 9. Unipolar and normalized acoustic PD signal based on (a) SG and (b) MA denoising methods

The 3D model in Figure 10 shows the visual representation of PD localization using both denoising techniques. Table 3 quantitatively compares the estimated and actual PD source locations across the x, y, and z axes for each method. The actual PD source

locations based on SG demonstrate small differences between estimated and actual PD source locations, with differences, Δ of 0.0039 m, 0.0132 m, and 0.0132 m along the x, y, and z axes, respectively. In contrast, the estimated PD source locations based on MA present slightly large differences, particularly along the x and y axes, with 0.0054 m and 0.0175 m, respectively.

Table 3

Comparison of actual PD source location based on SG and MA denoising methods

Type of filter	SG			MA		
Axes	x (m)	y (m)	z (m)	x (m)	y (m)	z (m)
Estimated	0.0739	0.0932	0.1668	0.0646	0.0975	0.1745
Actual	0.07	0.08	0.18	0.07	0.08	0.18
Difference, Δ	0.0039	0.0132	0.0132	0.0054	0.0175	0.0055

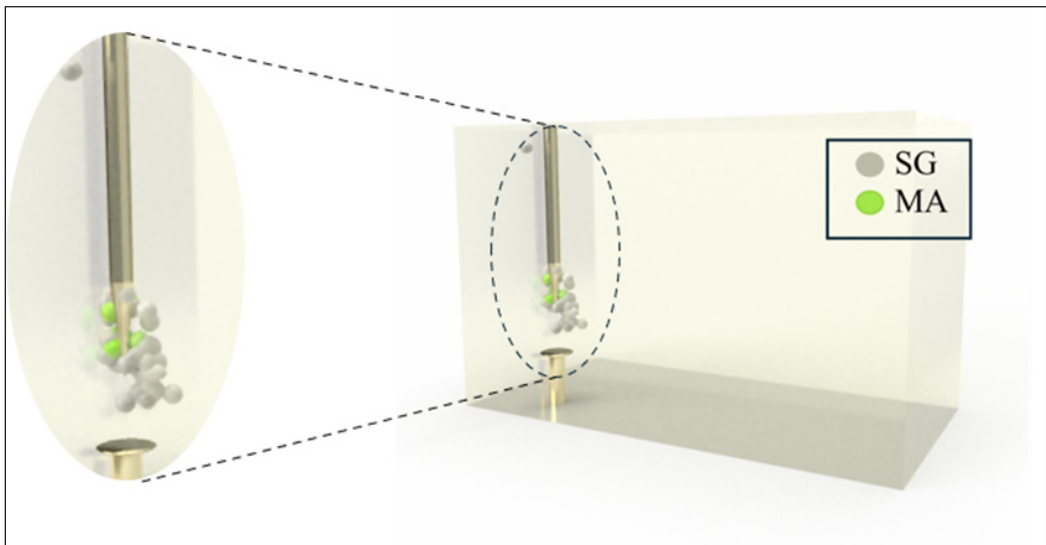


Figure 10. 3D model of PD localization based on SG and MA denoising methods

Table 4 highlights the location error and relative error for both denoising methods. The estimated PD source location based on SG achieves a lower location error of 0.0668 m compared to the MA with 0.0669 m. Although the absolute difference in location error is small, the relative error is slightly lower for SG, with 6.684%, compared to 6.691% for MA. This indicates that while both methods are relatively close in terms of PD localization accuracy in RBDPO, the SG consistently outperforms the MA, particularly in minimizing the deviation from the actual PD source location. The accuracy of the acoustic PD source localization achieved based on the SG-denoised acoustic PD signal in RBDPO is

comparable to that of mineral oil (Hashim et al., 2022). This highlights the ability of SG-denoised signals to improve acoustic PD source localization among different insulating fluids with distinct viscosities.

Table 4

Location error of the estimated PD source location based on SG and MA denoising methods

Evaluation	SG	MA
Location relative error (%)	6.684033005	6.691435483
Location error (m)	0.06684033	0.066914355

CONCLUSION

It is found that the SG can denoise the electrical and acoustic PD signals better than MA based on SNR, RMSE and CC analyses. The estimated PD source locations based on the denoised PD data by SG are more scattered than those by MA. Nevertheless, the estimated PD source locations at the x and y axes based on the denoised PD data by SG are closer to the actual PD source than those of MA. Future research could explore optimizing the SG parameters to further enhance the PD localization approach. In addition, advanced techniques could be explored for the denoising of electrical and acoustic PD signals and PD localization.

ACKNOWLEDGEMENT

This research was funded by Universiti Putra Malaysia, Inisiatif Putra Berkumpulan GP-IPB (GP-IPB/2022/9717000) funding. Special thanks to Advanced Lightning, Power and Energy Research (ALPER), and UPM for their technical support during this research.

REFERENCES

Ahmad, N. D., Hashim, A. H. M., Azis, N., Talib, M. A., Rezali, K. A. M., Nik Ali, N. H., Jasni, J., Masahiro, K., & Jamil, M. K. M. (2023). Partial discharge localization of refined bleached deodorized palm oil (RBDPO) based on acoustic emission method. In *2023 12th Asia-Pacific International Conference on Lightning (APL)* (pp. 1-5). IEEE. <https://doi.org/10.1109/APL57308.2023.10181667>

Azis, N., Jasni, J., Ab Kadir, M. Z. A., & Mohtar, M. N. (2014). Suitability of palm based oil as dielectric insulating fluid in transformers. *Journal of Electrical Engineering and Technology*, *9*(2), 662–669. <https://doi.org/10.5370/JEET.2014.9.2.662>

Chan, J. Q., Raymond, W. J. K., Illias, H. A., & Othman, M. (2023). Partial discharge localization techniques: A review of recent progress. *Energies*, *16*(6), Article 2863. <https://doi.org/10.3390/en16062863>

Chaudhuri, S., Ghosh, S., Dey, D., Munshi, S., Chatterjee, B., & Dalai, S. (2023). Denoising of partial discharge signal using a hybrid framework of total variation denoising-autoencoder. *Measurement: Journal of the International Measurement Confederation*, *223*, Article 113674. <https://doi.org/10.1016/j.measurement.2023.113674>

- CIGRE TB 676. (2017). *Partial discharges in transformers*. ECIGRÉ. <https://www.e-cigre.org/publications/detail/676-partial-discharges-in-transformers.html>
- Dombi, J., & Dineva, A. (2020). Adaptive savitzky-golay filtering and its applications. *International Journal of Advanced Intelligence Paradigms*, 16(2), 145–156. <https://doi.org/10.1504/IJAIP.2020.107011>
- Feizifar, B., Müller, Z., Fandi, G., & Usta, O. (2019, June). A collective condition monitoring algorithm for on-load tap-changers. In *2019 IEEE International Conference on Environment and Electrical Engineering and 2019 IEEE Industrial and Commercial Power Systems Europe (EEEIC/I&CPS Europe)* (pp. 1-6). IEEE. <https://doi.org/10.1109/EEEIC.2019.8783320>
- Firuzi, K., Vakilian, M., Phung, B. T., & Blackburn, T. R. (2019). Partial discharges pattern recognition of transformer defect model by LBP & HOG features. *IEEE Transactions on Power Delivery*, 34(2), 542–550. <https://doi.org/10.1109/TPWRD.2018.2872820>
- Fuhr, J. (2005). Procedure for identification and localization of dangerous PD sources in power transformers. *IEEE Transactions on Dielectrics and Electrical Insulation*, 12(5), 1005–1014. <https://doi.org/10.1109/TDEI.2005.1522193>
- Ghosh, R., Chatterjee, B., & Dalai, S. (2016, November). A new method for the estimation of time difference of arrival for localization of partial discharge sources using acoustic detection technique. In *2016 IEEE 7th Power India International Conference (PIICON)* (pp. 1-5). IEEE. <https://doi.org/10.1109/POWERI.2016.8077180>
- Guiñón, J. L., Ortega, E., García-Antón, J., & Pérez-herranz, V. (2007, September 3-7). *Moving average and savitzki-golay smoothing filters using mathcad*. [Paper presentation]. International Conference on Engineering Education (ICEE), Coimbra, Portugal.
- Hashim, A. H. M., Azis, N., Jasni, J., Radzi, M. A. M., Kozako, M., Jamil, M. K. M., & Yaakub, Z. (2023). Examination on the denoising methods for electrical and acoustic emission partial discharge signals in oil. *Indonesian Journal of Electrical Engineering and Informatics*, 11(3), 791–804. <https://doi.org/10.52549/ijeei.v11i3.4463>
- Hashim, A. H. M., Azis, N., Jasni, J., Radzi, M. A. M., Kozako, M., Jamil, M. K. M., & Yaakub, Z. (2022). Partial discharge localization in oil through acoustic emission technique utilizing fuzzy logic. *IEEE Transactions on Dielectrics and Electrical Insulation*, 29(2), 623–630. <https://doi.org/10.1109/TDEI.2022.3157911>
- Hussain, M. R., Refaat, S. S., & Abu-Rub, H. (2021). Overview and partial discharge analysis of power transformers: A literature review. *IEEE Access*, 9, 64587–64605. <https://doi.org/10.1109/ACCESS.2021.3075288>
- Javandel, V., Vakilian, M., & Firuzi, K. (2022). Multiple partial discharge sources separation using a method based on laplacian score and correlation coefficient techniques. *Electric Power Systems Research*, 210, Article 108070. <https://doi.org/10.1016/j.eprsr.2022.108070>
- Karami, H., Azadifar, M., Mostajabi, A., Rubinstein, M., Karami, H., Gharehpetian, G. B., & Rachidi, F. (2020). Partial discharge localization using time reversal: Application to power transformers. *Sensors*, 20(5), Article 1419. <https://doi.org/10.3390/s20051419>
- Kozako, M., Murayama, H., Hikita, M., Kashine, K., Nakamura, I., & Koide, H. (2012). New partial discharge location method in power transformer based on acoustic wave propagation characteristics using numerical simulation. In *2012 IEEE International Conference on Condition Monitoring and Diagnosis* (pp. 854–857). IEEE. <https://doi.org/10.1109/CMD.2012.6416284>

- Li, Y., Han, D., Tang, B., Li, K., Qiu, Z., & Zhang, G. (2021). The influence of electrode materials on the emission spectrum in SF₆ under AC corona discharge. In *2021 IEEE Electrical Insulation Conference (EIC)* (pp. 707-710). IEEE. <https://doi.org/10.1109/EIC49891.2021.9612340>
- Lonkwic, P., Szydło, K., & Molski, S. (2017). Savitzky-golay method for the evaluation of deceleration of the friction lift. *Advances in Science and Technology Research Journal*, *11*(1), 138–146. <https://doi.org/10.12913/22998624/68459>
- Mustam, M. M., Azis, N., Jasni, J., Halis, R., Talib, M. A., Yunus, R., Raof, N. A., & Yaakub, Z. (2023). Short-term ageing study on the palm oil and mineral oil in the presence of insulation paper, moisture, low molecular weight acid, and oxygen. *Pertanika Journal of Science and Technology*, *31*(6), 2931–2946. <https://doi.org/10.47836/pjst.31.6.16>
- Pattanadach, N., & Muhr, M. (2017). Comments on PDIV testing procedure according to IEC 61294. In *2017 IEEE 19th International Conference on Dielectric Liquids (ICDL)* (pp. 1-4). IEEE. <https://doi.org/10.1109/ICDL.2017.8124658>
- Purnamasari, D. N., Wibisono, K. A., & Sukri, H. (2021). Digital moving average filter application for echo signals and temperature. *E3S Web of Conferences*, *328*, Article 02007. <https://doi.org/10.1051/e3sconf/202132802007>
- Rafiq, M., Lv, Y. Z., Zhou, Y., Ma, K. B., Wang, W., Li, C. R., & Wang, Q. (2015). Use of vegetable oils as transformer oils-A review. *Renewable and Sustainable Energy Reviews*, *52*, 308–324. <https://doi.org/10.1016/j.rser.2015.07.032>
- Sarathi, R., Sheema, I. P. M., & Subramanian, V. (2014). Effect of barrier in the propagation of partial discharge signals. In *Proceedings of 2014 International Symposium on Electrical Insulating Materials* (pp. 249-252). IEEE. <https://doi.org/10.1109/ISEIM.2014.6870765>
- Seo, J., Ma, H., & Saha, T. K. (2018a). An improved spatial intersectional method for partial discharge (PD) source localization in power transformer. In *2018 12th International Conference on the Properties and Applications of Dielectric Materials (ICPADM)* 363-366. <https://doi.org/10.1109/ICPADM.2018.8401064>
- Seo, J., Ma, H., & Saha, T. K. (2018b). On savitzky – Golay filtering for online condition monitoring of transformer on-load tap changer. *IEEE Transactions on Power Delivery*, *33*(4), 1689–1698. <https://doi.org/10.1109/TPWRD.2017.2749374>
- Sinaga, H. H., Phung, B. T., & Blackburn, T. R. (2012). Partial discharge localization in transformers using UHF detection method. *IEEE Transactions on Dielectrics and Electrical Insulation*, *19*(6), 1891–1900. <https://doi.org/10.1109/TDEI.2012.6396945>
- Yang, J., Yan, K., Wang, Z., & Zheng, X. (2022). A novel denoising method for partial discharge signal based on improved variational mode decomposition. *Energies*, *15*(21), Article 8167. <https://doi.org/10.3390/en15218167>
- Zhang, G., Zhang, X., Tang, J., & Cheng, H. (2018). Study on localization of transformer partial discharge source with planar arrangement UHF sensors based on singular value elimination. *AIP Advances*, *8*(10), Article 105232. <https://doi.org/10.1063/1.5055668>

Performance of Recycling Aggregate Self-Compacting Concrete Incorporating Supplementary Cementitious Materials: An Overview

Said Mohammed Mostafa Aljamala, Nor Azizi Safiee*, Noor Azline Mohd Nasir and Farah Nora Aznieta Abdul Aziz

Department of Civil Engineering, Universiti Putra Malaysia, 43400 UPM Serdang, Selangor, Malaysia

ABSTRACT

Since the construction industry expands, the demand for environmentally friendly construction approaches becomes more urgent to preserve the environment and limited natural resource reserves. In the context of current concrete manufacturing, one of the primary issues with self-compacting concrete is its high cement requirement. Recent studies estimate that cement manufacturing contributes to at least 8% of worldwide carbon dioxide (CO₂) emissions. Using supplementary cementitious materials (SCMs), including silica fume (SF), ground granulated blast furnace slag (GGBS), fly ash (FA) and metakaolin (MK), is an alternate approach to reduce CO₂ emissions associated with concrete production. Cementitious and pozzolanic materials have been widely employed as SCMs to partially replace cement as a binding agent in concrete. Recycling accumulated construction waste, such as concrete aggregate, is a promising approach to reduce the adverse environmental impact and meet the growing global demand for raw resources. However, unlike natural aggregate (NA), recycled concrete aggregate (RCA) does not exhibit appropriate structural performance due to its inferior material qualities. This article intends to provide a review of the recent research on SCM in producing recycled concrete aggregate self-compacting concrete (RCA-SCC) with respect to its fresh and mechanical properties. Incorporating SCMs like FA, GGBS, and SF in RCA-SCC enhances workability. Ternary mixes, especially with FA and GGBS, demonstrate improved sustainability and

workability compared to binary mixes. Using SCMs is suggested to improve the quality of RCA and the interfacial transition zones (ITZ), potentially enhancing mechanical properties.

Keywords: Construction and demolition (C&D) waste, CO₂ emissions, mechanical Properties, recycled concrete aggregate (RCA), self-compacting concrete (SCC), supplementary cementitious materials (SCM)

ARTICLE INFO

Article history:

Received: 01 April 2024

Accepted: 10 April 2025

Published: 10 June 2025

DOI: <https://doi.org/10.47836/pjst.33.S4.08>

E-mail address:

s.eljamala@gmail.com (Said Mohammed Mostafa Aljamala)

norazizi@upm.edu.my (Nor Azizi Safiee)

nazline@upm.edu.my (Noor Azline Mohd Nasir)

farah@upm.edu.my (Farah Nora Aznieta Abdul Aziz)

*Corresponding author

INTRODUCTION

Self-compacting concrete (SCC) is a form of concrete that can be evenly distributed throughout a formwork solely through its weight, without the need for vibration compaction (Gupta et al., 2021; Malazdrewicz et al., 2023; Adesina, 2020; Al-Oran et al., 2022). Significant advancements in environmental and working conditions have resulted from the invention of SCC. These advancements include reduced energy consumption for easier concrete placing, vibration elimination, increased productivity, decreased noise, decreased labour requirements, and a high-quality surface (Kefelegn & Gebre, 2020). Conversely, normal concrete (NC) requires an external vibration for compaction. The quality of NC is affected when the compaction work is not properly done.

The binder content of SCC is higher, ranging from 430 to 700 kg/m³ of cement (Alsubari et al., 2015). The cement industry ranks high among the world's most energy-intensive and carbon-intensive manufacturing processes. Recent studies estimate that cement manufacturing contributes to at least 8% (1.4 gigatons annually) of worldwide carbon dioxide (CO₂) emissions (Carbone et al., 2022). Industrial by-products such as ground granulated blast furnace slag (GGBS), fly ash (FA), silica fume (SF), rice husk ash (RHA), metakaolin (MK) and palm oil fuel ash (POFA) are a major source of pollution and a financial burden for the economic and environmental sectors due to the enormous amounts of these waste items produced annually (Alsubari et al., 2015). Incorporating waste products as supplementary cementitious materials (SCM) decreases the quantity of trash sent to landfills and the emission of CO₂ during cement manufacture (Francis & Eldhose, 2017). The most common reactive industrial by-product materials with cementitious properties are GGBS, MK, SF and FA. Cementation and pozzolanic materials have been widely employed as SCMs to partially replace cement as a binding agent in concrete. This is primarily because their chemical compositions contain reactive components such as SiO₂, Al₂O₃, and CaO (Alobaidi et al., 2021).

Based on the estimation by Singh and Singh (2016b), it is projected that the worldwide volume of Construction and Demolition (C&D) waste will rise from 12.7 billion metric tonnes to 27 billion metric tonnes by the year 2050. This highlights the critical need for immediate action to limit the amount of C&D waste. Significant amounts of waste are produced annually during the construction, restoration, and demolition of structures and infrastructure. The global C&D waste production is reported to exceed 10 billion tonnes per year, with the US producing 700 million tonnes and the EU around 800 million tonnes (Wu et al., 2019). China generates around 2.3 billion tonnes of C&D waste annually due to rapid population growth and extensive urban regeneration initiatives (Huang et al., 2018). The global utilisation of construction natural aggregate is projected to increase to 62.9 billion metric tonnes by 2024, compared to 43.3 billion in 2016 (https://www.designingbuildings.co.uk/wiki/Construction_aggregates_market_2016_-_2024). Extensive

studies have been conducted on RCA's ability to manufacture new concrete. This approach helps to decrease the negative impact on landfills and the natural environment. This strategy has the potential to decrease the workload associated with the extraction of natural aggregate, which corresponds to around 50 billion tonnes annually globally (De Brito et al., 2016). This review study aims to compile prior research findings on SCM in RCA-SCC. Furthermore, the research aims to find out how the SCM affects the mechanical and fresh properties of RCA-SCC.

THE PROPERTIES OF SCMS

According to prior research, the chemical components of GGBS, FA, SF, and MK are summarised in Table 1. According to multiple studies, SF has a high concentration of amorphous silicon dioxide (ranging from 85.5% to 98.5%) and an ignition loss of less than 5%, which aligns with the recommendations made by ASTM C 1240. There is a significant difference between class C fly ashes and class F fly ashes in terms of their pozzolanic characteristics. The sum of the silica, alumina and iron ($\text{SiO}_2 + \text{Al}_2\text{O}_3 + \text{Fe}_2\text{O}_3$) content is used by ASTM C 618 to distinguish between Class C and Class F fly ash. The total sum of SiO_2 , Al_2O_3 , and Fe_2O_3 percentages in class C ash shall be equal to or greater than 50%, while the total shall be 70% or higher for class F fly ash. Class C fly ash differs in performance from low-calcium class F fly ash due to its high calcium content (15%–25%). Complying with ASTM C989 standards, GGBS is an SCM derived from the by-products of the iron and steel industry.

Its usual chemical make-up typically contains at least 32%–40% SiO_2 , 10-14.4% Al_2O_3 , and 34%–43% CaO . The chemical properties of FA significantly affect its reactivity and functionality in concrete. The stable glassy phase of silica-alumina in FA needs activation to improve the pozzolanic reaction. High SiO_2 and Al_2O_3 and low CaO content slow down early hydration, and chemical or thermal activation needs to break down the glassy network (Barbhuiya & Kumala, 2017). Activated FA functions like OPC but has better durability and corrosion resistance (Raghav et al., 2021). Yet, having high CaO and SiO_2 in GGBS facilitates the formation of C-S-H gel, leading to higher concrete strength and lower porosity (Khan & Sarker, 2019). It undergoes a similar hydration process to OPC and forms C-S-H gel, contributing to strength development (Raghav et al., 2021). Due to its extreme fineness and high silica content, silica fume is effectively used as a pozzolanic material (Khater, 2013). It enhances mechanical strength, reduces permeability, and improves durability by forming additional C-S-H gel through its reaction with calcium hydroxide. On the other hand, MK is an ultra-fine pozzolanic material and consists predominantly of silica and alumina (Curcio et al., 1998). MK is reported to increase the strength of concrete, especially during the early ages of hydration. Typically, the pozzolanic capabilities of MK are larger when the volume of SiO_2 and Al_2O_3 components is higher. MK is classified as a natural pozzolan according to ASTM C618.

Table 1
Chemical components of SCMs

Chemical Components	OPC [(Bingöl & Tohumcu, 2013; Gesoğlu et al., 2009; Ardalan et al., 2017; Mahalakshmi & Khed, 2020)]	GGBS [(Li et al., 2012; Kanamarlapudi et al., 2020; Gesoğlu et al., 2009; Ardalan et al., 2017)]	FA [Duan et al., 2020; Bingöl & Tohumcu, 2013; Gesoğlu et al., 2009; Gesoğlu et al., 2009]	SF [Bingöl & Tohumcu, 2013; Gesoğlu et al., 2009; Ardalan et al., 2017; Mahalakshmi & Khed, 2020)]	MK [(Tafraoui et al., 2016; Gómez-Casero et al., 2022; Tafraoui et al., 2016)]
Silicon dioxide (SiO ₂)	17.6–23.5	32–40	25–62	85.5–98.5	47–54.5
Aluminium oxide (Al ₂ O ₃)	3–6	10–14.4	10–30	0.35–1.5	37.5–43
Iron (III) oxide (Fe ₂ O ₃)	2.5–4.5	0.15–1.8	5–25	0.21	0.48–2
Magnesium oxide (MgO)	1–3	0.15–3.6	<1	0.09	0.1–0.28
Calcium oxide (CaO)	62–66	34–43	<10	1–3.1	0.1–0.16
Sodium oxide (Na ₂ O)	0.1–0.3	<1	<1	<0.55	<0.2
Potassium Oxide (K ₂ O)	0.3–1	<1	<1	<1	0.5–2
Sulphur trioxide (SO ₃)	1.5–3	<1	<1	0.42	<0.01
Loss on ignition (LOI)	1–3.5	<2	1–15	<5	0.44–1.28

Table 2 shows the physical properties of SCM based on previous studies. These properties significantly influence the characteristics of the concrete mixture. SF has a large surface area between 13,000 and 30,000 m²/kg. SF has an average particle size nearly one hundred times smaller than conventional cement particles. On the contrary, FA particles are not as tiny as silica fume particles. Fly ash particles exhibit a size variation from 14 µm to 100 µm. However, most fly ash particles are smaller than 35µm. Due to the increased mortar coverage required to coat the larger surface area of GGBS, less cement is subsequently available, which ultimately affects flowability. The specific surface area (SSA) of SCMs is vital for their reactivity, hydration rate, and overall influence on concrete properties. Materials with a higher SSA, like SF (approximately 13,000–30,000 m²/kg) and MK (around 23,000 m²/kg) which is approximately 100 times smaller than the average cement particle (around 290–326 m²/kg), tend to react more quickly with other components, which helps accelerate early strength development and lowers permeability. However,

this increased reactivity also raises water demand, necessitating careful adjustments to the mix. SF and MK improve durability by swiftly reacting with water, chloride, and sulphate ions, enhancing the matrix's resistance to chemical attacks. On the other hand, FA (approximately 287–500 m²/kg) and GGBS (around 350–650 m²/kg) aid in sulphate resistance by promoting ettringite formation, which helps reduce the risk of alkali-silica reaction (ASR). By optimising SSA in mix design, it can enhance concrete texture, boost strength, decrease porosity, and improve overall environmental performance, making SCMs essential for high-performance and durable construction projects.

Table 2
The physical properties of SCMs

Physical Properties	OPC [Gesoglu et al., 2009; De Matos et al., 2019; Ardalan et al., 2017; Singh et al., 2016]	GGBS [Gesoglu et al., 2009; Ardalan et al., 2017; Beycioğlu & Aruntaş, 2014]	FA [Gesoglu et al., 2009; Ardalan et al., 2017; Beycioğlu & Aruntaş, 2014]	SF [Gesoglu et al., 2009; Ardalan et al., 2017; Singh et al., 2016; Beycioğlu & Aruntaş, 2014]	MK [De Matos et al., 2019; Tafraoui et al., 2016]
Shape	Irregular and Angular	Spherical	Spherical	Spherical	Angular
Specific gravity g/cm ³	3.15	2.79–2.850	2.25–2.2	2.2–2.35	2.20–2.60
Average particle size (µm)	13.22	13.8–22.2	14–39	0.1–0.3	1.0–20.0
Surface area (m ² /kg)	290–326	350–650	287–500	13,000–30,000	23,000

DEVELOPMENT OF RCA-SCC

Recently, significant research efforts have focused on examining the physical, mechanical, and durability characteristics of RAC. These studies have shown that by employing appropriate design techniques and adopting reasonable mixing procedures, RAC can be effectively utilised in practical applications (Amario et al., 2017; Wang et al., 2019). The use of RCA in SCC production has recently garnered much attention from researchers (Tang et al., 2016; Singh et al., 2019; Duan et al., 2020). SCC needs to be more cost-effective in order to realise its full industry acceptance potential. Using RCA instead of natural aggregates may make SCC less costly and more environmentally friendly. Despite this, RCA could negatively impact concrete quality as it may absorb more water and lower density than natural aggregates. The low quality observed in RCA can be related to the adhered mortar and the NA. It also impacts the properties of the interfacial transition zones (ITZ) that exist

between aggregates and cement paste, which affects the strength properties of concrete (Singh & Singh, 2016b).

Tang et al. (2020) propose using SCMs like FA and MK to enhance the quality of RCA and ITZ. Figure 1 shows an infographic of the RCA-SCC combination produced by unary, binary and ternary binders. The cement is the only cementation binder used to prepare the mixture of unary RCA-SCC. In contrast, a combination of cement and one SCM is used to prepare binary RCA-SCC, and cement with two different SCMs is used to prepare ternary RCA-SCC. According to Kou et al. (2011), using pozzolanic elements such as SF and FA as partial cement replacements may increase the ITZ and cement matrix of RCA concrete. SCMs have pozzolanic properties, indicating that they react with the calcium hydroxide formed when cement hydrates. While the reaction of SCMs contributes additional cementitious materials that improve SCC properties, the effectiveness of this contribution is influenced by the characteristics of RCA itself. The shape and texture of RCA, being more angular and rough compared to natural aggregates, increase internal friction and may reduce workability. However, several treatment techniques of RCA can be used to eliminate or improve the quality of RCA, such as thermal treatment, mechanical treatment, chemical treatment, polymer treatment and incorporating pozzolanic materials. Therefore, SCMs can enhance the strength and durability by refining the microstructure and improving the ITZ.

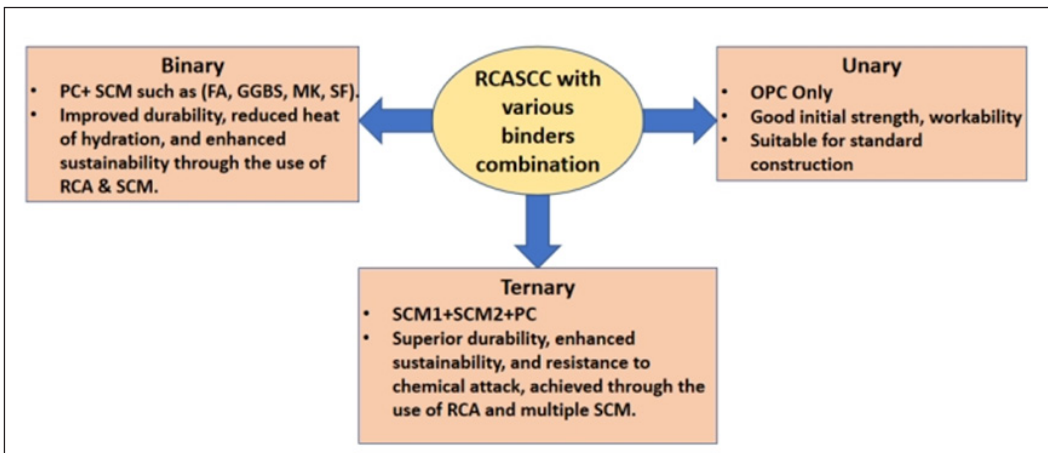


Figure 1. RCA-SCC with various binder combinations

The Fresh Properties Performance

The fundamental difference between SCC and normal concrete is its fresh properties and ability to flow, which are influenced by its consistency and cohesiveness. Slump flow, L-box, J-ring, V-funnel, and sieve segregation tests are among the most relevant SCC flowability

tests (Hani et al., 2018). The fresh state performances of SCC can be discussed based on the binder or combination of binders used in producing the concrete. However, it is important to note that SCC cannot be made without chemical admixtures. Chemical admixtures are used in SCC production to enhance workability and minimise segregation (Kumar et al., 2020). Superplasticisers, air-entraining agents, and retarders are most commonly used in SCC. It is utilised for various reasons, ensuring good mixing during transportation, pumping, placing, and curing, as well as ensuring the concrete's strength and durability. The following sub-section reviewed the SCC performances and their differences according to various binder combinations such as unary, binary and ternary.

The Fresh Properties of Unary Cementation Binder

The cement is the only cementation binder used to prepare the mixture of unary RCA-SCC. The fresh and mechanical properties of SCC are negatively impacted when RCA is used. RCA has high porosity, low density, and strength (Abed et al., 2020). Many researchers have examined the impact of RCA on SCC performance. Safiuddin et al. (2011) demonstrated that restricting the replacement rate of RCA to less than 50% can improve the workability of SCC. Tang et al. (2016) indicated that RCA can absorb more water because of its higher porosity than natural aggregates.

Furthermore, Sharobim et al. (2017) found that including 20%, 25%, and 50% RCA in SCC resulted in reduced cohesiveness compared to regular concrete, which increases the mortar's separation, leading to a larger segregation ratio. Nevertheless, the degree of segregation was diminished by using 75% and 100% RCA. The larger percentage of RCA increased angularity and surface roughness, leading to greater cohesiveness and decreased segregation ratio. Mohseni et al. (2017) stated that using 20% RCA decreased the slump flow diameter by 6%–8% compared to samples without RCA. Furthermore, the findings showed adequate homogeneity and unity in the mixtures, with no indication of segregation and leakage being detected.

Moreover, a study conducted by Castano and Abdel-Mohti (2024) used 0%, 10%, 30%, 50%, and 70% RCA to study the effect of different percentages of RCA on the fresh and mechanical properties. The result showed that the use of RCA up to 30% does not impact the filling and passing ability of SCC mixes; however, the reduction can be demonstrated when using a high quantity of RCA due to its high porosity and the weakly adhered mortar on the RCA surface.

Abed et al. (2020) used 25% and 50% RCA in SCC to examine its impact on the fresh properties. The results showed a decrease in slump flow and V-funnel values as the RCA ratio increased due to the rough surfaces of the RCA. Most research findings were consistent with the slump diameter's tendency to decrease as RCA increased. The observed impact of RCA was unremarkable, as all the combinations fell within the recommendation

of EFNARC (2005) values. Sasanipour and Aslani (2020) achieved the same result when replacing 25%, 50%, 75% and 100% RCA. The properties of RCA strongly depend on its source and the previous concrete component. However, some researchers can obtain the same results sometimes, even though the original source is different, due to some factors such as the use of chemical admixtures and the mix design adjustments with the w/c ratio.

The Fresh Properties of Binary Cementation Binder

The application of SCM, specifically GGBS, SF, and FA, is summarised in Table 3, which includes the results from multiple experiments. The addition of GGBS to SCC enhances the compatibility and consistency. GGBS has a density that is nearly 10% lower than that of cement. Therefore, replacing an equivalent cement mass with GGBS leads to an increased paste volume. This has increased the segregation resistance, as well as flowability, significantly (Tangadagi et al., 2021). Abhishek et al. (2021) examined the performance of SCC using 20%, 25%, 30% and 35% RCA, and GGBS in percentages of 30% and 35% replacement of OPC. The results showed that the workability decreases as the RCA content increases. This can be due to the increased water absorbability associated with higher RCA content. All the mixes were within the suggested guidelines per the EFNARC (2005).

Djelloul et al. (2018) examined the impact of GGBS on the fresh properties of RCA-SCC. Combining RCA with GGBS reduces SCC fresh density. This is because of the comparatively lower specific gravity of GGBS than cements. Moreover, the existence of old adhered porous cement mortar in RCA leads to lower specific gravity values for RCA mixes than for NA. RCA can replace NA in SCC mixtures without compromising the concrete's fresh characteristics like filling, passing, and segregation. According to RCA, workability improved by 25% and 50%, respectively. A similar effect is seen when 15% and 30% GGBS replace cement in SCC combined with RCA. The optimal proportion of GGBS in successful SCC mixtures was 15%, which prevented any indication of bleeding or segregation. Majhi et al. (2018) stated that increased GGBS leads to increased slump values. The enhanced workability can be related to the smooth surface properties and better distribution of GGBS particles compared to the other component materials. The findings also indicated a reduction in water absorption level with the rise in the cement replacement level of GGBS. Absorption reduction by 20.23% and 13% is observed for 15% and 30% GGBS mixes, respectively, compared to the control mix. This improvement can be attributed to the finer pore structure of GGBS. The positive effect of GGBS on the water absorption of SCC has already been reported in the literature (Ahari et al., 2015; Mohan & Mini, 2018).

Adding FA to SCC improved its flowability, passing ability, and viscosity. This is because the spherical shape and smooth surface of the FA reduced the water demand (Beycioğlu & Aruntaş, 2014). The fresh state of RCA-SCC with FA was examined by Abed

Table 3
Results of selected studies on the fresh properties of binary RCA-SCC

Ref	SCM	RCA(%)	Slump flow (mm)	T 50 (s)	V-funnel (s)	L-box (H2/H1)	Segregation (%)	J-ring (mm.)
Abhishek et al., 2021	GGBS 30%	0	658	-	8.5	0.8	-	-
		20	660	-	9.0	0.88	-	-
		25	673	-	9.5	0.94	-	-
		30	650	-	9.0	1.00	-	-
		35	645	-	9.8	0.94	-	-
Djelloul et al., 2018	GGBS 15%	0	730	4.0	12.50	0.95	6.90	-
		25	752	3.8	10.20	0.97	9.16	-
		50	783	2.5	6.16	1.00	12.20	-
		75	766	2.9	9.85	0.95	13.75	-
		100	737	4.2	15.18	0.90	11.80	-
Khodair & Bommareddy, 2017	GGBS 50%	0	762	4.51	16.20	0.94	8.93	543
		25	776	4.20	15.23	0.92	11.70	524
		50	792	3.90	12.63	0.83	14.70	543
		75	781	4.61	20.25	0.80	16.50	540
		100	749	4.97	23.20	0.75	15.80	538
Singh & Singh, 2016b	Low volume FA (up to 30%) High volume FA (more than 50%)	0	685	2	6.0	-	-	-
		50	688	2	5.8	-	-	-
		100	680	2	7.0	-	-	-
		0	695	3.3	5.5	-	-	-
		50	690	3.5	5.8	-	-	-
100	680	3.6	6.7	-	-	-		

Table 3 (continue)

Ref	SCM	RCA(%)	Slump flow (mm)	T 50 (s)	V-funnel (s)	L-box (H2/H1)	Segregation (%)	J-ring (mm.)
Khodair & Bommareddy, 2017	FA 50%	0	538	3	-	-	-	521
		25	558	5	-	-	-	512
		50	555	3	-	-	-	506
		75	579	2	-	-	-	525
		100	572	2	-	-	-	527
Kapoor et al., 2016	FA 30%	0	720	2.5	6	0.95	-	-
		50	710	2.8	7.1	0.92	-	-
		100	700	3.2	7.5	0.82	-	-
Katar et al., 2021	FA 15%	0	720	2.64	11.8	-	-	640
		25	780	2.74	8.38	-	-	720
		50	750	3.5	8.69	-	-	680
		75	660	2	6.58	-	-	560
Kapoor et al., 2020	FA 30%	0	730	2.5	6.5	0.95	-	-
		50	700	2.8	7.0	0.93	-	-
		100	680	3.0	8.0	0.82	-	-
		0	720	3.1	9.5	0.82	6.9	-
Nguyen, 2024	FA 50%	50	710	3.75	10	0.85	7.3	-
		75	705	4.20	11	0.89	8.1	-
		100	700	4.80	11.5	0.91	8.7	-
		0	600	6.0	12.5	0.92	-	-
Singh et al., 2022	SF 10%	25	590	5.8	12.8	0.93	-	-
		50	570	5.7	13	0.94	-	-
		75	560	5.6	13.1	0.97	-	-
		100	540	5.5	13.3	0.98	-	-
Sasanipour et al., 2019	SF 8%	25	625	5.0	-	-	-	585
		50	610	4.1	-	-	-	595
		75	600	3.2	-	-	-	590
		100	610	4.9	-	-	-	590

Table 3 (continue)

Ref	SCM	RCA(%)	Slump flow (mm)	T 50 (s)	V-funnel (s)	L-box (H2/H1)	Segregation (%)	J-ring (mm.)
Singh et al., 2023	SF 10%	0	630	8	12.5	0.85	-	-
		25	620	8.5	12.6	0.86	-	-
		50	610	8.7	12.7	0.87	-	-
		75	600	8.9	12.8	0.88	-	-
Singh & Singh, 2018	SF 15%	100	590	9	12.9	0.89	-	-
		0	701	-	7.0	0.87	-	-
		50	717	-	7.3	0.87	-	-
		100	695	-	7.9	0.82	-	-

and Nemes (2019). The results showed that fusing FA negatively affect the fresh properties. Tuyan et al. (2014) studied RCA-SCC with different replacement percentages, 0%, 20%, 40%, 60% and 30% FA. The results showed that the slump flow first increases with the 20% RCA. However, increasing the RCA percentage reduces the slump flow, while increasing the RCA percentage increases the V-funnel flow time. Kapoor et al. (2020) explored the fresh properties of SCC at 0%, 50%, and 100% RCA, along with 30% FA. The results showed that slump-flow decreases as the RCA replacement level increases. However, the T50 time increases as RCA increases the viscosity due to its highly porous nature. Moreover, a 54% increase in funnel flow time was observed once RCA was completely substituted. Similarly, 100% RCA replacement in the SCC mixture has no noticeable effect on the L-box ratio. Additionally, Benli (2019) stated that as the amount of FA increased, porosity and water absorption also increased. However, Golewski (2023) illustrated that the water absorption rate decreases with an FA level increase due to the general porosity reduction and the cement matrix homogenisation.

The addition of SF to SCC improves its mechanical and rheological characteristics. (Mahalakshmi & Khed, 2020). In similar behaviour, Sasanipour et al. (2019) observed that SF enhanced the workability and the fresh properties of SCCs. Nevertheless, the mixtures that did not contain SF exhibited good fresh characteristics and passing ability. The incorporation of SF reduces the water absorption by 7% to 12%. Mo et al. (2020) found that increasing the proportion of RCA had a drawback on the fresh properties of SCC. This was demonstrated by the decrease in slump flow diameter and the increase in V-funnel flow duration, indicating a drop in fluidity. The replacement of 10% SF decreases the reduction of fluidity.

The Fresh Properties of Ternary Cementation Binder

Table 4 summarises the findings of multiple experiments on the use of two types of SCMs in RCA-SCC. Guo et al. (2020) examined the sustainability aspect of binary and ternary (SF, GGBS and FA) of SCM materials in RCA-SCC. The result showed that increasing the w/c ratio with an increase in the content of FA may increase the slump flow, indicating that FA can improve the filling ability performance. The slump flow diameter of RCA-SCC mixes increased as the concentration of SCMs increased, notably for ternary mixes of FA and GGBS. The enhanced workability can be related to the smooth surface properties and good distribution of GGBS particles. The test results demonstrated that ternary mixes possess engineering benefits compared to binary mixes and have the potential to improve the sustainability of RCA-SCC. The combination of FA and GGBS improved flowability by increasing the diameter in the slump-flow test (Guo et al., 2020). Additionally, Singh et al. (2023) examined the impact of a ternary mixture (15% FA, 10% SF) in RCA-SCC. The findings indicated that using RCA at the optimal ratio of 25% resulted in a drop in Slump

Table 4
Results of some studies on the fresh state of ternary RCA-SCC

Ref	SCM	RCA (%)	Slump flow (mm)	T 50 (s)	V-funnel (s)	L-box (H2/H1)	Segregation (%)	J-ring (mm.)
Singh et al., 2023	SF 10%	0	630	8	12.4	0.84		
	FA 15%	25	610	6	12.5	0.85		-
Kapoor et al., 2016		50	600	5	12.6	0.87		
		75	590	4	12.7	0.88		
		100	580	3	12.9	0.90		
	SF 10%		730	2.6	6.3	0.93		
	FA 20%	0	710	2.9	6.8	0.91		-
Khodair & Bommareddy, 2017		50	680	3.2	7.1	0.85		
		100	725	2.7	6.4	0.94		
			715	2.9	6.9	0.92		-
			705	3.1	7.2	0.88		
Tiwari et al., 2021		0	621	2				574
		25	597	5				552
		50	624	2				587
		75	543	5				497
		100	602	3				567
Tiwari et al., 2021			710	3.3	8.5	0.93		
		25	700	2.7	8.0	0.93		-
			730	2.3	7.5	0.97		
			720	2.6	8.0	0.94		
			690	3.2	11	0.88		
Tiwari et al., 2021		50	750	2.5	9.5	0.92		-
			710	2.6	9.0	0.92		
			700	2.9	10	0.90		

Table 4 (continue)

Ref	SCM	RCA (%)	Slump flow (mm)	T 50 (s)	V-funnel (s)	L-box (H2/H1)	Segregation (%)	J-ring (mm.)
Guo et al., 2020	GGBS 25% FA 25%	50	615	6.6	-	-	-	589
	GGBS 35% FA 35%		560	6.9	-	-	-	533
	GGBS 30% FA 20%	100	663	5.6	-	-	-	633
	GGBS 35% FA 35%		675	6.9	-	-	-	648
Singh & Singh, 2018	SF 5%	0	740		5.2	0.82		
	FA 25%	100	715	-	5.6	0.89	-	-
	SF 5% FA 25%	25 50	700 720	3.7 3.9	-	0.95 0.97	7.7 6.3	-
Tang et al., 2016	SF 5% FA 25%	75 100	710 700	4.1 4.3	-	0.92 0.93	6.0 5.2	-
	MK 10% FA 20%	25 50	690 685	1.8 2.1	6.1	-	1.0 1.7	-
		75 100	685 680	2.2 2.5	6.3 6.5	-	1.2 1.5	-

Table 4 (continue)

Ref	SCM	RCA (%)	Slump flow (mm)	T 50 (s)	V-funnel (s)	L-box (H2/H1)	Segregation (%)	J-ring (mm.)
Singh et al., 2017	MK 5%		715	2.2	7.3	0.88		
	FA 25%	0	730	2.2	7.5	0.93	-	-
		50	750	2.0	7.0	0.91		
		100	720	3.1	6.1	0.86		
Kapoor et al., 2017	SF 5%		730	3.3	6.2	0.84		
	FA 25%		745	3.0	6.0	0.88		
	MK 10%	0	710	2.7	6.9	0.96		
	FA 20%	100	680	3.5	7.8	0.80		
Xuyong et al., 2025	GGBS 10%	15	682	11.32	23.47			662
	FA 20%	30	719	8.15	22.68	-		704
		50	698	9.07	24.46			680

Flow (mm), while the other tests, such as J-Ring, U-Box, L-Box, V-Funnel, and T-50 Time values, increased. The slump flow was reduced due to the high water absorption of RCA, which led to less workability and fluidity. However, for J-Ring, U-Box, L-Box, V-Funnel, and T-50, the times increased due to the ternary binder mix of FA and SF that makes the mix more cohesive and resistant to flow.

Kapoor et al. (2016) examined various RCA, FA, SF, and MK combinations. The authors achieved a good fresh behaviour in SCC by using an appropriate dosage of SCM. In addition, the findings of a research investigation carried out by Khodair and Bommareddy (2017) demonstrated that substituting cement with a ternary blend consisting of 25% of both FA and GGBS led to greater slump flow values with J-Ring in comparison to binary mixtures comprising 50% FA or 50% GGBS. The mixture of (50% RCA, 25% GGBS, and 25% FA) has the greatest slump flow and J-Ring value. Slump flow was also higher in all mixes when 50% GGBS was compared to mixes made with 50% FA. Additionally, Singh and Singh (2016b) studied the usage of RCA in low and high replacement levels of FA. The workability of SCC was studied using slump flow, V-funnel, and T500 tests. The results showed that increasing the RCA% reduced the slump flow due to the high water absorption of RCA, which negatively affected flowability. However, adding FA increases the workability due to enhanced paste volume. Otherwise, the addition of MK increases the cohesion and viscosity, which leads to an increase in the values of the V-funnel and T500 times. These results indicate that while FA improves flowability, MK makes the mixture denser, which raises the flowability resistance.

The Mechanical Properties Performance

The addition of RCA and SCM has a significant impact on compressive, tensile and flexural strengths, and modulus of elasticity. While several studies have studied the mechanical properties of RCA-NC with SCM, the mechanical properties of RCA-SCC with SCM have received less attention, with limited studies conducted in this area, as reviewed in the following sub-section.

The Mechanical Properties of Unary Cementation Binder

Most findings showed that the RCA generally exhibits lower compressive strength, mostly due to the limitations of RCA (Aslani et al., 2018; Uygunoğlu et al., 2014). According to Gesoglu et al. (2015), the compressive strength of 100% RCA replacement is reduced to 31%. Additionally, it also results in reduced tensile and flexural strength and modulus of elasticity. Additionally, Liu et al. (2021) discovered that using RCA in SCC reduces compressive strength by less than 23% compared to regular concrete, probably due to higher paste content strengthening the weak surface layer of RCA, resulting in a denser ITZ.

The study conducted by Sasanipour and Aslani (2020) revealed that using RCA decrease compressive strength at all ages. The reduction of compressive strength after 28 days was 32% when 25% RCA was used. Replacing 75% RCA resulted in a maximum reduction of 43% after 28 days. This is probably due to the high porosity of RCA and the insufficient bonding between the mortar paste and the RCA. Nevertheless, Abed et al. (2020) stated that using RCA up to 50% increases the compressive, flexural strength and elastic modulus due to the good bond between the RCA particles and the fresh cement paste. These results may be related to the quality of the parent concrete. This finding is supported by Kamar et al. (2024), who stated that increased durability and improved mechanical performance were achieved when recycled aggregates were sourced from high-strength parent concrete. However, the mechanical strength and durability of SCC decrease when recycled concrete aggregates derived from low-strength parent concrete are used in the mix.

Based on De Brito and Robles' (2010) study, using RCA reduces tensile strength at a slower rate than compressive strength. Tuyan et al. (2014) stated that increasing the percentage of RCA minimises the tensile strength reduction. The compressive and tensile strength results of the SCCs revealed that using RCA in percentages ranging from 25% to 75% had no significant impact on the strength of the SCC. However, compared to the control SCC, the 100% RCA modulus of elasticity was much lower, suggesting that there may be a brittleness problem with SCCs made completely of RCA (Tang et al., 2016). According to Tang et al. (2020), the mechanical properties of SCC that contain RCA are significantly affected by the properties of the RCA and the proportion of replacement. Compressive, flexural, and tensile strengths and the elastic modulus decreased as RCA replacement increased in SCC. However, it has been proposed that SCMs can enhance RCA and ITZ quality. The primary cause is the fact that the filler effect fills the inner pores of RAC efficiently, while the pozzolanic effect speeds up the hydration reaction of the cement and consumes $\text{Ca}(\text{OH})_2$ to generate a huge amount of C-S-H gel (Gao et al., 2022). Generating these gels results in dense particles, significantly enhancing the compactness of the inner structure of concrete. The enhancing effect is different for the various activities of the admixtures. The FA's effect on the micro-hardness and ITZs width of RAC is not obvious. The main reason is that FA reacts more slowly than cement, especially in the early stages. Even after 28 days, some FA remains unreacted in RAC, meaning fewer hydration products like calcium silicate and calcium aluminate are formed. On the other hand, SF is highly reactive, helping to consume excess calcium hydroxide $\text{Ca}(\text{OH})_2$ and speeding up cement hydration, which ultimately makes the RAC denser and more compact (Mohan & Mini, 2018).

The Mechanical Properties of Binary Cementation Binder

The compressive strength of SCC mixtures containing 30% FA decreases as RCA replacement increases because of the old ITZ in the concrete matrix (Kapoor et al., 2020).

Furthermore, Khodair and Luqman (2017) examined the high volume of fly ash of up to 70% FA with different percentages of RCA (0%, 25%, 50%, 75%). The compressive strength of all mixture combinations between HVFA and RCA decreased at all curing durations. Singh and Singh (2016b) discovered a maximum compressive strength decrease of 60% at 28 days for SCC control at 50% and 60% FA with 0%, 50%, and 100% RCA. The decrease in compressive strength can be attributed to the higher porosity of HVFA, which, according to Du et al. (2023), is attributed to the unreacted particles, which can act as inert fillers, failing to participate in the pozzolanic reaction. MK increased compressive strength by 50% and RCA by 100% compared to the control SCC mix for all HVFA at all curing ages.

However, another study by Kumar et al. (2017) observed that adding 33% FA with a low percentage of RCA achieved higher compressive strength compared to the control mix. Hu et al. (2017) found that compressive strength was improved when RCA and FA were used in conjunction with the arrangement of aggregate particles in the mixes. The compressive strength of the mixture containing 50% RCA exhibited a considerable improvement of around 17% compared to the control mixture. The findings can be explained by better particle packing, as the higher volume of excess paste improves bonding between cement and aggregate particles. Abed and Nemes (2019) found that mixes with RCA up to 50% and FA up to 15% had better strength performance compared to RCA-SCC mixes without FA. The result can be attributed to the submerged RCA in water for 24 hours before being used in the mixture, as the water absorption of RCA after 24 hours was 5.6%. According to Gesoğlu et al. (2009), the large FA particles in the RCA inter-crack could gradually gain strength over time. Even when FA with RCA replaced up to 30% of the cement, the tensile strength remained relatively unchanged, suggesting that the mixture may need more time to fully hydrate. Additionally, FA improved the flexural strength up to the point when 15% cement was replaced. There was no noticeable difference in the modulus of elasticity performance when FA was used instead of 15% of the cement.

Majhi et al. (2018) found that as the percentage of RCA, GGBS, or both increased, the mechanical characteristics decreased compared to the control sample. A combination of 50% RCA and 40% GGBS is likely to produce the optimum for sustainable concrete of M25 grade. The efficiency of GGBS in RCA-SCC increases with the age of the concrete at 90 days as compared to 7 and 28 days. Because GGBS has finer particles and RCA has a rougher surface, concrete mixes with varying percentages tend to have higher flexural and split tensile strengths than compressive strength. However, the comparison between RCA-SCC and RCA-NC incorporating GGBS has been studied by Abhishek et al. (2021). The comparison showed that the compressive strength of NC specimens decreased when RCA increased, but the SCC group specimens decreased rapidly as the RCA level increased. The scanning electron micrograph (SEM) analysis showed that the ITZ of RCA in SCC appeared loose and porous, leading to higher water absorption and negatively affecting the SCC mix.

Singh et al. (2022) studied the effect of SF in RCA-SCC and RCA-NC. The results showed a reduction in the compressive strength of SCC by 25% and 10% for RCA and SF, respectively, compared to NC. The same results were obtained by Sasanipour et al. (2019) when comparing RCA mixes with and without 8% SF. Singh and Singh (2016b) have noticed that using MK in RCA-SCC mixtures helps reduce the decrease in compressive strength. Incorporating MK into a combination of 50% RCA exhibited compressive strength comparable to the control sample. This can be due to the small particles of MK penetrating the pores of the RCA and the pozzolanic reaction of MK with calcium hydroxide. This process could be because of the completion of the reaction at early ages of chemically active MK, in which the resultant product helped in pore refinement of the mix (Çakır, 2014).

Figures 2 and 3 show the compressive strength results between the different percentages of SCMs with a constant percentage of 25% RCA. The results indicated that SCC with FA in binary form exhibited higher compressive strength than GGBS and SF, even with a smaller dosage of 15%. Table 5 tabulates the mechanical strength of SCC produced with a binary GGBS, FA and SF binder.

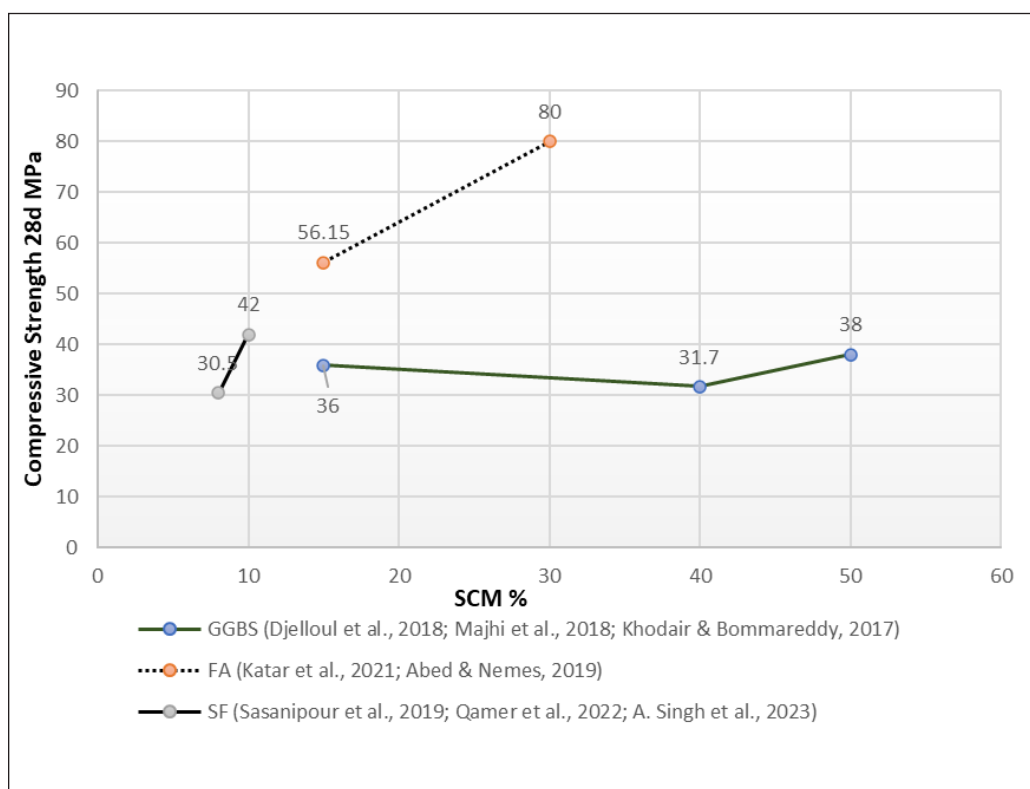


Figure 2. The compressive strength of 25% RCA SCC with various SCM levels (FA, GGBS, SF)

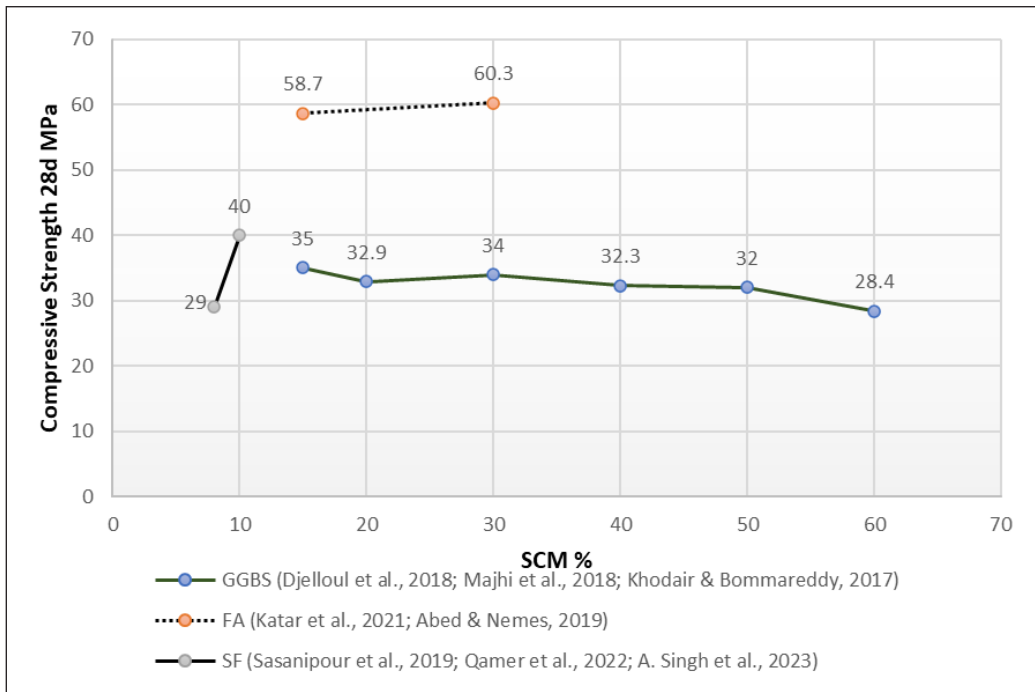


Figure 3. The compressive strength of 25% RCA SCC with various SCM levels (FA, GGBS, SF)

Table 5
Results of some studies on the mechanical properties of binary RCA-SCC

Ref	SCM	RCA (%)	Compressive Strength 28d. (MPa)	Tensile strength 28d. (MPa)	Flexural Strength 28d. (MPa)	Modulus of Elasticity 28d. (GPa)
Khodair & Bommareddy, 2017	GGBS	0	52	5.8	-	-
	50%	25	38	4.1	-	-
		50	32	3	-	-
		75	28	3.1	-	-
		100	19	1.9	-	-
Djelloul et al., 2018		0	39	-	-	-
	GGBS	25	36	-	-	-
	15%	50	35	-	-	-
		75	34	-	-	-
		100	33	-	-	-
		0	38	-	-	-
	GGBS	25	35	-	-	-
	30%	50	34	-	-	-
		75	33	-	-	-
		100	32	-	-	-

Table 5 (continue)

Ref	SCM	RCA (%)	Compressive Strength 28d. (MPa)	Tensile strength 28d. (MPa)	Flexural Strength 28d. (MPa)	Modulus of Elasticity 28d. (GPa)
Majhi et al., 2018	GGBS 20%	0	35.2	3.50	3.80	-
		25	34.0	2.86	3.70	-
		50	32.9	2.82	3.65	-
		100	28.4	2.65	3.55	-
	GGBS 40%	0	33.7	2.90	3.65	-
		25	31.7	2.70	3.60	-
		50	32.3	2.70	3.57	-
		100	27.0	2.55	3.42	-
	GGBS 60%	0	29.1	2.80	3.60	-
		25	28.0	2.56	3.50	-
		50	28.4	2.55	3.50	-
		100	24.4	2.36	3.15	-
Kapoor et al., 2016	FA 30%	0	38	-	-	-
		50	36.2	-	-	-
Katar et al., 2021	FA 15%	100	33	-	-	-
		0	55.9	3.10	-	-
		25	44.3	1.90	-	-
Kapoor et al., 2020	FA 30%	50	42.4	3.30	-	-
		75	41.8	3.00	-	-
		0	38	-	-	-
Nguyen, 2024	FA 50%	50	36.5	-	-	-
		100	33	-	-	-
		0	30.9	2.27	3.91	-
		50	26.6	1.70	2.93	-
Abed & Nemes, 2019	FA 15%	75	24.7	1.56	2.69	-
		100	29.5	2.20	3.79	-
		0	70	3.5	7.9	-
		25	68	3.4	7.8	-
		75	75	3.9	8.0	-
Sasanipour et al., 2019	FA 30%	50	63	3	7.0	-
		80	80	3.5	7.5	-
		85	85	3.8	7.4	-
		0	43	-	-	-
Singh et al., 2023	SF 10%	25	31	-	-	-
		50	29.5	-	-	-
		75	28	-	-	-
		100	23	-	-	-
Qamer et al., 2022	SF 8%	0	44	-	-	-
		25	42	-	-	-
		50	40	-	-	-
		0	42	-	-	-
		25	30	-	-	-
Singh et al., 2023	SF 10%	50	40	-	-	-
		75	25	-	-	-
		100	20	-	-	-
		0	42	-	-	-

The Mechanical Properties of Ternary Cementation Binder

According to Guo et al. (2020), using a ternary combination of FA and GGBS mixes has achieved higher compressive strength than binary mixes containing FA. The findings demonstrated that ternary mixtures possess engineering benefits in comparison to binary mixtures, hence enhancing the implementation of sustainable design principles in the field of structural engineering. Furthermore, including 100% RCA and 75% SCM in the RCA-SCC mixes resulted in a compressive strength of around 30 MPa, which is suitable for practical engineering use. The compressive strength of different SCC mixes increases by 1.26%–19.10% when incorporating various types of pozzolanic components such as FA, SF, and FA + SF, which generate more calcium-silicate-hydrate (C-S-H) gel (Singh et al., 2023).

Kapoor et al. (2016) studied the effect of adding SCMs (FA, SF, MK) in binary and ternary contents on the compressive strength of RCA-SCC. The replacement of 100% RCA for NCA resulted in a 13% reduction in 28-day compressive strength compared to the control SCC produced with NCA. Adding SF or MK to SCC with RCA at a dosage of 10% cement and 20% FA reduced the strength to 8% and 3%, respectively. The results show that using MK in a ternary mix produced a higher strength reduction compared to SF for 28 days of compressive strength. Furthermore, the results of Singh and Singh (2016a) showed that MK had a positive impact on SCC mixes with 25% and 50% RCA, which can be attributed to the filling of pores occurring by the pozzolanic reaction of MK with calcium hydroxide. This might be because the chemical reaction took place at an early stage in the life cycle of the chemically active MK, and the by-products helped improve the mix's pores. The amount of RCA plays an important role in determining the strength produced by ternary mixes containing MK and SF.

Khodair and Bommareddy (2017) noted that the 28-day compressive strength of SCC mixes with 25% FA and 25% GGBS was mid-range for 50% FA and 50% GGBS mixes. Compared to the mixes developed with 100% cement, SCMs mixes are relatively lower in compressive strength. The compressive strength of 50% GGBS was greater than the mixes of 50% FA, 25% FA, and 25% GGBS, except for 100% RCA mixes. GGBS initiates hydration by deconstructing the glass structure with hydroxide ions, releasing ions like Ca^{2+} , Al^{3+} , and SiO_4^{4-} , which contribute to the formation of an aluminium-substituted C-A-S-H gel, enhancing the microstructure and reducing porosity, making the concrete more robust (Pang et al., 2022). An increase in the RCA% exhibited a negative impact on tensile strength. All mixtures with 50% GGBS have the lowest split tensile strength drop compared to mixes with 50% FA, 25% FA, and 25% GGBS.

Adding 10% SF with 25% GGBS improved the compressive strength, even though the effect was more noticeable in mixes with greater w/b ratios (Gesoglu et al., 2015). This study discovered that mixtures with a w/b ratio of 0.30 and 0.43 showed a rise in compressive strength of 2.5%–4.4% and 8.8%–25.4%, respectively, when 10% SF was added. The compressive strength of RCA-SCC with ternary SCM was lower than that of

SCC integrating NCA without SCM for a given w/b ratio, and this difference increased as the quantity of RCA replacement increased. For splitting tensile and flexural strengths, mixes containing SCM and having a w/b ratio of 0.3 were better than those without SCM and having a w/b ratio 0.43. Table 6 tabulates the mechanical strength of SCC produced with a ternary binder of GGBS, FA, MK and SF.

Table 6
Results of some studies on the mechanical properties of ternary RCA-SCC

Ref	SCM	RCA (%)	Compressive strength,	Tensile strength,	Flexural Strength	Modulus of Elasticity
Tang et al., 2016		0	59.4	4.1		31.5
	SF 5%	25	63.7	4.9	-	30.3
	FA 25%	50	65.3	4.1		29.5
		75	60.0	3.9		28.5
		100	53.8	3.8		24.5
Khodair & Bommareddy, 2017		0	46	5.1	-	-
	GGBS 25%	25	35	3.8		
		50	30	2.9		
	FA 25%	75	24	2.8		
		100	20	2.4		
		SF 10%		41	-	-
	FA 20%	0	37			
50		34				
Kapoor et al., 2016	MK 10%	100	42	-	-	-
		FA 20%	40			
			35			
	Control (0,0)		48	-	-	-
	MK 10%	25	52			
Tiwari et al., 2021	GGBS 10%, 15%, 20%, 25%		51			
			48			
			45			
	Control (0,0)		44	-	-	-
	MK 10%	50	48			
Singh & Singh, 2016b	GGBS 10%, 15%, 20%, 25%		47			
			46			
			43			
	Control (0,0)	0	40	-	-	-
	MK 10%	25	42			
Singh & Singh, 2016b	FA 20%	50	38			
		75	35			
		100	36			
	MK 10%	0	43	-	-	-
Kapoor et al., 2017	FA 20%	100	37			
Singh et al., 2023	SF 10%	0	46.34	-	-	-
	FA 15%	25	45			
Xuyong et al., 2025	GGBS 10%	15	51.5	5.25	6.75	-
	FA 20%	30	53.7	5.35	6.42	
		50	45.2	4.75	5.75	

CONCLUSION

This paper draws the following conclusion from the extensive reviews on RCA-SCC with various by-product cementitious materials wastes:

- The chemical composition of SCMs plays a crucial role in their reactivity and contribution to concrete performance. The pozzolanic reactions induced by SF, with its high SiO₂ content, enhance strength and durability. FA needs activation because of its stable glassy phase. The high contents of CaO and SiO₂ for GGBS allow a higher degree of C-S-H gel formation, which increases strength and reduces porosity. MK is rich in silica and alumina, which promotes early strength development. Each SCM contributes uniquely to improving concrete durability, strength, and permeability reduction.
- The specific surface area (SSA) of SCM is vital for its reactivity, hydration rate, and overall influence on concrete properties. Materials with a higher SSA, like SF and MK, tend to react more quickly with other components, which helps accelerate early strength development and lowers permeability. On the other hand, FA and GGBS help in sulphate resistance by promoting ettringite formation, which helps reduce the risk of alkali-silica reaction (ASR).
- The increased porosity, decreased density, and decreased strength of RCA greatly influence workability and mechanical behaviour. Increased RCA replacement has an impact on fresh properties and mechanical properties; nevertheless, the workability of SCC can be enhanced by keeping RCA substitution to less than 50%. Slump flow values fall as RCA increases, owing to surface roughness. Generally, the replacement ratio and angularity of the aggregates determine how RCA affects SCC characteristics. However, incorporating GGBS alongside RCA mitigates this effect, and optimal proportions prevent issues like bleeding or segregation.
- Incorporating SCMs like FA, GGBS, and SF in RCA-SCC enhances workability. Ternary mixes, especially with FA and GGBS, demonstrate improved sustainability and workability compared to binary mixes. Ternary combinations influence slump flow, T-50 Time, and other properties of RCA-SCC.
- RCA generally exhibits lower compressive strength compared to NCA, with reductions influenced by factors like the porosity of RCA and the quality of the mortar matrix. Meanwhile, the rate of loss in tensile strength is typically lower compared to compressive strength. Using SCMs is suggested to improve the quality of RCA and the ITZ, potentially enhancing mechanical properties.
- Factors such as the quantity of SCM and curing duration affect the compressive strength of RCA-SCC. Higher RCA content generally leads to a decline in compressive strength, and the presence of large FA particles in the inter-crack of RCA may result in gradual

strength gain over time. The addition of GGBS to SCC enhances compatibility and consistency. MK mitigates the loss of compressive strength in RCA-SCC mixes, and its incorporation improves the ITZ bonding between paste and aggregates.

Additional investigation regarding the combining of SCC and RCA is still essential. Previous studies have focused on the strength and durability of SCC with RCA. Few investigations have focused on related properties, such as flexural, compressive, and splitting tensile strength. Few invest in the potential of these mixtures to achieve high strength levels, which is crucial for their practical application in structural elements, especially in SCC.

ACKNOWLEDGEMENT

The authors would like to express appreciation for the financial support granted for this research: Geran Inisiatif Putra Siswazah (UPM-IPS) [Project Number = GP-IPS/2023/9743300].

REFERENCES

- Abed, M., & Nemes, R. (2019). Mechanical properties of recycled aggregate self-compacting high strength concrete utilizing waste fly ash, cellular concrete and perlite powders. *Periodica Polytechnica Civil Engineering*, 63(1), 266-277. <https://doi.org/10.3311/ppci.13136>
- Abed, M., Nemes, R., & Tayeh, B. A. (2020). Properties of self-compacting high-strength concrete containing multiple use of recycled aggregate. *Journal of King Saud University: Engineering Sciences*, 32(2), 108–114. <https://doi.org/10.1016/j.jksues.2018.12.002>
- Abhishek, P., Ramachandra, P., & Niranjana, P. (2021). Use of recycled concrete aggregate and granulated blast furnace slag in self-compacting concrete. *Materials Today: Proceedings*, 42, 479–486. <https://doi.org/10.1016/j.matpr.2020.10.239>
- Alobaidi, Y. M., Hilal, N. N., & Faraj, R. H. (2021). An experimental investigation on the nano-fly ash preparation and its effects on the performance of self-compacting concrete at normal and elevated temperatures. *Nanotechnology for Environmental Engineering*, 6(1), Article 2. <https://doi.org/10.1007/s41204-020-00098-6>
- Al-Oran, A. A. A., Safiee, N. A., & Nasir, N. A. M. (2022). Fresh and hardened properties of self-compacting concrete using metakaolin and GGBS as cement replacement. *European Journal of Environmental and Civil Engineering*, 26(1), 379–392. <https://doi.org/10.1080/19648189.2019.1663268>
- Alsubari, B., Shafiq, P., & Jumaat, M. Z. (2015). Development of self-consolidating high strength concrete incorporating treated palm oil fuel ash. *Materials*, 8(5), 2154–2173. <https://doi.org/10.3390/ma8052154>
- Aslani, F., Ma, G., Wan, D. L. Y., & Muselin, G. (2018). Development of high-performance self-compacting concrete using waste recycled concrete aggregates and rubber granules. *Journal of Cleaner Production*, 182, 553–566. <https://doi.org/10.1016/j.jclepro.2018.02.074>

- Barbhuiya, S., & Kumala, D. (2017). Behaviour of a sustainable concrete in acidic environment. *Sustainability*, 9(9), Article 1556. <https://doi.org/10.3390/su9091556>
- Beycioğlu, A., & Aruntaş, H. Y. (2014). Workability and mechanical properties of self-compacting concretes containing LLFA, GBFS and MC. *Construction and Building Materials*, 73, 626–635. <https://doi.org/10.1016/j.conbuildmat.2014.09.071>
- Bingöl, A. F., & Tohumcu, İ. (2013). Effects of different curing regimes on the compressive strength properties of self compacting concrete incorporating fly ash and silica fume. *Materials in Engineering*, 51, 12–18. <https://doi.org/10.1016/j.matdes.2013.03.106>
- Çakır, Ö. (2014). Experimental analysis of properties of recycled coarse aggregate (RCA) concrete with mineral additives. *Construction and Building Materials*, 68, 17–25. <https://doi.org/10.1016/j.conbuildmat.2014.06.032>
- Carbone, C., Ferrario, D., Lanzini, A., Stendardo, S., & Agostini, A. (2022). Evaluating the carbon footprint of cement plants integrated with the calcium looping CO2 capture process. *Frontiers in Sustainability*, 3, Article 809231. <https://doi.org/10.3389/frsus.2022.809231>
- Castano, J. E., & Abdel-Mohti, A. (2024). Assessing the impact of recycled concrete aggregates on the fresh and hardened properties of self-consolidating concrete for structural precast applications. *Infrastructures*, 9(10), Article 177. <https://doi.org/10.3390/infrastructures9100177>
- Curcio, F., DeAngelis, B., & Pagliolico, S. (1998). Metakaolin as a pozzolanic microfiller for high-performance mortars. *Cement and Concrete Research*, 28(6), 803–809. [https://doi.org/10.1016/s0008-8846\(98\)00045-3](https://doi.org/10.1016/s0008-8846(98)00045-3)
- De Brito, J., & Robles, R. (2010). Recycled aggregate concrete (RAC) methodology for estimating its long-term properties. *Indian Journal of Engineering and Materials Sciences*, 17(6), 449-462.
- De Brito, J., Ferreira, J., Pacheco, J., Soares, D., & Guerreiro, M. J. (2016). Structural, material, mechanical and durability properties and behaviour of recycled aggregates concrete. *Journal of Building Engineering*, 6, 1–16. <https://doi.org/10.1016/j.jobe.2016.02.003>
- De Matos, P. R., Foiato, M., & Prudêncio, L. R. (2019). Ecological, fresh state and long-term mechanical properties of high-volume fly ash high-performance self-compacting concrete. *Construction and Building Materials*, 203, 282–293. <https://doi.org/10.1016/j.conbuildmat.2019.01.074>
- Djelloul, O. K., Mahdad, B., Wardeh, G., & Kenai, S. (2018). Performance of self-compacting concrete made with coarse and fine recycled concrete aggregates and ground granulated blast-furnace slag. *Advances in Concrete Construction*, 6(2), 103–121. <https://doi.org/10.12989/acc.2018.6.2.103>
- Du, S., Zhao, Q., & Shi, X. (2023). Quantification of the reaction degree of fly ash in blended cement systems. *Cement and Concrete Research*, 167, Article 107121. <https://doi.org/10.1016/j.cemconres.2023.107121>
- Duan, Z., Singh, A., Xiao, J., & Hou, S. (2020). Combined use of recycled powder and recycled coarse aggregate derived from construction and demolition waste in self-compacting concrete. *Construction and Building Materials*, 254, Article 119323. <https://doi.org/10.1016/j.conbuildmat.2020.119323>
- EFNARC (2005). *Specifications and guidelines for self-compacting concrete*. European federation for specialist construction chemicals & concrete systems. chrome-extension://efaidnbmninnibpcjpcglclefindmkaj/https://www.theconcreteinitiative.eu/images/ECP_Documents/EuropeanGuidelinesSelfCompactingConcrete.pdf

- Francis, A. K., & Eldhose, S. (2017). Study on the effect of replacement of portland cement by sugar cane bagasse ash and egg shell powder on HPC. *International Journal of Scientific & Engineering Research*, 8(3), 878-881.
- Gao, S., Guo, X., Ban, S., Ma, Y., Yu, Q., & Sui, S. (2022). Influence of supplementary cementitious materials on ITZ characteristics of recycled concrete. *Construction and Building Materials*, 363, Article 129736. <https://doi.org/10.1016/j.conbuildmat.2022.129736>
- Gesoğlu, M., Güneyisi, E., & Özbay, E. (2009). Properties of self-compacting concretes made with binary, ternary, and quaternary cementitious blends of fly ash, blast furnace slag, and silica fume. *Construction and Building Materials*, 23(5), 1847–1854. <https://doi.org/10.1016/j.conbuildmat.2008.09.015>
- Gesoğlu, M., Güneyisi, E., Öz, H. Ö., Taha, I., & Yasemin, M. T. (2015). Failure characteristics of self-compacting concretes made with recycled aggregates. *Construction and Building Materials*, 98, 334–344. <https://doi.org/10.1016/j.conbuildmat.2015.08.036>
- Golewski, G. L. (2023). Examination of water absorption of low volume fly ash concrete (LVFAC) under water immersion conditions. *Materials Research Express*, 10(8), Article 085505. <https://doi.org/10.1088/2053-1591/acedef>
- Gómez-Casero, M., De Dios-Arana, C., Bueno-Rodríguez, J., Pérez-Villarejo, L., & Eliche-Quesada, D. (2022). Physical, mechanical and thermal properties of metakaolin-fly ash geopolymers. *Sustainable Chemistry and Pharmacy*, 26, Article 100620. <https://doi.org/10.1016/j.scp.2022.100620>
- Guo, Z., Tao, J., Zhang, J., Kong, X., Chen, C., & Lehman, D. E. (2020). Mechanical and durability properties of sustainable self-compacting concrete with recycled concrete aggregate and fly ash, slag and silica fume. *Construction and Building Materials*, 231, Article 117115. <https://doi.org/10.1016/j.conbuildmat.2019.117115>
- Guo, Z., Zhang, J., Tao, J., Jiang, T., Chen, C., Bo, R., & Sun, Y. (2020). Development of sustainable self-compacting concrete using recycled concrete aggregate and fly ash, slag, silica fume. *European Journal of Environmental and Civil Engineering*, 26(4), 1453–1474. <https://doi.org/10.1080/19648189.2020.1715847>
- Gupta, N., Siddique, R., & Belarbi, R. (2021). Sustainable and greener self-compacting concrete incorporating industrial by-products: A review. *Journal of Cleaner Production*, 284, Article 124803. <https://doi.org/10.1016/j.jclepro.2020.124803>
- Hani, N., Nawawy, O. E., Ragab, K. S., & Kohail, M. (2018). The effect of different water/binder ratio and nano-silica dosage on the fresh and hardened properties of self-compacting concrete. *Construction and Building Materials*, 165, 504–513. <https://doi.org/10.1016/j.conbuildmat.2018.01.045>
- Hu, J., Souza, I. L., & Genarini, F. C. (2017). Engineering and environmental performance of eco-efficient self-consolidating concrete (Eco-SCC) with low powder content and recycled concrete aggregate. *Journal of Sustainable Cement-Based Materials*, 6(1), 2–16. <https://doi.org/10.1080/21650373.2016.1230901>
- Huang, B., Wang, X., Kua, H., Geng, Y., Bleischwitz, R., & Ren, J. (2018). Construction and demolition waste management in China through the 3R principle. *Resources, Conservation and Recycling*, 129, 36–44. <https://doi.org/10.1016/j.resconrec.2017.09.029>

- Kamar, D., Zohra, M. F., Sacia, K., Dallel, D., & Nouredine, A. (2024). Development of self-consolidating concretes based on recycled aggregates: Effect of parent concrete strength. *MATEC Web of Conferences*, 394, Article 02002. <https://doi.org/10.1051/mateconf/202439402002>
- Kanamarlapudi, L., Jonalagadda, K. B., Jagarapu, D. C. K., & Eluru, A. (2020). Different mineral admixtures in concrete: A review. *SN Applied Sciences*, 2(4), Article 760. <https://doi.org/10.1007/s42452-020-2533-6>
- Kapoor, K., Singh, S. P., & Singh, B. (2017). Permeability of self-compacting concrete made with recycled concrete aggregates and metakaolin. *Journal of Sustainable Cement-Based Materials*, 6(5), 293–313. <https://doi.org/10.1080/21650373.2017.1280426>
- Kapoor, K., Singh, S. P., Singh, B., & Singh, P. (2020). Effect of recycled aggregates on fresh and hardened properties of self compacting concrete. *Materials Today: Proceedings*, 32, 600–607. <https://doi.org/10.1016/j.matpr.2020.02.753>
- Kapoor, K., Singh, S., & Singh, B. (2016). Durability of self-compacting concrete made with recycled concrete aggregates and mineral admixtures. *Construction and Building Materials*, 128, 67–76. <https://doi.org/10.1016/j.conbuildmat.2016.10.026>
- Katar, I. M., Ibrahim, Y. E., Malik, M. A., & Khahro, S. H. (2021). Mechanical properties of concrete with recycled concrete aggregate and fly ash. *Recycling*, 6(2), Article 23. <https://doi.org/10.3390/recycling6020023>
- Kefelegn, A., & Gebre, A. (2020). Performance of self-compacting concrete used in congested reinforcement structural element. *Engineering Structures*, 214, Article 110665. <https://doi.org/10.1016/j.engstruct.2020.110665>
- Khan, M. N. N., & Sarker, P. K. (2019). Alkali silica reaction of waste glass aggregate in alkali activated fly ash and GGBFS mortars. *Materials and Structures*, 52(5), Article 93. <https://doi.org/10.1617/s11527-019-1392-3>
- Khater, H. M. (2013). Effect of silica fume on the characterization of the geopolymer materials. *International Journal of Advanced Structural Engineering*, 5(1), Article 12. <https://doi.org/10.1186/2008-6695-5-12>
- Khodair, Y., & Bommareddy, B. R. (2017). Self-consolidating concrete using recycled concrete aggregate and high volume of fly ash, and slag. *Construction and Building Materials*, 153, 307–316. <https://doi.org/10.1016/j.conbuildmat.2017.07.063>
- Khodair, Y., & Luqman, L. (2017). Self-compacting concrete using recycled asphalt pavement and recycled concrete aggregate. *Journal of Building Engineering*, 12, 282–287. <https://doi.org/10.1016/j.job.2017.06.007>
- Kou, S. C., Poon, C. S., & Agrela, F. (2011). Comparisons of natural and recycled aggregate concretes prepared with the addition of different mineral admixtures. *Cement and Concrete Composites*, 33(8), 788–795. d
- Kumar, B., Ananthan, H., & Balaji, K. V. (2017). Experimental studies on utilization of coarse and finer fractions of recycled concrete aggregates in self compacting concrete mixes. *Journal of Building Engineering*, 9, 100–108. <https://doi.org/10.1016/j.job.2016.11.013>

- Kumar, M. A., Magesh, R., Selvapraveen, S., & Vignesh, M. (2020). Assessment on fresh properties and hardened properties of self compacting concrete. *AIP Conference Proceedings*, 2235(1), Article 020021. <https://doi.org/10.1063/5.0007748>
- Li, Q., Li, Z., & Yuan, G. (2012). Effects of elevated temperatures on properties of concrete containing ground granulated blast furnace slag as cementitious material. *Construction and Building Materials*, 35, 687–692. <https://doi.org/10.1016/j.conbuildmat.2012.04.103>
- Liu, Y., Ling, T., & Mo, K. (2021). Progress in developing self-consolidating concrete (SCC) constituting recycled concrete aggregates: A review. *International Journal of Minerals, Metallurgy and Materials*, 28(4), 522–537. <https://doi.org/10.1007/s12613-020-2060-x>
- Mahalakshmi, S. H. V., & Khed, V. C. (2020). Experimental study on M-sand in self-compacting concrete with and without silica fume. *Materials Today: Proceedings*, 27, 1061–1065. <https://doi.org/10.1016/j.matpr.2020.01.432>
- Majhi, R. K., Nayak, A. N., & Mukharjee, B. B. (2018). Development of sustainable concrete using recycled coarse aggregate and ground granulated blast furnace slag. *Construction and Building Materials*, 159, 417–430. <https://doi.org/10.1016/j.conbuildmat.2017.10.118>
- Malazdrewicz, S., Ostrowski, K., & Sadowski, Ł. (2023). Self-compacting concrete with recycled coarse aggregates from concrete construction and demolition waste – Current state-of-the art and perspectives. *Construction and Building Materials*, 370, Article 130702. <https://doi.org/10.1016/j.conbuildmat.2023.130702>
- Mo, K. H., Ling, T., & Cheng, Q. (2020). Examining the influence of recycled concrete aggregate on the hardened properties of self-compacting concrete. *Waste and Biomass Valorization*, 12(2), 1133–1141. <https://doi.org/10.1007/s12649-020-01045-x>
- Mohan, A., & Mini, K. (2018). Strength and durability studies of SCC incorporating silica fume and ultra fine GGBS. *Construction and Building Materials*, 171, 919–928. <https://doi.org/10.1016/j.conbuildmat.2018.03.186>
- Mohseni, E., Saadati, R., Kordbacheh, N., Parpinchi, Z. S., & Tang, W. (2017). Engineering and microstructural assessment of fibre-reinforced self-compacting concrete containing recycled coarse aggregate. *Journal of Cleaner Production*, 168, 605–613. <https://doi.org/10.1016/j.jclepro.2017.09.070>
- Nguyen, H. C. (2024). The influence of recycled coarse aggregate content on the properties of high-fly-ash self-compacting concrete. *Civil Engineering Journal*, 10, 51–61. <https://doi.org/10.28991/cej-sp2024-010-04>
- Pang, L., Liu, Z., Wang, D., & An, M. (2022). Review on the application of supplementary cementitious materials in self-compacting concrete. *Crystals*, 12(2), Article 180. <https://doi.org/10.3390/cryst12020180>
- Qamer, M., Ashraf, A., Shad, M. A., Haider, W., Jan, M., Usman, M., Billah, M. B., & Ibrahim, M. (2022). Mechanical and durability properties of self-compacting concrete with recycled concrete aggregate, silica fume and nanosilica. *International Journal of Current Engineering and Technology*, 12(06), 412–418. <https://doi.org/10.14741/ijcet/v.12.5.4>
- Raghav, M., Park, T., Yang, H., Lee, S., Karthick, S., & Lee, H. (2021). Review of the effects of supplementary cementitious materials and chemical additives on the physical, mechanical and durability properties of hydraulic concrete. *Materials*, 14(23), Article 7270. <https://doi.org/10.3390/ma14237270>

- Safuiddin, M., Salam, M. A., & Jumaat, M. Z. (2011). Effects of recycled concrete aggregate on the fresh properties of self-consolidating concrete. *Archives of Civil and Mechanical Engineering*, 11(4), 1023–1041. [https://doi.org/10.1016/s1644-9665\(12\)60093-4](https://doi.org/10.1016/s1644-9665(12)60093-4)
- Sasanipour, H., & Aslani, F. (2020). Durability properties evaluation of self-compacting concrete prepared with waste fine and coarse recycled concrete aggregates. *Construction and Building Materials*, 236, Article 117540. <https://doi.org/10.1016/j.conbuildmat.2019.117540>
- Sasanipour, H., Aslani, F., & Taherinezhad, J. (2019). Effect of silica fume on durability of self-compacting concrete made with waste recycled concrete aggregates. *Construction and Building Materials*, 227, Article 116598. <https://doi.org/10.1016/j.conbuildmat.2019.07.324>
- Sharobim, K., Hassan, H. M., & Ragheb, S. (2017). Durability Improvement of self compacting recycled aggregate concrete using marble powder. *Port-Said Engineering Research Journal*, 21(2), 68–77. <https://doi.org/10.21608/psrj.2017.33292>
- Singh, N., & Singh, S. P. (2016a). Carbonation and electrical resistance of self compacting concrete made with recycled concrete aggregates and metakaolin. *Construction and Building Materials*, 121, 400–409. <https://doi.org/10.1016/j.conbuildmat.2016.06.009>
- Singh, N., & Singh, S. P. (2016b). Carbonation resistance and microstructural analysis of low and high volume fly ash self compacting concrete containing recycled concrete aggregates. *Construction and Building Materials*, 127, 828–842. <https://doi.org/10.1016/j.conbuildmat.2016.10.067>
- Singh, R. B., Kumar, N., & Singh, B. (2017). Effect of supplementary cementitious materials on rheology of different grades of self-compacting concrete made with recycled aggregates. *Journal of Advanced Concrete Technology*, 15(9), 524–535. <https://doi.org/10.3151/jact.15.524>
- Singh, R. B., & Singh, B. (2018). Rheological behaviour of different grades of self-compacting concrete containing recycled aggregates. *Construction and Building Materials*, 161, 354–364. <https://doi.org/10.1016/j.conbuildmat.2017.11.118>
- Singh, A., Duan, Z., & Liu, Q. (2019). Incorporating recycled aggregates in self-compacting concrete: a review. *Journal of Sustainable Cement-Based Materials*, 9(3), 165–189. <https://doi.org/10.1080/21650373.2019.1706205>
- Singh, A., Mehta, P. K., & Kumar, R. (2022). Recycled coarse aggregate and silica fume used in sustainable self-compacting concrete. *International Journal of Advanced Technology and Engineering Exploration*, 9(96), Article 1581. <https://doi.org/10.19101/ijatee.2021.876138>
- Singh, A., Mehta, P., & Kumar, R. (2023). Strength and microstructure analysis of sustainable self-compacting concrete with fly ash, silica fume, and recycled minerals. *Materials Today: Proceedings*, 78, 86–98. <https://doi.org/10.1016/j.matpr.2022.11.282>
- Tafraoui, A., Escadeillas, G., & Vidal, T. (2016). Durability of the ultra high performances concrete containing metakaolin. *Construction and Building Materials*, 112, 980–987. <https://doi.org/10.1016/j.conbuildmat.2016.02.169>
- Tang, W., Khavarian, M., Yousefi, A. A., & Cui, H. (2020). Properties of self-compacting concrete with recycled concrete aggregates. In R. Siddique (Ed.) *Self-Compacting Concrete: Materials, Properties, and Applications* (pp. 219–248). Woodhead Publishing. <https://doi.org/10.1016/b978-0-12-817369-5.00009-x>

- Tang, W., Ryan, P. C., Cui, H., & Liao, W. (2016). Properties of self-compacting concrete with recycled coarse aggregate. *Advances in Materials Science and Engineering*, 2016(1), Article 2761294. <https://doi.org/10.1155/2016/2761294>
- Tangadagi, R. B., Manjunatha, M., Seth, D., & Preethi, S. (2021). Role of mineral admixtures on strength and durability of high strength self compacting concrete: An experimental study. *Materialia*, 18, Article 101144. <https://doi.org/10.1016/j.mtla.2021.101144>
- Tiwari, P. K., Sharma, P., Sharma, N., Verma, M., & Rohitash. (2021). An experimental investigation on metakaoline GGBS based concrete with recycled coarse aggregate. *Materials Today: Proceedings*, 43, 1025–1030. <https://doi.org/10.1016/j.matpr.2020.07.691>
- Tuyan, M., Mardani-Aghabaglou, A., & Ramyar, K. (2014). Freeze–thaw resistance, mechanical and transport properties of self-consolidating concrete incorporating coarse recycled concrete aggregate. *Materials in Engineering*, 53, 983–991. <https://doi.org/10.1016/j.matdes.2013.07.100>
- Wang, Y., Zhao, B., Yang, G., Jia, Y., Liu, Y., Li, M., Xiang-Liang, T., Huang, Z., Jin, S., & Shen, W. (2019). Effect of recycled coarse aggregate on the properties of C40 self-compacting concrete. *Advanced Composites Letters*, 28, Article 096369351988512. <https://doi.org/10.1177/0963693519885128>
- Wu, H., Zuo, J., Zillante, G., Wang, J., & Yuan, H. (2019). Status quo and future directions of construction and demolition waste research: A critical review. *Journal of Cleaner Production*, 240, Article 118163. <https://doi.org/10.1016/j.jclepro.2019.118163>
- Xuyong, C., Jiawei, M., Qiaoyun, W., Jie, L., Shukai, C., & Zhuo, L. (2025). Study of the effect of pretreatment on coarse recycled aggregate in self-compacting concrete: Rheology, mechanical properties, and microstructures. *Journal of Building Engineering*, 101, Article 111744. <https://doi.org/10.1016/j.job.2024.111744>

Differences Between Research Log Datasets and Development Field Logs and the Creation of the Complexity Evaluation Index

Hironori Uchida^{1*}, Keitaro Tominaga², Hideki Itai², Yujie Li¹ and Yoshihisa Nakatoh¹

¹Kyushu Institute of Technology, Kitakyushu, 804-8550, Japan

²Panasonic System Design Co., Ltd, Yokohama, 222-0033, Japan

ABSTRACT

In the industrial domain, logs are widely applied in the management and maintenance of software systems to ensure reliability and availability. Furthermore, in the research field, various deep learning methods such as CNNs, LSTMs, and Transformers have been reported to achieve high accuracy in anomaly detection studies. However, there are challenges to their adoption in development fields. One reason is the limited datasets used in research, which lack a comprehensive evaluation for general applicability. To address this, we have prepared metrics to assess the complexity of log datasets necessary for creating a log generator for research purposes. We conducted a comparative study on the complexity of datasets in both research and industrial domains. Our evaluation of log sequence complexity, using frequency of occurrence and the Gini coefficient, showed that industrial logs are more complex across all metrics. This highlights the increased need for datasets close to the industrial domain for research purposes. Our study's findings suggest that a clear metric for dataset complexity can be achieved by converting logs into templates and then into sequences of size 10, evaluated using the Gini coefficient or kurtosis. Future work will involve developing a generator that produces logs close to those found in development environments, using these metrics as target values.

ARTICLE INFO

Article history:

Received: 01 April 2024

Accepted: 10 April 2025

Published: 10 June 2025

DOI: <https://doi.org/10.47836/pjst.33.S4.09>

E-mail address:

uchigzi@outlook.com (Hironori Uchida)
tominaga.keitaro@jp.panasonic.com (Keitaro Tominaga)
itai.hideki@jp.panasonic.com (Hideki Itai)
yzyjli@gmail.com (Yujie Li)
nakatoh@ecs.kyutech.ac.jp (Yoshihisa Nakatoh)

*Corresponding author

Keywords: Anomaly detection, complexity, evaluation index, log generator, system log

INTRODUCTION

Logs record vital information during system execution. In the industrial domain, particularly within large-scale systems, logs are extensively used to manage and maintain software systems to ensure reliability and

availability. In the research field, various deep learning methods such as CNNs (Du et al., 2017; Lu et al., 2018), LSTM (Meng, et al, 2019; Zhu et al, 2020), and Transformers (Guo et al, 2022; Nedelkoski et al, 2021) have been applied to anomaly detection studies. While these studies report high accuracy, there are challenges in their adoption in development fields (Le et al, 2022). One commonly used dataset in log anomaly detection research is Loghub (Zhu et al, 2023), which includes logs from multiple operating systems and applications such as HDFS (a distributed system), BGL (a supercomputer), and ThunderBird (a supercomputer). However, Loghub has only a few types of labeled logs, and there are only one or two instances of each type. This has raised concerns about the scarcity of datasets (He et al, 2022). For example, a study investigating the contents of the BGL dataset reported that specific logs were streaming continuously, and a particular log sequence pattern (e.g., logs extracted with a window size of 10 and stride of 1) accounted for about 40% of the total (Uchida et al, 2023). While this trend is frequent in system and server logs, it significantly differs from logs produced by systems comprising applications and operating systems that form a large part of societal systems. This discrepancy suggests a potentially significant difference in the complexity of anomaly detection problems.

Therefore, we believe that the choice of dataset is crucial for advancing log anomaly detection research that is also effective in development fields. However, publicly sharing logs from the development and post-development stages is challenging due to various rights. Our research aims to create logs as close as possible to those found in development fields.

In this study, we conducted the following investigations to develop a log dataset generator that closely resembles those in development environments:

1. Development of evaluation metrics to assess the complexity of log datasets.
2. Investigation of the differences in complexity between research log datasets and those from development environments using the metrics developed in point 1.

METHODS

Datasets

This discussion introduces the research dataset and the logs from the development fields used in this experiment.

Dataset in Research Fields

The dataset in the research fields utilized the Loghub dataset, commonly used in studies on log anomaly detection. Loghub contains a variety of datasets, such as operating systems and servers. We selected "Mac", "Linux", "Windows", "Android_v1", "BGL", and "Thunderbird" for our study. We applied a restriction for datasets exceeding 5,000,000 lines by removing logs beyond the 5,000,000th line.

Logs in the Development Fields

The logs from the development environment were extracted from a system presently undergoing development. This system is composed of multiple applications operating on a specific operating system, and the logs analyzed in this study originated from the output of these diverse systems. Specifically, the three logs utilized were denoted as "Dev_v1," "Dev_v2," and "Dev_v3," respectively.

Evaluation Metrics for Measuring Complexity

This discussion introduces the metrics used in this experiment to evaluate log complexity. As there is no standardized metric for assessing the complexity of logs, we compiled various metrics used across different datasets. Additionally, we set the following conditions for complexity in this experiment: If specific logs are continuously output or the number of specific logs is disproportionately high compared to the total logs, we consider the dataset's complexity low.

This is because complex systems that include an OS and multiple applications, specific logs are not continuously output; instead, various types of logs are generated concurrently. Thus, a balanced distribution of different types of logs indicates higher complexity. Under this condition, we used the frequency of each log type to measure complexity using various metrics.

Evaluation Metric 1: Number of Logs Per Second

One of the metrics we used is the number of logs per second. We assumed that the more logs and types per second, the more complex the system and the dataset. To determine whether a dataset is complex because of a high number of logs at specific times and due to a consistently high number of logs, we investigated the number of logs per second.

We calculated using the time part of each log format. Furthermore, as complexity metrics, we used the calculated number of logs per second to find the average, population standard deviation (pstdev), median, maximum, and minimum values.

The evaluation of complexity for each metric is as follows:

1. Mean and Standard Deviation: If the average is high and the standard deviation is low, it indicates that the variance in the number of logs per second is small and the average is high, suggesting a high complexity without bias.
2. Max, Min, Mean, Median: If there is a significant difference between the max and min values, and they are far from the mean and median, it indicates high complexity.

Evaluation Metric 2: Percentage of Data Types in Total Data Count (PDT)

Log type refers to the number of different types of data. In this study, there are three main data types: (1) original logs, (2) templates, and (3) sequence data. The "percentage of data types in total data count" is evaluated by dividing the total number of types by the total number of data points for these data types. A higher value indicates the presence of a larger variety of data types, suggesting higher complexity in the system.

Evaluation Metric 3: Frequency of Occurrence

We calculate the frequency of occurrence for each log type and use the average and standard deviation of these frequency values as complexity indicators. If the variation in frequency values is small, it is assumed that a variety of logs are being produced in large quantities, indicating high complexity.

Evaluation Metric 4: Kurtosis

Kurtosis is a statistical measure that characterizes the shape of a probability distribution, measuring the thickness of the tails and the sharpness of the central peak of the distribution. It allows us to assess how sharp the peak of the distribution is and how thick the tails are (DeCarlo et al., 1997).

In this experiment, kurtosis is calculated using the frequency of occurrence of each log as input. As a preprocessing step, we prepare two sequences of frequency values: one sorted in ascending order and the other in descending order, and then concatenate them to form a convex graph. This process enables the measurement of the kurtosis of frequency occurrence. A kurtosis greater than zero indicates that the distribution is sharper than a normal distribution, suggesting that certain logs occur frequently and there is bias in the data. Conversely, if kurtosis is less than zero, the distribution is not as sharp as a normal distribution and has wider tails, indicating less bias in frequency occurrence. The calculation formula (Fisher's definition) is as Equation 1:

$$Kurtosis = \frac{N(N-1)}{(N-1)(N-2)(N-3)} \sum_i^N \left(\frac{x_i - \bar{x}}{s} \right) \left(\frac{x_i - \bar{x}}{s} \right)^4 - \frac{3(N-1)^2}{(N-1)(N-3)} \quad [1]$$

where N represents the sample size, x_i represents each data point, \bar{x} is the sample mean, and s is the sample standard deviation. In this definition, the kurtosis of a normal distribution is 0.

Evaluation Metric 5: Gini Coefficient

The Gini coefficient is a measure of inequality commonly used in economics, ranging from 0 (complete equality) to 1 (complete inequality) (Sen et al., 1973). In this experiment, the Gini coefficient is calculated using the frequency of occurrence of each log as input. When the Gini coefficient is close to 0 (complete equality), it indicates a low bias in frequency of occurrence, suggesting high complexity in the dataset. Conversely, when the Gini coefficient is close to 1 (complete inequality), it indicates a high bias in the dataset, suggesting low complexity. In this experiment, we used the simplified formula in Equation 2:

$$\text{GiniCoefficient} = \frac{2 \sum_{i=1}^n ix_i}{n \sum_{i=1}^n x_i} - \frac{n+1}{n} \quad [2]$$

where x_i represents the sorted data, i represents the rank of the data (in sorted order), and n represents the total number of data points.

Evaluation Metric 6: Entropy

In the field of information theory, entropy is used to represent the uncertainty of data (Shannon et al., 1948). In this experiment, entropy is calculated using the frequency of occurrence of each log as input. High entropy indicates that the frequency of occurrence is relatively evenly distributed, suggesting high complexity. Low entropy indicates that a few logs occur frequently, suggesting low complexity. As a preprocessing step, the frequency of occurrence of each log is converted into a probability by dividing by the total frequency of occurrence. The preprocessing and the formula for calculating entropy are as Equation 3:

$$\text{Entropy} = - \sum p(x_i) * \log_2(p(x_i)) \quad [3]$$

where $p(x_i)$ represents the probability of each data point.

Evaluation Metric 7: Mean Absolute Deviation (MAD)

This metric represents how far data points are from the mean value. MAD, like the mean, indicates the central tendency of data but is less influenced by outliers (Huber et al. 1981). A small MAD indicates that the frequency of occurrence of logs is average, suggesting high complexity in the dataset (Equation 4):

$$\text{Mean Absolute deviation} = \frac{1}{N} \sum_{i=1}^N |x_i - \bar{x}| \quad [4]$$

where N is the size of the dataset, x_i represents each data point, and \bar{x} is the mean value of the dataset.

Experimental Procedure

To explore appropriate methods for investigating the complexity of log datasets, this study processed logs and converted them into the following five types of data analysis:

1. Original logs
2. Histogram of original logs (frequency of occurrence)
3. Histogram of log sequence data (frequency of occurrence)
4. Histogram of log templates (frequency of occurrence)
5. Histogram of log template sequence data (frequency of occurrence)

Experimental Procedure 1: Original Logs

In the complexity evaluation experiment of the original logs, we extract the contents part of the logs produced by each system and treat them as different logs if even one character in the string varies. For example, as shown in Table 1, logs Id1 to Id3 are considered different logs even though they only differ in parameters (numbers). This experiment investigates Metrics 1 (number of logs per second) and Metric 2.

Table 1
Examples of original logs

Id	Log
1	ddr: activating redundant bit steering: rank=0 symbol=25
2	ddr: activating redundant bit steering: rank=0 symbol=9
3	ddr: activating redundant bit steering: rank=0 symbol=23
4	1 ddr errors(s) detected and corrected on rank 0, symbol 2, bit 5
5	1 ddr errors(s) detected and corrected on rank 0, symbol 2, bit 0
6	30 ddr errors(s) detected and corrected on rank 0, symbol 9, bit 6

Experimental Procedure 2: Histogram of Original Logs (Frequency of Occurrence)

In this experiment, the complexity of original logs is evaluated by extracting the contents part of logs from each system and treating them as different logs if even one character in the string varies. Metrics 3 to 7 are investigated using the frequency of occurrence for logs.

Experimental Procedure 3: Log Sequence Data

The data uses the contents part of logs produced by each system, similar to Experimental Procedure 1. This data is converted into sequence data using a windowing process

(Window=10, Slide=1) from the chronological order in which the logs are output. These size 10 log sequence data are treated as one piece of data, and those that differ as sequences, as shown in Table 2, are treated as different data. Metrics 3 to 7 are investigated.

Table 2
Examples of log sequence data

Id	Log Sequence Data
1	[2, 2, 2, 2, 2, 2, 2, 2, 2, 2]
2	[2, 2, 2, 2, 2, 2, 2, 2, 2, 4]
3	[3, 3, 2, 2, 3, 2, 3, 2, 3, 2]

Experimental Procedure 4: Log Templates

Log templates extract and represent the common structure of the contents part of logs in a reusable format. They are commonly used as inputs for log analysis tools and deep learning models for anomaly detection. Templates differentiate between the variable parts (variables) and constant parts (constants) in a message, as shown in Table 3, with variable parts represented by `<*>`. In this study, we used Drain (He et al., 2017), a highly accurate tool for extracting parameters and creating templates. Drain employs a tree-structured learning technique with several parameters, including a threshold. For this experiment, we used the same parameters as those in a paper that investigated the accuracy of various DL models for log anomaly detection (Chen et al., 2022). The parameters used are shown in Table 4. Experimental Procedure 4 investigates Metrics 2 to 7.

Table 3
Examples of log templates

Id	Log Template
1	ddr: activating redundant bit steering: rank=0 <code><*></code>
2	<code><*></code> ddr errors(s) detected and corrected on rank 0, symbol <code><*></code> bit <code><*></code>
3	CE sym <code><*></code> at <code><*></code> mask <code><*></code>

Table 4
Drain parameters used in this study

Dataset type	Regex	Similarity threshold	Depth of all leaf nodes
BGL	[r'core\\.d+']	0.5	4
Android	[r'(/[w-]+)'+, r'(/[w-]+\.)\{2,\}[w-]+, r'\b(\-?\+?\d+)\b\ b0[XX][a-fA-F\d]+\b\ b[a-fA-F\d]\{4,\}b']	0.2	6
Thunderbird	[r'(\d+\.)\{3\}\d+']	0.5	4
Windows	[r'0x.*?\s']	0.7	5
Linux	[r'(\d+\.)\{3\}\d+ ', r'\d\{2\}:\d\{2\}:\d\{2\}']	0.39	6
Mac	[r'(/[w-]+\.)\{2,\}[w-]+']	0.7	6

Experimental Procedure 5: Sequence Data of Log Templates

Similar to Experimental Procedure 3, the data uses the contents of the logs produced by each system, and converts them into templates. These templates are converted into sequence data using a windowing process (Window=10, Slide=1) from the chronological order in which the templates are output. These size 10 template sequence data are treated as one piece of data, and those that differ as sequences, as shown in Table 5, are treated as different data. Metrics 3 to 7 are investigated.

Table 5
Examples of log template sequence data

Id	Log Template Sequence Data
1	[47, 47, 47, 47, 47, 47, 47, 47, 47, 26]
2	[47, 47, 47, 47, 47, 47, 47, 47, 47, 47]
3	[47, 47, 47, 47, 47, 48, 48, 48, 48, 48]

RESULTS

Experiment 1: Original Logs

We assessed the information quantity introduced in Experimental Procedure 1 using evaluation criteria 1 to 2. According to the definition original logs are treated as distinct logs if they do not fully match; each log is assigned a unique ID.

The results for each system are shown in Table 6. The criteria for high complexity include a high mean value, a small difference between the mean and median values, and small differences between the mean and the maximum and minimum values. The datasets that most closely meet these criteria are BGL and the three development field datasets. Linux has a small variance in the number of logs per second, but it is considered less complex

Table 6
Results of evaluation metrics 1 and 2 in Experiment 1

Dataset Name	Number of logs per second				PDT	Component
	mean	pstdev	median	max/min		
Mac	5.633	31.524	2	399 / 7	0.394	126
Linux	1.658	2.844	1	53 / 1	0.442	72
Windows	906.668	3855.942	18	35411 / 1	0.042	13
Android_v1	75.538	166.253	26	2568 / 1	0.180	1756
BGL	15.744	22.204	7	393 / 1	0.076	14
Thunderbird	7.862	58.545	3	10246 / 1	0.083	173
Dev_v1	402.952	402.509	163	1663 / 2	0.352	765
Dev_v2	61.113	78.237	36	379 / 1	0.375	11
Dev_v3	21.520	48.225	2	304 / 1	0.793	106

due to the low average number of logs. Other datasets have a large standard deviation and a significant difference between the mean and maximum values, indicating that logs are produced in large quantities at specific times, leading to a lower complexity rating.

Next, we summarize the results for the metric ratio of types to total log count. This metric investigates the diversity of log types within the dataset. Among the systems studied, Mac, Linux, and the three development field systems show relatively less bias in the types of logs.

Experiment 2: Histogram of Original Logs (Frequency of Occurrence)

We assessed the information quantity introduced in Experimental Procedure 1 based on evaluation criteria 3 through 7. According to the definition that original log histograms treat each log as a distinct entity unless they are an exact match, the histograms of each log are considered the sources of information.

Tables 7 and 8 show the results for each system. A notable result across all systems is that the median value is close to 1, indicating that most logs are infrequently produced (Table 7). Systems with a small difference between the mean and maximum values and a small standard deviation are Mac, Linux, and the three development field systems.

The systems with high complexity, as listed in Table 8, are summarized below:

1. Kurtosis: Mac, Linux, and the three development field systems are relatively complex. Notably, Development v2 and v3 show even less bias in frequency of occurrence compared to the other three.
2. Gini coefficient: Development v3 shows significantly less bias compared to the others.
3. Entropy: The results were almost identical across all systems.
4. Mean absolute deviation: Systems with relatively less bias are Mac, Linux, and the three development field systems.

Table 7
Results of evaluation metrics 3 in Experiment 2

Dataset Name	Histogram				
	mean	pstdev	median	max	min
Mac	2.537795	28.07699	1	2397	1
Linux	2.262353	11.82191	1	1043	1
Windows	23.86387	140.1128	4	34668	1
Android_v1	5.566029	131.1742	1	27822	1
BGL	13.1531	498.9645	1	152734	1
Thunderbird	12.08394	1126.886	1	382340	1
Dev_v1	2.838861	24.58524	1	2165	1
Dev_v2	2.663655	21.73202	1	387	1
Dev_v3	1.261637	1.853959	1	42	1

Table 8
Results of evaluation metrics 4 to 7 in Experiment 2

Dataset Name	Kurtosis	Gini coeff	Entropy	Mean abs dev
Mac	2138.922004	0.597588	11.96984	2.798122
Linux	5400.675048	0.521918	11.93911	2.095992
Windows	22940.91372	0.84988	14.62374	34.60172
Android_v1	14445.56889	0.811196	12.55274	8.451361
BGL	50994.03783	0.871437	13.26365	19.65518
Thunderbird	57462.50936	0.916109	8.629199	21.82688
Dev_v1	4434.076893	0.625783	11.23046	3.178633
Dev_v2	243.0334853	0.619438	7.827793	3.143811
Dev_v3	359.0682511	0.198355	9.90051	0.474979

Experiment 3: Log Sequence Data

We assessed the information quantity introduced in Experimental Procedure 3 using evaluation criteria 3 to 7. The log sequence data refers to sequence data generated by applying window processing to the logs in chronological order.

Looking at Table 9, it is observed that the three Development Field datasets have a small difference between the mean and standard deviation, indicating a low bias in frequency of occurrence. The systems with high complexity listed in Table 10 are summarized below:

1. Kurtosis: Linux, Windows, and the three Development Field systems show low values, indicating relatively high complexity.
2. Gini Coefficient: Mac and Development v1, in particular, show significantly less bias compared to others. Compared with the results of the log data in Experiment 2, the values for Mac, Linux, Development v1, and v2 have significantly decreased. The evaluation of log sequences measures whether the same logs are being output consecutively, so systems with low values indicate that logs are output in various orders, suggesting high complexity for anomaly detection datasets.
3. Entropy: The results were almost identical across all systems.
4. Mean Absolute Deviation: Systems with relatively less bias include Mac, Linux, and the three Development Field systems.

Table 9
Results of evaluation metrics 3 in Experiment 3

Dataset Name	Histogram of Log Sequence Data				
	mean	pstdev	median	max	min
Mac	25.692	186.8841	1	7685	1
Linux	50.912	501.259	8	10404	1

Table 9 (continue)

Dataset Name	Histogram of Log Sequence Data				
	mean	pstdev	median	max	min
Windows	1412.275	42682.57	1	1750733	1
Android_v1	99.82051	824.7748	3	40942	1
BGL	2550.591	42936.94	1	1706751	1
Thunderbird	4928.063	32883.25	45	660553	1
Dev_v1	8.265135	50.03262	1	2165	1
Dev_v2	88.84932	356.4681	2	2081	1
Dev_v3	2.655405	9.642574	1	147	1

Table 10

Results of evaluation metrics 4 to 7 in Experiment 3

Dataset Name	Kurtosis	Gini coeff	Entropy	Mean abs dev
Mac	29835.69004	0.023354	16.56222	0.047615
Linux	696.3898193	0.159301	14.02642	0.371192
Windows	266.4154937	0.813842	15.48659	18.17317
Android_v1	188736.1726	0.199083	19.14314	0.48477
BGL	397543.7988	0.578114	17.0855	2.614236
Thunderbird	3040665.057	0.297249	20.00339	0.817167
Dev_v1	1893.53867	0.089784	14.95477	0.194578
Dev_v2	244.9009545	0.946071	12.66111	46.71347
Dev_v3	472.3838329	0.141798	10.59842	0.321129

Experiment 4: Log Templates

We assessed the information quantity introduced in Experimental Procedure 4 using evaluation criteria 2 to 7. The log template refers to data in which the common components of each log are templated using a Log Parser.

Tables 11 and 12 present the results for each system. The three development field datasets have a small difference between the mean and standard deviation, indicating a low bias in frequency of occurrence (Table 11). Compared to the original logs (Experiment 2), the differences between systems in mean values and standard deviations become more discernible.

The systems with high complexity, as listed in Table 12, are summarized below:

1. Kurtosis: Thunderbird and Development v1, v2 show low values, indicating relatively high complexity.
2. Gini coefficient: Development v1 and Development v2 have significantly less bias compared to others.

3. Entropy: It is observed that the values for Android, Development v1, and Thunderbird are relatively high.
4. Mean absolute deviation: Development v1 and Development v2 show significantly less bias compared to others.

Table 11
Results of evaluation metrics 2 and 3 in Experiment 4

Dataset Name	Histogram of Templates					Template types
	mean	pstdev	median	max	min	
Mac	25.692	186.8841	1	7685	1	4000
Linux	50.912	501.259	8	10404	1	500
Windows	1412.275	42682.57	1	1750733	1	3538
Android_v1	99.82051	824.7748	3	40942	1	14898
BGL	2550.591	42936.94	1	1706751	1	1848
Thunderbird	4928.063	32883.25	45	660553	1	1013
Dev_v1	8.265135	50.03262	1	2165	1	5137
Dev_v2	88.84932	356.4681	2	2081	1	73
Dev_v3	2.655405	9.642574	1	147	1	592

Table 12
Results of evaluation metrics 4 to 7 in Experiment 4

Dataset Name	Kurtosis	Gini coeff	Entropy	Mean abs dev
Mac	779.8136527	0.929228	7.674175	44.10432
Linux	364.3586554	0.892429	4.195259	81.88374
Windows	1585.393851	0.997397	2.692711	2781.577
Android_v1	979.8777736	0.930228	9.664662	160.5336
BGL	1348.354829	0.987413	4.268589	4760.467
Thunderbird	192.1112006	0.931104	8.629199	7907.527
Dev_v1	785.1040542	0.817377	9.223006	11.61492
Dev_v2	18.75473595	0.930945	2.475725	157.9384
Dev_v3	125.3654616	0.585244	7.409572	2.678757

Experiment 5: Sequence Data of Log Templates

We assessed the information quantity introduced in Experimental Procedure 5 using evaluation criteria 3 to 7. The sequence data of log templates refers to data generated by applying window-based grouping to log template data extracted using a Log Parser in chronological order.

Tables 13 and 14 show the results for each system. The three development field datasets have a small difference between the mean and standard deviation, indicating a

low bias in frequency of occurrence (Table 13). Compared to the histogram of templates (Experiment 4), the differences between systems in terms of mean values and standard deviations become even more apparent.

The systems with high complexity, as listed in Table 14, are summarized below:

1. Kurtosis: The three development field systems show low values, indicating relatively high complexity.
2. Gini coefficient: Mac, Development v1, and Development v2 show significantly less bias compared to others.
3. Entropy: Linux, Windows, Thunderbird, and Development Field sub1 show high complexity.
4. Mean absolute deviation: Development v1 and Development v2 show significantly less bias compared to others.

Table 13
Results of evaluation metrics 3 in Experiment 5

Dataset Name	Histogram				
	mean	pstdev	median	max	min
Mac	1.599437	16.32902	1	3921	1
Linux	4.768928	135.1905	1	9584	1
Windows	231.894	16117.76	1	1663366	1
Android_v1	1.70683	38.48374	1	27045	1
BGL	29.85183	4498.018	1	1679174	1
Thunderbird	4.095916	202.1167	1	128936	1
Dev_v1	1.315677	3.431559	1	202	1
Dev_v2	7.9375	27.24916	1	248	1
Dev_v3	1.029644	0.229087	1	6	1

Table 14
Results of evaluation metrics 4 to 7 in Experiment 5

Dataset Name	Kurtosis	Gini coeff	Entropy	Mean abs dev
Mac	51686.09081	0.363217	14.66522	1.076106
Linux	4728.412527	0.768955	6.918843	6.516396
Windows	10354.70923	0.99097	4.084183	439.5919
Android_v1	292478.0814	0.405236	17.67513	1.277801
BGL	123606.2519	0.959574	6.279894	54.35098
Thunderbird	326215.3618	0.73049	16.12383	5.316484
Dev_v1	846.0012814	0.234677	14.29795	0.58936
Dev_v2	30.80765436	0.813872	7.034099	11.55499
Dev_v3	176.9035518	0.028296	10.54513	0.058

DISCUSSIONS

Evaluation Metrics

Firstly, regarding the transformation process of the datasets used, it was found that templates show a greater difference in metrics than original logs, making it easier to evaluate complexity. Moreover, converting to histogram sequence data rather than dealing with original logs or templates line by line clarified the differences in complexity. Converting to templates, which treat logs of the same format differing only in parameters, equally suggests that it is crucial to investigate datasets while preserving their significant parts. The reason sequence data showed clearer differences in complexity is likely due to the issue reported in related studies that "research datasets contain many consecutive logs," allowing us to identify biases in the frequency of specific sequence data occurrences.

These results suggest that the sequence data of templates is informative for evaluating dataset complexity, which is necessary for researching machine learning systems usable in the industrial domain.

As for which metrics are suitable, while consideration is needed for the number of data and types of logs regarding the average and variance of occurrence frequencies, it is clear that they can be easily evaluated.

Next, we discuss the development environment logs under the assumption that they are highly complex due to the system's inherent complexity. As shown in the results in Table 14, kurtosis and the Gini coefficient indicate that the development environment logs are more complex. In contrast, entropy produced different results. Based on these findings, kurtosis and the Gini coefficient are deemed appropriate metrics for evaluating complexity.

Kurtosis tends to exhibit extremely high values, particularly when a small number of data categories dominate, which can amplify differences between datasets. However, it is important to recognize that kurtosis primarily indicates how closely a distribution aligns with a normal distribution. Therefore, it should be applied cautiously when evaluating whether individual data logs are evenly distributed on average. While kurtosis is useful for identifying outliers and understanding distributional characteristics, its interpretation requires careful consideration, especially in contexts involving non-normal data distributions (Kim & White, 2004).

In contrast, the Gini coefficient directly measures inequality within a dataset and effectively quantifies the uniformity of data outputs. Gastwirth (1972) noted that the Gini coefficient provides a clear and straightforward metric for determining whether outputs are evenly distributed across categories. This characteristic makes the Gini coefficient particularly well-suited for evaluating the fairness or uniformity of data outputs, thereby complementing kurtosis-based analysis.

By integrating both metrics into the methodology, kurtosis highlights the sharpness of the distribution, whereas the Gini coefficient evaluates its equality. Together, these metrics enable a more comprehensive assessment of data characteristics.

Differences in Data Characteristics: Research Datasets vs. Industrial Logs

The results from all metrics used in this study showed that logs from development fields exhibited higher complexity. This confirms that there is indeed a difference between research datasets and industrial logs. This discrepancy poses a significant challenge for current research in log anomaly detection, highlighting the need to create research datasets closer to those in the industrial domain.

CONCLUSION

In this study, we investigated metrics to evaluate the complexity of datasets. We examined the differences between research datasets and logs from development environments, aiming to create anomaly detection datasets in logs closer to those in industrial domains. Based on our investigations, we found the following approaches to be suitable:

1. Using sequence data derived from the frequency of occurrences in log templates.
2. Using mean, variance, kurtosis, and Gini coefficient based on the frequency of occurrences as evaluation metrics.

Logs from industrial domains showed higher complexity in all evaluation metrics prepared for this study. Similar to findings in reference studies, these results indicate that current research datasets are significantly different from those in industrial domains, underscoring the need for research datasets closer to the industrial context.

Future work will involve creating an automatic log generator that can be used for research, with the evaluation metrics identified in this study serving as target values. Furthermore, in this study, we only evaluated each complexity metric independently. For example, template types and the evaluation of the Gini coefficient for frequency of occurrences in template sequences reflect different aspects of complexity, namely the diversity of template types and the complexity of the log sequences, respectively. Therefore, to measure the overall complexity of a dataset, it is necessary to observe the balance of each complexity, making creating a comprehensive evaluation method a task for future research.

ACKNOWLEDGEMENTS

This work is supported by a grant from Panasonic System Design and JST, Kyutech Research Fellowship, with Grant Number JPMJFS2133. This work was supported by JST, Kyutech Research Fellowship, Grant Number JPMJFS2133.

REFERENCES

- Chen, Z., Liu, J., Gu, W., Su, Y., & Lyu, M. R. (2021). *Experience report: Deep learning-based system log analysis for anomaly detection*. arXiv:2107.05908. <https://doi.org/10.48550/arXiv.2107.05908>

- DeCarlo, L. T. (1997). On the meaning and use of kurtosis. *Psychological Methods*, 2(3), 292. <https://doi.org/10.1037/1082-989X.2.3.292>
- Du, M., Li, F., Zheng, G., & Srikumar, V. (2017). Deeplog: Anomaly detection and diagnosis from system logs through deep learning. In *Proceedings of the 2017 ACM SIGSAC conference on computer and communications security* (pp. 1285-1298). Association for Computing Machinery. <https://doi.org/10.1145/3133956.3134015>
- Gastwirth, J. L. (1972). The estimation of the Lorenz curve and Gini index. *The Review of Economics and Statistics*, 54(3), 306–316. <https://doi.org/10.2307/1937992>
- Guo, H., Lin, X., Yang, J., Zhuang, Y., Bai, J., Zheng, T., Zhang, B., & Li, Z. (2021). *Translog: A unified transformer-based framework for log anomaly detection*. arXiv:2201.00016. <https://doi.org/10.48550/arXiv.2201.00016>
- He, P., Zhu, J., Zheng, Z., & Lyu, M. R. (2017). Drain: An online log parsing approach with fixed depth tree. In *2017 IEEE international conference on web services (ICWS)* (pp. 33-40). IEEE. <https://doi.org/10.1109/ICWS.2017.13>
- He, S., Zhang, X., He, P., Xu, Y., Li, L., Kang, Y., Ma, M., Wie, Y., Dang, Y., Rajmohan, S., & Lin, Q. (2022). An empirical study of log analysis at Microsoft. In *Proceedings of the 30th ACM Joint European Software Engineering Conference and Symposium on the Foundations of Software Engineering* (pp. 1465-1476). Association for Computing Machinery. <https://doi.org/10.1145/3540250.3558963>
- Huber, P. J. (1981). *Robust Statistics*. Wiley.
- Kim, T. H., & White, H. (2004). On more robust estimation of skewness and kurtosis. *Finance Research Letters*, 1(1), 56-73. [https://doi.org/10.1016/S1544-6123\(03\)00003-5](https://doi.org/10.1016/S1544-6123(03)00003-5)
- Le, V. H., & Zhang, H. (2022). Log-based anomaly detection with deep learning: How far are we?. In *Proceedings of the 44th International Conference on Software Engineering* (pp. 1356-1367). Association for Computing Machinery. <https://doi.org/10.1145/3510003.3510155>
- Lu, S., Wei, X., Li, Y., & Wang, L. (2018). Detecting anomaly in big data system logs using convolutional neural network. In *2018 IEEE 16th Intl Conf on Dependable, Autonomic and Secure Computing, 16th Intl Conf on Pervasive Intelligence and Computing, 4th Intl Conf on Big Data Intelligence and Computing and Cyber Science and Technology Congress (DASC/PiCom/DataCom/CyberSciTech)* (pp. 151-158). IEEE. <https://doi.org/10.1109/DASC/PiCom/DataCom/CyberSciTec.2018.00037>
- Meng, W., Liu, Y., Zhu, Y., Zhang, S., Pei, D., Liu, Y., Chen, Y., Zhang, R., Tao, S., Sun, P., & Zhou, R. (2019). Loganomaly: Unsupervised detection of sequential and quantitative anomalies in unstructured logs. *International Joint Conference on Artificial Intelligence*, 19(7), 4739-4745. <https://doi.org/10.24963/ijcai.2019/658>
- Nedelkoski, S., Bogatinovski, J., Acker, A., Cardoso, J., & Kao, O. (2020). Self-attentive classification-based anomaly detection in unstructured logs. In *2020 IEEE International Conference on Data Mining (ICDM)* (pp. 1196-1201). IEEE. <https://doi.org/10.1109/ICDM50108.2020.00148>
- Sen, A. (1973). *On economic inequality*. Oxford University Press.

- Shannon, C. E. (1948). A mathematical theory of communication. *The Bell System Technical Journal*, 27(3), 379-423. <https://doi.org/10.1002/j.1538-7305.1948.tb01338.x>
- Uchida, H., Tominaga, K., Itai, H., Li, Y., & Nakatoh, Y. (2023). Verification of generalizability in software log anomaly detection models. In V. K. Parimala (Ed.) *Anomaly Detection-Recent Advances, AI and ML Perspectives and Applications* (pp. 7). IntechOpen. <https://doi.org/10.5772/intechopen.111938>
- Zhu, B., Li, J., Gu, R., & Wang, L. (2020). An approach to cloud platform log anomaly detection based on natural language processing and LSTM. In *Proceedings of the 2020 3rd International Conference on Algorithms, Computing and Artificial Intelligence* (pp. 1-7). Association for Computing Machinery. <https://doi.org/10.1145/3446132.3446415>
- Zhu, J., He, S., He, P., Liu, J., & Lyu, M. R. (2023). Loghub: A large collection of system log datasets for ai-driven log analytics. In *2023 IEEE 34th International Symposium on Software Reliability Engineering (ISSRE)* (pp. 355-366). IEEE. <https://doi.org/10.1109/ISSRE59848.2023.00071>

REFEREES FOR THE PERTANIKA JOURNAL OF SCIENCE & TECHNOLOGY

Vol. 33 (S4) 2025

The Editorial Board of the Pertanika Journal of Science and Technology wishes to thank the following:

Abdul Rahman Mohd. Sam
UTM, Malaysia

Noor Kamal Al-Qazzaz
University of Baghdad, Iraq

Choon Sen Seah
UTM, Malaysia

Norazura Muhamad Bunnori
UM, Malaysia

Darwin Gouwanda
Monash University, Malaysia

Nur Ashida Salim
UiTM, Malaysia

Hendri Masdi
Universitas Negeri Padang, Indonesia

Raja Nor Firdaus Kashfi
UTeM, Malaysia

Hiroaki Yamada
Yamaguchi University, Japan

Sawal Hamid Md Ali
UKM, Malaysia

Kunihisa Tashiro
Shinshu University, Japan

Syahrun Nizam Md Arshad@
Hashim
UNIMAP, Malaysia

Mohammad Lutfi Othman
UPM, Malaysia

Tevhit Karacali
Ataturk University, Türkiye

Mohd Fairouz Mohd Yousof
UTHM, Malaysia

Yunus Kaya
Bayburt University, Türkiye

Mohd Salahuddin Mohd Basri
UPM, Malaysia

Zuraidah Zan
UPM, Malaysia

Nik Norsyahariati Nik Daud
UPM, Malaysia

UiTM - Universiti Teknologi MARA
UKM - Universiti Kebangsaan Malaysia
UM - Universiti Malayq
UNIMAP - Universiti Malaysia Perlis

UPM - Universiti Putra Malaysia
UTeM - Universiti Teknikal Malaysia Melaka
UTHM - Universiti Tun Hussein Onn
UTM - Universiti Teknologi Malaysia

While every effort has been made to include a complete list of referees for the period stated above, however if any name(s) have been omitted unintentionally or spelt incorrectly, please notify the Chief Executive Editor, *Pertanika* Journals at executive_editor.pertanika@upm.edu.my

Any inclusion or exclusion of name(s) on this page does not commit the *Pertanika* Editorial Office, nor the UPM Press or the university to provide any liability for whatsoever reason.

Performance of Recycling Aggregate Self-Compacting Concrete Incorporating
Supplementary Cementitious Materials: An Overview 129

*Said Mohammed Mostafa Aljamala, Nor Azizi Safiee, Noor Azline Mohd Nasir
and Farah Nora Aznieta Abdul Aziz*

Differences Between Research Log Datasets and Development Field Logs and the
Creation of the Complexity Evaluation Index 161

Hironori Uchida, Keitaro Tominaga, Hideki Itai, Yujie Li and Yoshihisa Nakatoh

Pertanika Journal of Science & Technology

Vol. 33 (S4) 2025

Content

Preface	i
<i>Siti Anom Ahmad, Nashiren Farzilah Mailah and Roseliza Kadir Basha</i>	
Bibliometric Review on Geopolymer Modified with Nanomaterials Using VOS Viewer	1
<i>Maryam Firas Al-Baldawi, Farah Nora Aznieta Abdul Aziz , Al Ghazali Noor Abbas, Noor Azline Mohd Nasir, Khalina Abdan and Norsuzailina Mohamed Sutan</i>	
Material Characterization and Electrical Performance of <i>Prosopis africana</i> Conductive Ink for Antenna Applications	27
<i>Suleiman Babani, Mohd Nizar Hamidon, Alyani Ismail, Haslina Jaafar, Intan Helina Hasan, Farah Nabilah Shafee, Ibrahim Garba Shitu, Jamila Lamido, Sani Halliru Lawan and Zainab Yunusa</i>	
Effect of Coil Diameter on the Performance of Interior and Embedded Permanent Magnet for Double-stator Generator	45
<i>Nur Amira Ibrahim, Norhisam Misron, Hairul Faizi Hairulnizam, Chockalingam Aravind Vaithilingam, Nashiren Farzilah Mailah and Ishak Aris</i>	
Psychology-informed Natural Language Understanding: Integrating Personality and Emotion-aware Features for Comprehensive Sentiment Analysis and Depression Detection	57
<i>Jing Jie Tan, Ban-Hoe Kwan, Danny Wee-Kiat Ng and Yan Chai Hum</i>	
Development of Digital Twin Data-driven Modelling for Gas Turbine Operation Behaviour	81
<i>Balbir Shah Mohd Irwan Shah, Asnor Juraiza Ishak, Mohd Khair Hassan and Nor Mohd Haziq Norsahperi</i>	
Evaluation of Multimodal Dataset for Continuous Air-writing Multidigit Number Recognition Using Wearable Sensor	99
<i>Yusuke Takei and Eiichi Inohira</i>	
Acoustic Partial Discharge Localization in Refined, Bleached and Deodorized Palm Oil (RBDPO) Based on the Savitzky-Golay and Moving Average Denoising Methods	115
<i>Nur Darina Ahmad, Norhafiz Azis, Jasronita Jasni, Khairil Anas Md Rezali, Mohd Aizam Talib, Nik Hakimi Nik Ali and Masahiro Kozako</i>	



Pertanika Editorial Office, Journal Division,
Putra Science Park,
1st Floor, IDEA Tower II,
UPM-MTDC Center,
Universiti Putra Malaysia,
43400 UPM Serdang,
Selangor Darul Ehsan
Malaysia

<http://www.pertanika.upm.edu.my>
Email: executive_editor.pertanika@upm.edu.my
Tel. No.: +603- 9769 1622

PENERBIT
UPM
UNIVERSITI PUTRA MALAYSIA
PRESS

<http://penerbit.upm.edu.my>
Email: penerbit@upm.edu.my
Tel. No.: +603- 9769 8855

